

Mesonic and Isobar modes in matter

Vom Fachbereich Physik
der Technischen Universität Darmstadt

zur Erlangung des Grades
eines Doktors der Naturwissenschaften
(Dr. rer. nat.)

genehmigte Dissertation von
Dipl.-Phys. Felix C. Riek
aus Frankfurt a.M.

Referent: Prof. Dr. J. Wambach
Korreferent: PD Dr. M. Lutz

Tag der Einreichung: 16.10.2007
Tag der Prüfung: 12.12.2007

Darmstadt 2007

D17

Contents

1. Zusammenfassung	5
2. Introduction	7
2.1. Motivation	7
2.2. Historical overview	9
3. Pions and vector-mesons at finite temperature	13
3.1. Fields and model interactions	13
3.2. The approximation scheme	13
3.3. Computational details	16
3.3.1. Pion self-energy and polarisation loops	16
3.3.2. Four transversality of vector mesons	19
3.3.3. Vector meson self-energies	22
3.4. Determination of the parameters	28
3.5. Results	30
3.5.1. Influence of the projection method	30
3.5.2. Results for the mesonic system	33
4. Pions and Δ-isobars at finite density	41
4.1. Fields and model interactions	41
4.2. The approximation scheme	42
4.3. Computational details	45
4.3.1. Pion self-energy and polarisation loops	45
4.3.2. Pion-nucleon scattering	47
4.3.3. Isobar self-energy in the presence of vertex corrections	55
4.4. Determination of the parameters	57
4.4.1. Vacuum scattering amplitude	58
4.4.2. Photo absorption	62
4.5. Results	74
5. Relations to the Φ-functional	87
6. Conclusions and Outlook	93

7. Appendix	97
A. $\pi\rho$ loop tensor coefficients	97
B. Coefficient functions $H^{[lm,ij]}$, $H^{[T,ij]}$, $H^{[lm,T]}$ and $H^{[T,T]}$	99
C. Ghost states in the pion self-energy	100
D. Different gauges	102
E. Coefficients of the vector-meson self-energies	104
F. Analytic estimates for the ρ -meson self-energy	108
G. Nucleon- and isobar-hole loop functions	110
H. Coefficient functions $V_{[ij]}^{(p,q)}$	113
I. Coefficient functions $J_{[ij]}^{(p,q)}$ and master functions J_i	115
J. Reformulation of the master loop functions J_i	122
K. Reformulations in the dispersion integrals	125
L. Coefficient functions $c_{[ij]}^{(p,q)}$	127
M. u-channel contributions to the πN scattering amplitude	128
N. Photon transition function U	130
O. Contractions of the isobar propagator	131
P. Nucleon contributions to the Photoabsorption	133
 Bibliography	 137

1. Zusammenfassung

Im Rahmen der Untersuchung von Schwerionenkollisionen wie sie zum Beispiel bei der GSI durchgeführt werden versucht man Erkenntnisse über den Aufbau und die Struktur von Materie zu gewinnen. Dabei ist eine theoretische Beschreibung der Eigenschaften von Mesonen und Baryonen in Materie für das Verständnis der aus den Experimenten gewonnenen Daten von entscheidender Bedeutung.

Ziel dieser Arbeit war es zunächst eine selbstkonsistente Beschreibung der Eigenschaften der leichten Vektor-Mesonen ρ und ω und des Pions bei endlicher Temperatur in einer baryonfreien Umgebung zu erreichen. Eine Verallgemeinerung dieser Rechnungen zu endlichen Dichten benötigt zunächst eine zuverlässige Beschreibung des Pions und der $\Delta(1232)$ Resonanz. Hier wurden die bisher in der Literatur diskutierten Ansätze durch Hinzunahme von Vertex-Korrekturen und eine selbstkonsistente durchgehend relativistische Rechnung verbessert. Im Rahmen unserer Modelle konnten wir zeigen, dass sich die Eigenschaften des ρ -Mesons auch bei hohen Temperaturen nicht dramatisch ändern, wenn keine Effekte der Baryon-Dichte berücksichtigt werden. Das Verhalten von Pion und Δ -Resonanz bei endlicher Dichte ändert sich hingegen stark. Eine Änderung der Masse des Isobars kann in unserem Modell durch eine geeignete Wahl der mittleren Felder gesteuert werden. Eine endgültige Aussage über eine mögliche Massenänderung kann im Rahmen des hier diskutierten Modells noch nicht getroffen werden. Hierzu sind weitere Verbesserungen, insbesondere die konsistente Berücksichtigung der In-Medium Effekte in den Hintergrundbeiträgen zur Photoabsorption, notwendig. Ferner müssen Korrekturen zum $\gamma N \Delta$ -Vertex in die Rechnung mit einbezogen werden.

Weiterhin konnte im Rahmen dieser Arbeit durch die konsistente Berücksichtigung der Vertex-Korrekturen eine Beschreibung der Δ -Resonanz ohne weichen Formfaktor erreicht werden. Dies ist von entscheidender Bedeutung für die In-Medium Physik da nur so sichergestellt werden kann, dass das Modell weiche Moden konsistent behandelt.

Die im Rahmen dieser Arbeit entwickelten technischen Methoden erlauben eine einfache Verallgemeinerung der hier behandelten Modelle hinsichtlich der Hinzunahme von weiteren Resonanzen und Kopplungen. Hierdurch kann die bisher erzielte Beschreibung der In-Medium Eigenschaften der betrachteten Teilchen weiter verbessert werden.

1. Zusammenfassung

2. Introduction

2.1. Motivation

Quantum Chromo Dynamics (QCD) is considered as the fundamental theory of strong interactions. Due to its nonabelian structure this gauge theory leads to perturbative interactions at high energies or small distance (asymptotic freedom), while at small energies the interaction becomes so strong that the quarks and gluons are confined into hadrons. Besides the iso-spin symmetry between up and down quarks QCD posses one particular symmetry which arises from the fact that the up and down quarks are nearly massless. This symmetry is called chiral symmetry, since massless quarks, though interacting with other quarks, preserve their helicity or handyness. It predicts degenerate pairs of hadrons with positive and negative parity, called chiral partners, provided the vacuum state is chirally symmetric. However, the experimentally observed hadron spectrum shows chiral partners with masses that are not degenerate but differ by about 500 MeV. Along with other observations this manifests that the chiral symmetry is spontaneously broken in vacuum leading to a finite value of the chiral condensate¹. The Goldstone theorem then predicts modes of zero mass which can be identified with the three pions. Their small but finite masses of 140 MeV, which is significantly lower than any other hadron mass, results from the remaining explicit symmetry breaking due to the small but finite masses of up and down quarks of 5 to 10 MeV.

The interesting point in the context of hadronic, i.e. strongly interacting matter is the conjecture that chiral symmetry becomes restored with increasing energy density along with the confinement – deconfinement phase transition. As chiral partners have to become degenerate in the chirally restored phase, this implies a strong change in the properties of the hadrons in the medium during the approach towards the phase border. This could be realised for example by mass-shifts and/or by broadening or more general by a change of their spectral functions. Apart from the Goldstone boson itself which stays gapless throughout the true Nambu-Goldstone phase, chiral symmetry considerations enforce no further constraints on other chiral partners. Therefore it is interesting to study the spectral properties of particles in the medium as a function of thermodynamic

¹Much like the rotational symmetry is broken in a ferro-magnet below the Curie temperature leading to a finite magnetisation with corresponding Goldstone modes, the spin waves, possessing a gapless spectrum.

2. Introduction

parameters such as density and temperature. Besides nuclear many-body effects which are interesting on their own, one expects to learn something about the fundamental symmetry features of strongly interacting matter. Finally a precise experimental and theoretical determination of the behaviour of particles together with their chiral partners (like the ρ - and a_1 -meson) is mandatory in order to draw quantitative conclusions [1].

One of the experimental accesses to observe the in-matter properties of hadrons is provided through the study of electron-positron- or muon anti-muon pairs, called dileptons both in hadron-nucleus and nucleus-nucleus collisions [2–8]. Compared to strong interacting particles, like pions or kaons, which suffer from strong and complicated final state interaction effects, such electromagnetic probes directly observe the centre of the reaction zone. While this method offers a quite clean possibility to study the behaviour of vector mesons, techniques to study their chiral partners are presently not established.

In order to address these questions from the theoretical side one needs reliable predictions about the in-medium behaviour of these particles. In order to develop the techniques further and especially study the effects due to self-consistency we will concentrate on two aspects which are, besides others, of importance.

- First we need to extend the existing studies of vector mesons in a hot environment because several techniques used to restore four-transversality had to be reconsidered.
- Secondly a good control about the in-medium properties of the pion is mandatory. Since the pion is the lightest degree of freedom in the hadron spectrum nearly every other hadron resonance has a decay-mode which includes the pion. Thus the behaviour of the pion will influence the behaviour of all other particles and therefore needs further investigation.

In this work we will address these problems from a nuclear and hadron many-body approach with the aim to improve the description of the Δ -isobar and the pion in the nuclear medium and to establish a more reliable self-consistent treatment of vector-mesons. For the pion and Δ -isobar we will use a fully relativistic treatment to guarantee that we have everywhere the right kinematical behaviour of the self-energies. Besides the standard RPA-type short range correlations we will further include vertex corrections. The problem of renormalisation will be addressed by dispersion relations thus avoiding possibly problematic soft formfactors. In addition we provide the nucleon with a scalar and vector-meanfield to be able to model the in-medium behaviour of the nucleon in a more realistic way. For the Δ -isobar we will also allow such meanfields. As compared to our earlier investigations [9] the model will be constrained by scattering and photo absorption data.

Concerning the vector-mesons an earlier treatment to restore four transversality [10] will be improved in order to avoid spurious modes arising from kinematical singularities.

Furthermore vertex corrections and short range correlations of the type used for the Δ -isobar will also be applied for the vector mesons. The account for both real and imaginary parts of the self energies makes it necessary to introduce particular renormalisation strategies with the perspective to extend the model towards the inclusion of further resonances and other decay processes.

The thesis is organised as follows. After a historical overview we will treat the vector-mesons in hot matter in Chapter 3. Afterwards the pion and Δ -isobar will be studied at zero temperature (Ch. 4). These two chapters will each start with a short description about the model used before going into the computational details. Results for the two investigated scenarios will be presented at the end of the corresponding chapters. Further relations which are not of direct relevance for the understanding of the model-calculations are stated in the Appendices where we also include some side-studies, like analytical estimates, which are not within the main focus of this work but turned out to improve the understanding.

2.2. Historical overview

Investigations of the in-medium behaviour of hadrons in nuclear matter have a long and diverse history. Many experiments focused on the investigation of pionic modes in nuclei [11] using e.g. electromagnetic probes, pion-nuclear reactions, and charge exchange reactions. Thereby it was found that the pion strongly couples to the $\Delta(1232)$ isobar resonance inducing Δ -hole excitations. The latter by itself would lead to a strong softening of the pion modes including the possibility of pion condensation which, however, becomes compensated by repulsive short-range correlations known as Migdal correlations [12,13]. The microscopic description challenged many investigations [9,13–25] with diverging results. With a few exceptions [19,20] non-relativistic many-body techniques were applied throughout. Short range correlation effects were studied systematically in refs. [15,18,21], while self-consistent approaches [9,16,17,20,21,23] are in the minority.

First estimates about the in-medium properties of the Δ -isobar at nuclear saturation density inferred from the phenomenological spreading potential [26] suggest a small repulsive mass shift of the isobar together with an increase of its width. With the exceptions of refs. [15,20] most recent models claim such a mass shift. This seems consistent with recent data on electroproduction of isobars off helium three [27] and with the observed shift of the peak in photo-absorption cross sections on nuclei relative to that on the nucleon. However the situation may be more subtle, as the photo absorption process is significantly affected by short range correlation [15,20,28] with the option even of a downwards shift of the Delta mass [22].

A further source of concern are the soft form-factors used in most calculations which omit vertex corrections, c.f. [16,17]. Such form-factors suppress pionic modes already at

2. Introduction

rather soft energy scales relevant for the isobar dynamics [20]. Since scales are not cleanly separated, models with soft form-factors are not able to properly explain the vacuum phenomenology, to which they are fitted. Thus, extrapolations to the nuclear medium are problematic. Strong temperature, density, energy and momentum dependences of the form-factors may come into play. Arve and Helgesson [18] or Oset et al. [15, 28] avoided soft form-factors and claimed a strong attractive isobar mass shift of about 65 MeV at nuclear saturation density consistent with photo absorption data.

Longitudinal and transverse isobar modes can split in the nuclear environment [15, 18, 20, 22]. Contrary to refs. [15, 20, 22] Arve et. al. [18] even quotes sizable splittings which, however, depend sensitively on the choice of their form-factors.

Since the Δ -isobar lies only 140 MeV above the πN -threshold, the feedback of a dressed pion back on the isobar itself can be very essential [9, 16, 17, 20, 21, 23] pledging for a self-consistent treatment. Further effects then arise through the fact that the Delta-hole correlations themselves are also modified [18, 20, 21].

Recently Lutz [29] formulated a covariant Delta-hole model. It differs significantly from the non-relativistic versions [13, 14, 30]. Sizable alterations in the self-energies occur close to the light-cone and in the time-like region, since factors proportional to the square of the pion four-momentum q^2 appear in the relativistic treatment [29, 30], compared to the square of the three-momentum \vec{q}^2 appearing non-relativistically [13, 14]. In this context quite a variety of prescriptions (see e.g. [18, 31]) were suggested with great spread in the values of the Migdal parameters [18, 21, 30, 32]. In a recent work [20] a first manifestly covariant and self-consistent computation of the pion spectral function was presented, and successfully used to compute the nuclear photo absorption [22], still using rather soft form-factors instead of vertex corrections. A further clarification of the isobar properties in nuclear matter is therefore vital, both for the application to nucleus-nucleus collisions [23] and for the calculation of the vector-meson properties.

Besides the motivations given by theory, e.g. in the context of chiral restoration, special interest in the vector-meson question arose from dilepton spectra observed in nucleus-nucleus collisions. There a significant enhancement in the dilepton rates was observed [2–8, 33], compared to rates estimated from straight extrapolations of elementary processes. While at low invariant pair-masses Bremsstrahlung and controllable Dalitz decays of the pion and other resonances dominantly contribute to the di-lepton rates, at invariant pair-masses above 400 MeV electromagnetic decays from light vector-mesons are the main source.

The enhanced nuclear yields triggered quite a variety of explanations, which range from a lowering of the ρ -meson mass to a significant increase of its damping width [9, 10, 34–41]. Presently the high precision data of the NA60 collaboration [8] are best described assuming a strong broadening of the ρ -meson width in the medium [42, 43]. A simple lowering of the ρ -meson mass [44] seems to be excluded. So far most theoretical investigations were done on a perturbative level. This allows to include large

numbers of excitation modes [39,40,45,46] contributing to the ρ -meson spectral function in the medium. Self-consistent treatments [9,10,47–49] showed interesting new effects. However so far the model space in the latter studies was rather limited. Contrary to the importance of baryonic effects, Refs. [10,47–49] solely investigated mesonic systems only. In a previous work [9] we already improved the situation by considering baryon effects on the in-medium pionic modes. Yet, certain aspects of conceptual importance such as vertex corrections [34,35] were still neglected. In addition large effort has been made [50–52] to describe the different mesons and baryons in vacuum using coupled channel approaches. In [52] this input was then used to draw conclusions about the in-medium behaviour of vector-mesons. Here quite different effects as compared to the calculations of Post et. al. [40] were found due to the smaller coupling of the ρ -meson to the $N^*(1520)$ resonance.

On the level of QCD sum-rules have been considered [53–58]. However they could so far only provide rough constraints on but no quantitative predictions for the spectral shape of the ρ -meson. Also recent lattice QCD studies [59] are trying to address these questions, however, with limited precision which defers a quantitative comparison to data.

The in-medium behaviour of the ω -meson is an even more challenging problem both theory wise [2,7,54,60–65] as well as experimentally. Suppressed in its coupling compared to the ρ -meson, the ω -meson signal will be quite difficult to be isolated in the dilepton spectrum. The alternative observation through the $\omega \rightarrow \pi^0\gamma \rightarrow 3\gamma$ channel as recently observed in photo-production off nuclei [66] point towards interesting density effects on the ω -meson. A preliminary analysis [67] shows a two peak structure of the in-medium ω -meson possibly arising from resonance-hole excitations [52]. Furthermore it was found [68] that also vertex corrections are needed in order to get a proper description already at the vacuum level.

In our previous exploratory study [9] we were able to calculate the modified spectral functions of both vector-mesons in a self-consistent coupling scheme. Thereby the process $\rho \rightarrow \omega + \pi$ leads to a strong interplay between the vector mesons. In particular the ω -width showed to be very sensitive to the space-like, i.e. low energy component of the pion modes caused by its coupling to nucleon nucleon-hole states.

Recently we had initiated a clarifying discussion [48,49] on spurious modes arising from kinematical singularities in self consistent treatments [47,49] of vector particles. This issue will be also part of this thesis.

2. Introduction

3. Pions and vector-mesons at finite temperature

In this chapter we study the interplay of the pion with the ρ - and ω -mesons in a hot but baryon free environment. Effects from nuclear density will be not be considered. We will analyse several ways how to restore four transversality of the vector-meson polarisation tensors in self-consistent calculations. The realtime formalism [69] will be used.

3.1. Fields and model interactions

The Lagrangian defining the interaction between pions and ρ - and ω -mesons is given by [70]

$$\begin{aligned} \mathcal{L}_{\pi\rho\omega} = & \frac{1}{2}(\partial_\mu - ig_{\rho\pi\pi}\rho_\mu^c T_c^1)\pi \cdot (\partial_\mu - ig_{\rho\pi\pi}\rho_\mu^c T_c^1)\pi - \frac{1}{2}m_\pi^2\pi \cdot \pi \\ & - \frac{1}{4}\rho_{\mu\nu}\rho^{\mu\nu} + \frac{1}{2}m_\rho^2\rho_\mu\rho^\mu \\ & - \frac{1}{4}\omega_{\mu\nu}\omega^{\mu\nu} + \frac{1}{2}m_\omega^2\omega_\mu\omega^\mu + g_{\omega\rho\pi}\epsilon^{\alpha\beta\mu\nu}\omega_\alpha\partial_\beta\rho_\mu(\partial_\mu - ig_{\rho\pi\pi}\rho_\mu^c T_c^1)\pi \end{aligned} \quad (3.1)$$

where π and ρ^μ denote the isospin triplet fields of the pion and the ρ -meson and we have $T_c^1 = -i\epsilon_{abc}$ with isospin indices a, b, c . Thereby the vector-meson field strength tensors are denoted by $\rho_{\mu\nu} = \partial_\mu\rho_\nu - \partial_\nu\rho_\mu$ and $\omega_{\mu\nu} = \partial_\mu\omega_\nu - \partial_\nu\omega_\mu$ respectively. The $\pi\rho\omega$ -vertex is given by the standard Wess-Zumino-Witten term [71–73] where we also have to use the covariant derivative.

3.2. The approximation scheme

Before explaining the technical details of the approach we first give an overview of the approximation. Main focus of this chapter will be on the determination of the behaviour of the light vector mesons ρ and ω and the pion at finite temperature. To do so we like to determine the full retarded propagators G_π , $G_{\mu\nu}^{(\rho)}$ and $G_{\mu\nu}^{(\omega)}$ of pion, ρ - and ω -meson

3. Pions and vector-mesons at finite temperature

given as solution to the coupled set of Dyson equations

$$\begin{aligned}
 G_{\pi}(w, u) &= G_{\pi}^{(0)}(w) + G_{\pi}^{(0)}(w) \Pi_{\pi}(w, u) G_{\pi}(w, u), \\
 G_{\mu\nu}^{(\rho)}(w, u) &= G_{\mu\nu}^{(\rho,0)}(w) + G_{\mu\alpha}^{(\rho,0)}(w) \Pi_{(\rho, P)}^{\alpha\beta}(w, u) G_{\beta\nu}^{(\rho)}(w, u), \\
 G_{\mu\nu}^{(\omega)}(w, u) &= G_{\mu\nu}^{(\omega,0)}(w) + G_{\mu\alpha}^{(\omega,0)}(w) \Pi_{(\omega, P)}^{\alpha\beta}(w, u) G_{\beta\nu}^{(\omega)}(w, u). \quad (3.2)
 \end{aligned}$$

Here the free propagators

$$\begin{aligned}
 G_{\pi}^{(0)}(w) &= \frac{1}{w^2 - m_{\pi}^2 + i\epsilon}, \\
 G_{\mu\nu}^{(\rho,0)}(w) &= \frac{g_{\mu\nu} - \frac{w_{\mu}w_{\nu}}{m_{\rho}^2}}{w^2 - m_{\rho}^2 + i\epsilon}, \quad G_{\mu\nu}^{(\omega,0)}(w) = \frac{g_{\mu\nu} - \frac{w_{\mu}w_{\nu}}{m_{\omega}^2}}{w^2 - m_{\omega}^2 + i\epsilon}, \quad (3.3)
 \end{aligned}$$

are indicated with an index zero and the retarded self energies or polarisation tensors will be defined in the following. The additional index P used at the vector-meson self-energies indicates a projection of these quantities in order to recover four-transversality. A detailed discussion of such projections will be given in a the following chapter.

From our choice of the interaction (3.1) we have several contributions to the self-energies of all particles which could be discussed. Our strategy assumes that the contributions with the lowest threshold will play the most dominant part and has to be resummed while further interactions implied by (3.1) are suppressed by phase space. Key ingredient for the pion self-energy of this approach is therefore the basic correlation loop

$$\begin{aligned}
 \chi_{\mu\nu}^{(\rho\pi)}(w, u) &= \langle \text{diagram} \rangle \\
 &= 8g_{\rho\pi\pi}^2 \int \frac{d^4l}{2(2\pi)^4} G_{\mu\nu}^{(\rho)}(l, u) G_{\pi}(l - w, u), \quad (3.4)
 \end{aligned}$$

which in a relativistic treatment takes the form of a Lorentz polarisation tensor. Here and in the following w denotes the external four momentum while u denotes the four velocity of the equilibrated matter (in the c.m. frame of the matter $u = (1, \vec{0})$). The $\pi\rho$ loop contains an isospin factor of two due to isospin symmetry. Other possible diagrams like the $\pi\omega$ -loops or $\rho\omega$ -loops which would also be allowed by the interaction are suppressed due to phase space restrictions and will therefore be neglected. For the $\rho\omega$ -loop this is clear due to the high mass in the intermediate state whereas the $\pi\omega$ -loop is less important in the low energy range due to the smaller width of the ω -meson.

With this basic diagram we then generate the following RPA resummed expressions

$$\begin{aligned}
 \Pi_{\mu\nu}^{(\rho\pi)} &= \begin{array}{c} \text{---} \\ \bullet \quad \text{---} \Pi^{\mu\nu} \quad \text{---} \\ \bullet \end{array} = \begin{array}{c} \rho \\ \text{---} \text{---} \\ \bullet \quad \text{---} \text{---} \text{---} \text{---} \bullet \\ \pi \end{array} + \begin{array}{c} \rho \quad \rho \\ \text{---} \text{---} \text{---} \\ \bullet \quad \text{---} \text{---} \bullet \quad \text{---} \text{---} \bullet \\ \pi \quad \pi \end{array} + \dots \\
 &= \left[\chi^{(\rho\pi)} \cdot (\mathbb{1} - \chi^{(\rho\pi)})^{-1} \right]^{\mu\nu} \\
 \Gamma_{\mu}^{(\rho\pi)} &= \begin{array}{c} \text{---} \\ \bullet \quad \text{---} \Gamma^{\mu} \quad \text{---} \\ \bullet \end{array} = q_{\mu} + \Pi_{\mu\nu}^{(\rho\pi)} q^{\nu},
 \end{aligned} \tag{3.5}$$

where q_{μ} denotes the pion momentum. They are relevant for the short range correlations and the corresponding vertex corrections. Using these building blocks we can now define the self-energies entering the self-consistent scheme. In the case of the pion we get

$$\begin{aligned}
 \Pi_{\pi} &= \text{---} \text{---} \bullet \text{---} \begin{array}{c} \text{---} \\ \bullet \quad \text{---} \Pi^{\mu\nu} \quad \text{---} \\ \bullet \end{array} \text{---} \text{---} \\
 &= -4 w^{\mu} \Pi_{\mu\nu}^{(\rho\pi)}(w, u) w^{\nu} + \delta m_{\pi} + w^2 \delta,
 \end{aligned} \tag{3.6}$$

which corresponds to a resummation of the backinfluence of the ρ -meson on the pion. The renormalisation terms δm_{π} and δ will be adjusted in vacuum to guarantee that the pion has its pole at $m^2 = (139 \text{ MeV})^2$ with residuum 1.

The self-energy for the ρ -meson will be given by

$$\begin{aligned}
 \Pi_{\rho}^{\mu\nu} &= \begin{array}{c} \times \\ \text{---} \\ \bullet \end{array} + \begin{array}{c} \text{---} \\ \bullet \quad \text{---} \text{---} \text{---} \text{---} \bullet \\ \Gamma^{\mu} \quad \Gamma^{\nu} \end{array} + \begin{array}{c} \text{---} \\ \bullet \quad \text{---} \text{---} \text{---} \text{---} \bullet \\ \Gamma^{\mu} \quad \Gamma^{\nu} \end{array} \\
 &+ \begin{array}{c} \text{---} \\ \bullet \quad \text{---} \text{---} \text{---} \text{---} \bullet \\ \Gamma^{\mu} \quad \Gamma^{\nu} \end{array} + \begin{array}{c} \text{---} \\ \bullet \quad \text{---} \text{---} \text{---} \text{---} \bullet \\ \Gamma^{\mu\nu} \end{array}
 \end{aligned} \tag{3.7}$$

$$= \Pi_{(\rho,1)}^{\mu\nu} + \Pi_{(\rho,2)}^{\mu\nu} + \Pi_{(\rho,3)}^{\mu\nu} \tag{3.8}$$

3. Pions and vector-mesons at finite temperature

with

$$\begin{aligned}
\Pi_{(\rho,1)}^{\mu\nu}(w,u) &= g_{\rho\pi\pi}^2 \int \frac{d^4l}{2(2\pi)^4} \left[(\Gamma_{(\rho\pi)}^\mu(l,u) + \Gamma_{(\rho\pi)}^\mu(l-w,u)) \right. \\
&\quad \left. (\Gamma_{(\rho\pi)}^\nu(l,u) + \Gamma_{(\rho\pi)}^\nu(l-w,u)) G_\pi(l,u) G_\pi(l-w,u) \right] \\
\Pi_{(\rho,2)}^{\mu\nu}(w,u) &= g_{\omega\rho\pi}^2 \int \frac{d^4l}{2(2\pi)^4} \left[\epsilon^{\mu\alpha\beta\gamma} \epsilon^{\nu\alpha'\beta'\gamma'} \Gamma_\alpha^{(\rho\pi)}(l-w,u) l_\beta \Gamma_{\alpha'}^{(\rho\pi)}(l-w,u) l_{\beta'} \right. \\
&\quad \left. G_{\gamma\gamma'}^{(\omega)}(l,u) G_\pi(l-w,u) \right] \\
\Pi_{(\rho,3)}^{\mu\nu}(w,u) &= g_{\rho\pi\pi}^2 \int \frac{d^4l}{2(2\pi)^4} \Pi_{(\rho\pi)}^{\mu\nu}(l,u) G_\pi(l+w,u)
\end{aligned} \tag{3.9}$$

Here the bare pion momentum q^μ at the vertex got dressed by correlations (3.5). The ω -meson receives a similar self-energy corrections as the ρ -meson,

$$\begin{aligned}
\Pi_{(\omega)}^{\mu\nu} &= \text{diagram} + \text{diagram} \\
&= g_{\omega\rho\pi}^2 \int \frac{d^4l}{2(2\pi)^4} \left[\epsilon^{\mu\alpha\beta\gamma} \epsilon^{\nu\alpha'\beta'\gamma'} \Gamma_\alpha^{(\rho\pi)}(l-w,u) l_\beta \Gamma_{\alpha'}^{(\rho\pi)}(l-w,u) l_{\beta'} \right. \\
&\quad \left. G_{\gamma\gamma'}^{(\rho)}(l,u) G_\pi(l-w,u) \right].
\end{aligned} \tag{3.10}$$

3.3. Computational details

3.3.1. Pion self-energy and polarisation loops

Since we will need structures arising from the polarisation loops (3.5) we start with the construction of these quantities and the pion self-energy.

For the computation of short range correlation effects we take advantage of the decompositions into the set of Lorentz structures $L_{\mu\nu}^{(ij)}(w,u)$ and $T_{\mu\nu}(w,u)$ (e.g. [29])

$$\begin{aligned}
L_{\mu\nu}^{(22)}(w,u) &= \left[\frac{(w \cdot u)}{w^2} w_\mu - u_\mu \right] \frac{w^2}{w^2 - (w \cdot u)^2} \left[\frac{(w \cdot u)}{w^2} w_\nu - u_\nu \right], \\
L_{\mu\nu}^{(12)}(w,u) &= L_{\nu\mu}^{(21)}(w,u) = w_\mu \sqrt{\frac{1}{w^2 - (w \cdot u)^2}} \left[\frac{(w \cdot u)}{w^2} w_\nu - u_\nu \right], \\
L_{\mu\nu}^{(11)}(w,u) &= \frac{w_\mu w_\nu}{w^2}, \quad T_{\mu\nu}(w,u) = g_{\mu\nu} - \frac{w_\mu w_\nu}{w^2} - L_{\mu\nu}^{(22)}(w,u).
\end{aligned} \tag{3.11}$$

Here $T^{\mu\nu}$ and $L_{(22)}^{\mu\nu}$ project onto the three physical degrees of freedom of a vector-meson, the two spatially transversal and the one spatially longitudinal, respectively. The other

four-longitudinal projectors are then needed to obtain a closed algebra. These projectors satisfy the following relations:

$$\begin{aligned} g^{\alpha\beta} L_{\mu\alpha}^{(ij)} L_{\beta\nu}^{(lm)} &= \delta_{jl} L_{\mu\nu}^{(im)}, & g^{\alpha\beta} L_{\mu\alpha}^{(ij)} T_{\beta\nu} &= g^{\alpha\beta} T_{\mu\alpha} L_{\beta\nu}^{(ij)} = 0, \\ g^{\alpha\beta} T_{\mu\alpha} T_{\beta\nu} &= T_{\mu\nu}. \end{aligned} \quad (3.12)$$

Now we can decompose the correlation loop (3.4)

$$\chi_{\mu\nu}^{(\rho\pi)}(w, u) = \sum_{i,j=1}^2 \chi_{ij}^{(\rho\pi)}(w, u) L_{\mu\nu}^{(ij)}(w, u) + \chi_T^{(\rho\pi)}(w, u) T_{\mu\nu}(w, u). \quad (3.13)$$

It leads to a decoupling of the Dyson-equation into the longitudinal and transversal sector [29]. The derivation of the explicit expressions for the longitudinal and transverse loop functions is relegated to Appendix A. The latter follow by simple contractions of the tensors $\chi_{\mu\nu}(w, u)$ with the projectors (3.11). The decompositions (3.13) also easily allows to include vertex corrections. To see how this works we compute this first contributions to the pion self-energy including correlations.

$$\begin{aligned} \Pi_\pi(w, u) &= -4 w^\mu \Pi_{\mu\nu}^{(\rho\pi)}(w, u) w^\nu + \delta m_\pi + w^2 \delta \\ &= -4 w^\mu \chi_{\mu\nu}^{(\rho\pi)} w^\nu - 4 g^{\alpha\beta} w^\mu \chi_{\mu\alpha}^{(\rho\pi)} \chi_{\beta\nu}^{(\rho\pi)} w^\nu + \dots + \delta m_\pi + w^2 \delta \end{aligned} \quad (3.14)$$

The decomposition (3.13) permits to evaluate the needed contractions

$$g^{\alpha\beta} \chi_{\mu\alpha}^{(\rho\pi)} \chi_{\beta\nu}^{(\rho\pi)} = \left[\sum_{im} \sum_j \chi_{ij}^{(\rho\pi)} \chi_{jm}^{(\rho\pi)} L_{\mu\nu}^{(im)} + \chi_T^{(\rho\pi)} \chi_T^{(\rho\pi)} T_{\mu\nu} \right]. \quad (3.15)$$

upon decomposing the contraction of two loop functions into the projector basis. Since the transversal parts do not mix with the other projectors we obtain a decoupled set of equations in this space. In contrast to this the longitudinal components do mix such that the new coefficients can be obtained from the old ones by a matrix multiplication. The generalisation to higher orders follows along the same lines. For example the coefficient function for the longitudinal projector $L_{ln}^{\mu\nu}$ in the next order is given by

$$\sum_{i,j} \chi_{li}^{(\rho\pi)} \chi_{ij}^{(\rho\pi)} \chi_{jn}^{(\rho\pi)}. \quad (3.16)$$

Now that we know how the projector structure has to be treated in the summation we can establish a convenient way for the calculation of the pion self-energy. We first define a loop matrix $\chi^{(L)}$ and $\chi^{(T)}$

$$\chi^{(L)} = \begin{pmatrix} \chi_{11}^{(\rho\pi)} & \chi_{12}^{(\rho\pi)} \\ \chi_{21}^{(\rho\pi)} & \chi_{22}^{(\rho\pi)} \end{pmatrix}, \quad \chi^{(T)} = \left(\chi_T^{(\rho\pi)} \right). \quad (3.17)$$

3. Pions and vector-mesons at finite temperature

The quantity $\Pi_{\mu\nu}^{(\rho\pi)}(w, u)$, which sums up all contributions in (3.14), then results to

$$\Pi_{\mu\nu}^{(\rho\pi)}(w, u) = \sum_{i,j=1}^2 \Pi_{(ij)}^{(\rho\pi)}(w, u) L_{\mu\nu}^{(ij)}(w, u) + \Pi_{(T)}^{(\rho\pi)}(w, u) T_{\mu\nu}(w, u) \quad (3.18)$$

with coefficient functions $\Pi_{ij}^{(\rho\pi)}$ and $\Pi_T^{(\rho\pi)}$ defined as

$$\begin{aligned} \Pi_{(11)}^{(\rho\pi)} &= \left[\left(\mathbb{1} - \chi^{(L)} \right)^{-1} \chi^{(L)} \right]_{11} & \Pi_{(12)}^{(\rho\pi)} &= \left[\left(\mathbb{1} - \chi^{(L)} \right)^{-1} \chi^{(L)} \right]_{12} \\ \Pi_{(21)}^{(\rho\pi)} &= \left[\left(\mathbb{1} - \chi^{(L)} \right)^{-1} \chi^{(L)} \right]_{21} & \Pi_{(22)}^{(\rho\pi)} &= \left[\left(\mathbb{1} - \chi^{(L)} \right)^{-1} \chi^{(L)} \right]_{22} \\ \Pi_{(T)}^{(\rho\pi)} &= \left[\left(\mathbb{1} - \chi^{(T)} \right)^{-1} \chi^{(T)} \right]_{11}. \end{aligned} \quad (3.19)$$

Due to the derivative structure of the interactions (4.1, 3.1) and the structure of the four particle interactions the Γ -bubble insertions simply lead to a replacement of the bare pion momentum q^μ at the vertex by a dressed one

$$q_\nu \rightarrow \Gamma_\nu^{(\rho\pi)}(q, u) = q^\nu + q^\mu \Gamma_{\mu\nu}^{(\rho\pi)}(q, u) = q_\nu \Gamma_1^{(\rho\pi)}(q, u) + u_\nu \Gamma_2^{(\rho\pi)}(q, u), \quad (3.20)$$

with contributions proportional q^μ and u^μ given by the vertex functions $\Gamma_i^{(\rho\pi)}$. These vertex functions are obtained by contracting the full correlation sum $\Pi_{\mu\nu}^{(\rho\pi)}(q, u)$ over q^μ because one vertex directly couples to the pion while the other one stems from the four point coupling. The two Vertex functions $\Gamma_1^{(\rho\pi)}(q, u)$ and $\Gamma_2^{(\rho\pi)}(q, u)$ are explicitly given by

$$\begin{aligned} \Gamma_1^{(\rho\pi)} &= 1 + 2 \left[\left(\mathbb{1} - \chi^{(L)} g^{(L)} \right)^{-1} \chi^{(L)} g^{(L)} \right]_{11} \\ &\quad + \frac{2(u \cdot q)}{\sqrt{q^2 - (u \cdot q)^2}} \left[\left(\mathbb{1} - \chi^{(L)} g^{(L)} \right)^{-1} \chi^{(L)} g^{(L)} \right]_{12} + \delta\Gamma \\ \Gamma_2^{(\rho\pi)} &= \frac{-2q^2}{\sqrt{q^2 - (u \cdot q)^2}} \left[\left(\mathbb{1} - \chi^{(L)} g^{(L)} \right)^{-1} \chi^{(L)} g^{(L)} \right]_{12} \end{aligned} \quad (3.21)$$

in terms of the loop functions. We introduced a finite renormalisation $\delta\Gamma$ to impose the condition $\Gamma_1(w^2 = m_\pi^2) = 1$ in vacuum. There are two important technical issues to be emphasised here. First, the application of the longitudinal and transverse projectors in (3.13) implies that the loop functions have to satisfy specific constraints. They follow from the observation that the polarisation tensor $\chi_{\mu\nu}^{(\rho\pi)}(q, u)$ is regular. In particular at $q^2 = 0$ and at $q^2 = (q \cdot u)^2$ it must hold

$$\begin{aligned} \chi_{22}^{(\rho\pi)}(q, u) &= \chi_{11}^{(\rho\pi)}(q, u) - i \chi_{12}^{(\rho\pi)}(q, u) - i \chi_{21}^{(\rho\pi)}(q, u) + \mathcal{O}(q^2), \\ \chi_{22}^{(\rho\pi)}(q, u) &= \chi_T^{(\rho\pi)}(q, u) + \mathcal{O}((q \cdot u)^2 - q^2). \end{aligned} \quad (3.22)$$

This turns out to be important when specifying the real parts of the loop functions (see Appendix A. Furthermore a finite renormalisation has to be constructed such that it suppresses the formation of ghosts in the pion self energy [74] (see Appendix C). The construction of the latter has to comply with the constraints (3.22).

3.3.2. Four transversality of vector mesons

Before we proceed with the determination of the vector meson self-energies we have to deal with a conceptual problem concerning the four transversality of the polarisation-tensor. In self-consistent Dyson approaches, where one sums up a restricted subclass of self-energy diagrams, one generally¹ violates Ward identities, arising from the fact that the interaction (3.1) has a conserved current [35, 76], on the correlator level. Thus the polarisation tensor may contain additional four-longitudinal background contributions, which have to be excluded in our present model where the photon couples via vector dominance. From general grounds, this deficiency can be cured by corresponding vertex corrections which lead to presently intractable schemes of Bethe-Salpeter equations resumming t -channel ladder diagrams required by crossing symmetry.

The simplest ansatz to restore four transversality on a more pragmatic level is to project out the unphysical four-longitudinal components of the polarisation tensor $\Pi_{(\rho)}^{\mu\nu}$ as implicitly done in ref. [47] through the Stückelberg Formalism. One is then left with a new projected tensor $\Pi_{(\rho, P)}^{\mu\nu}$ containing the 3 physical modes, the 2 spatially transverse and the spatially longitudinal mode

$$\Pi_{(\rho, P)}^{\mu\nu}(w, u) = L_{(22)}^{\mu\nu}(w, u) \Pi_{(\rho, P)}^{(22)}(w, u) + T^{\mu\nu}(w, u) \Pi_{(\rho, P)}^{(T)}(w, u), \quad (3.23)$$

where

$$\Pi_{(\rho, P)}^{(22)} = L_{\mu\nu}^{(22)} \Pi_{(\rho)}^{\mu\nu} \quad \Pi_{(\rho, P)}^{(T)} = T_{\mu\nu} \Pi_{(\rho)}^{\mu\nu}. \quad (3.24)$$

This procedure, however, has the side effect that although regular before the projection due to the kinematical singularity of the projector $L_{(22)}$ at $w^2 = 0$ the projected tensor becomes singular on the light cone. As a result this scheme leads to a spurious and thus unphysical mode with zero mass that seriously spoils the self-consistent dynamics. For details see the comment [48] to ref. [47].

Alternatively H. van Hees and J. Knoll [10] proposed a scheme that respects particular dynamical properties of the polarisation tensor and in addition avoids the above singular behaviour. From transport considerations it is known that polarisation tensors have at least two relaxation times. Because of charge conservation, one of these times has to be infinite, implying that the component $\Pi_{(\rho)}^{00}(w_0, \vec{w})$ vanishes exactly for $\vec{w} = 0$ and $w_0 \neq 0$, while the second relaxation time is clearly finite.

¹An exception is the tensor representation of the vector mesons [75] where the form of the interaction enforces four-transversality also in a self-consistent calculation.

3. Pions and vector-mesons at finite temperature

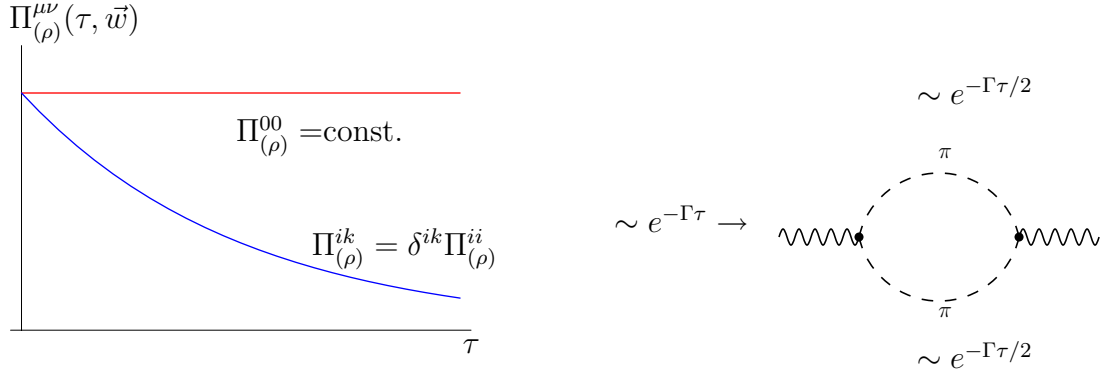


Figure 3.1.: Typical relaxation behaviour of the polarisation tensor.

Such a result can never be reached in a truncated Dyson-resummation scheme where all relaxation times are finite, because they are determined by the damping-time scale of the dressed propagators involved in the loops. On the other hand, the spatial components of the polarisation tensor, given by the autocorrelation of spatial currents, have solely finite and short correlation times which can be expected to be safely approximated within a Dyson resummation scheme. Therefore their strategy assumes the spatial components of the polarisation tensors $\Pi_{(\rho)}^{\mu\nu}$ to be given by the self-consistent loops, while the time-components are to be corrected such that the full tensor becomes four-transversal. Within this scheme the scalar functions $\Pi_{(\rho,P)}^{(22)}$ and $\Pi_{(\rho,P)}^{(T)}$ of (3.23) can be calculated solely from the spatial parts of the polarisation tensors using the following spatial traces

$$\begin{aligned} \Pi_1 &= \frac{w_i w_k}{\vec{w}^2} \Pi_{(\rho)}^{ik} & 3\Pi_3 &= -g_{ik} \Pi_{(\rho)}^{ik} \\ \Pi_{(\rho,P)}^{(22)} &= \frac{w^2}{(u \cdot w)^2} \cdot \Pi_1; & \Pi_{(\rho,P)}^{(T)} &= \frac{1}{2} (3\Pi_3 - \Pi_1). \end{aligned} \quad (3.25)$$

This scheme avoids the light-cone singularity, since $\Pi_{(\rho,P)}^{(22)}$ vanishes there by construction. However unless Π_1 does not vanish quadratically towards zero energy $w^0 = (u \cdot w)$ a singularity occurs there. Placed in the space-like region the corresponding spurious zero energy mode does not directly affect physical observable such as dilepton spectra. It can however influence the self-consistent dynamics, if the coupling of the vector mesons back onto other particles in the system such as the pions is considered². This back-coupling was unimportant in ref. [10], became however important for the case considered in ref. [47] where indeed the self-consistent dynamics is spoiled seriously by this zero energy mode as can be seen in Fig. 3.2 .

The advantage of the improved scheme is that it is free of singularities in the entire time-like region, where the singularities of the two spatial components at vanishing

²Note that in our previous calculation [9] where we used this scheme the propagation of spurious modes was blocked due to the structure of the $\pi\omega\rho$ -vertex.

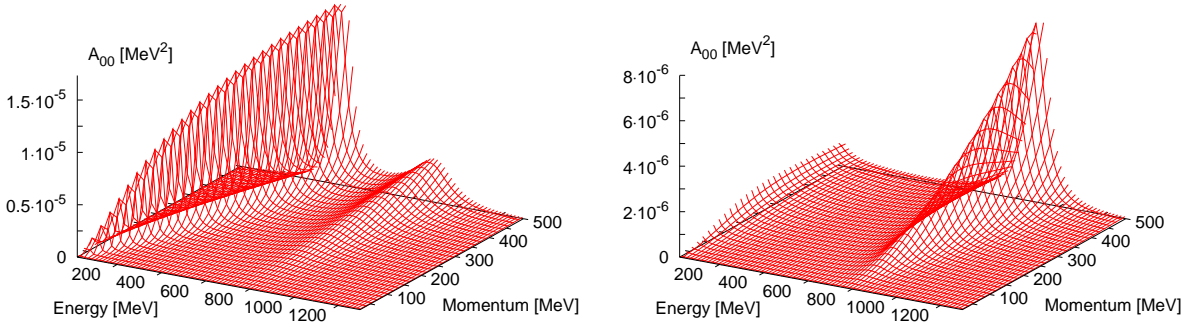


Figure 3.2.: Time-time component $A^{00}(w)$ of the ρ -meson spectral function at $T = 160$ MeV as a function of energy and three momentum for the Ruppert-Renk projection method (left figure) and for the method by van Hees and Knoll (right figure) calculated for the model presented in [47]. Please note the difference in the ordinate scales.

spatial momentum (in the rest frame) $\vec{w}^2 = (u \cdot w)^2 - w^2$ exactly compensate. It therefore opens the perspective to construct a singularity free tensor by some cut-off procedure solely applied to the spatial longitudinal component $\Pi_{(\rho, P)}^{(22)}$ in the space-like region close to vanishing energy. Therefore we have to have a more detailed look on the decomposition

$$\Pi_{(\rho)}^{\mu\nu}(w, u) = \sum_{i,j=1}^2 L_{(ij)}^{\mu\nu}(w, u) \Pi_{(\rho)}^{(ij)}(w, u) + T^{\mu\nu}(w, u) \Pi_{(\rho)}^{(T)}(w, u), \quad (3.26)$$

of the self-energy where the behaviour of the projectors enforce the relations

for $w^2 \rightarrow 0$

$$\Pi_{(\rho)}^{(11)} - \Pi_{(\rho)}^{(22)} - i \Pi_{(\rho)}^{(12)} - i \Pi_{(\rho)}^{(21)} \sim \mathcal{O}(w^2)$$

for $(u \cdot w)^2 - w^2 \rightarrow 0$

$$\begin{aligned} \Pi_{(\rho)}^{(12)} &\sim \mathcal{O}\left(\sqrt{(u \cdot w)^2 - w^2}\right) & \Pi_{(\rho)}^{(21)} &\sim \mathcal{O}\left(\sqrt{(u \cdot w)^2 - w^2}\right) \\ \Pi_{(\rho)}^{(22)} - \Pi_{(\rho)}^{(T)} &\sim \mathcal{O}\left((u \cdot w)^2 - w^2\right) \end{aligned} \quad (3.27)$$

between the coefficient functions. Now the longitudinal projector relation (3.25) can be rewritten as

$$\Pi_{(\rho, P)}^{(22)} = \Pi_{(\rho)}^{(22)} - \frac{(u \cdot w)^2 - w^2}{(u \cdot w)^2} \Pi_{(\rho)}^{(11)} + 2i \frac{\sqrt{(u \cdot w)^2 - w^2}}{(u \cdot w)} \Pi_{(\rho)}^{(12)} \quad (3.28)$$

3. Pions and vector-mesons at finite temperature

where we used $\Pi_{(\rho)}^{(21)} = \Pi_{(\rho)}^{(12)}$ due to the symmetry of the tensor. The singularities stem from the factors in front of $\Pi_{(\rho)}^{(11)}$ and $\Pi_{(\rho)}^{(12)}$. Thus one can attempt to construct the $\Pi_{(\rho, P)}^{(22)}$ and $\Pi_{(\rho, P)}^{(T)}$ coefficients in the space-like region as:

$$\Pi_{(\rho, P)}^{(T)} = \Pi_{(\rho)}^{(T)} \quad \Pi_{(\rho, P)}^{(22)} = \Pi_{(\rho)}^{(22)} - \lambda(w, u) \Pi_{(\rho)}^{(11)} - 2i \sqrt{\lambda(w, u)} \Pi_{(\rho)}^{(12)}, \quad (3.29)$$

with a coefficient function $\lambda(w, u)$ which has to fulfill

$$\lambda(w^2 = 0, u) = 1 \quad (3.30)$$

and should stay finite towards $(u \cdot w) = 0$. A possible choice that provides a smooth transition to the form (3.28) to be used in the time-like region is given by

$$\lambda(w, u) = \begin{cases} \frac{(u \cdot w)^2 - w^2 + \Lambda^2}{2((u \cdot w)^2 + \Lambda^2)} + \frac{(u \cdot w)^2 - w^2}{2(u \cdot w)^2 - w^2} & \text{for } w^2 < 0 \\ \frac{(u \cdot w)^2 - w^2}{(u \cdot w)^2} & \text{for } w^2 > 0 \end{cases}. \quad (3.31)$$

The sensitivity of the results on the regularisation parameter Λ then has to be investigated.

3.3.3. Vector meson self-energies

After our consideration of the options to suppress longitudinal background modes we now turn to the actual calculation of the self-energies for the vector mesons.

In order to avoid contributions from non-physical modes such as ghosts the vector meson propagators will be treated in the unitary gauge limit (for different gauges see Appendix D), which pushes all non-physical modes to infinite masses. The expressions for the free propagators thus read

$$G_{\mu\nu}^{(\rho,0)}(w) = \frac{g_{\mu\nu} - \frac{w_\mu w_\nu}{m_\rho^2}}{w^2 - m_\rho^2 + i\epsilon} \quad G_{\mu\nu}^{(\omega,0)}(w) = \frac{g_{\mu\nu} - \frac{w_\mu w_\nu}{m_\omega^2}}{w^2 - m_\omega^2 + i\epsilon}. \quad (3.32)$$

Let us start with a calculation where we exclude vertex corrections for simplicity. In this case we have two contributions

$$\Pi_{(\rho)}^{\mu\nu} = \Pi_{(\rho,1)}^{\mu\nu} + \Pi_{(\rho,2)}^{\mu\nu} = \text{diagram 1} + \text{diagram 2}. \quad (3.33)$$

to the ρ -meson self-energy. The first diagram (3.33) corresponds to the two pion decay of the ρ -meson which is responsible for nearly the complete vacuum width. The second diagram is suppressed in vacuum because of the higher mass in the intermediate state.

However as we found out in [9] this decay mode can be enhanced in the medium due to low energy excitations of the pion which reduce the mass of the intermediate state. In addition broadening of the ω -meson due to collisions will enhance its damping width such that this diagram can become important. The calculation of the imaginary parts of these diagrams has already been done in [9]. In addition self-consistent effects within such a system have been studied by [10, 47] where also a broadening was observed. In this work we will now extend the previous calculations by including the realparts of the self-energies and vertex corrections. In a first step we decompose the propagators (3.32) and self-energies (3.9, 3.11)

$$\begin{aligned}
 G_{\mu\nu}^{(\rho/\omega,0)}(w) &= T_{\mu\nu}(w, u) G_{(T)}^{(\rho/\omega,0)}(w) + \sum_{i,j=1}^2 L_{\mu\nu}^{(ij)}(w, u) G_{(ij)}^{(\rho/\omega,0)}(w) \\
 G_{\mu\nu}^{(\rho/\omega)}(w, u) &= T_{\mu\nu}(w, u) G_{(T)}^{(\rho/\omega)}(w, u) + \sum_{i,j=1}^2 L_{\mu\nu}^{(ij)}(w, u) G_{(ij)}^{(\rho/\omega)}(w, u) \quad (3.34) \\
 \Pi_{(\rho/\omega,i)}^{\mu\nu}(w, u) &= T^{\mu\nu}(w, u) \Pi_{(\rho/\omega,i)}^{(T)}(w, u) + \sum_{i,j=1}^2 L_{(ij)}^{\mu\nu}(w, u) \Pi_{(\rho/\omega,i)}^{(ij)}(w, u) \\
 \Pi_{(\rho/\omega,i,P)}^{\mu\nu}(w, u) &= T^{\mu\nu}(w, u) \Pi_{(\rho/\omega,i,P)}^{(T)}(w, u) + L_{(22)}^{\mu\nu}(w, u) \Pi_{(\rho/\omega,i,P)}^{(22)}(w, u)
 \end{aligned}$$

according to the projector-basis defined in (3.11). Note that according to (3.23) the projected self-energies have 4-transversal components only. The same automatically holds also for the propagators. The coefficients $G_{(T)}^{(\rho/\omega,0)}$ and $G_{(ij)}^{(\rho/\omega,0)}$ of the free propagator (3.32) are easily determined

$$\begin{aligned}
 G_{(T)}^{(\rho/\omega,0)}(w) &= G_{(22)}^{(\rho/\omega,0)}(w) = \frac{1}{w^2 - m_{\rho/\omega}^2 + i\epsilon} \\
 G_{(11)}^{(\rho/\omega,0)}(w) &= G_{(12)}^{(\rho/\omega,0)}(w) = G_{(21)}^{(\rho/\omega,0)}(w) = 0. \quad (3.35)
 \end{aligned}$$

The projection scheme now allows for a simple solution of the Dyson equation (3.2) by matrix inversion. Imposing four transversality on Π through the projection introduced in the pervious section (3.29) we obtain

$$\begin{aligned}
 G_T^{(\rho/\omega)}(w, u) &= \frac{1}{w^2 - m_{\rho/\omega}^2 - \Pi_{(\rho/\omega,P)}^{(T)}(w, u)} \\
 G_{(22)}^{(\rho/\omega)}(w, u) &= \frac{1}{w^2 - m_{\rho/\omega}^2 - \Pi_{(\rho/\omega,P)}^{(22)}(w, u)} \quad (3.36)
 \end{aligned}$$

$$G_{(11)}^{(\rho/\omega)}(w, u) = G_{(12)}^{(\rho/\omega)}(w, u) = G_{(21)}^{(\rho/\omega)}(w, u) = 0$$

$$\Pi_{(\rho,P)}^{(T)}(w, u) = \sum_{i=1}^2 \Pi_{(\rho,i,P)}^{(T)}(w, u) \quad \Pi_{(\rho,P)}^{(22)}(w, u) = \sum_{i=1}^2 \Pi_{(\rho,i,P)}^{(22)}(w, u) \quad (3.37)$$

3. Pions and vector-mesons at finite temperature

two decoupled equations for the dressed propagator. Taking now the interactions defined in (3.1) we compute the imaginary part of the retarded self-energy arising from the first diagram of (3.33):

$$\Im \Pi_{(\rho,1)}^{\mu\nu}(w, u) = g_{\rho\pi\pi}^2 \int \frac{d^4 l}{2(2\pi)^4} (2l^\mu - w^\mu) (2l^\nu - w^\nu) A_\pi(l, u) A_\pi(l - w, u) (n_B((l - w) \cdot u) + n_B(l \cdot u)), \quad (3.38)$$

where the pion spectral function $A_\pi(l)$ is defined as

$$A_\pi(l) = -2 \Im G_\pi \quad (3.39)$$

and $n_B((l \cdot u))$ are the usual Bose functions. The coefficient functions of the decomposition (3.34) are listed in Appendix E. The polarisation tensor (3.38) is not yet four transversal and has to be projected following the procedure (3.29) ff.

We have also to take care about the computation of the realparts. Applying an unsubtracted dispersion relations one would be left with power divergencies since none of the imaginary parts drops to zero for large energies. Within the framework of an effective field theory we would like to absorb all power divergencies into counter terms leading us to a scheme of subtracted dispersion relations. In addition one has to take care that along with the imaginary parts also the realparts are free of kinematical singularities. This enforces certain relations between several coefficient functions (3.27) which have to be fulfilled.

We begin our discussion of the renormalisation with the vacuum case. Here a subtracted dispersion relation

$$\Pi_{(\rho,1,P)}^{(22/T)}(w) = \frac{1}{\pi} w^4 \int d\bar{w}_0 \frac{\Im \Pi_{(\rho,1,P)}^{(22/T)}(\bar{w})}{\bar{w}^4 (w_0 - \bar{w}_0 + i\epsilon)} \quad (3.40)$$

is used with $w = (w_0, \vec{w})$ and $\bar{w} = (\bar{w}_0, \vec{w})$, which automatically guarantees that the polarisation tensor and its derivative vanish at the lightcone. This is the technically preferred renormalisation because of the vector dominance used for the coupling to photons. It guarantees that the photon stays massless and has a pole with residuum 1. In addition this scheme automatically complies with the required cancellation of the kinematical singularities because the chosen subtraction leads to realparts vanishing on the lightcone so that all constraints (3.27) are naturally fulfilled. For the in-medium case this scheme has to be abandoned because it crucially requires the imaginary parts and their derivatives to vanish at the lightcone which is no longer true if medium effects come into play which effectively remove all thresholds. In addition the behaviour of the realpart with s^2 which is fine in vacuum where every function has to be Lorentz invariant becomes artificial when going into medium where we have a preferred frame and would expect separate dependence on energy and momentum. Thus we then need a different

prescription. Let us first consider the kinematical constraints. These constraints arise only due to our special choice of the projector-basis. If one uses a decomposition into singularity free Lorentz tensors like

$$\begin{aligned} \Pi_{(\rho,1,P)}^{\mu\nu}(w,u) = & g^{\mu\nu} P_g(w,u) + w^\mu w^\nu P_{ww}(w,u) + u^\mu u^\nu P_{uu}(w,u) \\ & + (w^\mu w^\nu + w^\mu u^\nu) P_{wu}(w,u). \end{aligned} \quad (3.41)$$

instead of

$$\Pi_{(\rho,1,P)}^{\mu\nu}(w,u) = L_{(22)}^{\mu\nu}(w,u) \Pi_{(\rho,1,P)}^{(22)}(w,u) + T^{\mu\nu}(w,u) \Pi_{(\rho,1,P)}^{(T)}(w,u) \quad (3.42)$$

one avoids such problems and has no special constraints on the coefficient functions P . However in such a basis the interpretation of the results becomes less transparent since the four transversality condition is less obvious and the Dyson equation does not decouple. The idea is now to combine both advantages. Therefore we first will compute the coefficient functions in the basis (3.11, 3.42) then convert the results to the singularity free basis (3.41) evaluate the realparts and then convert back.

First one observes that the new coefficient functions are not all independent because they are solely build up form the two functions $\Pi_{(\rho,1,P)}^{(22)}$ and $\Pi_{(\rho,1,P)}^{(T)}$

$$\begin{aligned} P_g(w,u) = -\Pi_{(\rho,1,P)}^{(T)} \quad P_{ww}(w,u) &= \frac{w^2 \Pi_{(\rho,1,P)}^{(T)} - (w \cdot u)^2 \Pi_{(\rho,1,P)}^{(22)}}{w^2 (w^2 - (w \cdot u)^2)} \\ P_{uu}(w,u) &= \frac{w^2 \left(\Pi_{(\rho,1,P)}^{(T)} - \Pi_{(\rho,1,P)}^{(22)} \right)}{w^2 - (q \cdot u)^2} \\ P_{wu}(w,u) &= \frac{(w \cdot u)^2 \left(\Pi_{(\rho,1,P)}^{(22)} - \Pi_{(\rho,1,P)}^{(T)} \right)}{w^2 - (w \cdot u)^2}. \end{aligned} \quad (3.43)$$

On the other hand now the dispersion relations can be established for these new coefficient functions and via

$$\begin{aligned} \Pi_{(\rho,1,P)}^{(T)} &= -P_g(w,u) \\ \Pi_{(\rho,1,P)}^{(22)} &= \frac{-w^2(w^2 - (w \cdot u)^2)}{(w \cdot u)^2} P_{ww}(w,u) - \frac{w^2}{(w \cdot u)^2} P_g(w,u) \end{aligned} \quad (3.44)$$

can be reconverted to the old projector basis. This properly deals deals with the kinematical singularities which in the standard basis would require to guess special subtraction conditions. The dispersion relation used for the coefficient functions in the none singular basis is

$$P_{g,ww}(w,u) = \int \frac{(u \cdot w)^2 \Im P_{g,ww}(\bar{w},u)}{(u \cdot \bar{w})^2 \bar{w}_0 - w_0 + i\epsilon} d\bar{w}_0. \quad (3.45)$$

3. Pions and vector-mesons at finite temperature

Since the imaginary part has to go to zero for $w_0 = 0$ it is a natural choice to use a subtraction in w_0 to regularise the UV behaviour. However a logarithmic divergence is still left which will be regularised by a cutoff Λ . Unfortunately such a dispersion relation procedure induces medium dependent counter terms. This is not ideal because all the divergencies in the theory should result from vacuum terms such that a proper renormalisation prescription would work with vacuum terms only [77]. However at the moment there is no tractable scheme at hand which would allow us such a calculation. To properly approach the vacuum limit (3.40) one first has to subtract the vacuum part of the loop. Collecting all intermediate results we arrive at

$$\begin{aligned}\Pi_{(\rho,1,P)}^{(T)}(w,u) &= \Pi_{(\rho,1,vac)}^{(T)}(w,u) + \int \frac{(u \cdot w)^2 \Im \Pi_{(\rho,1,P)}^{(T)}(\bar{w},u) - \Im \Pi_{(\rho,1,vac)}^{(T)}(\bar{w},u)}{(u \cdot \bar{w})^2 (\bar{w}_0 - w_0 + i\epsilon)} d\bar{w}_0 \\ \Pi_{(\rho,1,P)}^{(22)}(w,u) &= \Pi_{(\rho,1,vac)}^{(22)}(w,u) + \int \frac{w^2 \Im \Pi_{(\rho,1,P)}^{(22)}(\bar{w},u) - \Im \Pi_{(\rho,1,vac)}^{(22)}(\bar{w},u)}{\bar{w}^2 (\bar{w}_0 - w_0 + i\epsilon)} d\bar{w}_0.\end{aligned}\tag{3.46}$$

Here it is understood that the vacuum terms $\Pi_{(\rho,1,vac)}^{(T)}$ and $\Pi_{(\rho,1,vac)}^{(22)}$ contain the projection (3.29) already. The factor w^2 in the 3 longitudinal is essential to cancel the $1/w^2$ singularity arising from the projector. This then defines the scheme for the calculation of the first self-energy diagram in (3.33). Note that we now automatically have a separate dependence on energy and momentum of real and imaginary part.

We come now to the calculation of the second diagram in (3.33). Here we will follow the same steps as for the first diagram. The imaginary part is given by:

$$\begin{aligned}\Im \Pi_{(\rho,2)}^{\mu\nu}(w,u) &= g_{\omega\rho\pi}^2 \int \frac{d^4l}{2(2\pi)^4} \epsilon^{\mu\alpha\beta\gamma} \epsilon^{\nu\alpha'\beta'\gamma'} q_\alpha l_\beta q_{\alpha'} l_{\beta'} A_{\gamma\gamma'}^{(\omega)}(l,u) A_\pi(l-w,u) \\ &\quad (n_B(l \cdot u) + n_B((l-w) \cdot u)),\end{aligned}\tag{3.47}$$

where the spectral function $A_{\gamma\gamma'}^{(\omega)}$ of the ω -meson is defined as the imaginary part of the propagator (3.32).

$$\begin{aligned}A_{\mu\nu}^{(\omega)}(l,u) &= L_{\mu\nu}^{(22)}(l,u) A_{(22)}^{(\omega)}(l,u) + T_{\mu\nu}(l,u) A_{(T)}^{(\omega)}(l,u) \\ A_{(22)}^{(\omega)}(l,u) &= -2 \Im G_{(22)}^{(\omega)}(l,u) \quad A_{(T)}^{(\omega)}(l,u) = -2 \Im G_{(T)}^{(\omega)}(l,u)\end{aligned}\tag{3.48}$$

The expressions for the coefficients of the decomposition (3.34) are listed in Appendix E. In vacuum the realpart of the functions $\Pi_{(\rho,2,P)}^{(22/T)}$ is determined by a dispersion relation:

$$\Pi_{(\rho,2,P)}^{(22/T)}(w,u) = \frac{1}{\pi} \int d\bar{w}_0 \frac{w^6 \Im \Pi_{(\rho,2,P)}^{(22/T)}(\bar{w},u)}{\bar{w}^6 (w_0 - \bar{w}_0 + i\epsilon)}\tag{3.49}$$

where one has to take the higher degree of divergence into account. In the medium case the same scheme as before (3.46) will be used however due to the higher degree of the

divergence one is left with a linear divergence left also to be regularised by the cutoff. This is unfavourable because one would like to move all power divergencies into counter terms. However a higher subtraction would require to make additional definitions how to handle the dispersion integral because of the requirement that also the derivative of the imaginary part has to vanish at zero energy. That implies that the actual mass shifts in medium depend on this cutoff which is an additional free parameter in the model and thus the values of the meanfields used to give the vector-mesons the desired in-medium mass may depend on this cutoff.

Now we come to the inclusion of vertex corrections. As already stated the vertex corrections just require to replace the bare pion momentum at the vertex by the dressed one

$$q^\mu \rightarrow q^\mu \Gamma_1^{(\rho\pi)} + u^\mu \Gamma_2^{(\rho\pi)}, \quad (3.50)$$

with vertex functions $\Gamma_1^{(\rho\pi)}$ and $\Gamma_2^{(\rho\pi)}$ as defined in (3.21). In order to simplify the notation we introduce the following effective spectral functions of the pion:

$$A_\pi^{[ij]}(q, u) = -2 \Im \left[\frac{\Gamma_i^{\rho\pi}(q, u) \Gamma_j^{\rho\pi}(q, u)}{q^2 - m_\pi^2 - \Pi_\pi(q, u)} \right], \quad (3.51)$$

where we additionally define $\Gamma_0^{\rho\pi}(q) = 1$ which allows us to write the normal pion spectral function (3.39) as $A_\pi^{[00]}(q, u)$. Collecting then the vertex tensors Γ_i into the pion spectral functions as defined in (3.51) the expressions for the several self-energy diagrams:

$$\begin{aligned} \Pi_\rho &= \Pi_{(\rho,1)}^{\mu\nu} + \Pi_{(\rho,2)}^{\mu\nu} + \Pi_{(\rho,3)}^{\mu\nu} \\ \Pi_{(\rho,1)}^{\mu\nu} &= \text{diagram 1} + \text{diagram 2} + \text{diagram 3} \\ \Pi_{(\rho,2)}^{\mu\nu} &= \text{diagram 4} \\ \Pi_{(\rho,3)}^{\mu\nu} &= \text{diagram 5} \end{aligned} \quad (3.52)$$

get modified. Besides these vertex corrections Γ in loops also the new diagram containing $\bar{\Pi}$ has to be considered. Its imaginary part is readily expressed through:

$$\Im \Pi_{(\rho,3)}^{\mu\nu}(w, u) = g_{\rho\pi\pi}^2 \int \frac{d^4 l}{2(2\pi)^4} \Im \Pi_{(\rho\pi)}^{\mu\nu}(l, u) A_\pi(l + w, u) (n_B((l + w) \cdot u) + n_B(l \cdot u)) \quad (3.53)$$

3. Pions and vector-mesons at finite temperature

with the shortrange correlation tensor $\Im\Pi_{(\rho\pi)}^{\mu\nu}(l, u)$ defined in (4.20). The coefficients of the decomposition (3.34) for all diagrams (3.9, 3.52) are readily evaluated also in the presence of vertex corrections. The results for the imaginary parts can be found in Appendix E. The scheme for the determination of the realparts (3.46) can be taken over from the case without vertex corrections. Hereby the new diagram $\Pi_{(\rho,3)}^{\mu\nu}$ is treated like the two pion decay $\Pi_{(\rho,1)}^{\mu\nu}$.

The self-energy of the ω meson is given by the second diagram in (3.33) with ρ and ω meson exchanged. Therefore we can use the same equations where we only have to take care of the different isospin factors. Thus the equivalent of (3.47) becomes

$$\Im\Pi_{(\omega)}^{\mu\nu}(w) = 3 g_{\omega\rho\pi}^2 \int \frac{d^4l}{2(2\pi)^4} \epsilon^{\mu\alpha\beta\gamma} \epsilon^{\nu\alpha'\beta'\gamma'} w_\alpha l_\beta w_{\alpha'} l_{\beta'} A_{\gamma\gamma'}^{(\rho)}(l, u) A_\pi(l-w, u) (n_B(l \cdot u) + n_B((l-w) \cdot u)). \quad (3.54)$$

The vertex corrections and correlation parts of $\Pi_{(\omega)}$, c.f. Eq. (3.11), can likewise be constructed following the above strategy for $\Pi_{(\rho)}$ c.f. Eqs. (3.49) ff. The relevant coefficients for the decomposition (3.34) are listed in Appendix E.

3.4. Determination of the parameters

For the vector mesons two coupling constants are to be fitted. The first one, $g_{\rho\pi\pi}$, determines the coupling of the ρ meson to the two pion channel. It also controls the vertex corrections and is fitted to $\pi - \pi$ scattering phase-shifts in the vector channel. A reasonable description of the electromagnetic formfactor of the pion can also be obtained using slightly different values of the parameters. However since here one would also have to consider $\rho\omega$ mixing and perhaps a small violation of vector dominance [78] we solely use the phaseshifts to determine the value of the coupling constant. For the mesonic system we get the following values for the bare vacuum mass and the coupling constant:

$$\begin{aligned} m_\rho &= 782 \text{ MeV}, & g_{\rho\pi\pi} &= 5.65 & \text{fitting the phaseshifts} \\ \text{and} \\ m_\rho &= 773 \text{ MeV}, & g_{\rho\pi\pi} &= 5.3 & \text{fitting the formfactor.} \end{aligned}$$

These values are consistent with the ones obtained in a perturbative approach (e.g. [82]) indicating that the self-consistent corrections can be neglected for the vacuum physics.

For the coupling of the ω meson $g_{\omega\rho\pi}$ one has several options. We choose to determine this value from the vacuum decay width of the ω -meson into the $\pi^0 \gamma$ channel because this is a more clean method. A direct fit to the full width of the ω -meson for $g_{\omega\rho\pi}$ would lead to a larger value because other decay channels are still neglected. For calculating the decay into $\pi^0 \gamma$ we use strict vector dominance and restrict the calculation to the lowest perturbative order [68]

3.4. Determination of the parameters

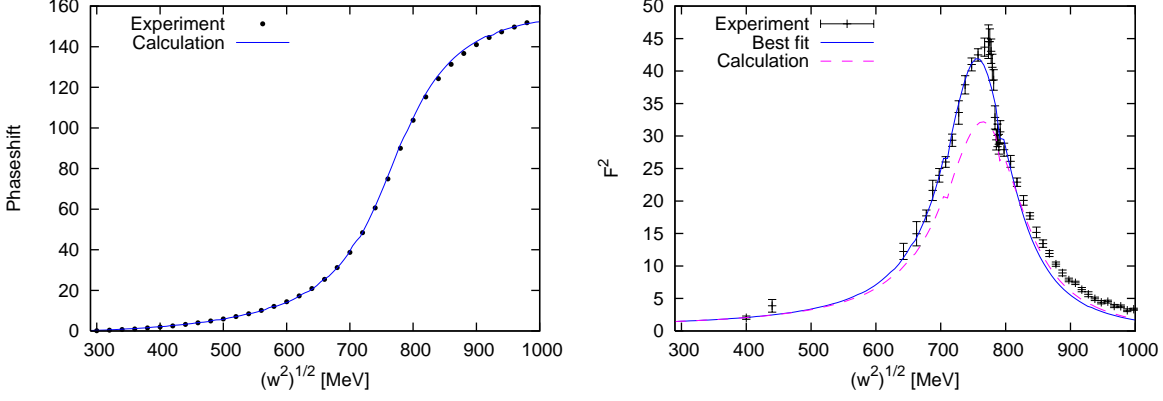


Figure 3.3.: Comparison of our model with the vacuum data. Pion phaseshifts in the vector channel [79] (left figure) and electromagnetic formfactor F of the pion [80, 81] (right figure). For the formfactor we present the best fit (best fit) solution and the one obtained using the parameters from the best fit of the $\pi - \pi$ phase-shifts (calculation).

$$\begin{aligned}
 \Gamma_{\pi^0 \gamma} &= \frac{1}{3} \frac{1}{2 m_\omega} \int \frac{d^3 k}{2 k^0 (2\pi)^3} \frac{d^3 p}{2 \sqrt{p^2 + m_\pi^2} (2\pi)^3} 2 \vec{k}^2 \left(\frac{e g_{\omega\rho\pi}}{g_{\rho\pi\pi}} \right)^2 (2\pi)^4 \delta^4(q - k - p) \\
 &\text{with } q = (m_\omega, \vec{0}) \\
 &= \frac{\alpha}{48 m_\omega} \left(\frac{g_{\omega\rho\pi}}{g_{\rho\pi\pi}} \right)^2 \left(\frac{m_\omega^2 - m_\pi^2}{m_\omega} \right)^3 \left(\left(\frac{m_\omega^2 - m_\pi^2}{2 m_\omega} \right)^2 + m_\pi^2 \right)^{-1/2}. \quad (3.55)
 \end{aligned}$$

Neglecting the pion mass whenever compared to the mass of the ω meson we then arrive at the following expression for the coupling constant:

$$g_{\omega\rho\pi} = \frac{1}{m_\omega} \sqrt{\frac{24 \Gamma_{\pi^0 \gamma}}{m_\omega \alpha} g_{\rho\pi\pi}^2 \left(1 - \frac{m_\pi^2}{m_\omega^2} \right)^{-3}}. \quad (3.56)$$

The partial decay width $\Gamma_{\pi^0 \gamma} = 0.75$ MeV taken from the particle data book [83] together with the value of $g_{\rho\pi\pi}$ obtained in the fit of the phaseshifts determines $g_{\omega\rho\pi} = 0.0155$. This value is slightly higher than the one found by Wachs [68] using a perturbative treatment. However we have to state that using only the decay of the ω meson into $\rho\pi$ still underestimates the total width. This has also been stated by Wachs [68] who claimed that additional vertex corrections are needed, which are beyond the model presented here. Thus the analysis has to be seen as a conservative estimate of the effects concerning the ω -meson.

3.5. Results

3.5.1. Influence of the projection method

Before we can study the influence of the vertex corrections and the different decay and scattering processes we have to analyse the influence of the additional freedom introduced by the projection scheme ((3.29) to (3.31)). Our studies of the $\pi\rho$ system show that the presence of kinematical singularities has a strong influence on the self-consistent results and may lead to unphysical effects. Therefore correction methods like the scheme described in (3.29, 3.31) are mandatory. However in such a scheme the strength of the far space-like modes in the 3d longitudinal part of the vector-mesons is controlled by the choice of the function $\lambda(w, u)$ parameterised here by the parameter Λ (3.31). This additional dependence on Λ has to be studied. In order to keep the discussion as simple as possible we restrict this study to a reduced model where only pions and ρ -mesons void of vertex corrections are kept. The same system was also studied in [10, 47, 49] using different techniques to restore four transversality.

The behaviour of the

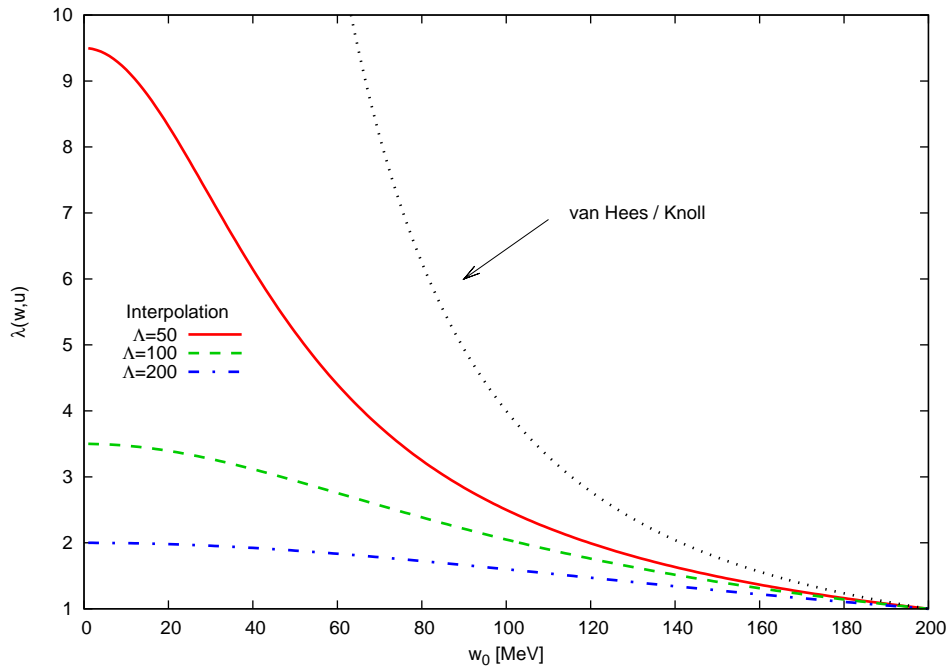


Figure 3.4.: Comparison of different choices for $\lambda(w, u)$ (3.31) at a 3 momentum of 200 MeV for three different values of the parameter Λ . For comparison we also show the function λ implicitly used in the method by H. van Hees and J. Knoll which develops a singularity at vanishing w_0 .

function $\lambda(w, u)$ is shown in Fig. 3.4 for some typical values of Λ in (3.31). This function determines how much strength is contained in the far space-like components. A low value of Λ results in a higher strength of these components while a large value suppresses strength. In addition we shall compare the results also to a calculation where the value of the spectral function for the ρ -meson is set to zero for all spacelike momenta referred to as 'with cut'³. The results of this study are stated in Figs. 3.5 and 3.6. The numerical evaluations shows that the dependence on the actual choice of Λ is quite moderate even though the actual value of $\lambda(w, u)$ changes by more than a factor of two. The largest difference is obtained between the calculations using the interpolation scheme (3.31) and the one using the cut. Here we observe that the width of the ρ -meson is reduced by about 30 MeV for the interpolation scheme instead of the cut, while the width changes only about 10 MeV when Λ is increased from 50 MeV to 200 MeV. In contrast to this the pion shows a larger sensitivity on the value of Λ which even increases with temperature. We observe that especially the introduction of the cut leads to a reduction of the width. In contrast to this the effect of Λ is small and becomes important only for very high temperatures. This behaviour of the pion and the ρ -meson is generic and similar for all momenta. We therefore show results (Fig. 3.5 and 3.6) for a momentum of 200 MeV only. The rather large influence of the cut on the pion spectral function can be understood. The cut effectively reduces the decay possibilities of the pion such that the width decreases as can be seen in Fig. 3.6. This then self-consistently influences back on the ρ -meson which becomes broader because the phase space for the decay modes is larger. In addition the pion spectral function has now less strength on the low energy side since strength has been shifted to high energy reducing phase space for the decay (see also Appendix F). This effect also causes that we see nearly no temperature influence on the width of the ρ -meson because with increasing temperature pion strength is shifted towards higher energies which in part compensates the Bose enhancement effect. To conclude this analysis of the influence of the value of Λ used in the calculation we observe that as expected the influence of the Λ increases with temperature because the low energy tail becomes stronger populated. The effect of changing Λ turned out to be small for the ρ -meson and somewhat larger for the pion. However as we will see in the next chapter where effects of baryonic particle-hole contributions on the pion self-energy are studied the influence resulting from $\pi\rho$ -loops becomes relatively small and the actual variations with Λ are therefore no source of concern.

³Since analyticity is violated when artificially setting some part of the spectral function to zero this procedure can be taken as some extreme example only.

3. Pions and vector-mesons at finite temperature

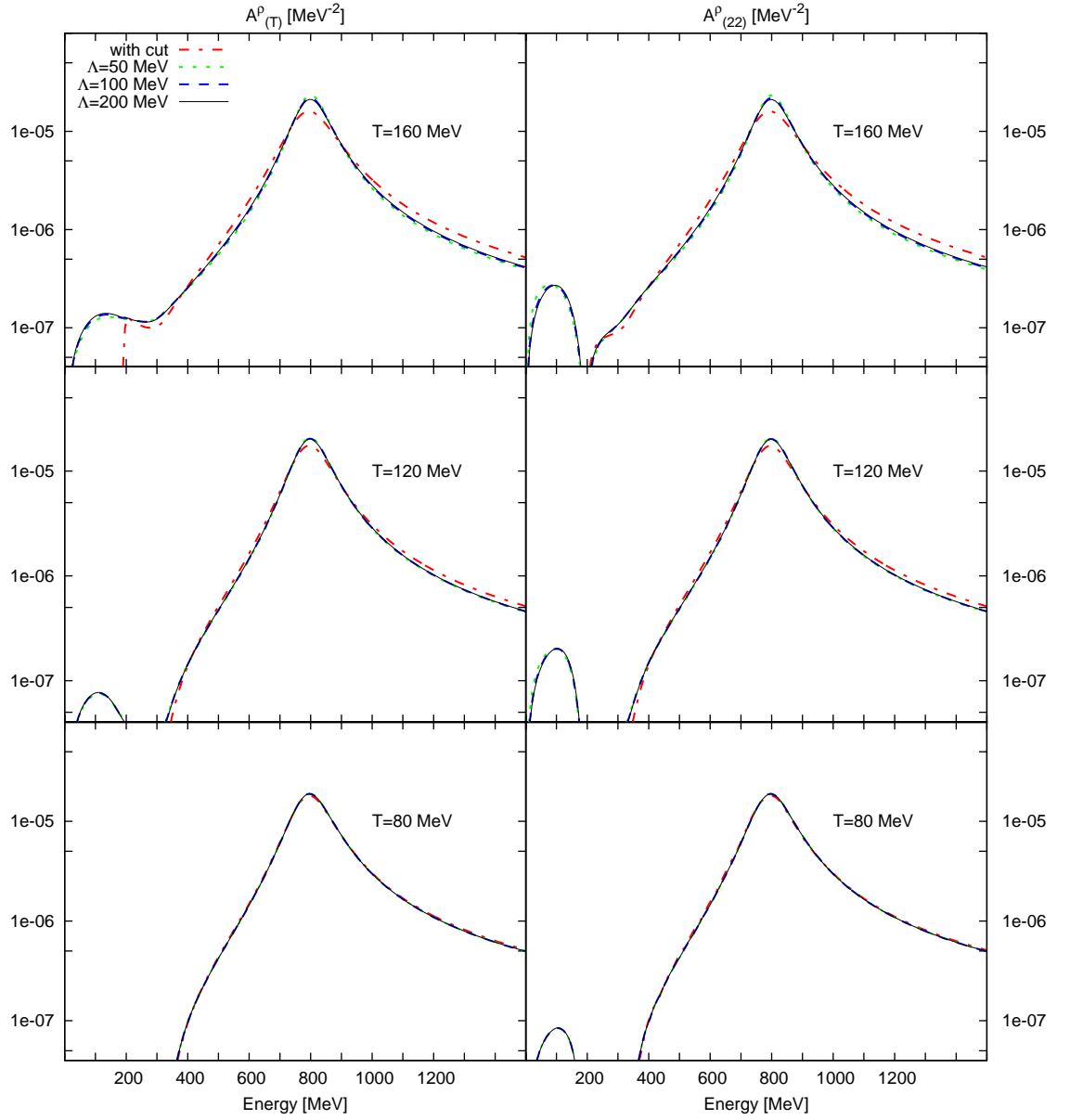


Figure 3.5.: Spatial transversal (left panels) and longitudinal (right panels) parts of the ρ -meson spectral function at a momentum of 200 MeV. The four choices used for the regularisation of the projection method are specified in the upper left panel.

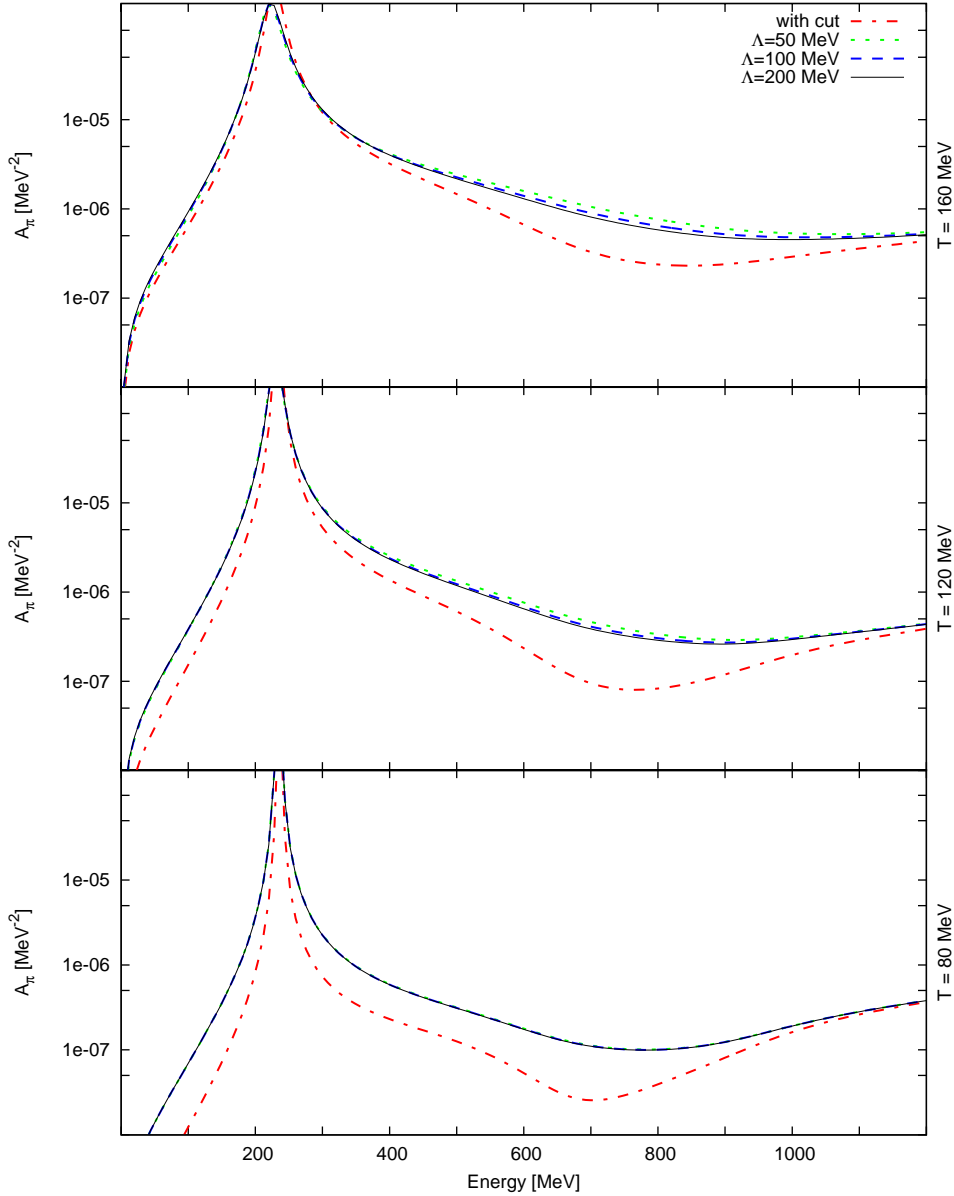


Figure 3.6.: Same as in Fig. 3.5 for the pion spectral function at a momentum of 200 MeV.

3.5.2. Results for the mesonic system

In the previous section we studied the influence from the uncertainty in the determination of the spacelike parts in the 3d longitudinal components of the vector mesons. It turned out that we have only a small sensitivity to the choice of the interpolation and therefore use a value of $\Lambda = 200$ MeV in the following. The next step is now to isolate effects coming from the various parts of the model like the vertex corrections or the

3. Pions and vector-mesons at finite temperature

coupling to the omega meson and to study the temperature dependence of the spectral distributions. From the analytic estimate (see Appendix F) and earlier calculations [9] we expect no dramatic changes of the spectral distribution of the ρ -meson. For the ω -meson we expect some broadening due to the interplay with the ρ -meson. However since in the pure mesonic model no large spacelike components appear in the pion spectral function which turned out [9] to be responsible for large fractions of this broadening we expect less strong changes. The most interesting point then will be what influence the vertex corrections have on the result and to what extent the pion gets modified.

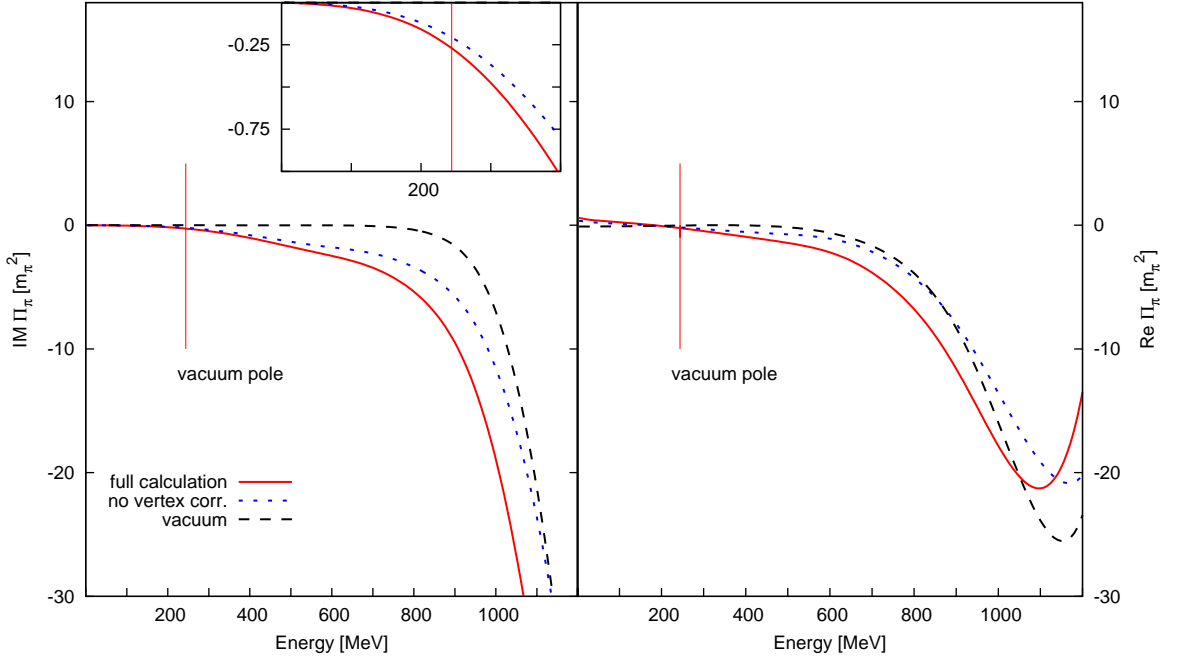


Figure 3.7.: Imaginary (left plot) and real part (right plot) of the pion self-energy at at temperature of 120 MeV and 200 MeV momentum in the full calculation (full line) and without vertex-corrections and short-range correlations (dotted line). Vacuum results for the full calculation are given for comparison (dashed line).

We begin with the effects on the pion. The self-energy at $T=120$ MeV temperature can be seen in Fig. 3.7. We observe that in the medium the pion width is around 35 MeV and becomes a bit smaller without the vertex correction. This width results from new scattering effects present at finite T . In vacuum we only have the free pion pole and the continuum from the decay of the pion into the $\rho\pi$ -channel, (Fig. 3.8). At finite T the continuum remains essentially unchanged (Fig. 3.8), while the pion pole gets broadened by scattering. Here the pion can scatter off an other pion from the heat-bath and convert into a ρ -meson, a process which becomes the more effective the

more the low energy time-like components of the ρ -meson become enlarged. This leads then to self-energy contributions at low masses which are responsible for the broadening of the main pion mode. Short-range correlations have some but small influence on the self-energy which becomes a bit larger in general.

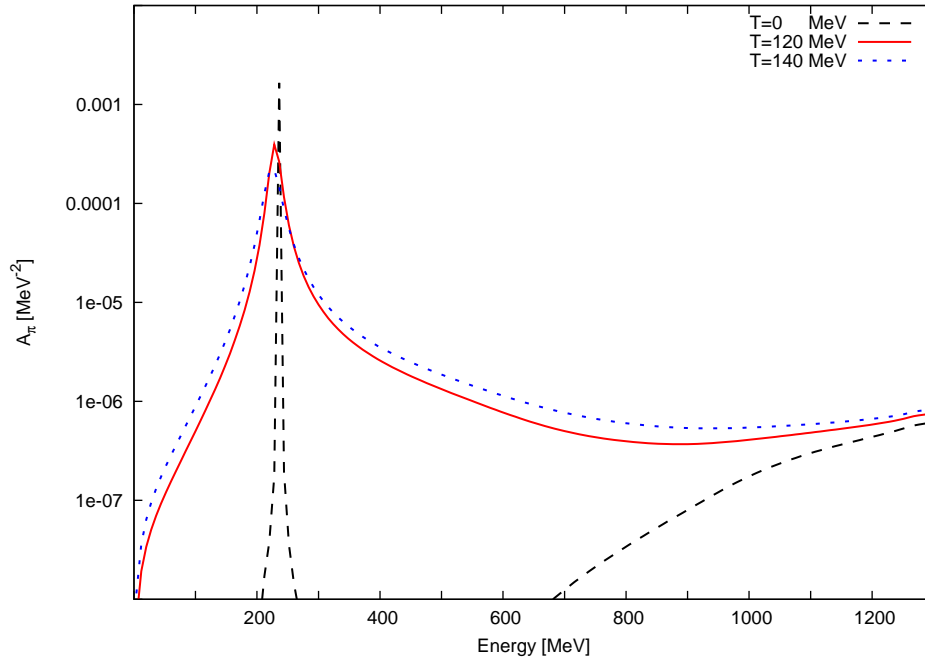


Figure 3.8.: Pion spectral function for three different temperatures at a momentum of 200 MeV.

From Fig. 3.8⁴ we also learn that the changes in the pion spectral function are not symmetric with respect to the vacuum mass but show a preference for higher masses. This then leads to a suppression of the ρ -meson decay thus reducing the width.

The ρ -meson shows only minor changes and we especially have to note that the width given though the thermally enhanced decay into two pion becomes reduced (see Fig. 3.13) as compared to the perturbative case (See Appendix F). This can be explained because here we have to deal with a pion spectral function which is no longer symmetric around the pole mass but receives more contributions on the high mass side resulting from the $\rho\pi$ cut. Since this attracts some strength into a mode where the ρ -meson can not decay into we have some lowering of the width. The resulting net effect between this reduction and the thermal enhancement turns out to be quite small such that the actual enhancement of the ρ -meson width is mainly given by the two new decay modes into $\omega\pi$ and $\rho\pi\pi$ which become now possible since the thresholds for these decays are

⁴The small width of the pion pole at zero temperature results from a minimal width required in the numerical calculations.

3. Pions and vector-mesons at finite temperature

reduced when all particles become broad. However even with the additional scattering and decay possibilities into $\omega\pi$ and $\rho\pi\pi$ the width is only increased by 35 MeV at 140 MeV temperature (see Fig. 3.10).

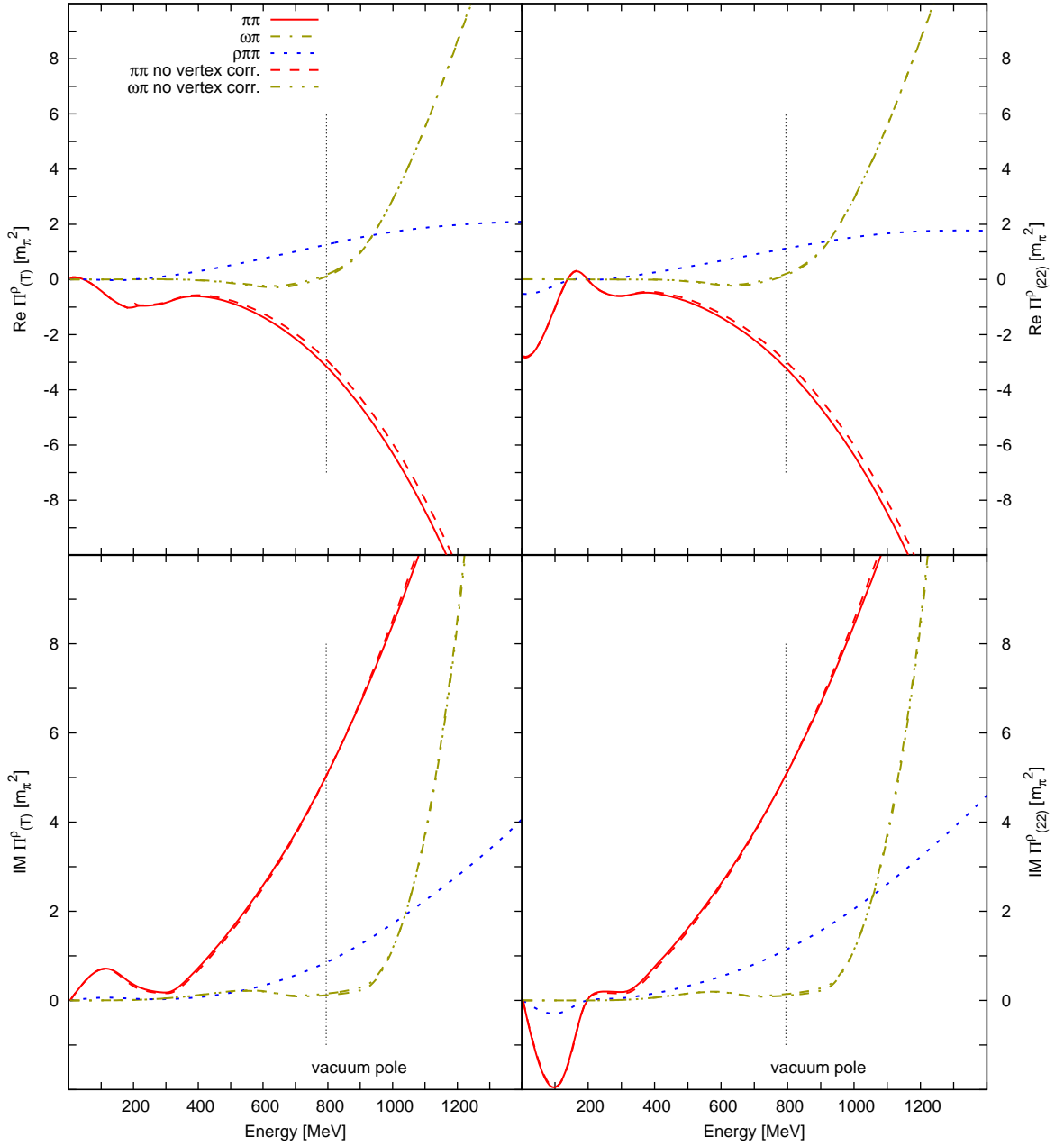


Figure 3.9.: Contributions (see upper left plot for explanations) to the 3 transversal (left plots) and 3 longitudinal (right plots) part of the ρ -meson self-energy at a temperature of 120 MeV and three momentum of 200 MeV.

In Fig. 3.9 we see the three different contributions to the ρ -meson self-energy. We observe that in the whole low energy range until about 1.2 GeV the decay into two pions ($\pi\pi$) dominates the self-energy. In contrast to this the contributions from the interplay with the ω -meson ($\omega\pi$) and the vertex corrections ($\rho\pi\pi$) give only small corrections. In addition we see that all processes receive contributions at very low energy from scattering off thermally excited particles. Therefore all spectral functions have support also in this regions leading then to the vanishing of the thresholds in all self-energies.

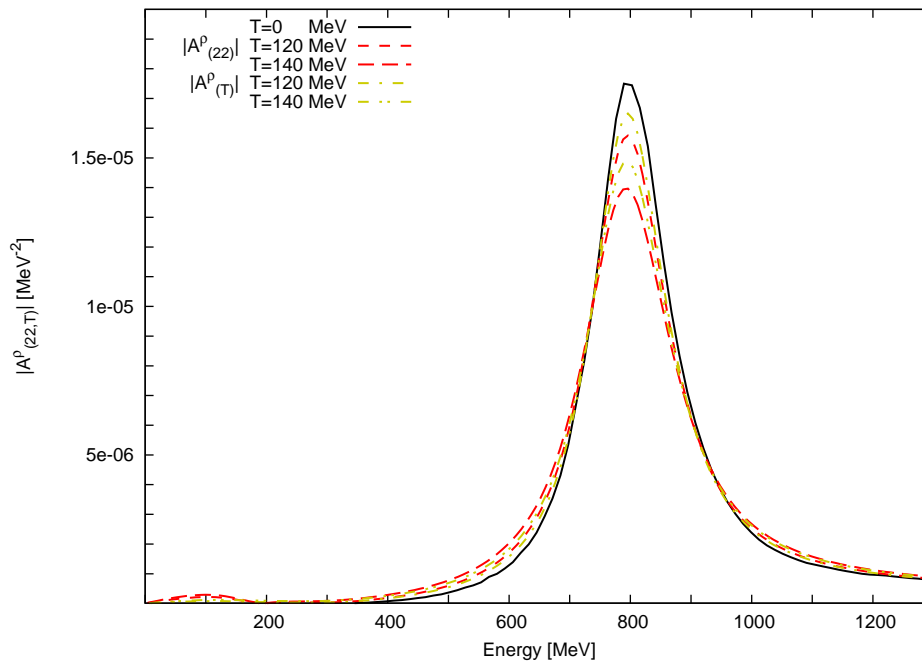


Figure 3.10.: 3 longitudinal and transversal part of the ρ -meson spectral function for three a momentum of 200 MeV and different temperatures.

The effect of the vertex corrections and short-range correlations is seen to be negligible. This is due to the fact that they lead only to a reordering of spectral strength of the pion. However since the ρ -meson has a much larger mass than the pion it is quite insensitive on this reordering. For the ω -meson we observe (see Fig. 3.11) also a small effect of the vertex corrections. At $T=120$ MeV the ω -meson width is increased to about 30 MeV which is about half of the value compared to earlier studies [9]. This however is due to the leak of low energy pion components which could arise from interactions with baryons.

3. Pions and vector-mesons at finite temperature

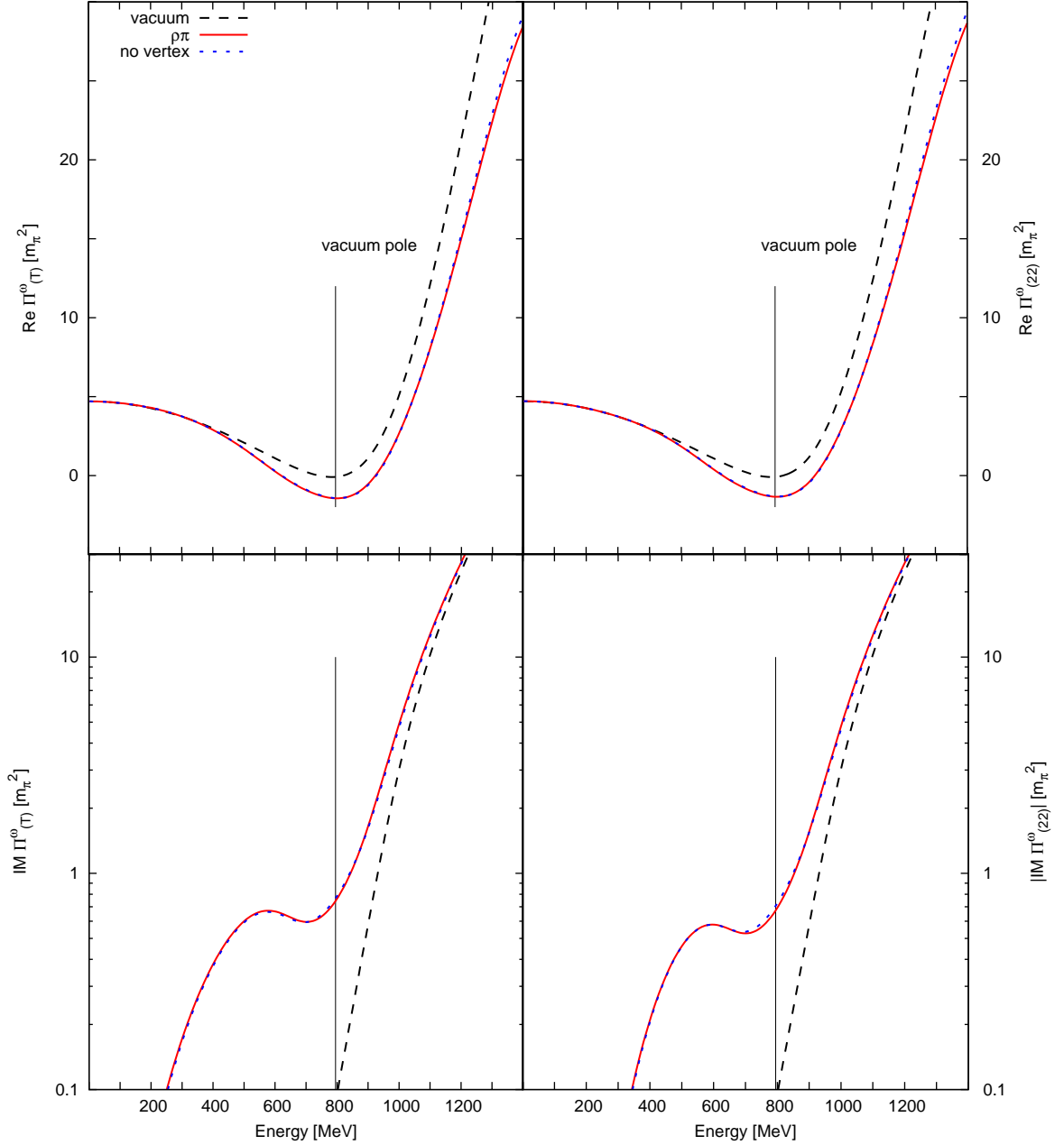


Figure 3.11.: 3 longitudinal and transversal part of the ω -meson self-energy at a temperature of 120 MeV and three momentum of 200 MeV in the full calculation (full line) and without vertex-corrections and short-range correlations (dotted line). Vacuum results for the full calculation are given for comparison (dashed line).

To gain some further understanding of the vertex corrections we have to look at the results for the vertex tensors Γ_i (4.22). Here we observe that at low momenta the

realpart of Γ_1 is, for energies in the region of the pion mass, larger then 1 which implies that the vertex corrections essentially enhance the process where they are applied.

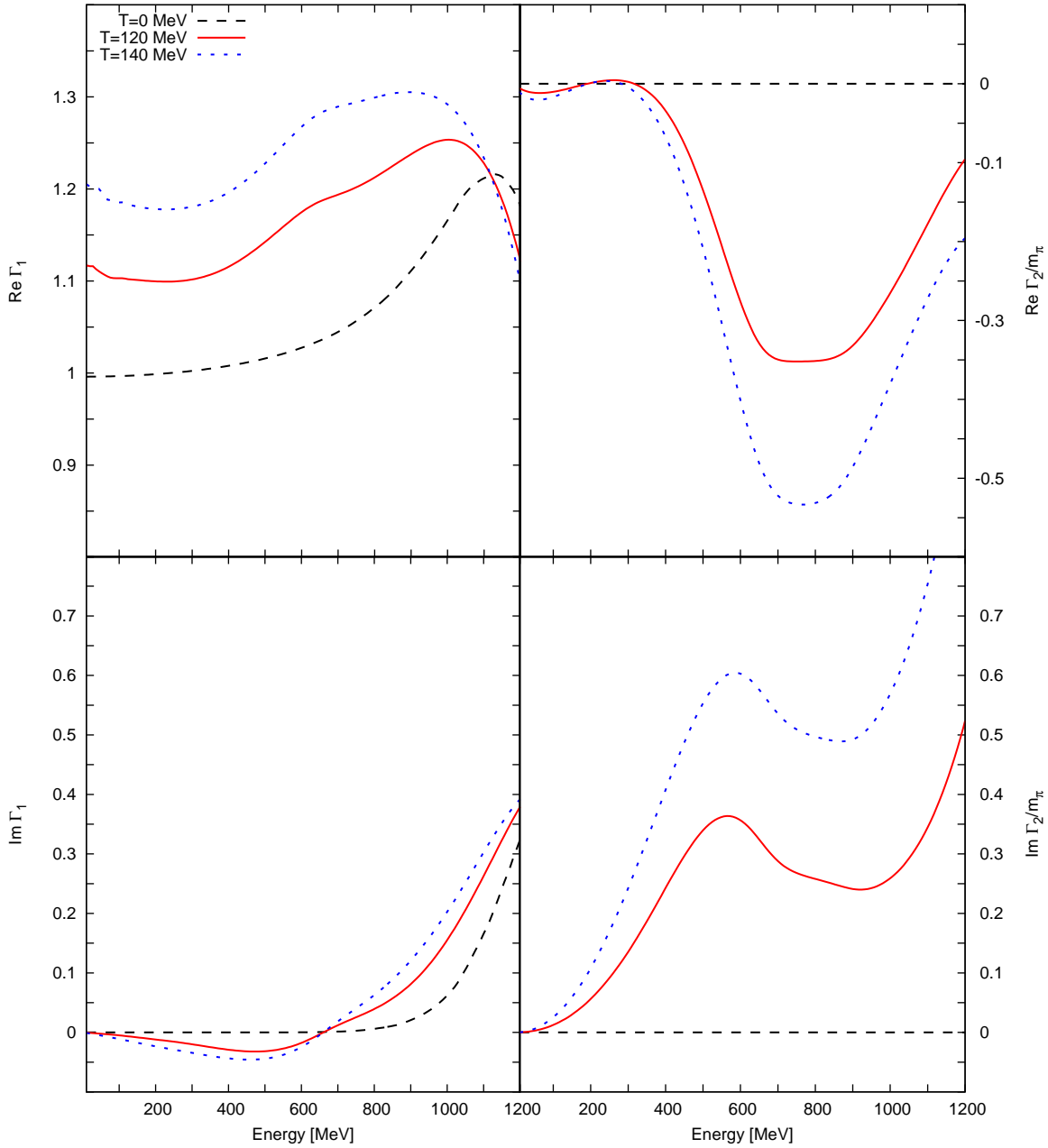


Figure 3.12.: Real and imaginary part of the vertex functions Γ_1 and Γ_2 at a three momentum of 200 MeV and three different temperatures.

In contrast to this the effects coming from the imaginary part of Γ_1 and especially from Γ_2 are much less pronounced.

3. Pions and vector-mesons at finite temperature

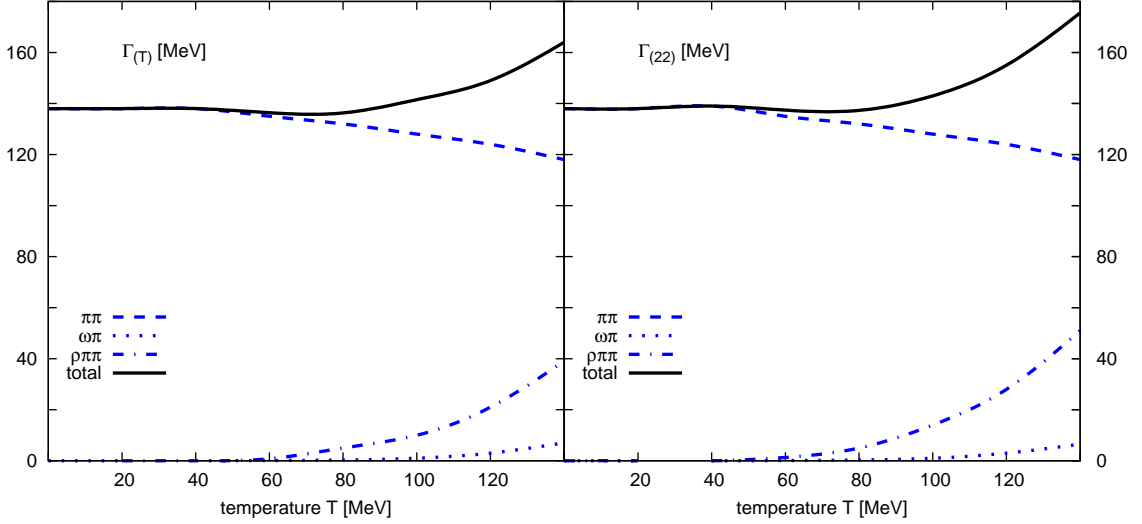


Figure 3.13.: ρ -meson width $\Gamma_{(22,T)} = -\Im\Pi_{(22,T)}(m_\rho, 0)/m_\rho$ versus temperature. We give results for the total width and the three different contributions $\rho \rightarrow \pi\pi$ (dashed line), $\rho \rightarrow \omega\pi$ (dotted line), $\rho \rightarrow \rho\pi\pi$ (dashed dotted line).

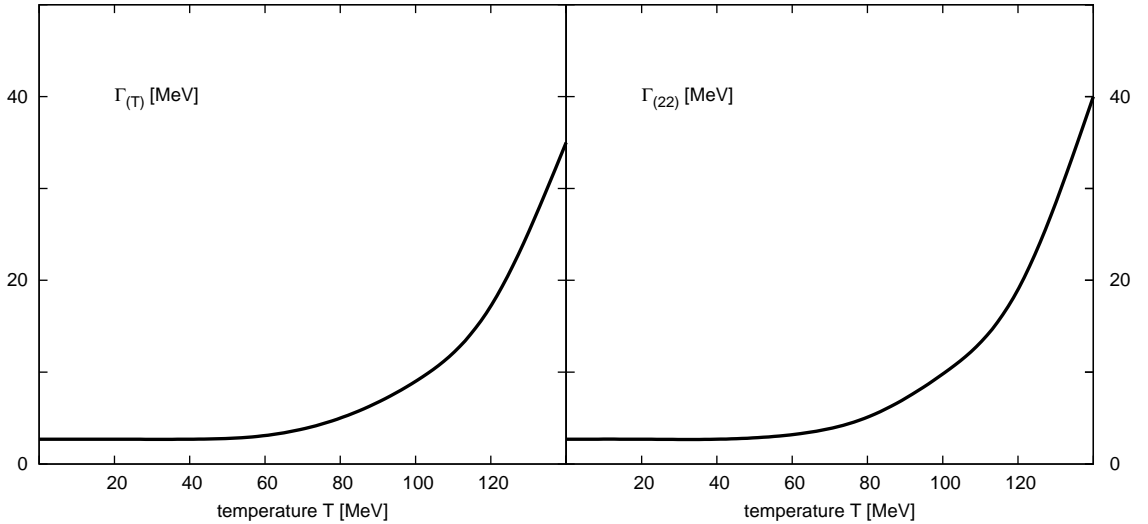


Figure 3.14.: ω -meson width $\Gamma_{(22,T)} = -\Im\Pi_{(22,T)}(m_\omega, 0)/m_\omega$ versus temperature.

From these results we learn that the self-consistency in the meson sector proved being not very important for the ρ -meson where the results are comparable with the perturbative treatment. On the other hand self-consistent effects come into play when considering the pion and the ω -meson. The vertex correctons proved to small in all cases as could already be expected from the rather high threshold of the $\rho\pi$ -loop as compared to the pion mass. The momentum dependence proved to be small in all cases.

4. Pions and Δ -isobars at finite density

In order to extend our considerations of the vector-mesons towards finite density we need a good understanding of the pion and baryon properties in a hot and dense environment. To approach this problem we will now study the interaction of the pion with nucleon and Δ -isobar at finite density and zero temperature.

4.1. Fields and model interactions

The interaction between pions, nucleons and the Δ -isobar is modelled by the leading order vertices [29] resulting from the low energy limit of QCD. Therefor we consider the leading order vertices

$$\mathcal{L}_{\pi N \Delta} = \frac{f_N}{m_\pi} \bar{N} \gamma_5 \gamma^\mu (\partial_\mu \vec{\pi}) \vec{\tau} N + \frac{f_\Delta}{m_\pi} \left(\bar{\Delta}^\mu (\partial_\mu \vec{\pi}) \vec{T} N + \text{h.c.} \right) \quad (4.1)$$

resulting from the chiral lagrangian. Here τ_i and T_i denote the standard iso-spin Pauli and iso-spin 1/2 to 3/2 transfer matrices, respectively which obey $T_i^\dagger T_j = \delta_{ij} - \tau_i \tau_j / 3$. Following ref. [84] the coupling constants are chosen to be $f_N = 0.988$ and $f_\Delta = 1.85$. Pion, nucleon and Δ -isobar fields are denoted by π , N and Δ^μ , respectively¹.

Taken at one loop level the interactions (4.1) lead to a strong softening of the pion mode. This can be prevented by short range correlations as suggested by Migdal. In its

¹Considering the form of the interaction (4.1) one has to note that for the Δ as a spin 3/2 particle it leads to the propagation of additional spin 1/2 modes. Since the Δ -isobar is supposed to be a spin 3/2 particle one could call these additional modes unphysical and try to prevent them from propagating. One method to do this has been proposed by Pascalutsa [85] which uses a new type of gauged interaction

$$\mathcal{L} = \frac{f_\Delta}{m_\pi} \left(\epsilon^{\mu\nu\alpha\beta} \partial_\mu \bar{\Delta}_\nu \gamma_5 \gamma_\alpha \vec{T} N (\partial_\beta \vec{\pi}) + \text{h.c.} \right), \quad (4.2)$$

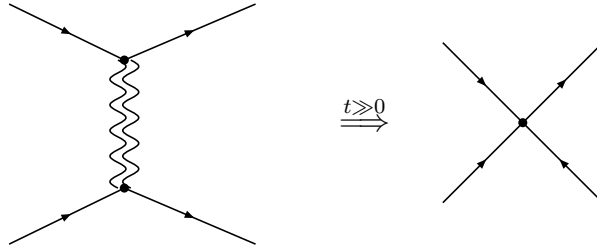
for the Δ such that only spin 3/2 modes can be propagated. However he showed [86] that the difference between these two coupling schemes are background terms which have to be adjusted to data anyway. Thus we decided to use the standard interaction (4.1) to be also in line with earlier studies such that a comparison is easier possible.

4. Pions and Δ -isobars at finite density

relativistic version [29, 32] this four baryon interaction reads

$$\begin{aligned}
\mathcal{L}_{\text{Migdal}} &= g'_{11} \frac{f_N^2}{m_\pi^2} \left(\bar{N} \gamma_5 \gamma_\mu \vec{\tau} N \right) \left(\bar{N} \gamma_5 \gamma^\mu \vec{\tau} N \right) \\
&+ g'_{22} \frac{f_\Delta^2}{m_\pi^2} \left(\left(\bar{\Delta}_\mu \vec{T} N \right) \left(\bar{N} \vec{T}^\dagger \Delta^\mu \right) + \left(\left(\bar{\Delta}_\mu \vec{T} N \right) \left(\bar{\Delta}^\mu \vec{T} N \right) + \text{h.c.} \right) \right) \\
&+ g'_{12} \frac{f_N f_\Delta}{m_\pi^2} \left(\bar{N} \gamma_5 \gamma_\mu \vec{\tau} N \right) \left(\left(\bar{\Delta}^\mu \vec{T} N \right) + \text{h.c.} \right), \tag{4.3}
\end{aligned}$$

with Migdal parameters g'_{ij} . It accounts, in particular, for t -channel exchange interactions mediated by heavy mesons



to be treated as local couplings on the Hartree level. The Fock contribution can be cast into the form of a Hartree contribution by a simple Fierz transformation just simply renormalising the coupling strengths in (4.3). These additional interactions give not only rise to changes in the pion self-energy but introduce also corrections to the $\pi N \Delta$ vertex which will be an essential part of this work. Besides these interactions we treat the binding effects in the baryon sector by scalar Σ_S and vector Σ_V mean fields which depend on the nuclear density ρ and will be specified later.

4.2. The approximation scheme

As also done in the previous chapter we first give an overview about the model in form of diagrams. The main focus is on the study of the in-medium behaviour of the propagators of the pion G_π and the Δ -isobar $S^{\mu\nu}$ as the solution of the Dyson equation

$$\begin{aligned}
G_\pi(w, u) &= G_\pi^{(0)}(w) + G_\pi^{(0)}(w) \Pi_\pi(w, u) G_\pi(w, u), \\
S_{\mu\nu}(w, u) &= S_{\mu\nu}^{(0)}(w - \Sigma_V^\Delta u) + S_{\mu\alpha}^{(0)}(w - \Sigma_V^\Delta u) \Sigma_\Delta^{\alpha\beta}(w, u) S_{\beta\nu}(w, u), \tag{4.4}
\end{aligned}$$

where we use the free propagators

$$\begin{aligned}
 G_\pi^{(0)}(w) &= \frac{1}{w^2 - m_\pi^2 + i\epsilon} \\
 S_0^{\mu\nu}(w) &= \frac{-1}{\psi - m_\Delta + i\epsilon} \left(g^{\mu\nu} - \frac{\gamma^\mu \gamma^\nu}{3} - \frac{2 w^\mu w^\nu}{3 m_\Delta^2} - \frac{\gamma^\mu w^\nu - w^\mu \gamma^\nu}{3 m_\Delta} \right) \\
 &\quad + \frac{Z}{6 m_\Delta^2} \left[\gamma^\mu (Z \psi - 2(Z-1) m_\Delta) \gamma^\nu - 2 \gamma^\mu w^\nu - 2 w^\mu \gamma^\nu \right], \quad (4.5)
 \end{aligned}$$

indicated with the index zero. The vector meanfield of the Δ -isobar Σ_V^Δ will be included by an energy shift in the free propagator (4.4). We take

$$m_\Delta = m_\Delta^{vac} + \Sigma_S^\Delta \quad (4.6)$$

as the free Δ mass and scalar meanfield Σ_S^Δ whereas Z accounts for ambiguities in the interpolating field. The four vector u^μ characterises the nuclear matter frame and will be taken $u^\mu = (1, \vec{0})$ in the following. It remains to specify the self-energies entering in the Dyson equation (4.4). Interested in the soft modes of the system which we would like to resum we consider particle- and Delta-hole excitations as key ingredients of the model. The corresponding nucleon- and isobar-hole loop tensors,

$$\chi_{\mu\nu}^{(Nh)}(w, u) = \text{Diagram with two vertices, top arc labeled } N, \text{ bottom arc labeled } N^{-1} \text{ ; } \chi_{\mu\nu}^{(\Delta h)}(w, u) = \text{Diagram with two vertices, top arc labeled } \Delta, \text{ bottom arc labeled } N^{-1} \text{ ; } \quad (4.7)$$

which we define by

$$\begin{aligned}
 \chi_{\mu\nu}^{(\Delta h)}(w, u) &= \frac{4}{3} \frac{f_\Delta^2}{m_\pi^2} \int \frac{d^4 p}{(2\pi)^4} i \text{tr} \Delta S(p, u) S_{\mu\nu}(p+w, u) + (w_\mu \rightarrow -w_\mu), \\
 \chi_{\mu\nu}^{(Nh)}(w, u) &= 2 \frac{f_N^2}{m_\pi^2} \int \frac{d^4 p}{(2\pi)^4} i \text{tr} \left(\Delta S(p, u) \gamma_5 \gamma_\mu \frac{1}{\not{p} - \Sigma_V^N \not{\psi} + \not{p} - m_N} \gamma_5 \gamma_\nu \right. \\
 &\quad \left. + \frac{1}{2} \Delta S(p, u) \gamma_5 \gamma_\mu \Delta S(p+w, u) \gamma_5 \gamma_\nu \right) + (w_\mu \rightarrow -w_\mu), \quad (4.8)
 \end{aligned}$$

take in a relativistic treatment the form of Lorentz polarisation tensors. They depend on the choice of the nucleon propagator which in our case will contain scalar and vector meanfields only

$$\begin{aligned}
 S_N(p, u) &= \frac{1}{\not{p} - \Sigma_V^N \not{\psi} - m_N + i\epsilon} + \Delta S(p, u), \quad m_N = m_N^{vac} - \Sigma_S^N, \\
 \Delta S(p, u) &= 2\pi i \Theta \left[p \cdot u - \Sigma_V^N \right] \delta \left[(p - \Sigma_V^N u)^2 - m_N^2 \right] \\
 &\quad \times \left(\not{p} - \Sigma_V^N \not{\psi} + m_N \right) \Theta \left[k_F^2 + p^2 - (u \cdot p)^2 \right], \quad (4.9)
 \end{aligned}$$

In the case of the pion we get an equivalent contribution as compared to (3.6)

$$\begin{aligned} \Pi_\pi &= \text{---} \bullet \text{---} \text{---} \text{---} \text{---} \text{---} \text{---} \\ &= -w^\mu \Pi_{\mu\nu}^{(\Delta N)}(w, u) w^\nu - 4\pi \left(1 + \frac{m_\pi}{m_N}\right) b_{\text{eff}} \rho, \end{aligned} \quad (4.14)$$

only the building blocks have been changed and correspond now to the well known nucleon- and isobar-hole contributions modified by short range interactions. In addition we supply a correction term linear in density in order to be able to reproduce the pion nucleon scattering length in vacuum in the context of a virial expansion.

4.3. Computational details

4.3.1. Pion self-energy and polarisation loops

Since we will need structures arising from the polarisation loops (4.12) we start with the construction of these quantities and the pion self-energy. For the computation of short range correlation effects we take advantage of the decompositions into the set of Lorentz structures $L_{\mu\nu}^{(ij)}(w, u)$ and $T_{\mu\nu}(w, u)$ (3.11) and write

$$\begin{aligned} \chi_{\mu\nu}^{(Nh)}(w, u) &= \sum_{i,j=1}^2 \chi_{ij}^{(Nh)}(w, u) L_{\mu\nu}^{(ij)}(w, u) + \chi_T^{(Nh)}(w, u) T_{\mu\nu}(w, u), \\ \chi_{\mu\nu}^{(\Delta h)}(w, u) &= \sum_{i,j=1}^2 \chi_{ij}^{(\Delta h)}(w, u) L_{\mu\nu}^{(ij)}(w, u) + \chi_T^{(\Delta h)}(w, u) T_{\mu\nu}(w, u). \end{aligned} \quad (4.15)$$

It leads to a decoupling of the Dyson-equation in the longitudinal and transversal sector [29]. The derivation of the explicit expressions for the longitudinal and transverse loop functions is relegated to Appendix G. The latter follow by simple contractions of the tensors $\chi_{\mu\nu}^{(\Delta h)}(w, u)$ and $\chi_{\mu\nu}^{(Nh)}(w, u)$ with the projectors (3.11). As in the previous chapter we define the loop and coupling matrices χ and g

$$\begin{aligned} \chi^{(L)} &= \begin{pmatrix} \chi_{11}^{(Nh)} & \chi_{12}^{(Nh)} & 0 & 0 \\ \chi_{21}^{(Nh)} & \chi_{22}^{(Nh)} & 0 & 0 \\ 0 & 0 & \chi_{11}^{(\Delta h)} & \chi_{12}^{(\Delta h)} \\ 0 & 0 & \chi_{21}^{(\Delta h)} & \chi_{22}^{(\Delta h)} \end{pmatrix} & g^{(L)} &= \begin{pmatrix} g'_{11} & 0 & g'_{12} & 0 \\ 0 & g'_{11} & 0 & g'_{12} \\ g'_{12} & 0 & g'_{22} & 0 \\ 0 & g'_{12} & 0 & g'_{22} \end{pmatrix}, \\ g^{(T)} &= \begin{pmatrix} g'_{11} & g'_{12} \\ g'_{12} & g'_{22} \end{pmatrix}, & \chi^{(T)} &= \begin{pmatrix} \chi_T^{(Nh)} & 0 \\ 0 & \chi_T^{(\Delta h)} \end{pmatrix}. \end{aligned} \quad (4.16)$$

where now the projector and coupled channel structure has to be included. The pion self-energy can then be brought in the same form as in (3.14)

$$\Pi_\pi(w, u) = -w^\mu \Pi_{\mu\nu}^{(\Delta N)}(w, u) w^\nu - 4\pi \left(1 + \frac{m_\pi}{m_N}\right) b_{\text{eff}} \rho. \quad (4.17)$$

4. Pions and Δ -isobars at finite density

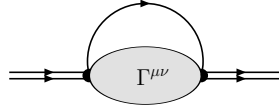
After decomposition the quantity $\Pi_{\mu\nu}^{(\Delta N)}(w, u)$, which sums up all contributions in (3.14), results to

$$\Pi_{\mu\nu}^{(\Delta N)}(w, u) = \sum_{i,j=1}^2 \Pi_{(ij)}^{(\Delta N)}(w, u) L_{\mu\nu}^{(ij)}(w, u) + \Pi_T^{(\Delta N)}(w, u) T_{\mu\nu}(w, u) \quad (4.18)$$

with coefficient functions $\Pi_{ij}^{(\Delta N)}$ and $\Pi_T^{(\Delta N)}$ defined as

$$\begin{aligned} \Pi_{(11)}^{(\Delta N)} &= \sum_{i \in \{1,3\} j \in \{1,3\}} \left[\left(\mathbb{1} - \chi^{(L)} g^{(L)} \right)^{-1} \chi^{(L)} \right]_{ij} \\ \Pi_{(12)}^{(\Delta N)} &= \sum_{i \in \{1,3\} j \in \{2,4\}} \left[\left(\mathbb{1} - \chi^{(L)} g^{(L)} \right)^{-1} \chi^{(L)} \right]_{ij} \\ \Pi_{(21)}^{(\Delta N)} &= \sum_{i \in \{2,4\} j \in \{1,3\}} \left[\left(\mathbb{1} - \chi^{(L)} g^{(L)} \right)^{-1} \chi^{(L)} \right]_{ij} \\ \Pi_{(22)}^{(\Delta N)} &= \sum_{i \in \{2,4\} j \in \{2,4\}} \left[\left(\mathbb{1} - \chi^{(L)} g^{(L)} \right)^{-1} \chi^{(L)} \right]_{ij} \\ \Pi_T^{(\Delta N)} &= \sum_{i=1}^2 \left[\left(\mathbb{1} - \chi^{(T)} g^{(T)} \right)^{-1} \chi^{(T)} \right]_{ii}. \end{aligned} \quad (4.19)$$

Here the coupled channel structure requires the additional summations. For the correlation diagram



in (4.13) one needs the corresponding correlation tensors

$$\Gamma_{(\Delta N)}^{\mu\nu}(w, u) = \sum_{i,j=1}^2 \Gamma_{(ij)}^{(\Delta h)}(w, u) L_{(ij)}^{\mu\nu}(w, u) + \Gamma_T^{(\Delta h)}(w, u) T^{\mu\nu}(w, u) \quad (4.20)$$

with coefficient functions Γ_{ij} and Γ_T defined as

$$\begin{aligned} \Gamma_{(11)}^{(\Delta h)} &= \left[g^{(L)} \left(\mathbb{1} - \chi^{(L)} g^{(L)} \right)^{-1} \right]_{33} & \Gamma_{(12)}^{(\Delta h)} &= \left[g^{(L)} \left(\mathbb{1} - \chi^{(L)} g^{(L)} \right)^{-1} \right]_{34} \\ \Gamma_{(21)}^{(\Delta h)} &= \left[g^{(L)} \left(\mathbb{1} - \chi^{(L)} g^{(L)} \right)^{-1} \right]_{43} & \Gamma_{(22)}^{(\Delta h)} &= \left[g^{(L)} \left(\mathbb{1} - \chi^{(L)} g^{(L)} \right)^{-1} \right]_{44} \\ \Gamma_T^{(\Delta h)} &= \left[g^{(T)} \left(\mathbb{1} - \chi^{(T)} g^{(T)} \right)^{-1} \right]_{22} \end{aligned} \quad (4.21)$$

which represents a truncated version of $\Pi_{\mu\nu}^{(\Delta N)}$ where the outermost loops are stripped off.

Like in the $\pi\rho\omega$ -system considered previously the vertex corrections are introduced by replacing the bare pion momentum q^μ at the vertex by a dressed one

$$q_\mu \rightarrow \Gamma_\mu^{(N\Delta)}(q, u) = q_\mu \Gamma_1^{(N\Delta)}(q, u) + u_\mu \Gamma_2^{(N\Delta)}(q, u) \quad (4.22)$$

$$\begin{aligned} \Gamma_1^{(N\Delta)} &= 1 + \sum_{i \in \{3\} j \in \{1,3\}} \left[\left(\mathbb{1} - \chi^{(L)} g^{(L)} \right)^{-1} \chi^{(L)} g^{(L)} \right]_{ij} \\ &+ \sum_{i \in \{4\} j \in \{1,3\}} \frac{(u \cdot q)}{\sqrt{q^2 - (u \cdot q)^2}} \left[\left(\mathbb{1} - \chi^{(L)} g^{(L)} \right)^{-1} \chi^{(L)} g^{(L)} \right]_{ij} \end{aligned} \quad (4.23)$$

$$\Gamma_2^{(N\Delta)} = \sum_{i \in \{4\} j \in \{1,3\}} \frac{-q^2}{\sqrt{q^2 - (u \cdot q)^2}} \left[\left(\mathbb{1} - \chi^{(L)} g^{(L)} \right)^{-1} \chi^{(L)} g^{(L)} \right]_{ij}.$$

4.3.2. Pion-nucleon scattering

One important issue of this work is the study of the in-medium isobar propagator $S_{\mu\nu}(w, u)$ and its interplay with the pion in a self-consistent framework where we also would like to include short-range-correlations and modifications of the vertex [87, 88]. The in-medium modifications of the nucleon will be treated by the inclusion of scalar and vector meanfields. We will start our discussion with the case without vertex corrections in order to introduce our renormalisation scheme in this more simple case. Afterwards we then state the changes introduced by the inclusion of the vertex corrections.

The isobar self-energy tensor in nuclear matter is a quite complicated object which depends on the time-like 4-vector u_μ specifying the nuclear matter frame. For symmetric nuclear matter at rest it follows $u_\mu = (1, \vec{0})$. The solution of the Dyson equation (4.4) requires a detailed study of the Lorentz-Dirac structure of the propagator. This can most easily be done by using an appropriate decomposition of all objects. The projectors used for the case of the Δ -isobar, where we have in addition to the behaviour as a Lorentz tensor a spinor structure, $P_{[ij]}^{\mu\nu}(w, u)$ and $Q_{[ij]}^{\mu\nu}(w, u)$, have already been introduced by Lutz and Korpa in [89]. Introducing the auxiliary Dirac structures

$$\begin{aligned} P_\pm(w) &= \frac{1}{2} \left(1 \pm \frac{\psi}{\sqrt{w^2}} \right), \quad U_\pm(w, u) = P_\pm(w) \frac{-i \gamma \cdot u}{\sqrt{(w \cdot u)^2/w^2 - 1}} P_\mp(w), \\ V_\mu(w) &= \frac{1}{\sqrt{3}} \left(\gamma_\mu - \frac{\psi}{w^2} w_\mu \right), \quad X_\mu(w, u) = \frac{(w \cdot u) w_\mu - w^2 u_\mu}{w^2 \sqrt{(w \cdot u)^2/w^2 - 1}}, \\ R_\mu(w, u) &= +\frac{1}{\sqrt{2}} \left(U_+(w, u) + U_-(w, u) \right) V_\mu(w) - i \sqrt{\frac{3}{2}} X_\mu(w, u), \\ L_\mu(w, u) &= +\frac{1}{\sqrt{2}} V_\mu(w) \left(U_+(w, u) + U_-(w, u) \right) - i \sqrt{\frac{3}{2}} X_\mu(w, u). \end{aligned} \quad (4.24)$$

4. Pions and Δ -isobars at finite density

which satisfy some useful relations

$$\begin{aligned}
P_{\pm} P_{\pm} &= P_{\pm} = U_{\pm} U_{\mp}, & P_{\pm} P_{\mp} &= 0 = U_{\pm} U_{\pm}, \\
V \cdot L &= 0 = R \cdot V, & L \cdot V &= -\frac{\sqrt{8}}{3} (U_+ + U_-) = V \cdot R, \\
V \cdot V &= L \cdot R = R \cdot L = 1, & R \cdot R &= L \cdot L = \frac{1}{3}, \\
P_{\pm} V_{\mu} &= V_{\mu} P_{\mp}, & P_{\pm} L_{\mu} &= L_{\mu} P_{\pm}, & P_{\pm} R_{\mu} &= R_{\mu} P_{\pm}, \\
U_{\pm} V_{\mu} &= -\frac{1}{3} V_{\mu} U_{\mp} - \frac{\sqrt{8}}{3} L_{\mu} P_{\mp}, & U_{\pm} L_{\mu} &= R_{\mu} U_{\pm}, \\
V_{\mu} U_{\pm} &= -\frac{1}{3} U_{\mp} V_{\mu} - \frac{\sqrt{8}}{3} R_{\mu} P_{\mp}, & U_{\pm} R_{\mu} &= L_{\mu} U_{\pm},
\end{aligned} \tag{4.25}$$

one defines two sets of projectors. The q-space projectors recover the helicity 3/2 modes

$$\begin{aligned}
Q_{[11]}^{\mu\nu} &= \left(g^{\mu\nu} - \hat{w}^{\mu} \hat{w}^{\nu} \right) P_+ - V^{\mu} P_- V^{\nu} - L^{\mu} P_+ R^{\nu}, \\
Q_{[22]}^{\mu\nu} &= \left(g^{\mu\nu} - \hat{w}^{\mu} \hat{w}^{\nu} \right) P_- - V^{\mu} P_+ V^{\nu} - L^{\mu} P_- R^{\nu}, \\
Q_{[12]}^{\mu\nu} &= \left(g^{\mu\nu} - \hat{w}^{\mu} \hat{w}^{\nu} \right) U_+ + \frac{1}{3} V^{\mu} U_- V^{\nu} \\
&\quad + \frac{\sqrt{8}}{3} \left(L^{\mu} P_+ V^{\nu} + V^{\mu} P_- R^{\nu} \right) - \frac{1}{3} L^{\mu} U_+ R^{\nu}, \\
Q_{[21]}^{\mu\nu} &= \left(g^{\mu\nu} - \hat{w}^{\mu} \hat{w}^{\nu} \right) U_- + \frac{1}{3} V^{\mu} U_+ V^{\nu} \\
&\quad + \frac{\sqrt{8}}{3} \left(L^{\mu} P_- V^{\nu} + V^{\mu} P_+ R^{\nu} \right) - \frac{1}{3} L^{\mu} U_- R^{\nu},
\end{aligned} \tag{4.26}$$

where $\hat{w}_{\mu} = w_{\mu}/\sqrt{w^2}$. The projection onto the helicity 1/2 modes (p-space) is obtained via

$$\begin{aligned}
P_{[11]} &= P_+, & P_{[12]} &= U_+, & P_{[21]} &= U_-, & P_{[22]} &= P_-, \\
P_{[31]}^{\mu} &= V^{\mu} P_+, & P_{[32]}^{\mu} &= V^{\mu} U_+, & \bar{P}_{[13]}^{\mu} &= P_+ V^{\mu}, & \bar{P}_{[23]}^{\mu} &= U_- V^{\mu}, \\
P_{[41]}^{\mu} &= V^{\mu} U_-, & P_{[42]}^{\mu} &= V^{\mu} P_-, & \bar{P}_{[14]}^{\mu} &= U_+ V^{\mu}, & \bar{P}_{[24]}^{\mu} &= P_- V^{\mu}, \\
P_{[51]}^{\mu} &= \hat{w}^{\mu} P_+, & P_{[52]}^{\mu} &= \hat{w}^{\mu} U_+, & \bar{P}_{[15]}^{\mu} &= P_+ \hat{w}^{\mu}, & \bar{P}_{[25]}^{\mu} &= U_- \hat{w}^{\mu}, \\
P_{[61]}^{\mu} &= \hat{w}^{\mu} U_-, & P_{[62]}^{\mu} &= \hat{w}^{\mu} P_-, & \bar{P}_{[16]}^{\mu} &= U_+ \hat{w}^{\mu}, & \bar{P}_{[26]}^{\mu} &= P_- \hat{w}^{\mu}, \\
P_{[71]}^{\mu} &= L^{\mu} P_+, & P_{[72]}^{\mu} &= L^{\mu} U_+, & \bar{P}_{[17]}^{\mu} &= P_+ R^{\mu}, & \bar{P}_{[27]}^{\mu} &= U_- R^{\mu}, \\
P_{[81]}^{\mu} &= L^{\mu} U_-, & P_{[82]}^{\mu} &= L^{\mu} P_-, & \bar{P}_{[18]}^{\mu} &= U_+ R^{\mu}, & \bar{P}_{[28]}^{\mu} &= P_- R^{\mu},
\end{aligned}$$

$$P_{[ij]}^{\mu\nu} = P_{[i1]}^{\mu} \bar{P}_{[1j]}^{\nu} = P_{[i2]}^{\mu} \bar{P}_{[2j]}^{\nu}, \tag{4.27}$$

where we directly extended the algebra to include objects with one or no Lorentz index [89]. Using the various relations (4.24) it is now easy to prove the properties:

$$\begin{aligned}
Q_{[ik]}^{\mu\alpha} g_{\alpha\beta} P_{[lj]}^{\beta\nu} &= P_{[ik]}^{\mu\alpha} g_{\alpha\beta} Q_{[lj]}^{\beta\nu} = 0, \\
Q_{[ik]}^{\mu\alpha} g_{\alpha\beta} Q_{[lj]}^{\beta\nu} &= \delta_{kl} Q_{[ij]}^{\mu\nu}, & P_{[ik]}^{\mu\alpha} g_{\alpha\beta} P_{[lj]}^{\beta\nu} &= \delta_{kl} P_{[ij]}^{\mu\nu},
\end{aligned} \tag{4.28}$$

showing that the $Q_{[ij]}^{\mu\nu}$ and $P_{[ij]}^{\mu\nu}$ indeed form a projector algebra. This particular basis facilitates the computation of the in-medium part of the isobar self-energy significantly.

In particular the algebra (4.28) illustrates the decoupling of helicity one-half (p-space) and three-half modes (q-space). Concerning the objects with one or no Lorentz index the set of identities (4.28) extends naturally

$$\begin{aligned} P_{[ik]} \cdot P_{[lj]} &= \delta_{kl} P_{[ij]}, & P_{[ik]}^\mu \bar{P}_{[lj]}^\nu &= \delta_{kl} P_{[ij]}^{\mu\nu}, & \bar{P}_{[ik]}^\mu g_{\mu\nu} P_{[lj]}^\nu &= \delta_{kl} P_{[ij]}, \\ Q_{[ik]}^{\mu\alpha} g_{\alpha\beta} P_{[lj]}^\beta &= 0 = \bar{P}_{[ik]}^\alpha g_{\alpha\beta} Q_{[lj]}^{\beta\nu}. \end{aligned} \quad (4.29)$$

As a first application we consider the isobar propagator, $S_{\mu\nu}(w, u)$, in the nuclear medium. We will drop the index Δ in the following. From covariance we expect a general decomposition of the form,

$$S^{\mu\nu}(w, u) = \sum_{i,j=3}^8 S_{[ij]}^{(p)}(v, u) P_{[ij]}^{\mu\nu}(v, u) + \sum_{i,j=1}^2 S_{[ij]}^{(q)}(v, u) Q_{[ij]}^{\mu\nu}(v, u), \quad (4.30)$$

in terms of invariant functions, $S_{[ij]}^{(p,q)}(v, u)$, and the complete set of Dirac-Lorentz tensors $P_{[ij]}^{\mu\nu}(v, u)$ and $Q_{[ij]}^{\mu\nu}(v, u)$. For later convenience we introduce a shifted energy variable

$$v_\mu = w_\mu - \Sigma_V^N u_\mu \quad (4.31)$$

which accounts for the nucleon vector meanfield Σ_V^N . Decomposing likewise the isobar self-energy in the shifted basis

$$\Sigma^{\mu\nu}(w, u) = \sum_{i,j=3}^8 \Sigma_{[ij]}^{(p)}(v, u) P_{[ij]}^{\mu\nu}(v, u) + \sum_{i,j=1}^2 \Sigma_{[ij]}^{(q)}(v, u) Q_{[ij]}^{\mu\nu}(v, u), \quad (4.32)$$

and the bare propagator

$$S_0^{\mu\nu}(w) = \sum_{i,j=3}^8 S_{0,[ij]}^{(p)}(v, u) P_{[ij]}^{\mu\nu}(v, u) + \sum_{i,j=1}^2 S_{0,[ij]}^{(q)}(v, u) Q_{[ij]}^{\mu\nu}(v, u), \quad (4.33)$$

it is straightforward to evaluate the Dyson equation (4.4). It can be mapped onto two simple matrix equations which in compact notation read

$$\begin{aligned} S^{(p)}(v, u) &= S_0^{(p)}(v, u) \left[1 - \Sigma^{(p)}(v, u) S_0^{(p)}(v, u) \right]^{-1}, \\ S^{(q)}(v, u) &= S_0^{(q)}(v, u) \left[1 - \Sigma^{(q)}(v, u) S_0^{(q)}(v, u) \right]^{-1}, \end{aligned} \quad (4.34)$$

involving the six-dimensional matrix $\Sigma^{(p)}(v, u)$ and two-dimensional matrix $\Sigma^{(q)}(v, u)$.

Due to the projector formalism the in-medium isobar propagator as implied by the interaction vertex (4.1) at the one-loop level can be computed in a manifestly covariant fashion [22]. Since we aim at generalising the latter work towards vertex correction effects, it proves convenient to extract the isobar propagator from a corresponding model

4. Pions and Δ -isobars at finite density

for the pion-nucleon scattering amplitude. The conceptual path is already laid out in Ref. [89].

Since we want to use pion-nucleon scattering data to constrain our model we need to solve the according scattering equation. Without vertex corrections is evident that also the isobar self-energy can be computed by considering a Bethe-Salpeter scattering equation of the pion-nucleon system

$$\begin{aligned}\mathcal{T}(\bar{k}, k; w, u) &= \mathcal{V}(\bar{k}, k; w, u) + \int \frac{d^4l}{(2\pi)^4} \mathcal{V}(\bar{k}, l; w, u) \mathcal{G}(l; w, u) \mathcal{T}(l, k; w, u), \\ \mathcal{G}(\frac{1}{2}w - l; w, u) &= -i S_N(w - l, u) \left[l^2 - m_\pi^2 - \Pi_\pi(l, u) \right]^{-1},\end{aligned}\quad (4.35)$$

where q, p, \bar{q}, \bar{p} are the initial and final pion and nucleon 4-momenta and

$$w = p + q = \bar{p} + \bar{q}, \quad k = \frac{1}{2}(p - q), \quad \bar{k} = \frac{1}{2}(\bar{p} - \bar{q}). \quad (4.36)$$

The two-particle propagator, $\mathcal{G}(l; w, u)$, is specified in terms of the free nucleon propagator (4.9), and the pion propagator written in terms of the in-medium self-energy $\Pi_\pi(l, u)$ of (4.17). The latter will be determined self-consistently based on the interaction (4.1, 4.3). This generalises the study of [29].

In order to generate the isobar self-energy $\Sigma^{\mu\nu}(w, u)$, we introduce the interaction kernel

$$\mathcal{V}(\bar{k}, k; w, u) = -\frac{f_\Delta^2}{m_\pi^2} \bar{q}_\mu S_0^{\mu\nu}(w - \Sigma_V^\Delta u) q_\nu, \quad (4.37)$$

where we allow for the presence of a vector mean field Σ_V^Δ . The isospin projector $P_{I=\frac{3}{2}}$ is suppressed in (4.37) (see e.g. [20]). The particular choice (4.37) implies a scattering amplitude, which determines the isobar propagator, $S_{\mu\nu}(w, u)$, by

$$\mathcal{T}(\bar{k}, k; w, u) = -\frac{f_\Delta^2}{m_\pi^2} \bar{q}_\mu S^{\mu\nu}(w, u) q_\nu. \quad (4.38)$$

The system is solved conveniently by decomposing the interaction kernel into a set of projectors based on the shifted 4-momentum $v_\mu = w_\mu - \Sigma_V^N u_\mu$:

$$\mathcal{V} = \sum_{i,j=3}^8 V_{[ij]}^{(p)}(v, u) \bar{q}_\mu P_{[ij]}^{\mu\nu}(v, u) q_\nu + \sum_{i,j=1}^2 V_{[ij]}^{(q)}(v, u) \bar{q}_\mu Q_{[ij]}^{\mu\nu}(v, u) q_\nu. \quad (4.39)$$

For the general case with $\Sigma_V^\Delta \neq \Sigma_V^N$ the derivation of $V_{[ij]}^{(p,q)}(v, u)$ as implied by (4.37) is somewhat tedious though straight forward to derive. The expressions are listed in

Appendix H. In the limit $\Sigma_V^\Delta \rightarrow \Sigma_V^N$ the expressions simplify with:

$$\begin{aligned}
 V_{[11]}^{(q)} = V_{[77]}^{(p)} &= + \frac{f_\Delta^2}{m_\pi^2} \frac{1}{\sqrt{v^2} - m_\Delta}, & V_{[22]}^{(q)} = V_{[88]}^{(p)} &= - \frac{f_\Delta^2}{m_\pi^2} \frac{1}{\sqrt{v^2} + m_\Delta}, \\
 V_{[55]}^{(p)} &= - \frac{2}{3} \frac{f_\Delta^2}{m_\pi^2} \frac{\sqrt{v^2} + m_\Delta}{m_\Delta^2} - \frac{1}{3} \frac{f_\Delta^2}{m_\pi^2} \frac{1}{m_\Delta} \left[\frac{\sqrt{v^2}}{2 m_\Delta} Z (Z - 4) - Z (Z - 1) \right], \\
 V_{[66]}^{(p)} &= + \frac{2}{3} \frac{f_\Delta^2}{m_\pi^2} \frac{\sqrt{v^2} - m_\Delta}{m_\Delta^2} + \frac{1}{3} \frac{f_\Delta^2}{m_\pi^2} \frac{1}{m_\Delta} \left[\frac{\sqrt{v^2}}{2 m_\Delta} Z (Z - 4) + Z (Z - 1) \right], \\
 V_{[53]}^{(p)} = V_{[35]}^{(p)} &= + \frac{1}{\sqrt{3}} \frac{f_\Delta^2}{m_\pi^2} \frac{1}{m_\Delta} \left[1 - \frac{\sqrt{v^2}}{2 m_\Delta} Z (Z - 2) + Z (Z - 1) \right], \\
 V_{[64]}^{(p)} = V_{[46]}^{(p)} &= - \frac{1}{\sqrt{3}} \frac{f_\Delta^2}{m_\pi^2} \frac{1}{m_\Delta} \left[1 + \frac{\sqrt{v^2}}{2 m_\Delta} Z (Z - 2) + Z (Z - 1) \right], \\
 V_{[33]}^{(p)} &= - \frac{f_\Delta^2}{m_\pi^2} \frac{Z}{m_\Delta} \left[\frac{\sqrt{v^2}}{2 m_\Delta} Z - (Z - 1) \right], \\
 V_{[44]}^{(p)} &= + \frac{f_\Delta^2}{m_\pi^2} \frac{Z}{m_\Delta} \left[\frac{\sqrt{v^2}}{2 m_\Delta} Z + (Z - 1) \right], \tag{4.40}
 \end{aligned}$$

where only non-zero components are specified. A corresponding decomposition is implied for the in-medium scattering amplitude

$$\begin{aligned}
 \mathcal{T} &= \sum_{i,j=3}^8 T_{[ij]}^{(p)}(v, u) \bar{q}_\mu P_{[ij]}^{\mu\nu}(v, u) q_\nu + \sum_{i,j=1}^2 T_{[ij]}^{(q)}(v, u) \bar{q}_\mu Q_{[ij]}^{\mu\nu}(v, u) q_\nu, \\
 T^{(p)}(v, u) &= V^{(p)}(v, u) \left[1 - J^{(p)}(v, u) V^{(p)}(v, u) \right]^{-1}, \\
 T^{(q)}(v, u) &= V^{(q)}(v, u) \left[1 - J^{(q)}(v, u) V^{(q)}(v, u) \right]^{-1}. \tag{4.41}
 \end{aligned}$$

The scattering amplitude \mathcal{T} is determined by the interaction kernel (4.40) and two matrices of loop functions $J_{[ij]}^{(p)}(v, u)$ and $J_{[ij]}^{(q)}(v, u)$. Comparing (4.41) with (4.37) and (4.34) we identify

$$\Sigma_{[ij]}^{(p)}(v, u) = - \frac{f_\Delta^2}{m_\pi^2} J_{[ij]}^{(p)}(v, u), \quad \Sigma_{[ij]}^{(q)}(v, u) = - \frac{f_\Delta^2}{m_\pi^2} J_{[ij]}^{(q)}(v, u). \tag{4.42}$$

The evaluation of the real parts of the loop functions requires great care. The imaginary parts of the loop functions, $\Delta J_{[ij]}^{(p,q)}(w_0, \vec{w})$, behave like w_0^n for large w_0 with n not always smaller or equal to zero. Thus power divergencies arise if the real parts are evaluated by means of an unsubtracted dispersion-integral ansatz. The task is to devise a subtraction scheme that eliminates all the power divergent terms systematically. The latter are unphysical and in a consistent effective field theory approach must be absorbed into counter terms. Only the residual strength of the counter terms may be estimated by a naturalness assumption reliably. Since we want to neglect such counter terms

4. Pions and Δ -isobars at finite density

it is crucial to set up the renormalisation in a proper manner. We suggest [88] to introduce a subtraction scheme that in the free-space limit recovers the loop functions as renormalised in [90]. There the representation was motivated by properties of the loop functions manifest within dimensional regularisation [90]. Its form follows from the Passarino Veltman representation [91] supplemented by a subtraction of reduced tadpole contributions [90].

The loop functions $J_{[ij]}^{(p,q)}(w_0, \vec{w})$ are expressed in terms of a basis spanned by 13 master loop functions, $J_n^{(p,q)}(w_0, \vec{w})$ as detailed in Appendix I. However the renormalisation procedure has also to comply with the behaviour of the projectors used in the decomposition. These projectors are singular at $v^2 = 0$ and $(u \cdot v) = v^2$ which imposes a certain behaviour of the coefficient functions. A careful consideration of the projector properties leads to the requirements

$$\begin{aligned}
J_1 + \frac{(v \cdot u)}{\sqrt{(v \cdot u)^2}} J_2 &= \mathcal{O}(\sqrt{v^2}) , \\
J_4 + J_5 + 2 \frac{(v \cdot u)}{\sqrt{(v \cdot u)^2}} J_6 &= \mathcal{O}(\sqrt{v^2}) , \\
J_7 + \frac{(v \cdot u)}{\sqrt{(v \cdot u)^2}} J_8 &= \mathcal{O}(\sqrt{v^2}) , \\
J_{10} + J_{11} + 2 \frac{(v \cdot u)}{\sqrt{(v \cdot u)^2}} J_{12} &= \mathcal{O}(\sqrt{v^2}) , \\
\frac{(v \cdot u)}{\sqrt{(v \cdot u)^2}} J_9 + 3 J_{10} + J_{11} + 3 \frac{(v \cdot u)}{\sqrt{(v \cdot u)^2}} J_{12} &= \mathcal{O}(v^2) , \tag{4.43}
\end{aligned}$$

which have to be fulfilled at $v^2 = 0$ and

$$J_2 = J_3 + J_5 = J_6 = J_8 = J_7 + J_{12} = 0 \tag{4.44}$$

needed at $v^2 = (u \cdot v)^2$.

Let us begin the consideration with the vacuum case which proves much easier than the in-medium calculation. Here the 13 basis loops are given by

$$\begin{aligned}
J_i(v, u) &\xrightarrow{\rho=0} N_i(v, u) \int_0^\infty \frac{d\bar{v}^2 v^2}{\pi \bar{v}^2 \bar{v}^2 - v^2 - i\epsilon} \rho(\bar{v}) \\
&+ \Delta_i^{(4)}(v) \int_0^\infty \frac{d\bar{v}^2}{\pi} \left(\frac{v^2}{\bar{v}^2}\right)^2 \rho(\bar{v}) + \Delta_i^{(6)}(v) \int_0^\infty \frac{d\bar{v}^2}{\pi} \left(\frac{v^2}{\bar{v}^2}\right)^3 \rho(\bar{v}), \tag{4.45}
\end{aligned}$$

with

$$\begin{aligned}
 \rho(v) &= \frac{\Theta\left[v^2 - (m_N + m_\pi)^2\right]}{16 \pi \sqrt{v^2}} \sqrt{v^2 - 2(m_N^2 + m_\pi^2) + \frac{(m_N^2 - m_\pi^2)^2}{v^2}}, \\
 N_0 &= 1, \quad N_1 = \frac{v^2 + m_N^2 - m_\pi^2}{2\sqrt{v^2}}, \quad N_2 = N_6 = N_8 = 0, \\
 N_3 &= -N_5 = -\frac{[(m_N - m_\pi)^2 - v^2][(m_N + m_\pi)^2 - v^2]}{12 v^2}, \quad N_4 = N_1^2 \\
 N_7 &= -N_{12} = N_1 N_3, \quad N_9 = N_1^3, \quad N_{10} = N_{11} = 0. \\
 \Delta_3^{(4)} &= -\Delta_5^{(4)} = \frac{(m_N^2 - m_\pi^2)^2}{3(v^2)^2}, \quad \Delta_9^{(4)} = -\frac{1}{8} \frac{(m_N^2 - m_\pi^2)^3}{\sqrt{v^2}^5} \\
 \Delta_7^{(4)} &= -\Delta_{12}^{(4)} = -\left(\frac{N_1}{12} - \frac{N_1 N_5}{v^2} - \frac{(m_N^2 - m_\pi^2)^2}{8\sqrt{v^2}^3}\right) \\
 \Delta_7^{(6)} &= -\Delta_{12}^{(6)} = \left(\frac{(m_N^2 - m_\pi^2)^2 N_1}{12(v^2)^2} + \frac{(m_N^2 - m_\pi^2)^2}{8\sqrt{v^2}^3} + \frac{(m_N^2 - m_\pi^2)^3}{24\sqrt{v^2}^5}\right). \quad (4.46)
 \end{aligned}$$

The higher order subtractions $\Delta_i^{(j)}$ are to enforce the kinematical constraints² (4.43,4.44). However the energy dependence of these additional terms is trivial because it is given by the $(v^2)^n$ factor from the subtraction and the energy dependence of the $\Delta_j^{(i)}(v^2)$ only. In contrast to this the first term in (4.45) shows a more complicated structure. One has to note that the constraints (4.43,4.44) do not require that the loops are finite at the lightcone or at $v^2 = (u \cdot v)^2$. As long as (4.43) and (4.44) are fulfilled we will always get singularity free results.

For the in-medium case the situation becomes even more involved because we have to define the additional loops which are zero in vacuum³. Guided from the approach in vacuum we also make an ansatz with terms including at most one subtraction in v^2/\bar{v}^2 and a remainder term

$$J_n(v_0, \vec{w}) = \int_{-\infty}^{+\infty} \frac{d\bar{v}_0}{\pi} \frac{\Delta J_n(\bar{v}_0; v_0, \vec{w})}{\bar{v}_0 - v_0 - i\epsilon(\bar{v}_0 - \mu)} + J_n^C(v_0, \vec{w}), \quad (4.47)$$

where we introduce spectral weight functions, $\Delta J_n(v_0, \bar{v}_0, \vec{w})$, that depend on 'external'

²As a more simple cure one could try to cut out the singularities by restricting all $S_{[ij]}^{(p,q)}$ to the region $v^2 \geq m^2$ with some $m \geq 0$. However this has the disadvantage that when using vector meanfields of about 300 MeV the main mode of the Δ -isobar will be chopped off for higher momenta making the influence of this cut rather high.

³In principal one could use the technique as for the vector-meson case (3.41) and use the trick of converting to a singularity free basis in order to deal with the kinematical singularities. However the fact that we need to define some loops which are zero in vacuum makes this approach inefficient.

4. Pions and Δ -isobars at finite density

and 'internal' energies $v_0 = w_0 - \Sigma_V^N$ and \bar{v}_0 . We identify

$$\begin{aligned} \Delta J_n(\bar{v}_0; v_0, \vec{w}) &= \int \frac{d^3l}{2(2\pi)^3} \left(m_N^2 + \vec{l}^2\right)^{-\frac{1}{2}} \\ &\times \left\{ K_n(l_+, \bar{v}_0; v_0, \vec{w}) A_\pi(|\bar{v}_+|, \vec{w} - \vec{l}) \left[\Theta(+\bar{v}_+) - \Theta(k_F - |\vec{l}|) \right] \right. \\ &\quad \left. + K_n(l_-, \bar{v}_0; v_0, \vec{w}) A_\pi(|\bar{v}_-|, \vec{w} - \vec{l}) \Theta(-\bar{v}_-) \right\}, \\ l_\pm^\mu &= (\pm \sqrt{m_N^2 + \vec{l}^2}, \vec{l}), \quad \bar{v}_\pm = \bar{v}_0 \mp \sqrt{m_N^2 + \vec{l}^2}, \end{aligned} \quad (4.48)$$

Here the pion spectral function A_π is defined as the imaginary part of the corresponding propagator (4.5)

$$\begin{aligned} A_\pi(\omega, \vec{q}) &= -\Im \frac{1}{\omega^2 - \vec{q}^2 - m_\pi^2 - \Pi_\pi(\omega, \vec{q})} \quad \text{for } \omega > 0, \\ A_\pi(-\omega, \vec{q}) &= -A_\pi(\omega, \vec{q}), \end{aligned} \quad (4.49)$$

including the self-energy computed in the previous section (4.17). The subtraction terms, $J_i^C(v, u)$, of (4.47) are determined (see Appendix I) by the coefficients,

$$\begin{aligned} \bar{C}_{a,n}^{ijk}(\vec{w}) &= \int_{-\infty}^{+\infty} \frac{d\bar{v}_0}{\pi} \int \frac{d^3l}{2(2\pi)^3} \left((m_N - \Sigma_S)^2 + \vec{l}^2 \right)^{-\frac{1}{2}} \\ &\times \left\{ (\bar{v} \cdot u)^a \frac{(\bar{l}_\pm \cdot \bar{v})^i (\bar{l}_\pm \cdot u)^j (\bar{l}_\pm^2)^k}{(\bar{v}^2)^n} A_\pi(\bar{v}_+, \vec{w} - \vec{l}) \left[\Theta(+\bar{v}_+) - \Theta(k_F - |\vec{l}|) \right] \right. \\ &\quad \left. + (\bar{v} \cdot u)^a \frac{(\bar{l}_\pm \cdot \bar{v})^i (\bar{l}_\pm \cdot u)^j (\bar{l}_\pm^2)^k}{(\bar{v}^2)^n} A_\pi(\bar{v}_-, \vec{w} - \vec{l}) \Theta(-\bar{v}_-) \right\}, \\ \bar{l}_\pm^\mu &= l_\pm^\mu - \frac{1}{2} \bar{v}^\mu, \quad \bar{v}^2 = (\bar{v} \cdot u)^2 - (v \cdot u)^2 + v^2, \quad u^\mu = (1, \vec{0}), \end{aligned} \quad (4.50)$$

expanded up to second order

$$C_{a,n}^{ijk}(\vec{w}) = \bar{C}_{a,n}^{ijk}(0) + \frac{1}{2} \vec{w}^2 (\nabla_{\vec{w}} \cdot \nabla_{\vec{w}}) \bar{C}_{a,n}^{ijk}(0), \quad (4.51)$$

(see Appendix I and tabular I.1). Note that similar as in the vacuum case the higher subtraction terms have trivial energy dependence given by the external energy variable only. In addition the $\bar{C}_{a,n}^{ijk}(\vec{w})$ become constant numbers in the vacuum limit. Even though we could also fulfill all requirements (4.43, 4.44) by defining the subtractions $J_i^C(v, u)$ directly in terms of the $\bar{C}_{a,n}^{ijk}(\vec{w})$ we have to use the expanded ones for several reasons. First of all the interpretation of the J_i^C as counter terms requires a polynomial behaviour which is automatically imposed by (4.51). In contrast to this the use of $\bar{C}_{a,n}^{ijk}(\vec{w})$ in the $J_i^C(v, u)$ terms leads to additional, unwanted, structures. Secondly we have to state that the integrals for the higher order subtraction are strictly speaking not defined as soon as the imaginary part gets support at the lightcone. At zero temperature this causes no problems when using the expanded version because the support of

the imaginary part on the lightcone is always zero for reasonable small momenta and meanfields. The situation is different at finite temperature where different prescriptions have to be used (see Appendix I).

4.3.3. Isobar self-energy in the presence of vertex corrections

The evaluation of the delta self-energy in the presence of vertex corrections

$$\Sigma_{\Delta}^{\mu\nu} = \text{diagram 1} + \text{diagram 2} + \text{diagram 3}, \quad (4.52)$$

requires several modifications of the formulas used so far. This is due to the fact that the third contribution to the self-energy in (4.52) can't be generated by a πN scattering equation like in the previous section and we have to consider the Dyson-equation directly. Still it is useful to identify a set of master loop functions, in terms of which the full loop matrix can be constructed. The latter are renormalised applying the scheme introduced in the previous section. The proper generalisation of (4.48) is readily worked out. The pion spectral function, distorted by vertex correction functions, leads to effective spectral densities, which we denote with $A_{\pi}^{ab}(\omega, \vec{q})$. For a given spectral distribution we introduce

$$\begin{aligned} \Delta J_{ab,n}(\bar{v}_0; v_0, \vec{w}) &= \int \frac{d^3l}{2(2\pi)^3} \left(m_N^2 + \vec{l}^2\right)^{-\frac{1}{2}} \\ &\times \left\{ K_n(l_+, \bar{v}_0; v_0, \vec{w}) A_{\pi}^{ab}(|\bar{v}_+|, \vec{w} - \vec{l}) \left[\Theta(+\bar{v}_+) - \left(\frac{\bar{v}_+}{|\bar{v}_+|}\right)^{a+b} \Theta(k_F - |\vec{l}|) \right] \right. \\ &\left. + \left(\frac{\bar{v}_-}{|\bar{v}_-|}\right)^{a+b} K_n(l_-, \bar{v}_0; v_0, \vec{w}) A_{\pi}^{ab}(|\bar{v}_-|, \vec{w} - \vec{l}) \Theta(-\bar{v}_-) \right\}, \\ l_{\pm}^{\mu} &= (\pm \sqrt{m_N^2 + \vec{l}^2}, \vec{l}), \quad \bar{v}_{\pm} = \bar{v}_0 \mp \sqrt{m_N^2 + \vec{l}^2}, \end{aligned} \quad (4.53)$$

where $n = 0, \dots, 12$. The kernels $K_n(l, \bar{v}_0; v_0, \vec{w})$ are identical to those encountered in (4.48). They are listed in Appendix I. The real part of the loop functions is computed applying the dispersion-integral representation (4.47). A corresponding generalisation holds for the second term in (4.47).

We identify the effective spectral distributions, $A_{\pi}^{ab}(\omega, \vec{q})$ as implied by the diagrams (4.52). The vertex vector and tensor may be decomposed into invariants

$$\begin{aligned} \Gamma_{\mu}^{(\Delta N)}(q, u) &= q_{\mu} \Gamma_1^{(\Delta N)}(q, u) + u_{\mu} \Gamma_2^{(\Delta N)}(q, u), \\ \Gamma_{\mu\nu}^{(\Delta N)}(q, u) &= q_{\mu} q_{\nu} \bar{\Gamma}_{11}^{(\Delta N)}(q, u) + q_{\mu} u_{\nu} \bar{\Gamma}_{12}^{(\Delta N)}(q, u) + u_{\mu} q_{\nu} \bar{\Gamma}_{12}^{(\Delta N)}(q, u) \\ &\quad + u_{\mu} u_{\nu} \bar{\Gamma}_{22}^{(\Delta N)}(q, u) + g_{\mu\nu} \bar{\Gamma}_{00}^{(\Delta N)}(q, u), \end{aligned} \quad (4.54)$$

4. Pions and Δ -isobars at finite density

in terms of which we introduce the spectral distributions

$$A_\pi^{00}(\omega, \vec{q}) = -\Im \left(\bar{\Gamma}_{00}^{(\Delta N)}(\omega, \vec{q}) \right),$$

$$A_\pi^{ab}(\omega, \vec{q}) = -\Im \left(\frac{\Gamma_a^{(\Delta N)}(\omega, \vec{q}) \Gamma_b^{(\Delta N)}(\omega, \vec{q})}{\omega^2 - \vec{q}^2 - m_\pi^2 - \Pi_\pi(\omega, \vec{q})} + \bar{\Gamma}_{ab}^{(\Delta N)}(\omega, \vec{q}) \right). \quad (4.55)$$

where the vertex vectors $\Gamma_i^{(\Delta h)}$ are defined in (4.24). The explicit form of the tensor vertex

$$\begin{aligned} \bar{\Gamma}_{11}(q, u) &= -\frac{1}{q^2} \left(\Gamma_{11}^{(\Delta h)} + \frac{q \cdot u}{\sqrt{q^2 - (q \cdot u)^2}} (\Gamma_{12}^{(\Delta h)} + \Gamma_{21}^{(\Delta h)}) \right. \\ &\quad \left. + \frac{(q \cdot u)^2}{q^2 - (q \cdot u)^2} \Gamma_{22}^{(\Delta h)} - \frac{q^2}{q^2 - (q \cdot u)^2} \Gamma_T^{(\Delta h)} \right), \\ \bar{\Gamma}_{12}(q, u) &= \Gamma_{21}(q, u) = \frac{1}{\sqrt{q^2 - (q \cdot u)^2}} \Gamma_{12}^{(\Delta h)} + \frac{q \cdot u}{q^2 - (q \cdot u)^2} (\Gamma_{22}^{(\Delta h)} - \Gamma_T^{(\Delta h)}), \\ \bar{\Gamma}_{22}(q, u) &= -\frac{q^2}{q^2 - (q \cdot u)^2} (\Gamma_{22}^{(\Delta h)} - \Gamma_T^{(\Delta h)}), \quad \bar{\Gamma}_{00}(q, u) = -\Gamma_T^{(\Delta h)}, \end{aligned} \quad (4.56)$$

is given in terms of the longitudinal and transverse correlation functions $\Gamma_{ij}^{(\Delta h)}$ specified previously (4.20).

It is left to specify the isobar self energy in terms of the generic loop functions defined by (4.53). In a first step a matrix of loop functions, $J_{ab,[ij]}^{(p,q)}(v, u)$, is constructed in terms of $J_{ab,n}(v, u)$ as detailed in Appendix I. The evaluation of the self energy is analogous to the computation in the previous section with the complication that the effective vertex develops additional structures $q_\mu u_\mu + u_\mu q_\nu$, $u_\mu u_\nu$ and $g_{\mu\nu}$. The loops $J_{11,[ij]}^{(p,q)}(v, u)$, which are implied by the structure $q_\mu q_\nu$, contribute like the previous loops $J_{[ij]}^{(p,q)}(v, u)$ in (4.42). The remaining loop functions are readily worked out through the useful identities

$$\begin{aligned} u^\mu &= -i \sqrt{\frac{2}{3}} \sqrt{\frac{(v \cdot u)^2}{v^2} - 1} \left\{ \bar{P}_{[17]}^\mu + \bar{P}_{[28]}^\mu - \frac{1}{\sqrt{2}} (\bar{P}_{[14]}^\mu + \bar{P}_{[23]}^\mu) \right\} \\ &\quad + \frac{v \cdot u}{\sqrt{v^2}} (\bar{P}_{[15]}^\mu + \bar{P}_{[26]}^\mu) \\ &= -i \sqrt{\frac{2}{3}} \sqrt{\frac{(v \cdot u)^2}{v^2} - 1} \left\{ P_{[71]}^\mu + P_{[82]}^\mu - \frac{1}{\sqrt{2}} (P_{[41]}^\mu + P_{[32]}^\mu) \right\} \\ &\quad + \frac{v \cdot u}{\sqrt{v^2}} (P_{[51]}^\mu + P_{[62]}^\mu), \\ g^{\mu\nu} P_{[11]} &= Q_{[11]}^{\mu\nu} + P_{[44]}^{\mu\nu} + P_{[55]}^{\mu\nu} + P_{[77]}^{\mu\nu}, \\ g^{\mu\nu} P_{[22]} &= Q_{[22]}^{\mu\nu} + P_{[33]}^{\mu\nu} + P_{[66]}^{\mu\nu} + P_{[88]}^{\mu\nu}, \\ g^{\mu\nu} P_{[12]} &= Q_{[12]}^{\mu\nu} - \frac{1}{3} P_{[43]}^{\mu\nu} + P_{[56]}^{\mu\nu} + \frac{1}{3} P_{[78]}^{\mu\nu} - \frac{\sqrt{8}}{3} (P_{[73]}^{\mu\nu} + P_{[48]}^{\mu\nu}), \\ g^{\mu\nu} P_{[21]} &= Q_{[21]}^{\mu\nu} - \frac{1}{3} P_{[34]}^{\mu\nu} + P_{[65]}^{\mu\nu} + \frac{1}{3} P_{[87]}^{\mu\nu} - \frac{\sqrt{8}}{3} (P_{[84]}^{\mu\nu} + P_{[37]}^{\mu\nu}). \end{aligned} \quad (4.57)$$

It is now straight forward to write down the self energies, $\Sigma_{[ij]}^{(p,q)}(v, u)$, as

$$\begin{aligned}
 \Sigma_{[ij]}^{(q)}(v, u) &= -\frac{f_\Delta^2}{m_\pi^2} \left\{ J_{11,[ij]}^{(q)}(v, u) + J_{00,[ij]}^{(p)}(v, u) \right\}, \\
 \Sigma_{[ij]}^{(p)}(v, u) &= -\frac{f_\Delta^2}{m_\pi^2} \left\{ J_{11,[ij]}^{(p)}(v, u) + \sum_{a,b=1}^2 J_{22,[ab]}^{(p)}(v, u) c_{ai}(v, u) c_{bj}(v, u) \right. \\
 &\quad + \sum_{a=1}^2 \left(J_{12,[ia]}^{(p)}(v, u) c_{aj}(v, u) + J_{21,[aj]}^{(p)}(v, u) c_{ai}(v, u) \right) \\
 &\quad \left. + \sum_{a,b=1}^2 J_{00,[ab]}^{(p)}(v, u) c_{[ij]}^{(ab)}(v, u) \right\}, \\
 c_{aj}(v, u) &= \frac{v \cdot u}{\sqrt{v^2}} \delta_{4+a,j} - i \sqrt{\frac{2}{3}} \sqrt{\frac{(v \cdot u)^2}{v^2} - 1} \left(\delta_{6+a,j} - \frac{1}{\sqrt{2}} \delta_{5-a,j} \right), \\
 c_{[ij]}^{(ab)}(v, u) &= \delta_{a1} \delta_{b2} \left(\frac{1}{3} (\delta_{i7} \delta_{j8} - \delta_{i4} \delta_{j3}) + \delta_{i5} \delta_{j6} - \frac{\sqrt{8}}{3} (\delta_{i7} \delta_{j3} + \delta_{i4} \delta_{j8}) \right) \\
 &\quad + \delta_{ab} \delta_{ij} \left(\delta_{i,5-a} + \delta_{i,4+a} + \delta_{i,6+a} \right) \\
 &\quad + \delta_{a2} \delta_{b1} \left(\frac{1}{3} (\delta_{i8} \delta_{j7} - \delta_{i3} \delta_{j4}) + \delta_{i6} \delta_{j5} - \frac{\sqrt{8}}{3} (\delta_{i3} \delta_{j7} + \delta_{i8} \delta_{j4}) \right) \quad (4.58)
 \end{aligned}$$

with coefficients $c_{[ij]}^{(ab)}$ given in Appendix L.

4.4. Determination of the parameters

We now turn to the determination of the model parameters. The coupling constants f_Δ , f_N and f_γ as well as the values for the mean-fields used for the Delta isobar and the Migdal parameters g'_{ij} will be determined from both, scattering as well as photo absorption data.

For the scalar and vector mean fields of the nucleon we use the simple parametrisations

$$\Sigma_V^N = 280 \frac{\rho}{\rho_0} \text{ MeV}, \quad m_N = 939 \text{ MeV} + \Sigma_S^N \quad \Sigma_S^N = -350 \frac{\rho}{\rho_0} \text{ MeV}, \quad (4.59)$$

as a quite conservative estimate [92–96]. The corresponding mean-fields of the Δ -isobar will be adjusted together with the parameters g'_{ij} to nuclear photo absorption data.

The phenomenological relevance of the Z parameter in the definition of the isobar propagator was discussed in [97]. A value of $Z \simeq 0.72$ was suggested in [90] based on an analysis of pion- and kaon-nucleon scattering data.

In (4.17) we allowed for a background term linear in the nuclear density reflecting an s-wave pion-nucleon interaction. Such a term is required to compensate for the fact

4. Pions and Δ -isobars at finite density

that the vertices of (4.1) lead to a pion-nucleon isospin averaged scattering length of the form [90],

$$4\pi \left(1 + \frac{m_\pi}{m_N}\right) a_{\pi N} = -\frac{f_N^2}{m_N} - \frac{4}{9} \frac{f_\Delta^2}{m_\Delta} (2 - Z) \left(1 + Z + (2 - Z) \frac{m_N}{2m_\Delta}\right). \quad (4.60)$$

For $Z = 0$ this would lead to $a_{\pi N} \simeq -0.09$ fm and thus to a significant overestimation of the empirical scattering length of about -0.01 fm [90]. In order to improve on the s-wave part of our model we subtract that large term by identifying $b_{\text{eff}} \simeq 0.08$ fm in (4.17). The dependence of b_{eff} on $|Z| < 1$ is moderate. At $Z \simeq 0.72$, the value suggested in [90], it follows $b_{\text{eff}} \simeq 0.06$ fm.

The evaluation of the parameters for the pionic modes requires some care. Complications arise here due to different reasons. First we will see that a proper fit of the πN scattering amplitude requires more care than in the case of the $\pi\pi$ scattering used for the ρ -meson because u -channel contributions prove to be relevant at least close to threshold.

As a second point we have to keep in mind that since we would like to determine the Migdal parameters and mean-fields from photo absorption on the nucleus our vacuum model has to comply with the data for the same process on the nucleon. Here the only additional parameter is f_γ which however can only give rise to an overall factor in the photo absorption. Thus our model for the scattering amplitude has to give the right shape needed for the description of the photo absorption data without further tuning.

4.4.1. Vacuum scattering amplitude

For the adjustment of the πN scattering amplitude we compare our results with the empirical scattering amplitude as extracted from phase shifts [20, 98]. Since it is known [20] that u -channel effects are important in the threshold region we study these contributions on a perturbative level. Thus besides the s-channel isobar pole diagram

$$T_{\pi N}^{(\frac{3}{2}, +)} = \left[\text{Diagram} \right]_{\frac{3}{2} \frac{3}{2}} \quad (4.61)$$

which contributes to the πN scattering amplitude in the spin $3/2$ isospin $3/2$ channel $T_{\pi N}^{(\frac{3}{2}, +)}$ we also study the u -channel contributions

$$\left[\text{Diagram 1} + \text{Diagram 2} \right]_{\frac{3}{2} \frac{3}{2}} \quad (4.62)$$

resulting from the nucleon⁴ and isobar u -channel pole diagram. Details are given in Appendix M. These additional contributions solely modify the real part of the scattering amplitude. To get a feeling about possible changes in the imaginary part one can calculate the first iteration in the u -channel showing that also an improvement of the imaginary part close to threshold is possible. However since the scattering amplitude close to threshold is dominated by the real part we neglect these effects on the imaginary part in the following. The included diagrams give the lowest order in the modification of the scattering amplitude due to u -channel contributions and thus an estimate about possible effects. Since we only need the contribution to the P_{33} amplitude it is convenient to use a projection of these diagrams on the required spin and isospin $3/2$ channel. A convenient projector basis using projectors with good angular momentum has already been introduced in [90]. Such projectors allow to decompose the vacuum scattering amplitude into it's partial waves

$$\mathcal{T}(\bar{k}, k; w) = \sum_{n=0}^{\infty} (M_n^{(+)}(\sqrt{s}) Y_n^{(+)}(\bar{q}, q; w) + M_n^{(-)}(\sqrt{s}) Y_n^{(-)}(\bar{q}, q; w)) \quad (4.63)$$

For our case the relevant $J = 3/2$ projector is given by

$$Y_1^{(+)} = -3 \bar{q}_\mu \left(P_{[77]}^{\mu\nu}(w) + Q_{[11]}^{\mu\nu}(w) \right) q_\nu. \quad (4.64)$$

From our decomposition of the scattering amplitude (4.35) we read of

$$M_1^{(+)}(\sqrt{s}) = -3 \frac{f_\Delta^2}{m_\pi^2} S_{[77]}^{(p)} = -3 \frac{f_\Delta^2}{m_\pi^2} S_{[11]}^{(q)} \quad (4.65)$$

and can directly take our vacuum results for the Δ -propagator to determine the contribution of the s-channel diagram. The determination of the coefficient function in case of the u -channel diagrams can be done along the same lines. We therefore first decompose the scattering amplitude into the given projectors P^\pm

$$K_{u,\pi N}^{(x)}(\bar{p}, p; w) = K_{\pi N}^{(x,+)} P^+ + K_{\pi N}^{(x,-)} P^- \quad (4.66)$$

where $x \in \{N, \Delta\}$ and then project onto the required channel

$$M_1^{(x,+)}(\sqrt{s}) = \int \frac{dz}{2} \frac{K_{\pi N}^{(x,+)}(s, u)}{p_{\pi N}^2} P_1(z) + \int \frac{dz}{2} \frac{(E_N - m_N)^2}{p_{\pi N}^4} K_{\pi N}^{(x,-)}(s, u) P_2(z) \quad (4.67)$$

where P_1 and P_2 are the first and second Legendre polynomials. For the vacuum case the kinematics yields

$$\begin{aligned} p_{\pi N}^2 &= \frac{s + m_\pi^2 - m_N^2}{2\sqrt{s}} - m_\pi^2 & E_N &= \sqrt{s} - \frac{s + m_\pi^2 - m_N^2}{2\sqrt{s}} \\ u &= 2m_N^2 + 2m_\pi^2 + 2p_{\pi N}^2(1-z) - \sqrt{s}. \end{aligned} \quad (4.68)$$

⁴The nucleon s-channel diagram does not contribute in the partial wave studied here.

4. Pions and Δ -isobars at finite density

The interaction kernels $K_{\pi N}^{(x,\pm)}$ are derived in Appendix M. Within this scheme we can now determine the scattering amplitude resulting from our model. In order to reproduce the available data [98] we allow for a phenomenological dependence⁵ of the isobar mass on $s = \sqrt{w^2}$, i.e.

$$m_{\Delta} = m_{\Delta}^{vac}(\sqrt{w^2}) + \Sigma_S^{\Delta}. \quad (4.69)$$

The result is given by the dashed line in Fig. 4.4.1. In a fully consistent treatment this energy dependence would have to vanish. In contrast to this we find a large variation which could reflect the influence of left-handed branch points on the P33 amplitude.

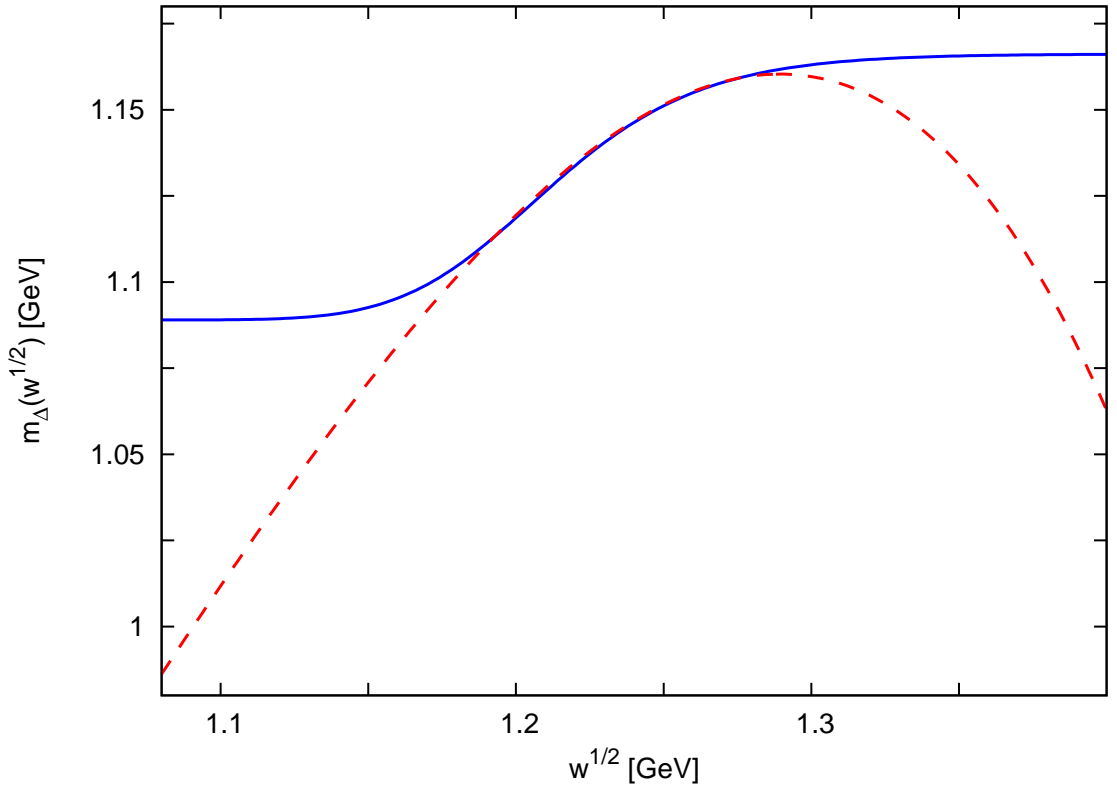


Figure 4.1.: Effective mass $m_{\Delta}^{vac}(\sqrt{w^2})$ of the Delta isobar. The dashed function leads to an exact reproduction of the amplitude while the full one, used in the calculations, only results in an approximation.

Thus a fully consistent calculation which would reproduce the amplitude much better,

⁵This treatment might lead to additional poles in the complex plain and thus to ghost states. Their contribution can be estimated from the analytic properties of the propagator and turn out to be small.

meaning with a much smaller variation of the mass function, would at least require the unitarisation of the sum of s-channel isobar and u-channel nucleon exchange processes. This however is beyond the scope of this work. In order to correct for the presence of such processes we include a phenomenological mass function determined by fitting the imaginary part of the amplitude in the resonance region only. Outside the resonance region we let the effective mass become a constant, full line in Fig. 4.4.1. While having a much smaller variation than the exactly required mass function this phenomenological mass function reproduces the empirical amplitude still quite well. Significant deviations are only seen close to threshold where we expect the largest influence from u-channel contributions.

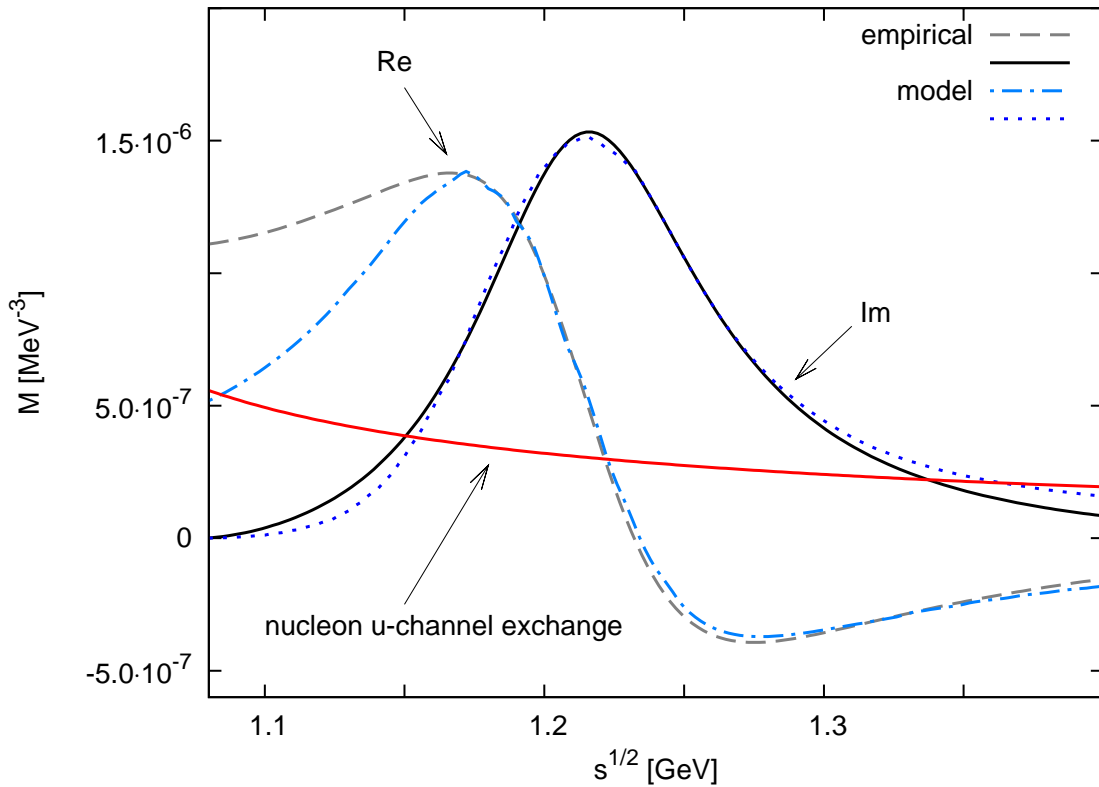
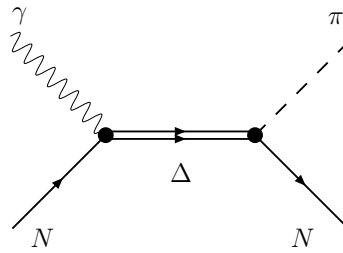


Figure 4.2.: Comparison of the empirical P33 amplitude of [20] and our model calculation. In addition we show the contribution of the nucleon u-channel diagram.

4.4.2. Photo absorption

Tuning the model to the photo absorption data, both, on the nucleon as well as on the nucleus will allow us to determine the values of the Migdal parameters and the isobar mean-fields at finite density. Since the photon receives no initial state interaction we can directly scale up the γN amplitude to get a model for the γ -nucleus amplitude. However for a description of even the photo absorption on the proton a simple model containing the s-channel Delta pole diagram



only is not sufficient. This can most easily be seen when we analyse not only the total photo absorption but the exclusive processes for scattering on the proton (p) $\gamma + p \rightarrow \pi^0 + p$ and $\gamma + p \rightarrow \pi^+ + n$ as well as the corresponding ones on the neutron (n) $\gamma + n \rightarrow \pi^0 + n$ and $\gamma + n \rightarrow \pi^- + p$ separately. Here it turns out that while the processes with a neutral pion in the final state are mostly dominated by the resonance there is a rather high background contribution in the case of a charged pion. This background consists of additional processes involving the nucleon. Especially relevant in the energy range of Δ -isobar are the nucleon s- and u-channel diagrams [99–102]:

Two Feynman diagrams representing s-channel and u-channel nucleon exchange. The left diagram shows an incoming nucleon (N) from the bottom left and an outgoing nucleon (N) from the bottom right, with a wavy photon (gamma) from the top left and a dashed pion (pi) from the top right. A horizontal nucleon line (N) connects the two vertices. The right diagram is similar but the photon and pion lines are crossed, representing u-channel exchange. The two diagrams are separated by a plus sign and followed by a comma and the equation number (4.70).

the Kroll-Ruderman term:

A Feynman diagram representing the Kroll-Ruderman term. It shows a wavy photon (gamma) and a dashed pion (pi) meeting at a vertex. From this vertex, two solid lines representing nucleons (N) emerge, one going to the bottom left and one to the bottom right. The diagram is followed by the equation number (4.71).

and the t-channel pion exchange:

$$(4.72)$$

Based on the interaction vertices (4.1, 4.3) and the photo couplings

$$\begin{aligned} \mathcal{L}_{\pi N} &= -e\bar{N} \left(\frac{\mathbf{1} + \tau_3}{2} \right) \gamma^\mu N A_\mu \\ &\quad - e \frac{f_N}{m_\pi} \bar{N} \gamma_5 \gamma^\mu A_\mu (\vec{\tau} \times \vec{\pi})_3 N - e (\vec{\pi} \times \partial^\mu \vec{\pi})_3 A_\mu \end{aligned} \quad (4.73)$$

$$\begin{aligned} \mathcal{L}_{\gamma N \Delta}^{mag.} &= \frac{f_\gamma}{m_\pi^2} i \epsilon_{\mu\nu\alpha\beta} \left(\partial^\alpha A^\beta - \partial^\beta A^\alpha \right) \bar{N} T_3^\dagger (\partial^\mu \Delta^\nu) + \text{h.c.} \\ \mathcal{L}_{\gamma N \Delta}^{el.} &= \frac{f'_\gamma}{m_\pi^2} \gamma_5 \left(\partial^\alpha A^\beta - \partial^\beta A^\alpha \right) \bar{N} T_3^\dagger (\partial^\mu \Delta^\nu) + \text{h.c.} \end{aligned} \quad (4.74)$$

the photon-nucleon cross section is reasonably well described. We allow a magnetic and electric⁶ coupling of the Delta isobar. The relevance of this electric coupling was claimed by [101, 102] in contrast to the simpler model used in [22]. As an important generalisation of [22] we incorporate short range correlation effects into the $\gamma N \Delta$ vertex of (4.1) as well as in the $\pi N \Delta$ and $\pi N N$ vertices. As already seen in the case of e.g. the pion self-energy these vertex corrections lead to a replacement of the pion momentum by a properly dressed momentum $\zeta^\beta(w, q, u)$ defined in (4.81). The modified $\gamma N \Delta$ vertex then becomes:

$$\Gamma_{\mu\nu}(q, p, u) = \epsilon_{\mu\nu\alpha\beta} q^\alpha \zeta^\beta(w, q, u), \quad w_\mu = p_\mu + q_\mu, \quad (4.75)$$

with the photon and nucleon 4-momenta q_μ and p_μ . The generalised vertex (4.75) is transverse with respect to the photon 4-momentum and therefore consistent with constraints set by gauge invariance. The vacuum limit is approached with the replacement $\zeta_\mu \rightarrow w_\mu$. The corrections to the $\pi N \Delta$ and $\pi N N$ vertices are incorporated in the very same way as in the previous chapter (4.22) for details see Appendix P. The computation of the total absorption cross section for each channel is performed in the nuclear matter rest frame. Fermi motion effects are considered:

$$\begin{aligned} \sigma_{\gamma A}^{channel}(q_0) &= \frac{4}{\rho} \int_0^{k_F} \frac{d^3 p}{(2\pi)^3} \frac{\Im A_{\gamma N}^{channel}(q, p, u)}{2(p - m_V u) \cdot q}, \\ p_0 &= \sqrt{m_N^2 + \vec{p}^2} + \Sigma_V, \quad q_0 = |\vec{q}|, \quad u_\mu = (1, \vec{0}), \end{aligned} \quad (4.76)$$

⁶Note that with this choice of the electric coupling one receives contribution in the electric and magnetic multipole [101]

4. Pions and Δ -isobars at finite density

with

$$\begin{aligned}
A_{\gamma N}^{channel}(q, p, u) &= \int \frac{d^4 l}{(2\pi)^4} \frac{d^4 k}{(2\pi)^4} \left[\sum_{lm=1}^2 \sum_{ij=1}^2 K_{ij;lm}^{channel}(p, q, k, l, u) A_{ij;lm}^{eff}(k, u) \right. \\
&\quad \left. + \sum_{lm=1}^2 K_{g;lm}^{channel}(p, q, k, l, u) A_{g;lm}^{eff}(k, u) \right] \delta((l - m_V u)^2 - m_N^2) \delta(p + q - l - k)
\end{aligned} \tag{4.77}$$

and integration kernels $K_{ij;lm}^{channel}$ defined in Appendix P. The integration in (4.77) is performed over the momentum of the outgoing nucleon l_μ and the pion k_μ . In addition we define effective spectral functions

$$\begin{aligned}
A_{ab;lm}^{eff}(\omega, \vec{q}) &= -\Im \left(\frac{\Gamma_a^{(l)}(\omega, \vec{q}) \Gamma_b^{(m)}(\omega, \vec{q})}{\omega^2 - \vec{q}^2 - m_\pi^2 - \Pi_\pi(\omega, \vec{q})} - \Gamma_{ab}^{(lm)}(\omega, \vec{q}) \right) \\
A_{g;lm}^{eff}(\omega, \vec{q}) &= \Im \left(\Gamma_{00}^{(lm)}(\omega, \vec{q}) \right)
\end{aligned} \tag{4.78}$$

which are build up in a similar way then (4.55) however we have to consider additionally the possibility of connecting resonance with resonance terms as well as resonance with background terms and background terms among each other. Therefore we need additional vertex tensors Γ which are given in Appendix P. The total cross-section is in the end obtained by summing over the individual channels. For a particular model of the isobar propagator, $S_{\mu\nu}(w, u)$, and the vertex, $\zeta_\mu(w, q, u)$, the expressions (4.76) and (4.77) enable the computation of the nuclear photo absorption cross section in the isobar region. The required amplitude $A_{\gamma N}$ also involves vertex corrections given by a further isobar-hole tensor loop function, which takes the form

$$\begin{aligned}
\Pi_{\mu\nu,\alpha}^{(\Delta h)}(q, u) &= \frac{4}{3} \frac{f_\Delta^2}{m_\pi^2} \int \frac{d^4 p}{(2\pi)^4} i \text{tr} \Delta S(p, u) S_{\mu\nu}(p + q, u) p_\alpha \\
&\quad + (q_\mu \rightarrow -q_\mu).
\end{aligned} \tag{4.79}$$

The photon vertex tensor, $\Gamma_{\mu\nu}(q, p, u)$ couples to the transverse nucleon- and Delta-hole loops, $\Pi_T^{(Nh)}(q, u)$ and $\Pi_T^{(\Delta h)}(q, u)$, introduced in (4.15). Because of the ϵ -tensor structure in the bare photon vertex, only contributions proportional to either $g_{\mu\nu} u_\alpha$ or $g_{\nu\alpha} u_\mu$ are relevant. This requirement singles out transverse correlation effects:

$$\begin{aligned}
\Gamma_\nu^\mu(q, p, u) &= \epsilon^{\mu\tau\alpha\beta} g_{\tau\nu} q^\alpha \zeta^\beta(w, q, u) \\
&= q_\alpha \epsilon^{\mu\tau\alpha\beta} \left(g_{\tau\nu} p^\beta + \Pi_{\tau\kappa,\beta}^{(\Delta h)}(q, u) \left[\frac{1}{1 - g^{(T)} \chi^{(T)}(q, u)} g^{(T)} \right]_{22} T_\nu^\kappa(q, u) \right)
\end{aligned} \tag{4.80}$$

with matrix structures defined in (4.16). For further manipulations it is useful to offer a more explicit form of the photon vertex. As anticipated in (4.75) the vertex can be

written in terms of a 4-vector function $\zeta_\mu(w, q, u)$. Due to the presence of the ϵ -tensor in (4.79) it is sufficient to consider terms proportional to p_μ or u_μ . The p_μ part of the bare vertex is not renormalised by the short range interaction (4.3). The evaluation of the only non-trivial term requires a projection of the tensor, $\Pi_{\mu\nu,\alpha}^{(\Delta h)}$, onto the relevant structure. We obtain:

$$\zeta_\mu(w, q, u) = w_\mu + U(q, u) \left[\frac{1}{1 - g^{(T)} \chi^{(T)}(q, u)} g^{(T)} \right]_{22} u_\mu, \quad (4.81)$$

where

$$\begin{aligned} U(q, u) &= \frac{1}{2} T^{\mu\nu}(q, u) \frac{(q \cdot u) q^\alpha - q^2 u^\alpha}{(q \cdot u)^2 - q^2} \Pi_{\mu\nu,\alpha}^{(\Delta h)}(q, u) \\ &- \frac{1}{2} T^{\nu\alpha}(q, u) \frac{(q \cdot u) q^\mu - q^2 u^\mu}{(q \cdot u)^2 - q^2} \Pi_{\mu\nu,\alpha}^{(\Delta h)}(q, u). \end{aligned} \quad (4.82)$$

The evaluation of the invariant loop function, $U(q, u)$, in terms of a given isobar propagator, $S_{\mu\nu}(w, u)$, can be found in Appendix N. Next we have to consider a very important issue. The resonance amplitudes are gauge invariant by themselves due to the choice of the interaction (4.74). On the other side we need certain cancellations among the background terms to get a gauge invariant result. While these cancellations are easily fulfilled in the vacuum, problems arise as soon as in-medium spectral functions for the pion and vertex corrections come into play for the in-medium calculations. While this causes no problems in the neutral pion channels, a full calculation in the charged pion channels would require the evaluation of additional vertex corrections which are beyond the scope of this work. Therefore we restrict the calculation by setting

$$\begin{aligned} A_{11;12}^{eff} &= A_{11;21}^{eff} = A_{11;22}^{eff} = A_\pi^{vac.} \\ A_{ab;12}^{eff} &= A_{ab;21}^{eff} = A_{ab;22}^{eff} = 0 \quad \text{for } a \text{ and } / \text{ or } b = 2 \\ A_{g;12}^{eff} &= A_{g;21}^{eff} = A_{g;22}^{eff} = 0 \end{aligned} \quad (4.83)$$

thus removing all in medium effects of the pion in the background terms while keeping the mean-field shifts for the nucleon. A comparison with the full calculation in the neutral pion channels will then allow a first judgement about the influence of these in medium effects. For the consideration of the in-medium results we need to use the photo absorption on heavy nuclei such as Uranium or Lead. In this case however we have no reason to assume isospin symmetry any more like we did for the calculations up to now. In order to take such effects into account in a first approach we put a different weighting between the processes on the proton and on the neutron when summing up the contributions for the total cross-section. Before we turn to the discussion of the parameters let us first consider the kinematical situation. This will provide some rough

4. Pions and Δ -isobars at finite density

estimate about the values to be expected for the isobar mean-fields apart from corrections through the short range correlations. Energy and momentum conservation require

$$w_0 = \sqrt{m_N^2 + \vec{p}^2} + m_V + q_0, \quad |\vec{w}|_{min} = |q_0 - |\vec{p}||, \quad |\vec{w}|_{max} = q_0 + |\vec{p}|, \quad (4.84)$$

where w_0 and \vec{w} are the isobar energy and momentum, \vec{p} the nucleon momentum and q_0 the photo energy. Thus, for given photon energy and nucleon momentum the isobar is probed only in a very limited region of phase space. Considering the nuclear Fermi motion within the Fermi surface, we get a border line in the $w_0 - \vec{w}$ - plain which marks the region where the Delta is probed for each photon energy. In vacuum the situation is even more simple because there one can choose the frame where the nucleon is at rest. Therefore this region shrinks to a point and we can draw a single kinematical curve on which the isobar is probed when varying the photo energy (see Fig. 4.3).

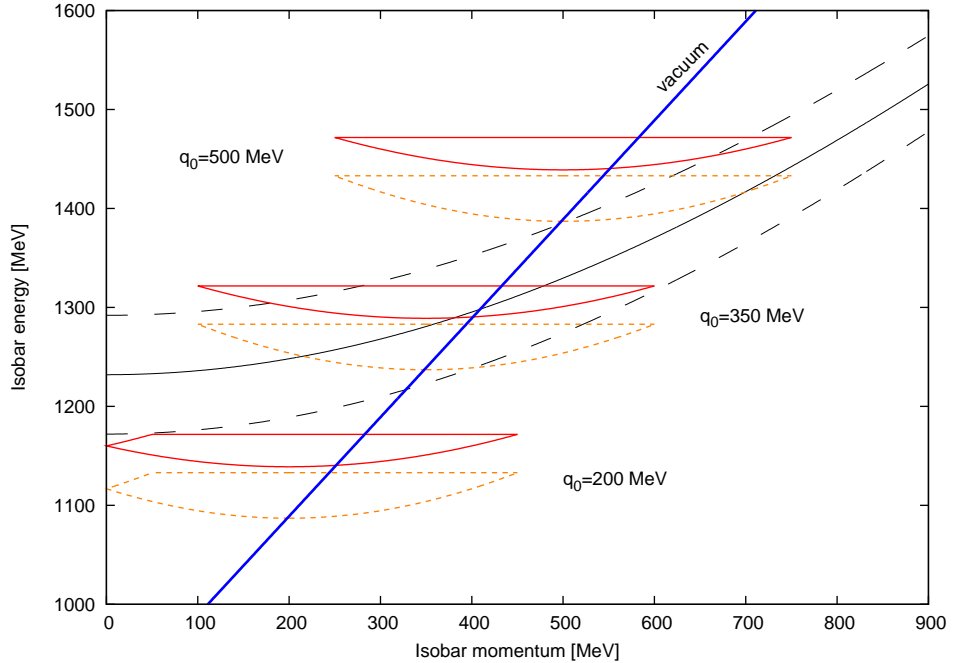


Figure 4.3.: Kinematics for the photo absorption. Shown are the areas where the Δ -isobar is probed at different photon energies q_0 . Full areas state the situation when no mean-fields for the nucleon are present and the dashed areas when mean-fields are applied ($k_F = 250$ MeV in both cases). We additionally give the free isobar kinematic and the line along which the isobar is probed in vacuum.

The in-medium case is discussed in Fig. 4.3 where we plot the region probed by a photon with energy from 200 MeV to 500 MeV which is most relevant for the peak seen in the

experimental data. In addition we draw a helping line at a photon energy of 350 MeV where the maximum in the experimental data is observed. We learn that, if no vertex corrections are applied, we expect quite similar mean-field-shifts for nucleon and Delta to explain the experimental fact that the peak position of the cross section is nearly unshifted from vacuum to in-medium.

We will now turn to the determination of the parameters. First we have to adjust the coupling constants f_γ and f'_γ (4.74) using the data for photo absorption on the proton. The absorption is here nearly completely dominated by pion nucleon final states. The result for the total absorption cross-section is displayed in Fig. 4.4. From this figure we also learn that in order to describe especially the data points for energies bellow 250 MeV the background terms are very important. Still we are missing some strength here. This fact may - as in the case of the $\pi\pi$ -scattering - be related to missing u-channel contributions in the isobar self-energy.

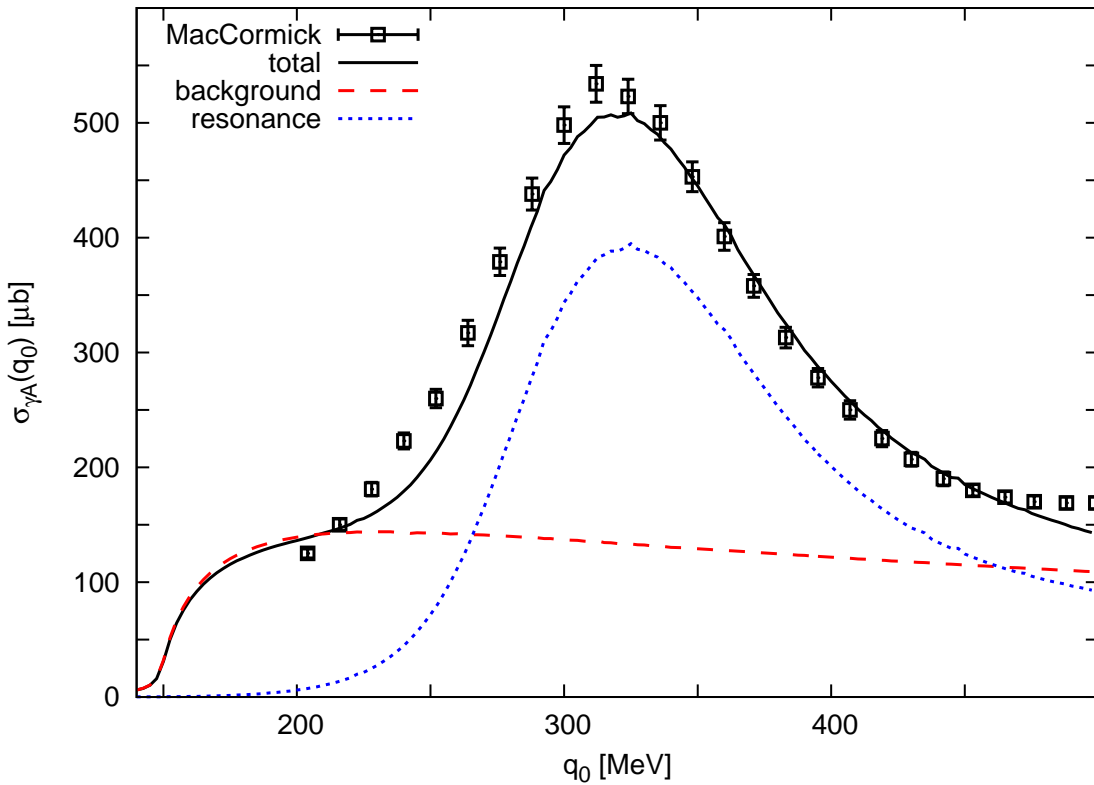


Figure 4.4.: Calculation of the photo absorption on the nucleon compared to data for the photo absorption on the proton ($\gamma p \rightarrow \text{hadrons}$) [103]. We display the full calculation (full line) and the resonance (dotted line) and background (dashed line) contributions separately.

However as we pointed already out for a complete description we need not only to

4. Pions and Δ -isobars at finite density

describe the total photo absorption but also the individual exclusive processes $\gamma + p \rightarrow \pi^0 + p$ and $\gamma + p \rightarrow \pi^+ + n$. Additionally we would have the corresponding processes for absorption on the neutron. However the data quality is naturally much better in the proton case so that we stick to this to adjust the the parameters. In order to determine the magnetic coupling f_γ and electric coupling f'_γ the photo absorption is calculated in vacuum. A good fit leads a value of $f_\gamma = 0.0114$ and $f'_\gamma = 0.024$ which is in the same range as the values found in [101, 102]. In addition we get a quite reasonable description of the exclusive processes. This would be different when we would try to adjust the the parameters without the background terms. Even though we would achieve a reasonable description of the total absorption cross-section we have no chance describing the exclusive processes. In this case one would clearly overestimate the process $\gamma + p \rightarrow \pi^0 + p$ and underestimate $\gamma + p \rightarrow \pi^+ + n$.

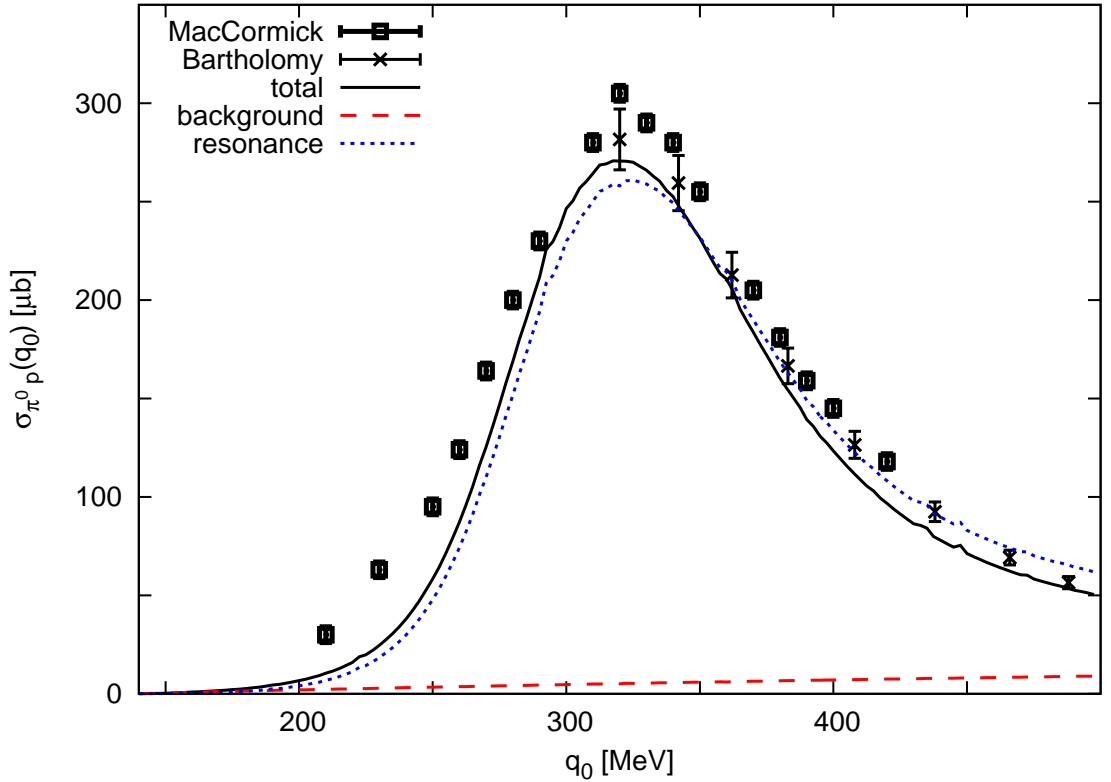


Figure 4.5.: Calculation of the $\pi^0 p$ channel compared to data for the photo absorption on the proton [103, 104]. We display the full calculation (full line) and the resonance (dotted line) and background (dashed line) contributions separately.

The result for $\gamma + p \rightarrow \pi^0 + p$ is shown in Fig. 4.5. This process is dominated by the Δ -resonance. The background terms have only a minor influence on the results.

This can be understood from the theoretical side because here only the s- and u-channel nucleon pole diagrams (4.70) enter which don't give rise to strong effects. The situation changes drastically when one considers the charged pion channel $\gamma + p \rightarrow \pi^+ + n$. Here the Kroll-Rudermann term (4.71) and the t-channel pion exchange (4.72) lead to a much higher background contribution which is clearly visible in Fig. 4.6. Nearly half of the cross-section is given by the background terms. The peak position turns out to be at a bit too high photon energies in our calculation. This is caused by the strict adjustment of our isobar propagator to the $\pi\pi$ -scattering data. A more global fit of the parameters would certainly lead to an improved result.

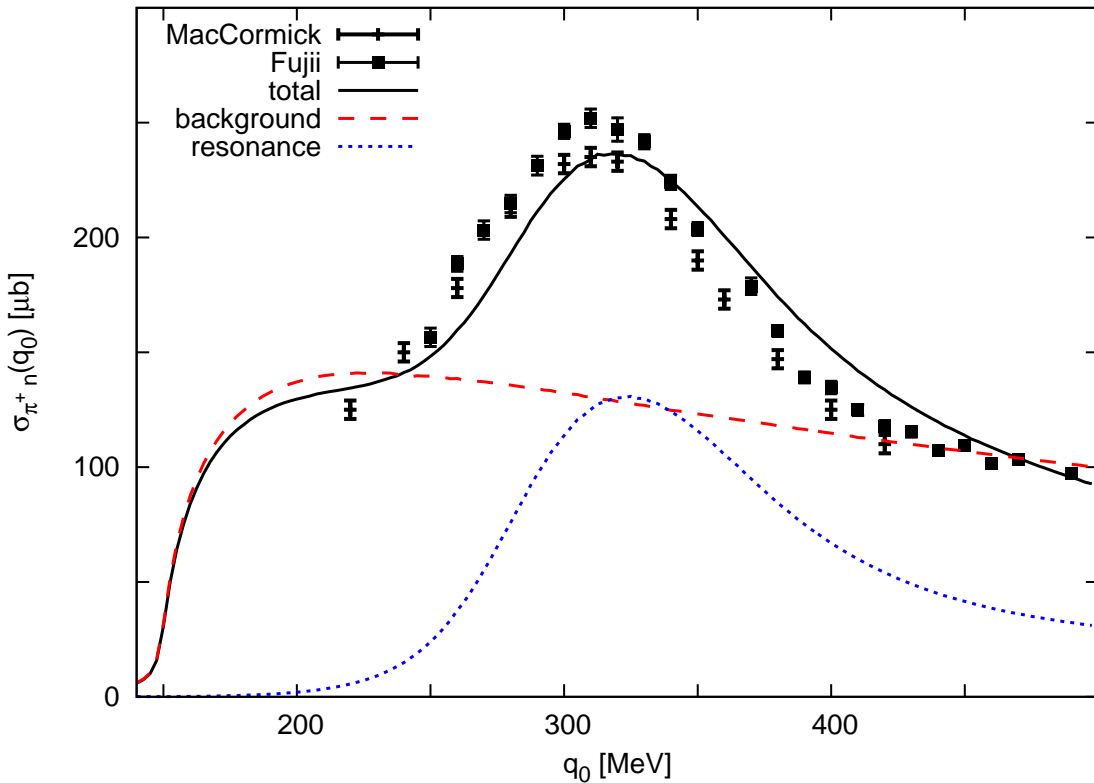


Figure 4.6.: Calculation of the π^+n channel compared to data for the photo absorption on the proton [103,105]. We display the full calculation (full line) and the resonance (dotted line) and background (dashed line) contributions separately.

We now turn to the discussion of the Migdal parameters g'_{ij} . These should be adjusted together with the mean-fields for the Δ -isobar to reproduce the photo absorption data on the nucleus. Since the model for the in-medium calculations of the photo absorption includes the serious approximation of treating the background terms without vertex

4. Pions and Δ -isobars at finite density

corrections and a realistic pion spectral function we can't draw a final conclusion here but will study different scenarios. We choose the following two parameters sets

Set 1:

$$\begin{aligned}\Sigma_V^\Delta &= 360 \frac{\rho}{\rho_0} \text{ MeV}, & \Sigma_S^\Delta &= \frac{\rho}{\rho_0} 350 \text{ MeV} \\ g'_{11} &= 0.58 & g'_{12} &= 0.2 & g'_{22} &= 0.2\end{aligned}\quad (4.85)$$

Set 2:

$$\begin{aligned}\Sigma_V^\Delta &= 440 \frac{\rho}{\rho_0} \text{ MeV}, & \Sigma_S^\Delta &= \frac{\rho}{\rho_0} 350 \text{ MeV} \\ g'_{11} &= 0.58 & g'_{12} &= 0.2 & g'_{22} &= 0.6\end{aligned}\quad (4.86)$$

where the value of the scalar mean-field is chosen identical with the nucleon scalar mean-field. Both sets produce an attractive mass-shift of the isobar with respect to the vacuum (see next section). An unshifted Δ -isobar could also be obtained by using even higher values for the vector meanfield or by reducing the scalar one. This would result in a about 30 to 40 μb lower cross-section. To really determine these parameters the model has to be extended to incorporate the essential medium effects neglected by (4.83).

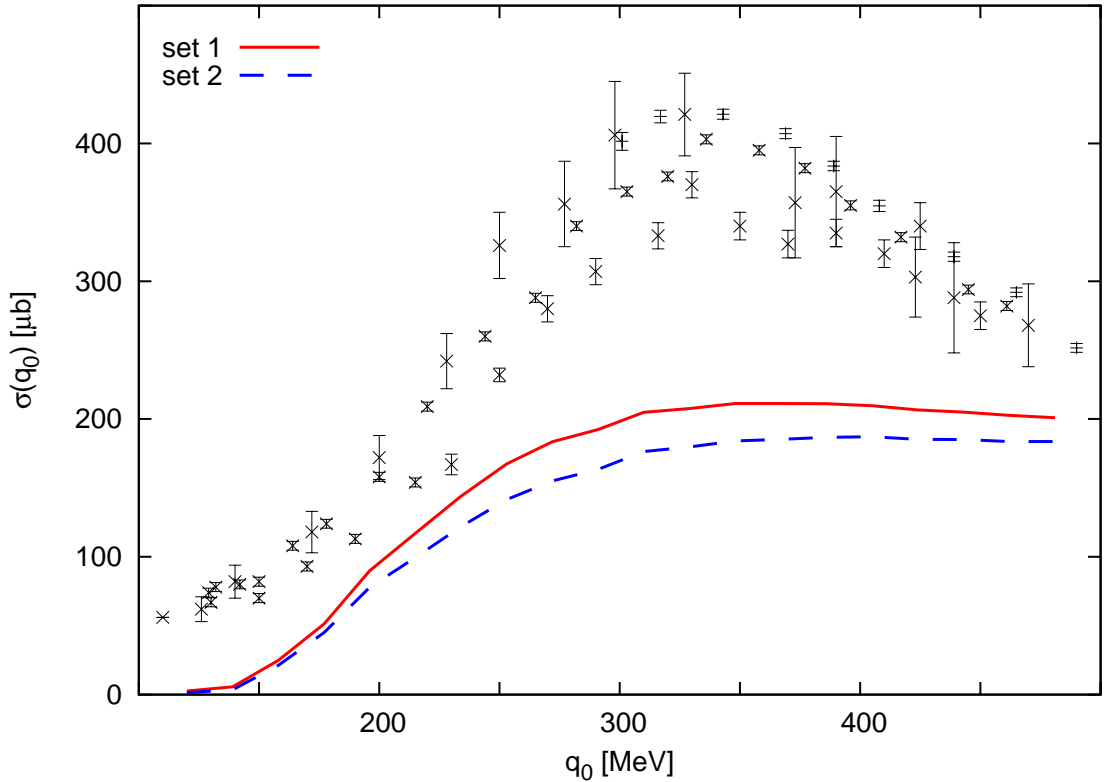


Figure 4.7.: Comparison of the total photo absorption cross-section for the two different parametersets defined in (4.86).

However it turned out that within the given sensitivity of the calculation we can only make a statement about the combination of scalar and vector-mean-field where the splitting between both influences the global shift of the isobar. The influence of the absolute magnitude of these mean-fields has only a minor effect. In Fig. 4.7 we show the corresponding results for the cross-section. We learn that within this restricted model setup we reproduce the magnitude of the cross-section rather well while the peak structure is less dominant in our calculation. This might result from the fact that the actual creation of the peak is a highly nontrivial effect within our model because due to the vertex correction (4.75) we do not probe the resonance peak itself but the high energy edge of the resonance. The actual peak is then created in the interplay of this edge with the vertex. The global magnitude is still about $120 \mu\text{b}$ too small.

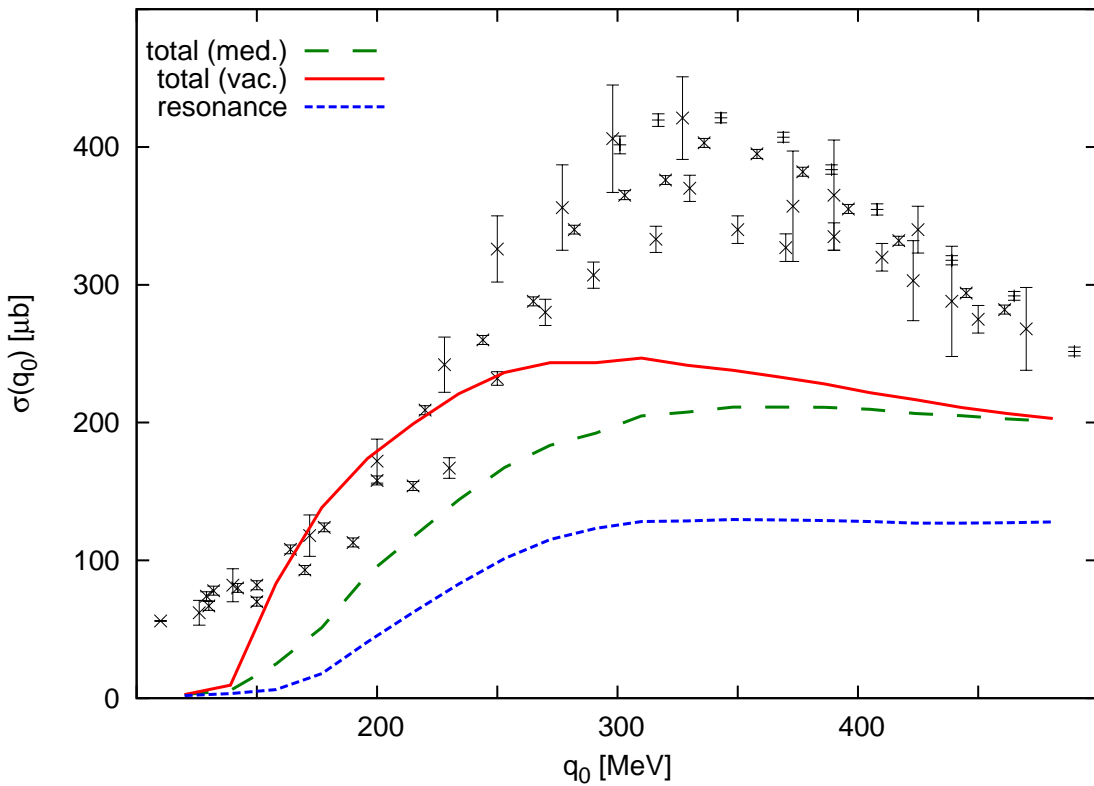


Figure 4.8.: Contributions of the resonance and background terms to the total photo absorption cross-section. For the full curve we added the vacuum background to the resonance contribution whereas the dashed line shows the cross-section when the medium effects are switched on. Parameters are according to set 1. Data is taken from [106, 107].

However in this approach we neglected important in-medium effects in the background terms. As can be seen from (4.83) we keep the mean-field shifts of the nucleon and

4. Pions and Δ -isobars at finite density

Pauli-blocking effects only. This results in an underestimation of the cross-section as can also be seen from Fig. 4.8 and Fig. 4.9. The relevance of the background terms for the in-medium calculation are visible from Fig. 4.8. We observe that their contribution is less strong than in the vacuum case. This is caused partially due to Pauli-blocking effects but also we expect quite some influence from the approximations made in the calculation of the background terms (4.83). While being less severe for the neutral pion channel as can be seen from Fig. 4.9 we expect that a calculation with the full pion spectral function should lead to stronger effects especially in the t-channel diagram which still have to be explored. The relevance of the different channels is shown in Fig. 4.10. Here we learn that the most dominating contribution comes from the absorption on the neutron which is not surprising since for the heavy systems studied here we have much more neutrons than protons.

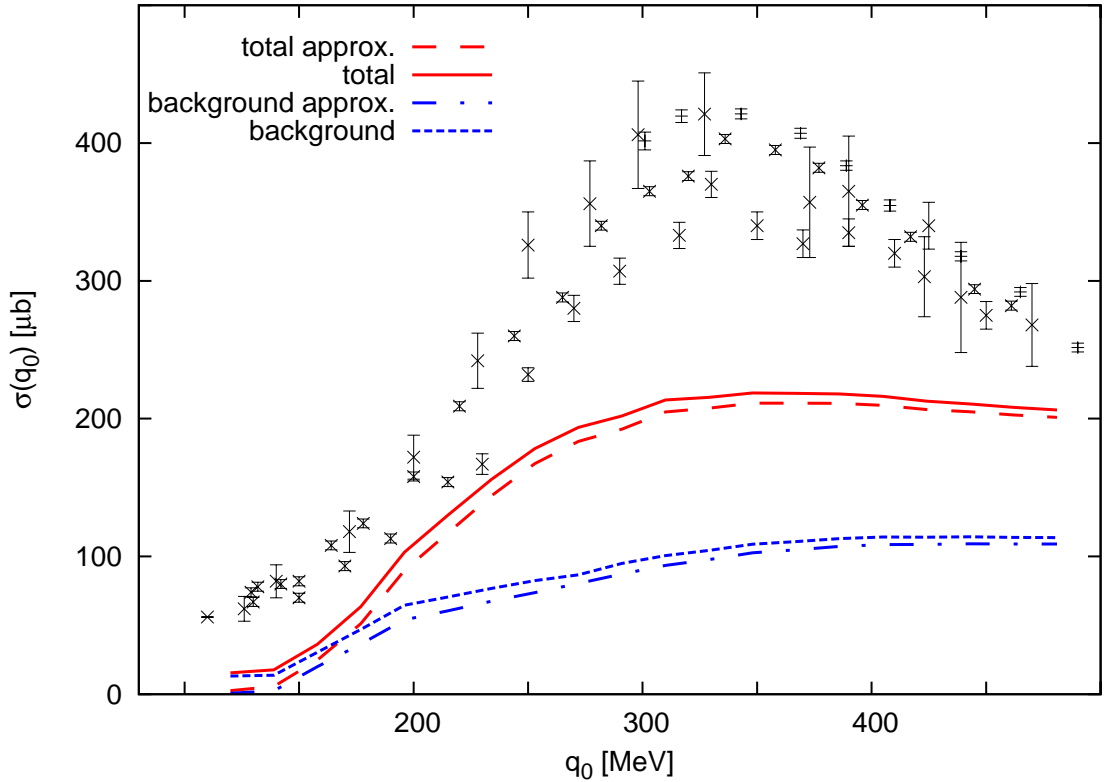


Figure 4.9.: Influence of the approximation made in (4.83). We compare the results for a calculation using the spectral functions of (4.83) compared to a calculation where this approximation has only been used in the charged pion channel while keeping the full structure (4.78) in the neutral pion channel.

In the fit it turns out that the photo absorption is quite insensitive on the choice of g_{11}

so that we take this value in accordance with literature [32]. The influence of the other two Migdal parameters turned out being small then expected.

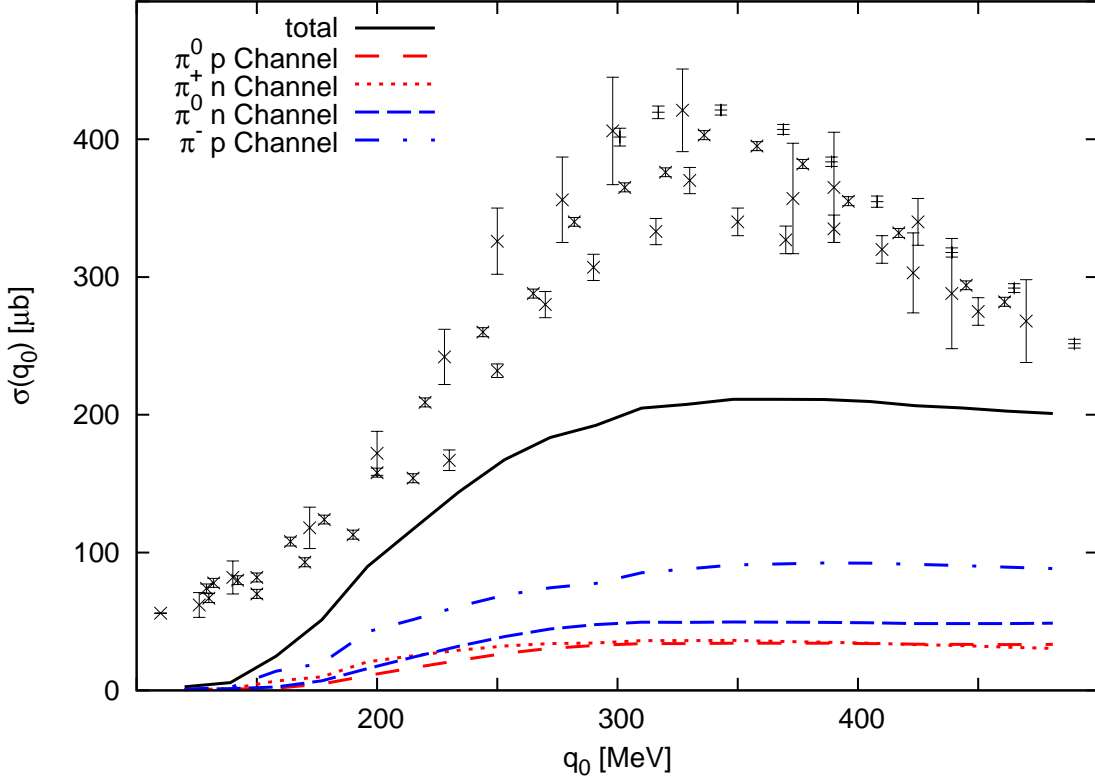


Figure 4.10.: Contributions of the several channels to the total photo absorption cross-section. Parameters are according to set 1. Data is taken from [106,107].

We observe that even a variation in g_{22} from 0.2 to 0.6 causes only relatively small change in the cross-section as can be seen in Fig. 4.7 when the mean-fields are readjusted. This effect is caused by compensating effects of the Migdal parameters in the different parts of the model. In the photon vertex a higher value of g_{22} would lead to a larger cross-section however on the other hand this effect is compensated by a different shape of the resonance mainly caused by the second diagram in (4.13). Our parameter choice 2 is also in agreement with values for g_{ij} suggested by Nakano et al. [32] who analysed Gamow-Teller transitions. They [32] deduce the constraint $g'_{11} = 0.585$ together with $g'_{12} = 0.191 + 0.051 g'_{22}$ insisting on an empirical quenching factor $Q = 0.9$ of the Gamow-Teller resonance [108]. In their consideration they assume the quenching exclusively to result from a mixing of the nucleon-hole and the isobar-hole state. As will be shown in the following section this choice of parameters produces a Δ -isobar with an attractive mass-shift which is quite conservative. On the other hand we could not find reasonable

fits using a high value of g'_{12} as suggested by the calculations of Arve et al. [18] where universality $g'_{11} = g'_{12} = g'_{22} = 0.60$ was found.

4.5. Results

Now we turn to the discussion of the results obtained in the $\pi N\Delta$ -system at finite density. Since the model for the photoabsorption still needs to be extended in order to allow for a reliable fit of the Migdal parameters g'_{ij} we will present the results for the parameter sets one and two on equal footing. Special care will be taken to show the effects of the vertex corrections which become much more important as in the case of the $\pi\rho\omega$ -system studied previously. We begin our discussion with the results for the in-medium Δ -isobar. Here the most relevant components of the spectral functions $S_{ij}^{(p)}$ and $S_{ij}^{(q)}$ (4.30) are the ones which contain the vacuum pole, namely $S_{77}^{(p)}$ and $S_{11}^{(q)}$ (4.33, 4.37, 4.40). Therefore we restrict our discussion to these two main components. However one has to keep in mind that the other components - even though small - are crucially needed to keep the whole scheme free of kinematical singularities. The results for the two main components can be found in Fig. 4.11 and 4.12 where we compare the calculations for both parameter sets for half times normal nuclear density (Fig. 4.11) and normal nuclear density (Fig. 4.12). Compared to the vacuum result we observe in both cases a significant attractive shift of the Δ -isobar of about 120 MeV for set 1 and about 80 MeV for set two at saturation density. However one has to note that also the nucleon receives an attractive shift of about 60 MeV due to the mean-fields (4.9, 4.59). Keeping in mind that previous calculations [15, 28] claimed attractive mass shifts of about 60 MeV using an unmodified nucleon our results confirm the possibility of such shifts. The splitting of the spin 3/2 and 1/2 mode increases with momentum reaching about 100 MeV for 600 MeV momentum. The width of the resonance is nearly unchanged for low momenta while a significant broadening is observed for momenta larger than about 300 MeV. Comparing the calculations for half times saturation density and saturation density we observe that already at rather low density we have significant attraction of the Δ -isobar of about 80 MeV (which is about 45 MeV larger than the shift of the nucleon.). This means that we have, especially for parameter set 2, a saturation behaviour already at rather low densities. This underlines the relevance of a self-consistent calculation since such a behaviour will never be possible in a low density expansion. We also learn that the change in g'_{22} has much stronger influence on the calculations at higher density as can be seen from the much larger deviations of the results for set 1 compared to those for set 2. This is natural since the contributions of the Delta-hole loops which are modified by g'_{22} become stronger with increasing density.

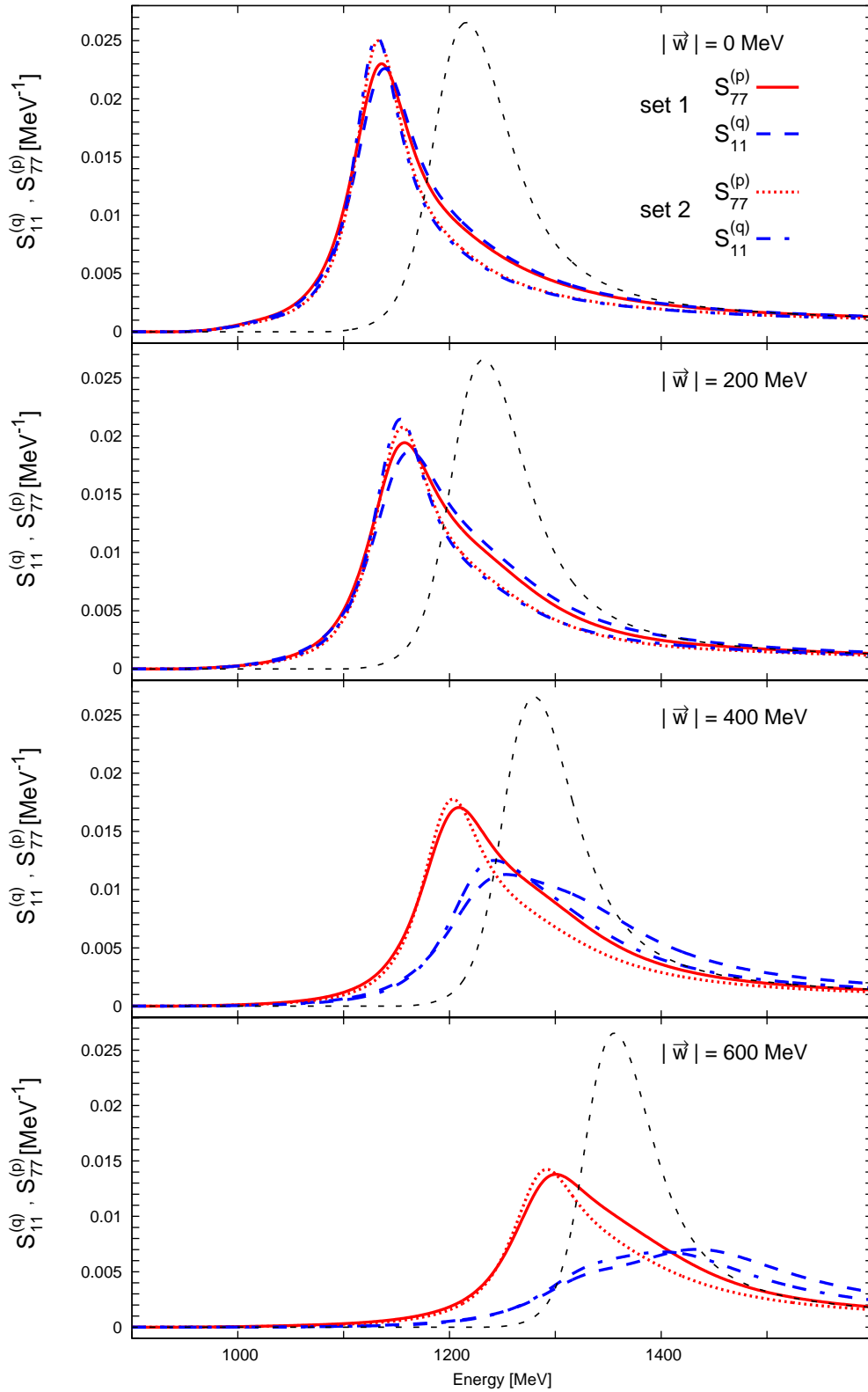


Figure 4.11.: Spectral functions $S_{77}^{(p)}$ and $S_{11}^{(q)}$ for parameter sets one and two and half normal nuclear density. For comparison we also show the vacuum result (long dotted line).

4. Pions and Δ -isobars at finite density

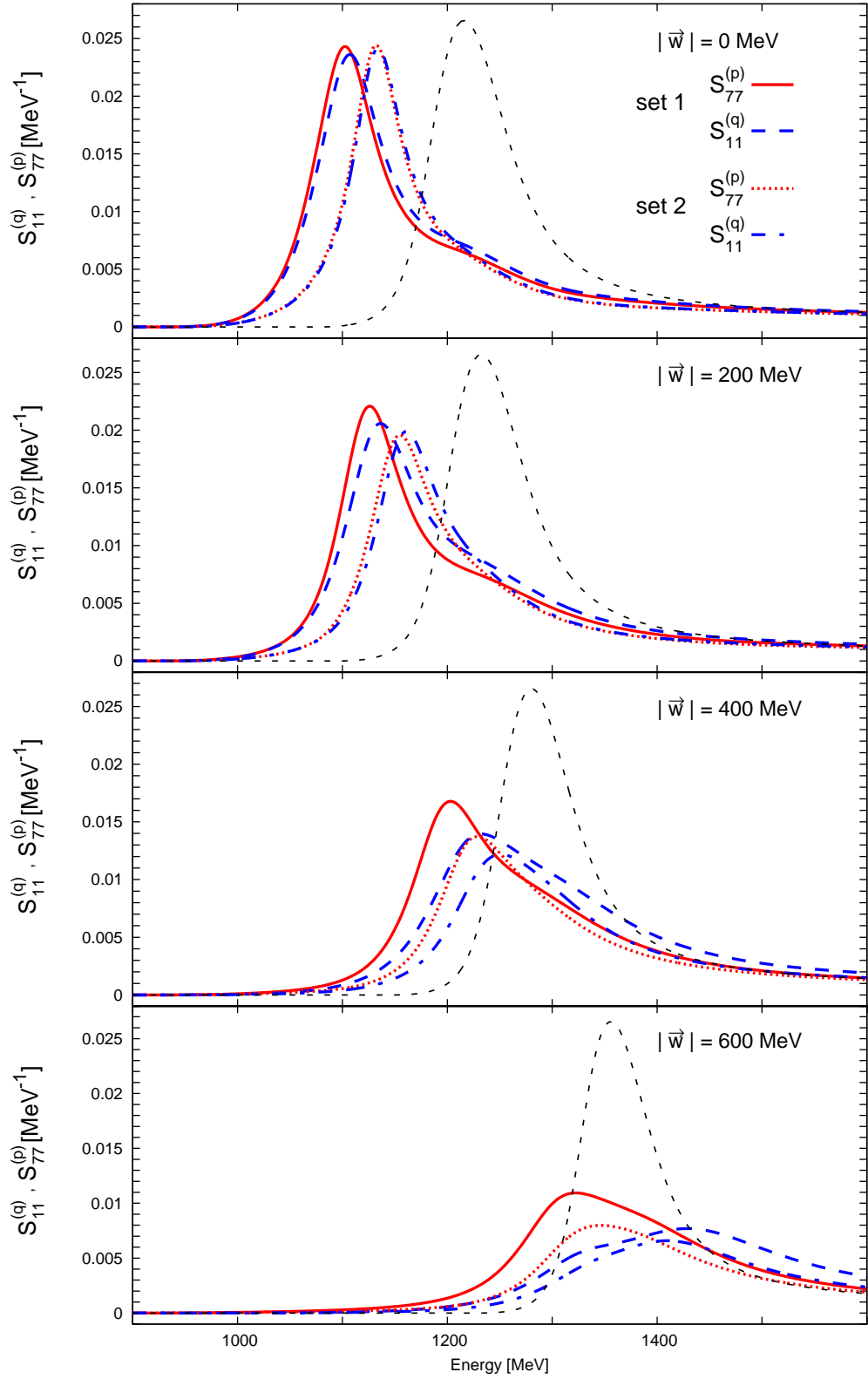


Figure 4.12.: Spectral functions $S_{77}^{(p)}$ and $S_{11}^{(q)}$ for parameter sets one and normal nuclear density. For comparison we also show the vacuum result (long dotted line).

Let us now discuss the results for the pion spectral function. The results for both parameter sets can be found in Fig. 4.13 and 4.14 where calculations for half times normal nuclear density and normal nuclear density are presented. In all cases the contribution of the nucleon-hole states is clearly visible at small energies while the Delta-hole mode is less pronounced. Generally there is the tendency that the pion receives a small attractive mass shift at small momenta which is due to level-level repulsion between the main and the Delta-hole mode. At momenta of about 200 to 300 MeV these two modes cross and for higher momenta the main peak of the spectral function is shifted toward higher energies. Besides these similarities there are also some distinct differences between the calculations with small g'_{22} (parameter set 1) and high g'_{22} (parameter set 2). Especially one observes that the crossing of the main pion mode with the Delta-hole mode happens at higher momenta for the high g'_{22} case. The reason for this effect which can also be seen from the pion self-energy given in Fig. 4.15 is that the Delta-hole mode is at about 100 MeV higher energies for the high g'_{22} case which is explainable since in this case the Δ -isobar receives less attraction. One further aspect concerns the normalisation of the pion. In a scheme where the self-energy is determined by a resummation of certain diagrams it is not a priori clear that the normalisation is preserved in the self-consistent treatment due the fact that additional ghost-states may appear (See the discussion in Appendix C.). We checked that with the scheme used for the calculations of the Delta-hole and nucleon-hole loops we indeed arrive at a procedure which conserves the normalisation of the pion throughout the whole self-consistency.

4. Pions and Δ -isobars at finite density

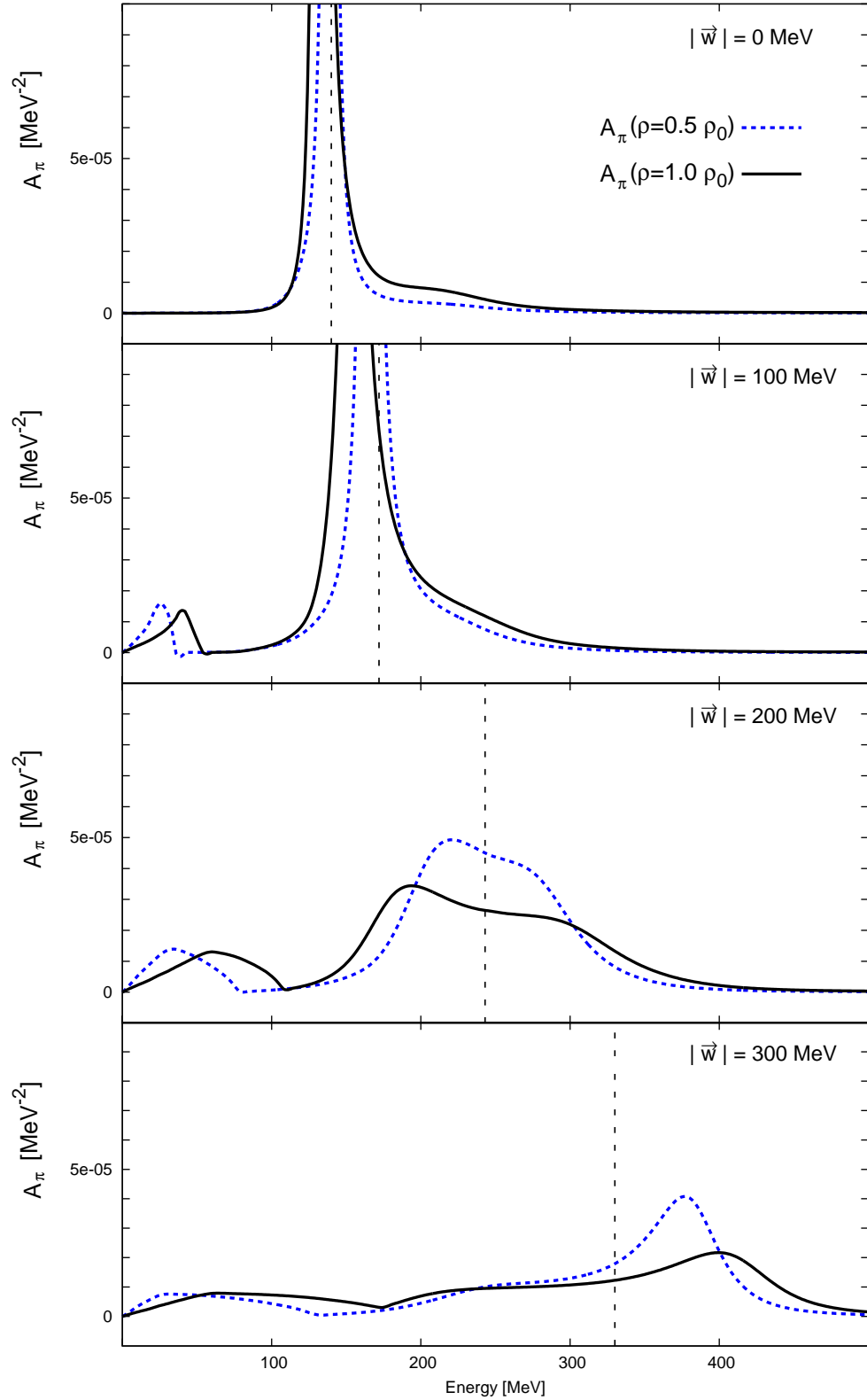


Figure 4.13.: Pion spectral function A_π for half normal nuclear density (dotted line) and normal nuclear density (full line) for parameter set 1. The vertical dashed line marks to position of the vacuum pole.

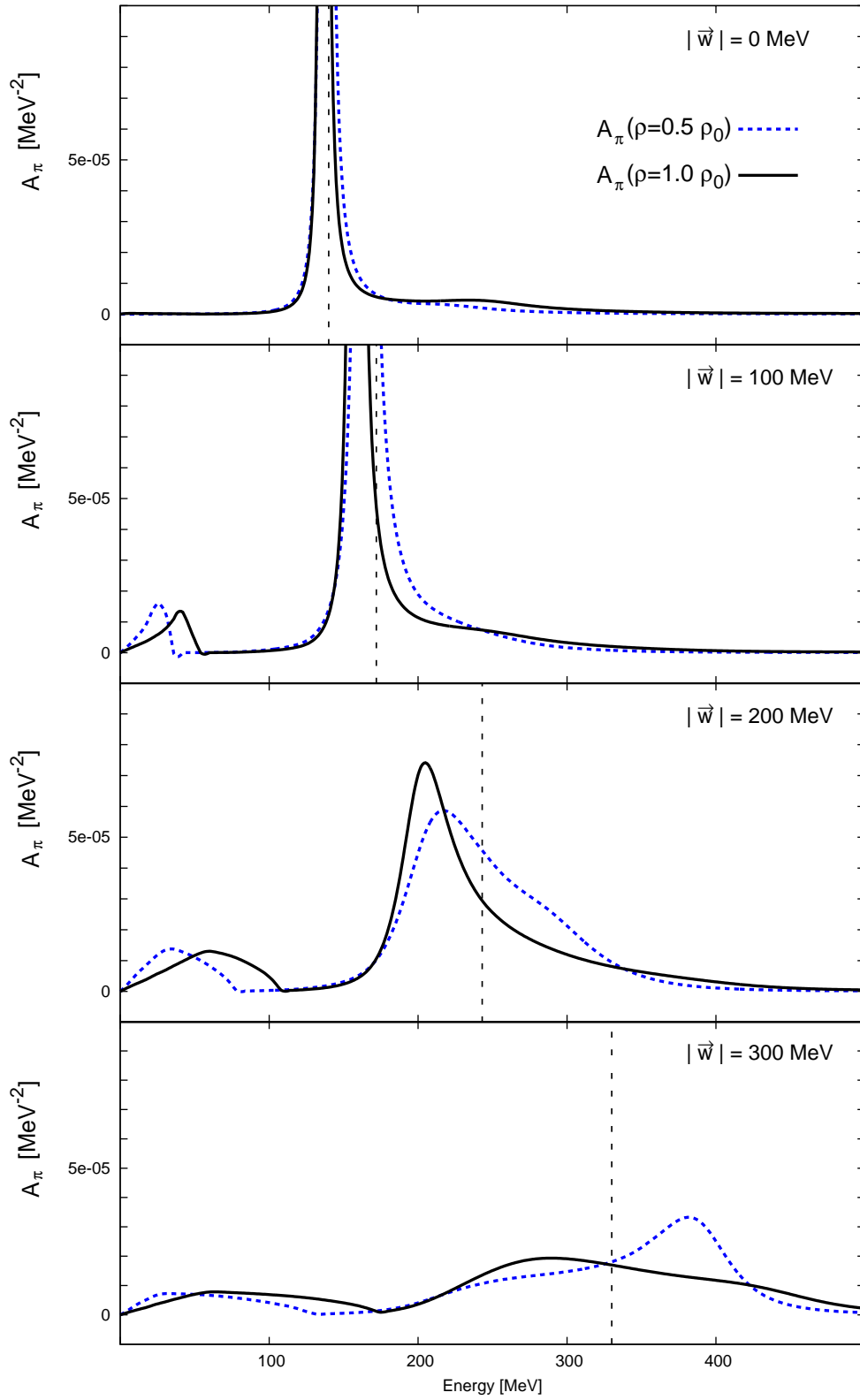


Figure 4.14.: Pion spectral function A_π for half normal nuclear density (dotted line) and normal nuclear density (full line) for parameter set 2. The vertical dashed line marks to position of the vacuum pole.

4. Pions and Δ -isobars at finite density

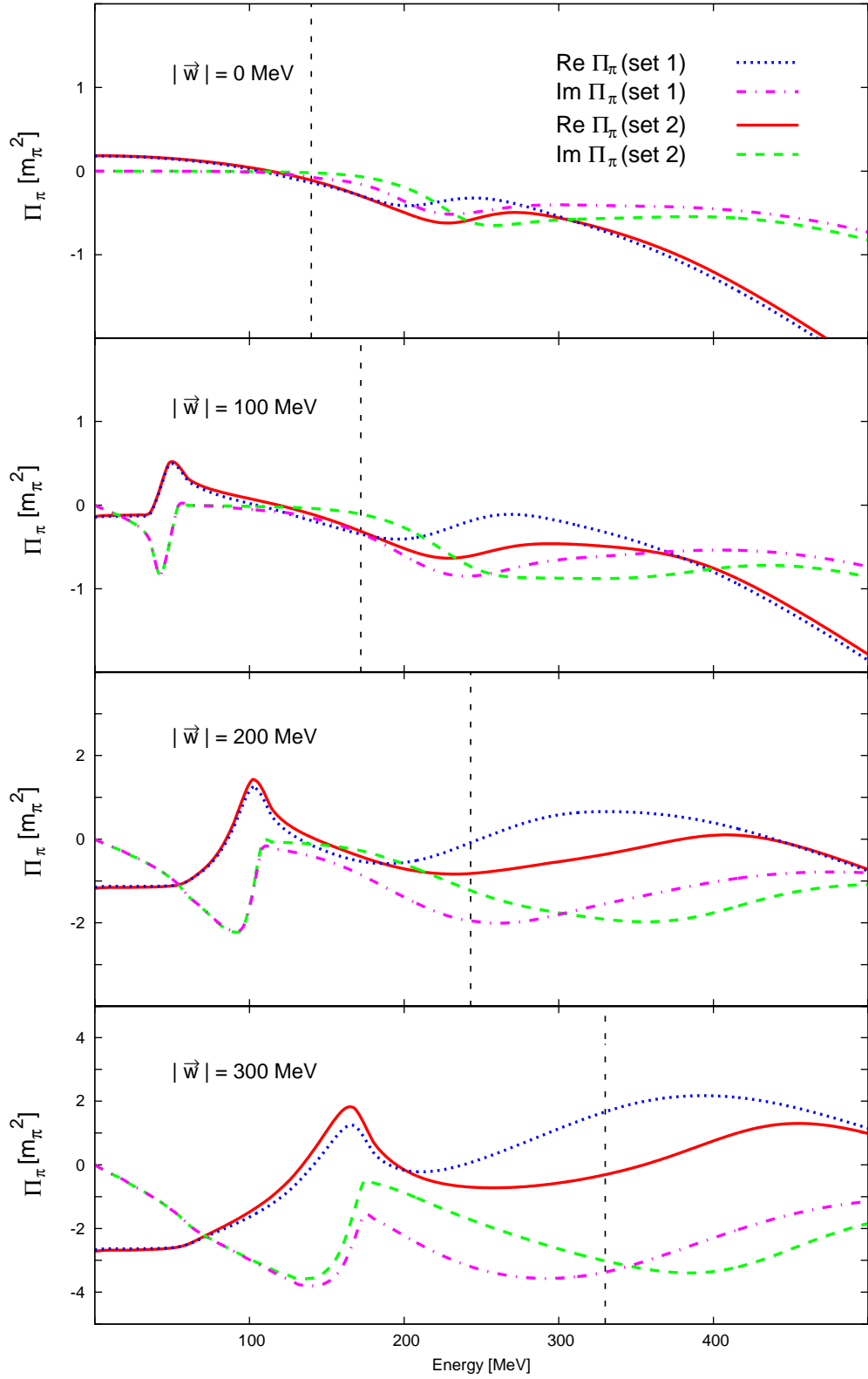


Figure 4.15.: Pion selfenergy for normal nuclear density and both parameter sets.

The relevance of the vertex corrections can be seen from Fig. 4.16 and 4.17 where we compare the pion spectral function with the effective spectral function which is modified due to the vertex tensors (4.55). Here it turns out that the A_{11}^π component plays the dominant part while the other effective spectral functions have only a minor influence on the result. We especially learn that the introduced vertex corrections indeed act like a formfactor in the spacelike region. Therefore the nucleon-hole contribution gets strongly suppressed which prevents the Δ -isobar from becoming too broad at finite density. The magnitude of the suppression can be deduced from Fig. 4.18 where the results for the vertex tensor Γ_1 can be found. We see that the realpart of this function is below 1 in the region where the nucleon-hole contribution dominates the spectral function thus leading to a suppression. In addition we see that the effective spectral function can even become negative. This is caused by an interplay of real and imaginary part of the vertex tensor. The fact that even when we insert these indefinite spectral functions in our calculation and still get a self-energy for the Δ -resonance that leads to a positive definite spectral function is highly non-trivial and can only be obtained when all vertex tensors are taken into account. Here also the contribution from the second diagram in (4.52) is mandatory. An additional observation is that the Delta-hole structure is much stronger pronounced in the effective spectral function. This is due to the fact that such a structure is not only provided by the self-energy but additionally by vertex Γ_1 . From Fig. 4.19 where the results for the vertex function Γ_2 are presented we also learn the reason for the fact that the effective spectral functions A_{12}^π and A_{22}^π are quite small. In contrast to the vertex function Γ_1 which has a real-part close to 1 the vertex function Γ_2 is nearly zero in the kinematical region where we have the main contributions from the pion spectral function. This effect is especially visible for small momenta. However even at large momenta no sizeable contribution can be generated. The relevance of self-consistence is also clearly visible from the rather large distortion of the spectral function by the vertex corrections. Since these vertex corrections crucially depend on the form of the isobar propagator, self-consistence is absolutely essential.

4. Pions and Δ -isobars at finite density

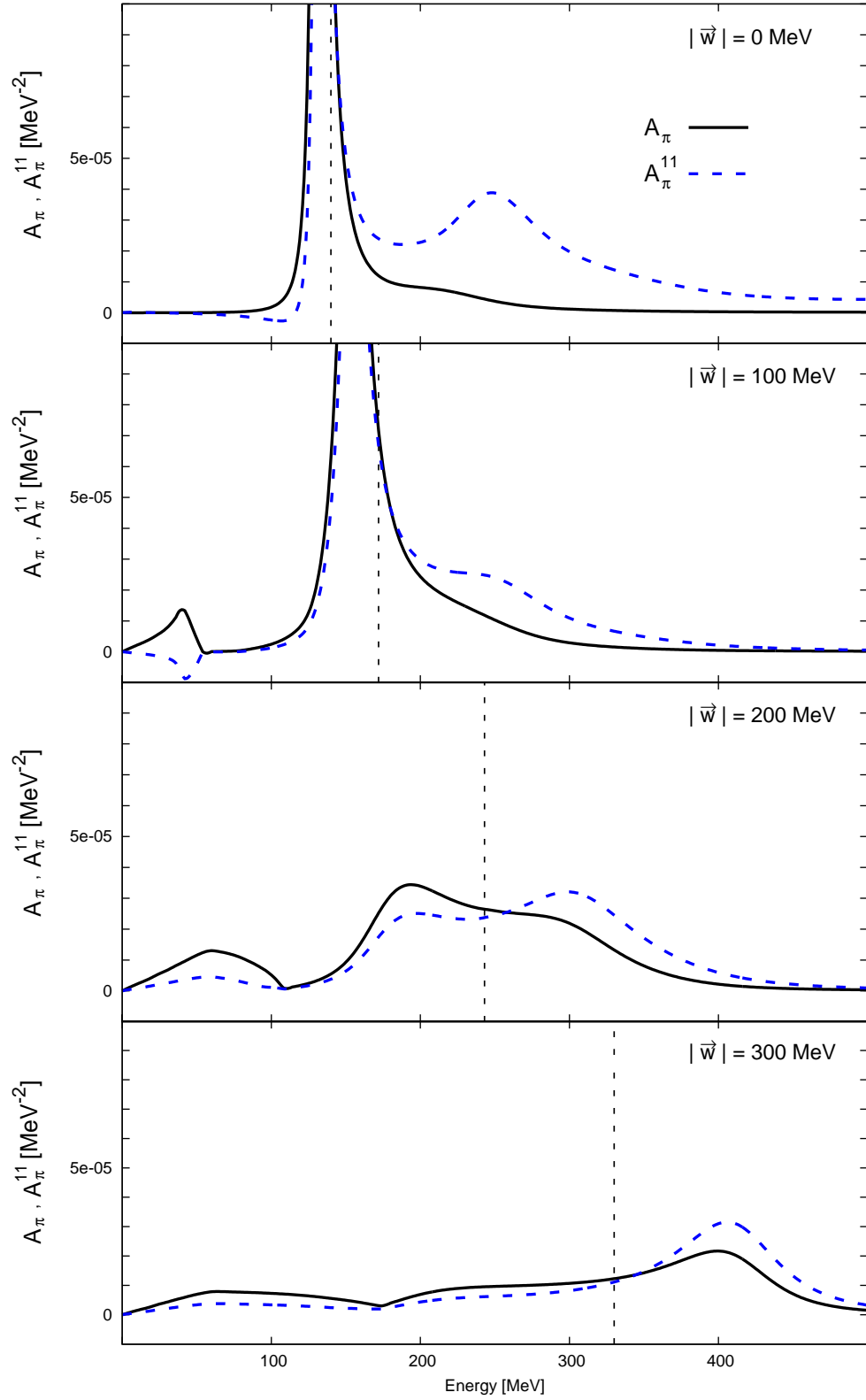


Figure 4.16.: Pion spectral function A_π (full line) and effective spectral function A_π^{11} (4.55) (dashed line) for parameter set 1 and normal nuclear density.

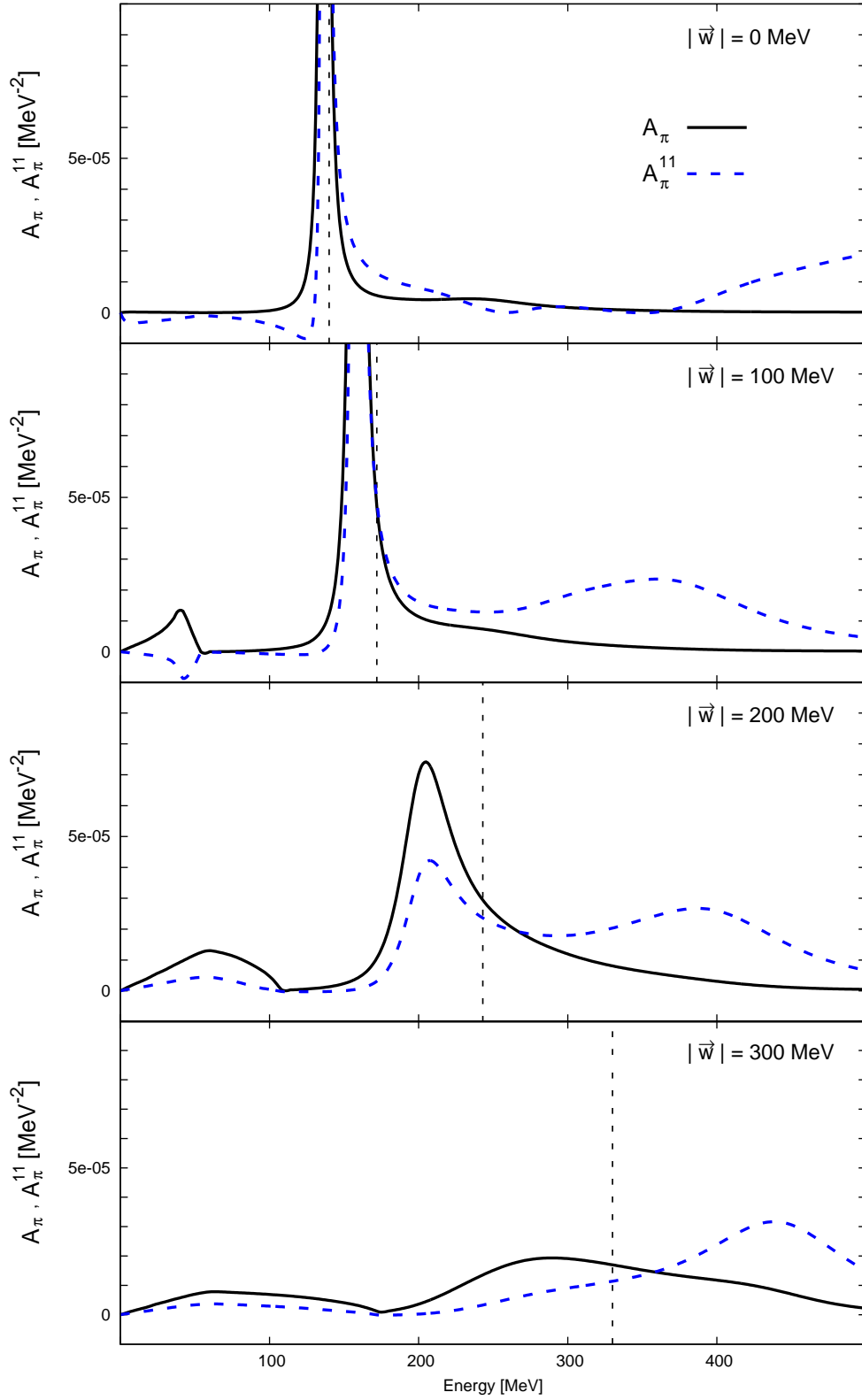


Figure 4.17.: Pion spectral function A_π (full line) and effective spectral function A_π^{11} (4.55) (dashed line) for parameter set 2 and normal nuclear density.

4. Pions and Δ -isobars at finite density

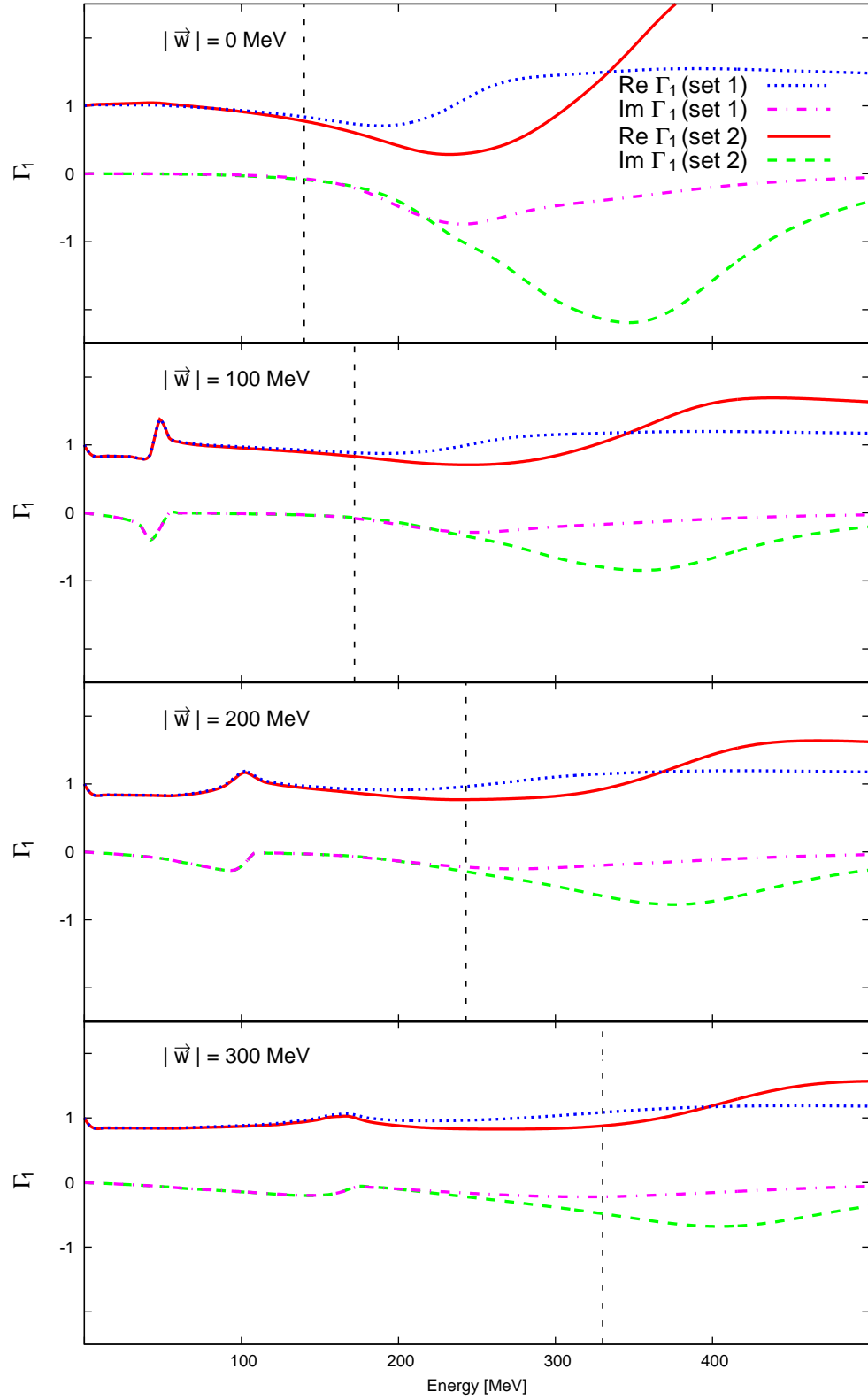


Figure 4.18.: Vertex function Γ_1 (4.24) for normal nuclear density and both parameter sets.

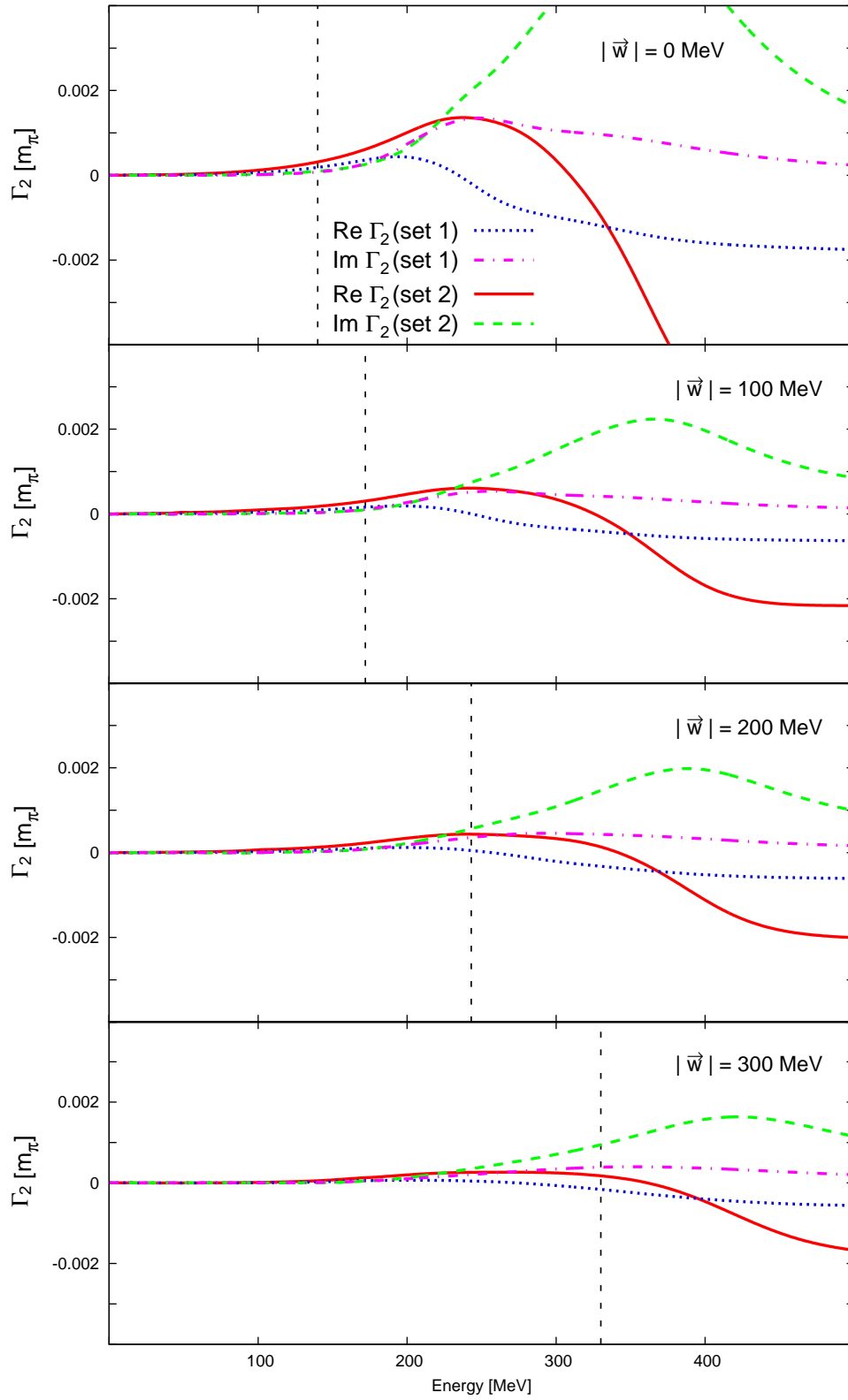


Figure 4.19.: Vertex function Γ_2 (4.24) for normal nuclear density and both parameter sets.

4. Pions and Δ -isobars at finite density

5. Relations to the Φ -functional

Before we draw the conclusions of what has been done in this work we would like to point out some relations of our approach to the Φ -functional method [109, 110]. Up to now we determined the self-energies (3.6, 3.9, 3.11, 4.14, 4.13) entering in our coupled set of coupled Dyson equations (3.2, 4.4) by the principal that we would like to sum up all soft modes in the system. However there is a more schematic method for the construction of the self-energies which could serve as a guidance. This method is provided by the Φ -functional approach. Within this method or, more general, in self-consistent two-particle irreducible (2PI) approximation schemes [109, 110], the self-energies Σ or Π for the baryons and mesons are derived from a generating functional, called Φ -functional. This functional is given by a truncated set of closed diagrams in accordance with the interaction Lagrangian where all lines denote dressed, i.e. self-consistent propagators. The self-energies result as functional variations with respect to the meson G and baryon S propagators, i.e.

$$-i\Sigma(x, y) = \frac{\delta i\Phi[G, S]}{\delta iS(y, x)} \quad \text{or} \quad -i\Pi(x, y) = \frac{\delta i\Phi[G, S]}{\delta iG(y, x)}. \quad (5.1)$$

This implies an opening of a corresponding propagator line in the diagrams of Φ . For the resulting set of coupled Dyson equations such 2PI approaches guarantee that even in a partial resummation of a single class of diagrams the conservation laws which are related to the symmetries of the system are fulfilled on the level of expectation values [109]. In addition such a set-up guarantees the thermodynamic consistency of the approximation. However we have to point out strongly that this scheme can only serve as a guide determining which diagrams are to be included in the calculations. This is due to the fact that the actual self-energies might have divergences which have to be absorbed in counter terms. At this point the Φ -functional approach and our scheme using dispersion relations deviate in the choice of these counter terms.

In the Φ -functional approach the procedure to generate the coupled Dyson equation would be like this. First our strategy is that all soft modes have to be resummed while all the hard modes can be treated as local point vertices. As already stated in sections 3.2 and 4.2 this implies that the key ingredients of this approach are correlation loops

5. Relations to the Φ -functional

resulting both from particle-hole and meson-meson channels

$$\chi^{\mu\nu} = \text{bubble}(\chi) = \left\{ \begin{array}{l} \text{bubble}(N) ; \text{bubble}(\Delta) ; \\ \text{bubble}(\rho) ; \text{bubble}(\omega) \end{array} \right\} \quad (5.2)$$

which in a relativistic treatment take the form of Lorentz polarisation tensors. With the help of the correlation loops (4.7) and using the interactions (3.1, 4.1, 4.3) which also allow to couple any of these loops directly using a four point vertex¹. It is possible to define a 2PI Φ -functional

$$\Phi = \begin{array}{l} \text{self-energy}(\chi) + \text{self-energy}(\Delta) + \text{self-energy}(\rho) + \text{self-energy}(\omega) \\ + \frac{1}{2} \text{triangle}(\chi, \pi) + \frac{1}{3} \text{triangle}(\chi, \chi, \pi) + \frac{1}{4} \text{triangle}(\chi, \chi, \chi, \pi) + \dots \\ + \frac{1}{2} \text{triangle}(\chi, \chi, \chi) + \frac{1}{3} \text{triangle}(\chi, \chi, \chi, \chi) + \frac{1}{4} \text{triangle}(\chi, \chi, \chi, \chi, \chi) + \dots, \end{array} \quad (5.3)$$

to be understood in a properly chosen regularisation scheme. As already mentioned the renormalisation of the resulting Dyson equations will not use the counter terms as following from this functional (5.3) but will use the dispersion relations stated in sections 3.3 and 4.3. Therefore we use the Φ -functional only as a book-keeping tool telling us which diagrams have to be resummed. The upper set of diagrams in (5.3) defines the

¹A generalisation of the interactions used in (3.1, 4.1, 4.3) to allow for all necessary four point couplings is straight forward.

Hartree mean-field terms, while the infinite set of ring diagrams with χ -loops of any sort given in (4.7) generate the following RPA resummed expressions²

$$\begin{aligned}
\Pi^{\mu\nu} &= \text{---} \bullet \text{---} \Pi^{\mu\nu} \text{---} \bullet \text{---} = \text{---} \bullet \text{---} \chi \text{---} \bullet \text{---} + \text{---} \bullet \text{---} \chi \text{---} \bullet \text{---} \chi \text{---} \bullet \text{---} + \dots \\
&= \left[\chi \cdot (1 - g' \cdot \chi)^{-1} \right]^{\mu\nu} \\
\Gamma^{\mu\nu} &= \text{---} \bullet \text{---} \Gamma^{\mu\nu} \text{---} \bullet \text{---} = g' \cdot \Pi^{\mu\nu} \cdot g' \\
\Gamma^\mu &= \text{---} \bullet \text{---} \Gamma^\mu \text{---} \bullet \text{---} = q^\mu + g' \cdot \Pi^{\mu\nu} q_\nu
\end{aligned} \tag{5.4}$$

They are relevant for the short range correlations and the corresponding vertex corrections. The difference between these expressions is given by the outer most vertices. In the case of Π we have two three-point vertices at the outer most positions while $\Gamma^{\mu\nu}$ has two four-point vertices and Γ^μ one three and one four-point vertex. In all these quantities we now set the $\rho\omega$ -loop to zero because it contributes at very high energies only.

Almost all self-energies used so far follow by variation of Φ (5.3) with respect to the propagators implying to open any of the corresponding propagator lines (5.1). For the nucleon the self-energy results to

$$\begin{aligned}
\Sigma_N &= \text{---} \bullet \text{---} \times \text{---} + \text{---} \bullet \text{---} \text{---} \Gamma^\mu \text{---} \bullet \text{---} \text{---} \Gamma^\nu \text{---} \bullet \text{---} + \text{---} \bullet \text{---} \text{---} \Gamma^\mu \text{---} \bullet \text{---} \text{---} \Gamma^\nu \text{---} \bullet \text{---} \\
&+ \text{---} \bullet \text{---} \text{---} \Gamma^{\mu\nu} \text{---} \bullet \text{---} + \text{---} \bullet \text{---} \text{---} \Gamma^{\mu\nu} \text{---} \bullet \text{---} \dots
\end{aligned} \tag{5.5}$$

The self-energies for the isobar is given by

$$\Sigma_\Delta = \text{=} \bullet \text{=} \times \text{=} + \text{=} \bullet \text{=} \text{---} \Gamma^\mu \text{---} \bullet \text{---} \text{---} \Gamma^\nu \text{---} \bullet \text{=} + \text{=} \bullet \text{=} \text{---} \Gamma^{\mu\nu} \text{---} \bullet \text{=} \dots \tag{5.6}$$

Here the correlation diagrams are instrumental in order to avoid the standard use of soft form-factors. In the case of the pion we get a first contribution when opening any of the

²Besides the Lorentz structure for χ , these are matrix relations also in the excitation channels $i \in \{NN^{-1}, \Delta N^{-1}, \pi\rho, \dots\}$. Thereby χ takes a diagonal form with values given by (4.7), while the channel-channel couplings are compiled in g' .

5. Relations to the Φ -functional

explicitate pion lines in (5.3). This produces the first diagram in (5.7)³

$$\Pi_\pi = \text{---} \bullet \text{---} \left[\text{---} \bullet \text{---} \right] + \left[\text{---} \bullet \text{---} \right] + \left[\text{---} \bullet \text{---} \right], \quad (5.7)$$

and corresponds to the well known nucleon- and isobar-hole contributions modified by short range interactions. However now we also have $\pi\rho$ loops hidden in the χ bubbles. Opening the corresponding pion lines gives two further self-energy terms given in brackets. The first one gives a correction to the $\pi\rho$ -loop in the pion self-energy where the vertices are dressed by short-range effects. The second one is similar to the main term but contains an additional ρ -meson.

The self-energy for the ρ -meson will be given by

$$\Pi_\rho = \text{---} \times \text{---} + \text{---} \left[\text{---} \right] + \text{---} \left[\text{---} \right] + \text{---} \left[\text{---} \right] + \text{---} \left[\text{---} \right] + \text{---} \left[\text{---} \right] \quad (5.8)$$

where all diagrams except the third one follow from the ϕ -functional (5.3). This third diagram is included for a more complete correction of the $\rho\pi\pi$ -vertex. The ω -meson receives a similar self-energy corrections as the ρ -meson, however, since we have no $\omega\pi$ -loops in our definition of χ we get the following terms

$$\Pi_\omega = \text{---} \times \text{---} + \text{---} \left[\text{---} \right] + \text{---} \left[\text{---} \right] \quad (5.9)$$

only. In the end we arrive at a set of coupled Dyson equations for the determination of the full retarded propagators in terms of the retarded self energies or polarisation tensors and the free propagators.

³We set some terms in brackets to indicated further approximations. Details follow bellow.

The model studied in this work uses only a subset of the self-energies indicated by this approach. We studied the baryonic part with the self-consistent interplay of the Δ -isobar together with the pion and nucleon at zero temperature and a pure mesonic model where we consider the interactions of the pion with the ρ - and ω -meson at finite temperature. These simplified treatments allowed us to introduce the new techniques on a less complicated level which proved to be mandatory to identify possible problems. In addition we neglected certain parts of the self-energies given above. For example we treated the nucleon with a sharp spectral function and thus all correlation terms in (5.5) were ignored keeping only the scalar and vector-meanfields. In addition all the terms in the brackets have been neglected due to phase-space suppression arguments. In a more complete treatment one could also start including these diagrams and establish the connection between the two subsystems studied so far.

For renormalisable theories Φ -derivable approximations can be proven to be renormalisable with counter term structures defined on the vacuum level [77, 111, 112]. Since our field theoretical model is not renormalisable in the standard sense we use dispersion relations instead of the procedure described in [77, 111, 112].

5. *Relations to the Φ -functional*

6. Conclusions and Outlook

Conclusions

In this work we studied the influence of the presence of nuclear matter on the spectral properties of the light vector-mesons ρ and ω as well as on the pion and the Δ -isobar in a self-consistent framework. Here the aim was to include not only short-range correlations of the usual Migdal type but in addition to include vertex corrections in order to consistently sum up all soft modes of the system. These short-range correlations which are normally used to describe the interactions of the pion with nucleon and Δ -isobar were also applied to the vector-mesons. Special emphasis was put on the determination of the real-parts of all self-energies and the proper avoiding of kinematical singularities in the self-consistent treatment [88]. The self-consistent treatment of vector-mesons within the current model setup requires great care due to the fact that the polarisation tensors have to be four transversal meaning that no unphysical degrees of freedom are propagated. In contrast to perturbation theory where Ward-Identities are conserved at each order of the expansion, conservation laws are spoiled as soon as self-consistency comes into play. The reason for this is that only certain sub-classes of diagrams are now summed up to infinite order thus violating Ward-Identities. One cure to restore four transversality is given by projection schemes which construct four transversal objects out of the given polarisation-tensors obtained in the resummation. We studied these techniques used up to now and found that some have severe problems arising from kinematical singularities which are introduced by the projection. Therefore we invented a new ad hoc method to circumvent these problems. In the baryonic system we now achieved a description of the isobar properties without relying on the usually used soft formfactors. This is conceptual important because the presence of soft formfactors, where the cutoff scale is of the same order as the physics one likes to describe, makes the in-medium extrapolation doubtful. In addition we used a fully relativistic treatment of all particles including the spin 3/2 Δ -isobar. This is important to guaranty the proper behaviour of the self-energies in all kinematical regions. In addition in a self-consistent treatment where new low energetic modes may emerge this is the more reasonable treatment because these new modes may not be heavy enough to allow for a non-relativistic expansion. Since a lot of preparatory work concerning the renormalisation and the proper avoiding of kinematical singularities had to be done we decided to first consider two independent systems namely a purely mesonic system where we have interactions of ρ - and ω -meson

6. Conclusions and Outlook

together with the pion and one baryonic system where we studied the dynamics of the $\pi N\Delta$ -system at zero temperature.

The parameters of the model were adjusted to reproduce $\pi\pi$ - and πN -scattering in the relevant channels as well as photo absorption on nucleon and nucleus. We found that in the meson sector we could achieve a good description of either the $\pi\pi$ -phaseshifts or of the electromagnetic formfactor only by a different choice of the parameters. A simultaneously fit of both quantities would require to take more vertex corrections beyond our model into account. Since the phase-shifts offer a more clean method to determine the parameters we then used this input only. In addition it turned out that a proper description of the ω -meson properties also requires to take more processes into account [68]. Therefore our model can only serve as a first estimate here. In the baryonic subsystem we can get a good simultaneous description of the scattering and photo absorption data. However for reproducing the empirical scattering amplitude we had to take a moderate energy dependence of the vacuum isobar mass into account. This variation serves for processes beyond the s -channel pole contribution of the Δ isobar important for the description of the πN scattering amplitude like unitarised u -channel contributions. The fit of the Migdal parameters g_{11} , g_{12} and g_{22} to the photoabsorption data turned out being quite involved. Previous calculations [22] used the resonance contributions of the Δ -isobar only to adjust the parameters. However there are considerable background terms [14, 99–101] which have to be taken into account before reliable conclusions can be drawn. Special care has also to be taken about vertex corrections. However despite these problems it turns out that the values for the Migdal parameters g_{11} , g_{12} and g_{22} used in other approaches [32] give also reasonable results in our scheme. The meanfield-shifts required for the isobar are repulsive however within the resolution of the model we cannot make detailed statements about the individual size of the scalar and vector meanfield but only about the total shift. In addition the current status of the model for the photo absorption allows not to draw detailed conclusions about the values of the Migdal parameters or the mean-fields. However we have to note that even a rather large attraction of the isobar could well be in agreement with the data.

In the purely mesonic system containing pion as well as ρ - and ω -meson we made the experience that no large medium effects are visible even at high temperatures and when taking correlations and vertex corrections into account. This complies with earlier studies [35, 36, 38, 40, 113] where it was found that the dominating in-medium effect on the light vector mesons results from the direct interaction with baryons. We only observe a moderate broadening of about 30 MeV for both vector-mesons even at 120 MeV temperature. The influence of the vertex corrections and short range correlations turned out to be quite small. In addition in such a purely mesonic scenario self-consistency was found to play only a minor role and has the most pronounced effects on the pion.

However this picture concerning vertex corrections and self-consistency might change when including direct baryon couplings because then new low energetic resonance-hole excitations become available.

In contrast to this in the baryonic system we have strong effects from the vertex corrections and the self-consistency requirement. The vertex corrections turn out to be essential in order to obtain an in-medium Δ -isobar which is not strongly broadened. This is due to the fact that these vertex corrections effectively suppress the nucleon-hole states in the pion propagator. A definite statement about the Migdal parameters and the in-medium mass-shift of the Δ -isobar could not be obtained within the present framework. We observe that the contribution of the s-channel isobar exchange to the photo absorption is only about 30 %, nearly independent of the parameters used. This makes a more detailed study of the background terms essential.

Outlook

The present status of the work suggests extensions in several directions. First of all it is essential to extend the calculations of the photoabsorption in order to determine the values of the Migdal parameters and the mean-fields of the isobar. Here a complete treatment requires to include further corrections of the $\gamma\pi\pi$ - and γNN -vertices. This will then modify especially the interference between the resonance and the t-channel pion exchange and will allow a much better understanding of the microscopic processes. After this the calculations already made in the pion-baryon sector could be applied to electron scattering or neutrino induced reactions. Additionally it would be straight forward to obtain the pion optical potential as resulting from our model and compare the results to data. With more effort one could also try to describe pion absorption or charge exchange reactions [11]. An interesting topic would also be to study pionic atoms using our model for the πN -amplitude. Here the possible strong attraction we can get for the isobar could possibly explain the rather strong imaginary part of the scattering length. All this would help to constrain the model further because different kinematical regions are probed. Having then a quite well settled model an extension of the calculations in the pion-baryon sector to finite temperatures is conceptual unproblematic. Further extensions could then point towards the unification of both parts of this work namely to study a combined system of baryons and vector-mesons at finite density and temperature. Concerning such applications to vector-mesons it would of course be necessary to describe also further resonances like the $N^*(1520)$ resonance in a similar framework. Such an extended model would then also allow applications of the so obtained spectral functions to dilepton spectra [43]. The latter would require to implement the so obtained microscopic results into some macro dynamical model, such as hydrodynamical or fireball evolution models. This could then allow for a proper description of the nuclear collision dynamics.

6. *Conclusions and Outlook*

7. Appendix

A. $\pi\rho$ loop tensor coefficients

The imaginary parts of the $\rho\pi$ loop functions χ_{ij} of Eq. (3.13) are given by

$$\begin{aligned}\Im\chi_{ij}^{(\rho\pi)}(w, u) &= 2g_{\rho\pi\pi} \int \frac{d^4l}{(2\pi)^4} (H^{[ij,22]} A_{22}^\rho(l, u) + H^{[ij,T]} A_T^\rho(l, u)) A_\pi(l - w, u) \\ &\quad (n_B(l \cdot u) - n_B((l - w) \cdot u)) F(w^2), \\ \Im\chi_T^{(\rho\pi)}(w, u) &= 2g_{\rho\pi\pi} \int \frac{d^4l}{(2\pi)^4} (H^{[T,22]} A_{22}^\rho(l, u) + H^{[T,T]} A_T^\rho(l, u)) A_\pi(l - w, u) \\ &\quad (n_B(l \cdot u) - n_B((l - w) \cdot u)) F(w^2),\end{aligned}\tag{A.1}$$

in terms of coefficients $H^{[11,22]}$ and $H^{[11,T]}$ given in Appendix B. The determination of the realparts requires some care for two reasons. First of all the imaginary parts don't tend to zero for large energies making renormalisation necessary. For example we consider the vacuum on-shell limit of the imaginary parts

$$\begin{aligned}\Im\chi_{11}^{(\rho\pi)} &= \frac{g_{\rho\pi\pi} |\vec{l}_\pi|^3}{2\pi m_\rho^2 \sqrt{s}} & \Im\chi_{22}^{(\rho\pi)} = \Im\chi_T^{(\rho\pi)} &= \frac{g_{\rho\pi\pi} (2m_\rho^2 + |\vec{l}_\pi|^2) |\vec{l}_\pi|}{12\pi m_\rho^2 \sqrt{s}} \\ \Im\chi_{12}^{(\rho\pi)} &= \Im\Pi_{21}^{(\rho\pi)} = 0 \\ |\vec{l}_\pi| &= \frac{1}{2} \left[\frac{((m_\rho - m_\pi)^2 - s)((m_\rho + m_\pi)^2 - s)}{s} \right]^{1/2}.\end{aligned}\tag{A.2}$$

As one clearly observes these functions don't tend to zero for large energies. This problem will be handled by a formfactor

$$F(q^2) = \left[\left(\exp\left(\frac{w^2 - \lambda^2}{\lambda^2}\right) \right)^2 \theta(w^2 - \lambda^2) + \theta(\lambda^2 - w^2) \right]\tag{A.3}$$

with $\lambda = 1250$ MeV. In addition we have to take care about the kinematical constraints. This can be done in the same way as for the baryonic loops by choosing a different

7. Appendix

representation:

$$\begin{aligned}
\chi_{11}^{(\rho\pi)}(\omega, \vec{q}) &= \frac{1}{q^2} \chi_1^{(\rho\pi)}(\omega, \vec{q}), \\
\chi_{12}^{(\rho\pi)}(\omega, \vec{q}) &= \frac{1}{\sqrt{q^2 - (q \cdot u)^2}} \left(\frac{q \cdot u}{q^2} \chi_1^{(\rho\pi)}(\omega, \vec{q}) - \chi_2^{(\rho\pi)}(\omega, \vec{q}) \right), \\
\chi_{22}^{(\rho\pi)}(\omega, \vec{q}) &= \frac{q \cdot u}{q^2 - (q \cdot u)^2} \left(\frac{q \cdot u}{q^2} \chi_1^{\Delta h}(\omega, \vec{q}) - 2 \chi_2^{(\rho\pi)}(\omega, \vec{q}) \right. \\
&\quad \left. + \frac{q^2}{q \cdot u} \chi_3^{(\rho\pi)}(\omega, \vec{q}) \right), \\
\chi_T^{(\rho\pi)}(\omega, \vec{q}) &= \frac{1}{2} \left(\chi_4^{(\rho\pi)}(\omega, \vec{q}) - \chi_{11}^{(\rho\pi)}(\omega, \vec{q}) - \chi_{22}^{(\rho\pi)}(\omega, \vec{q}) \right). \tag{A.4}
\end{aligned}$$

The functions $\chi_i^{(\rho\pi)}$ can now be build up, using the kernels defined in Appendix B,

$$\begin{aligned}
\chi_i^{(\rho\pi)}(\omega, \vec{q}) &= \left[\delta_{i4} \chi_3^{(\rho\pi)}(0, \vec{q}) \right. \\
&\quad \left. - 2g_{\rho\pi\pi} \int \frac{d^4 l}{(2\pi)^4} \int_{-\infty}^{+\infty} \frac{d\bar{\omega}}{\pi} \left(\frac{q^2}{\bar{q}^2} \right)^{n_i} \frac{(H^{[i,22]} A_{22}^\rho(l, u) + H^{[i,T]} A_T^\rho(l, u)) A_\pi(l - w, u)}{\bar{\omega} - \omega - i\epsilon} \right. \\
&\quad \left. (n_B(l \cdot u) - n_B((l - w) \cdot u)) F(w^2) \right] + (q_\mu \rightarrow -q_\mu), \tag{A.5}
\end{aligned}$$

for $i = 1, 3, 4$ with $n_{1,4} = 2$, $n_2 = 1$ and $q^2 = \omega^2 - \vec{q}^2$, $\bar{q}^2 = \bar{\omega}^2 - \vec{q}^2$. While for $n = 2$ we have

$$\begin{aligned}
\chi_i^{(\rho\pi)}(\omega, \vec{q}) &= \left[\delta_{i4} \chi_3^{(\rho\pi)}(0, \vec{q}) \right. \\
&\quad \left. - 2g_{\rho\pi\pi} \int \frac{d^4 l}{(2\pi)^4} \int_{-\infty}^{+\infty} \frac{d\bar{\omega}}{\pi} \left(\frac{\omega}{\bar{\omega}} \right) \frac{(H^{[i,22]} A_{22}^\rho(l, u) + H^{[i,T]} A_T^\rho(l, u)) A_\pi(l - w, u)}{\bar{\omega} - \omega - i\epsilon} \right. \\
&\quad \left. (n_B(l \cdot u) - n_B((l - w) \cdot u)) F(w^2) \right] - (q_\mu \rightarrow -q_\mu), \tag{A.6}
\end{aligned}$$

B. Coefficient functions $H^{[lm,ij]}$, $H^{[T,ij]}$, $H^{[lm,T]}$ and $H^{[T,T]}$

$$H^{[T,lm]} = \frac{1}{2} g^{\nu\alpha} g^{\mu\beta} T_{\mu\nu}(w, u) L_{\alpha\beta}^{(ij)}(l, u) \quad H^{[ij,T]} = g^{\nu\alpha} g^{\mu\beta} L_{\mu\nu}^{(ij)}(w, u) T_{\alpha\beta}(l, u)$$

$$H^{[ij,lm]} = g^{\nu\alpha} g^{\mu\beta} L_{\mu\nu}^{(ij)}(w, u) L_{\alpha\beta}^{(ij)}(l, u)$$

$$H^{[11,y]} = \frac{1}{w^2} H^{[1,y]}$$

$$H^{[12,y]} = \frac{1}{\sqrt{w^2 - (u \cdot w)^2}} \left[\frac{(u \cdot w)}{w^2} H^{[1,y]} - H^{[2,y]} \right]$$

$$H^{[22,y]} = \frac{(u \cdot w)}{w^2 - (u \cdot w)^2} \left[\frac{(u \cdot w)}{w^2} H^{[1,y]} - 2 H^{[2,y]} + \frac{w^2}{(u \cdot w)} H^{[3,y]} \right]$$

$$H^{[T,y]} = \frac{1}{2} [H^{[4,y]} - H^{[11,y]} - H^{[22,y]}] \quad y \in \{ij, T\}$$

$$H^{[1,11]} = \frac{(l \cdot w)^2}{l^2} \quad H^{[2,11]} = \frac{(u \cdot l)(l \cdot w)}{l^2} \quad H^{[3,11]} = \frac{(u \cdot l)^2}{l^2} \quad H^{[4,11]} = 1$$

$$H^{[1,12]} = \frac{(l \cdot w)((u \cdot l)(l \cdot w) - l^2(u \cdot w))}{l^2 \sqrt{l^2 - (u \cdot l)^2}} \quad H^{[2,12]} = -\frac{(l \cdot w) \sqrt{l^2 - (u \cdot l)^2}}{l^2}$$

$$H^{[3,12]} = \frac{w^2(u \cdot l)^3 - l^2((u \cdot w)(l \cdot w) + (u \cdot l)(w^2 - (u \cdot w)^2))}{l^2 \sqrt{l^2 - (u \cdot l)^2}} \quad H^{[4,12]} = 0$$

$$H^{[1,22]} = \frac{((u \cdot l)(l \cdot w) - l^2(u \cdot w))^2}{l^2(l^2 - (u \cdot l)^2)} \quad H^{[2,22]} = (u \cdot w) - \frac{(u \cdot l)}{l^2}$$

$$H^{[3,22]} = 1 - \frac{(u \cdot l)^2}{l^2} \quad H^{[4,22]} = 1$$

$$H^{[1,T]} = -\frac{(l \cdot w)^2 - 2(u \cdot w)(u \cdot l)(l \cdot w) + (u \cdot l)^2 w^2 + l^2((u \cdot w)^2 - w^2)}{2(l^2 - (u \cdot l)^2)}$$

$$H^{[2,T]} = 0 \quad H^{[3,T]} = 0 \quad H^{[4,T]} = 1$$

$$H^{[T,21]} = H^{[T,12]} \quad H^{[22,21]} = H^{[22,12]} \quad H^{[11,21]} = H^{[11,12]}$$

$$H^{[12,21]} = H^{[21,12]} \quad H^{[21,21]} = H^{[12,12]}$$

$$H^{[21,22]} = H^{[12,22]} \quad H^{[21,T]} = H^{[12,T]} \quad H^{[21,11]} = H^{[12,11]} \quad (B.1)$$

C. Ghost states in the pion self-energy

The occurrence of ghost causes a severe problem [74]. It implies that the pion self energy does not satisfy a Lehman representation anymore. A ghost state is present if the pion self energy has a pole for complex energies, i.e.

$$D(\omega) = \det[1 - \Pi^{(L)}(\omega, \vec{q}) g^{(L)}] = 0 \quad \text{with} \quad \Im\omega \neq 0. \quad (\text{C.1})$$

Note that a function that satisfies a Lehman representation can have poles only on the 2nd or higher Rieman sheets. In fact, we claim that such artifacts are avoided all together once a finite renormalisation is implemented such that all elements $\Pi_{ij}(\omega, \vec{q})$ are bounded for large energies, i.e.

$$\lim_{\omega \rightarrow \pm\infty} |\Pi_{ij}(\omega, \vec{q})| < \infty. \quad (\text{C.2})$$

It is noted that the condition (C.2) may be viewed as a construction rule how to define additional terms of the form (4.3) involving a finite number of time or spatial derivatives¹. The latter amount to introducing effective energy and momentum dependent coupling constants $g'_{ij}(\omega, \vec{q})$ to be used in (4.16). In this work, rather than constructing such counter terms explicitly we impose the condition (C.2) on the loop functions directly.

Our argument that (C.2) indeed avoids the formation of ghost states goes as follows [74]: According to a theorem² proven by Symanzik [114] and Weinberg [115] one may represent the determinant

$$\begin{aligned} D(\omega) &= R(\omega) H(\omega), \\ H(\omega) &= H_0 + H_1 \omega + \int_{\text{thres}}^{\infty} \frac{dz}{\pi} \frac{\omega}{z} \frac{\Im H(z)}{z - \omega - i\epsilon}, \end{aligned} \quad (\text{C.3})$$

in terms of a so-called Herglotz function $H(\omega)$ [116] and a rational function $R(\omega)$. Here we use the fact that all elements $\Pi_{ij}(\omega, \vec{q})$ are analytic functions with branch cuts on the real axis only. A Herglotz function is characterised by $\Im H(\omega) > 0$ and $H_1 > 0$ in (C.3). The spectral density $\Im H(\omega)$ may contain a finite number of positive δ -function terms. An important property of the Herglotz functions is that it does not support zeros at complex ω . Moreover the number of zeros permitted at real energies exceeds the number of poles at most by one³. From the assumption (C.2) it follows that $D(\omega)$

¹The imaginary parts of the particle and isobar hole loops are bounded due to kinematics. For the $\rho\pi$ -loop we achieve the same by using a formfactor.

²We reject here the pathological case where $\Im D(\omega)$ changes sign infinitely many times.

³This property follows once the Herglotz function with a finite number of pole terms is decomposed in terms of a Wigner R-function [117] and a Herglotz function with no pole terms. A Wigner R-function has simple poles and zeros only, that interlace [118]. A function $R(z)$ is called an R-function if it has the following properties: $R(z)$ is meromorphic, $\Im R(z) \Im z \geq 0$. Adding to a R-function a monotonic function, i.e. a Herglotz function without poles, can not lead to additional zeros.

is asymptotically bounded by a constant, and also that $D(\omega)$ does not have any pole in the complex plane. Since the Herglotz function behaves asymptotically like [116]

$$\frac{H(\omega)}{\omega} \longrightarrow H_1 \quad \text{as } |\omega| \longrightarrow \infty \quad (\text{C.4})$$

we conclude the the rational function $R(\omega)$ must in this case vanish like

$$R(\omega) \longrightarrow \frac{1}{\omega}. \quad (\text{C.5})$$

As a consequence it is also excluded that $D(\omega)$ develops zeros at complex ω . This follows because all poles in $R(\omega)$ must be cancelled by the zeros of the Herglotz function $H(\omega)$. Furthermore any pole in the Herglotz function must be compensated for by corresponding zeros in $R(\omega)$. Trouble may be induced by possibly complex zeros in $R(\omega)$ that are not associated with poles in $H(\omega)$. The latter are excluded by the asymptotic properties of $D(\omega)$. This can be seen as follows. Let m and n be the number of poles and zeros of the Herglotz function and j and i the number of poles and zeros of the rational function respectively. Since $D(\omega)$ has no poles we need to have

$$i \geq m \quad n \geq j. \quad (\text{C.6})$$

Further it holds

$$j - i = 1 \quad n = m + 1 \quad (\text{C.7})$$

due to the properties of $D(\omega)$ and $H(\omega)$ ⁴. This leads us the the conclusion

$$m + 1 \geq j \quad j \geq m + 1 \quad (\text{C.8})$$

which can only be fulfilled if

$$j = m + 1 \Rightarrow i = m = n - 1 \quad (\text{C.9})$$

and therefore can't have a pole in the complex plain because we need all i allowed zeros in $R(\omega)$ to cancel the poles of $H(\omega)$.

⁴The case with $m = n$ which automatically requires $i = j$ can be treated along the same lines.

D. Different gauges

Up to now we only stated that we use unitary gauge for the vector mesons. In order to clarify the reason for this we will now analyse different possible choices for the t'Hooft gauge. The essential differences can already be seen in vacuum and on a perturbative level so that we can restrict the discussion to this case. Our choice of the interaction (3.1) is a special case (unitary gauge) of the more general Stückelberg model. For details about the this model we refer to [78] and references within. From the Stückelberg Lagrangian

$$\begin{aligned} \mathcal{L}_{\text{Stückel.}} = & -\frac{1}{4}\rho_{\mu\nu}\rho^{\mu\nu} + \frac{m_\rho}{2}\rho^\mu\rho_\mu - \frac{1}{2\xi}(\partial_\mu\rho^\mu)^2 + \frac{1}{2}(\partial_\mu\phi)(\partial^\mu\phi) \\ & -\frac{\xi m_\rho^2}{2}\phi^2 + (\partial_\mu\eta^*)(\partial^\mu\eta) - \xi m_\rho\eta^*\eta \end{aligned} \quad (\text{D.1})$$

where we have in addition to the vector meson field ρ^μ or $\rho^{\mu\nu} = \partial^\mu\rho^\nu - \partial^\nu\rho^\mu$ respectively the ghost field η and the Stückelberg ghost ϕ we can directly read of the form

$$G_{\mu\nu}^{-1}(w) = (w^2 - m_\rho^2)g_{\mu\nu} + \frac{1 - \xi}{\xi}w_\mu w_\nu \quad (\text{D.2})$$

of the free inverse propagator containing the parameter ξ which interpolates between the renormalisable R_ξ gauges with $0 \leq \xi < \infty$ and the unitary gauge with $\xi = \infty$. After matrix inversion the retarded propagator turns into

$$G_{\mu\nu}(w) = \frac{g_{\mu\nu}}{w^2 - m_\rho^2 + i(w_0)\epsilon} - \frac{w_\mu w_\nu (1 - \xi)}{(w^2 - m_\rho^2 + i(w_0)\epsilon)(w^2 - m_\rho^2\xi + i(w_0)\epsilon)} \quad (\text{D.3})$$

The spectral function of the vector meson is the given through the imaginary part of this propagator

$$\begin{aligned} A_{\mu\nu}(w) = -2\Im[G_{\mu\nu}(w)] = & 2\pi \left[g_{\mu\nu} - \frac{w_\mu w_\nu}{w^2} \right] \delta(w^2 - m_\rho^2) (\theta(w_0) - \theta(-w_0)) \\ & + 2\pi \frac{w_\mu w_\nu}{m_\rho^2} \delta(w^2 - m_\rho^2\xi) (\theta(w_0) - \theta(-w_0)). \end{aligned} \quad (\text{D.4})$$

Note that this function needs a $i\epsilon$ prescription for all poles which appear in order to make the complete function retarded. We observe that in addition to the mode of the vector meson we have an additional ghost mode with a mass of $m_\rho\sqrt{\xi}$ in the spectra. This additional mode is four longitudinal and due to that recives no modifications from the self-energy which couples only to transverse modes. In addition the coupling of the ρ - and ω -meson within our model is such that this contribution modifies the pion self-energy only. In all other diagrams like $\omega \rightarrow \rho\pi$ we have to take only the transversal part into account thus making the result independent of the value of ξ . Within an arbitrary

choice of ξ the vacuum pion self-energy is given by

$$\begin{aligned} \Im\Pi_\pi(w) &= \frac{w^2}{8\pi m_\rho^2 w^2} \left[\sqrt{(w^2 - m_-^2)(w^2 - m_+^2)}^3 \theta(w^2 - m_+^2) \right. \\ &\quad \left. + (w^2 - m_\pi^2)^2 \sqrt{(w^2 - \bar{m}_-^2)(w^2 - \bar{m}_+^2)} \theta(w^2 - \bar{m}_+^2) \right] \\ m_\pm &= m_\rho \pm m_\pi \quad \bar{m}_\pm = m_\rho \sqrt{\xi} \pm m_\pi \end{aligned} \quad (\text{D.5})$$

Results for Landau ($\xi = 0$), Feynman ($\xi = 1$) and unitary gauge ($\xi = \infty$) are presented in Fig. D.1.

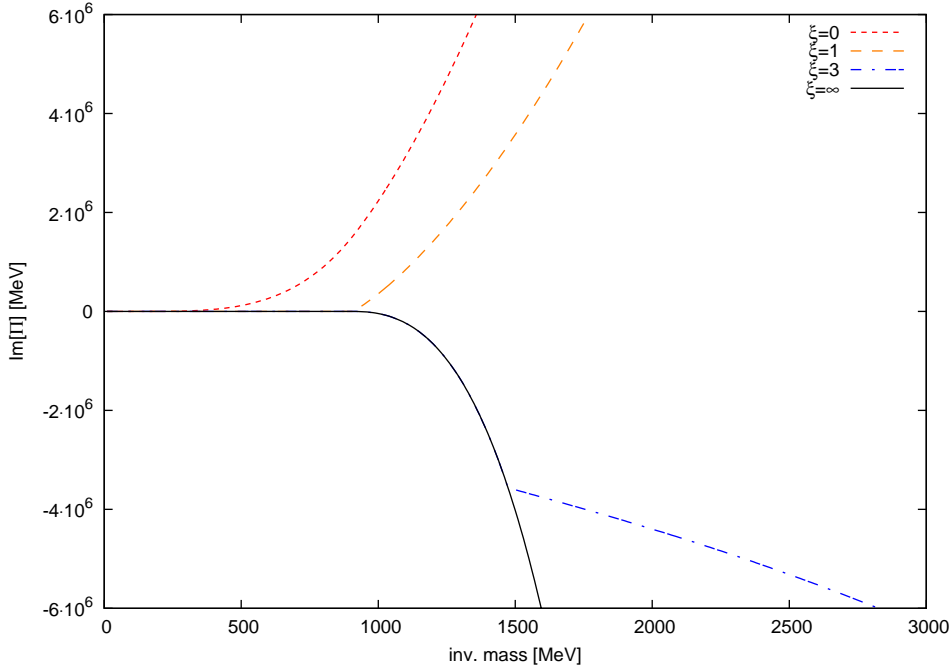


Figure D.1.: Results for the perturbative pion selfenergy in vacuum.

As we can already conclude from (D.5) the unitary gauge is special with respect to the UV behaviour where the imaginary part is proportional s^2 whereas in all other R_ξ gauges we have a behaviour proportional to s only. This is due the fact that when $\xi \rightarrow \infty$ is applied the ghost field which is responsible for the reduction of the UV behaviour is moved to infinite mass. This change of the UV behaviour is clearly visible by comparing the case of $\xi = 3$ with $\xi = \infty$. An other interesting effect arises when we set $\xi = 0$. Here we observe that the self-energy has the 'wrong' sign. This is clearly a signal from the unphysical ghost state at zero mass which now enters the calculation. In order to avoid these problems with ghost states we work in unitary gauge.

E. Coefficients of the vector-meson self-energies

We specify the imaginary parts of the coefficients $\Pi_{(\rho,i)}^{(ij)}$ and $\Pi_{(\rho,i)}^{(T)}$ in Eq. (3.34). In the case with vertex corrections we have:

$$\begin{aligned}
\Im\Pi_{(\rho,1)}^{(T,ij)}(w,u) &= g_{\rho\pi\pi}^2 \int \frac{d^4l}{2(2\pi)^4} (n_B((l-w)\cdot u) + n_B(l\cdot u)) \\
&\quad (B_{(T,ij)}^{[ll]} (A_{\pi}^{[11]}(l,u) A_{\pi}^{[00]}(l-w,u) + 2 A_{\pi}^{[10]}(l,u) A_{\pi}^{[10]}(l-w,u) \\
&\quad + A_{\pi}^{[00]}(l,u) A_{\pi}^{[11]}(l-w,u)) + B_{(T,ij)}^{[ww]} (A_{\pi}^{[00]}(l,u) A_{\pi}^{[11]}(l-w,u)) \\
&\quad - (B_{(T,ij)}^{[lw]} + B_{(T,ij)}^{[wl]}) (A_{\pi}^{[10]}(l,u) A_{\pi}^{[10]}(l-w,u) + A_{\pi}^{[00]}(l,u) A_{\pi}^{[11]}(l-w,u)) \\
&\quad + (B_{(T,ij)}^{[ul]} + B_{(T,ij)}^{[lu]}) (A_{\pi}^{[20]}(l,u) A_{\pi}^{[10]}(l-w,u) + A_{\pi}^{[10]}(l,u) A_{\pi}^{[20]}(l-w,u) \\
&\quad + A_{\pi}^{[12]}(l,u) A_{\pi}^{[00]}(l-w,u) + A_{\pi}^{[00]}(l,u) A_{\pi}^{[21]}(l-w,u)) \\
&\quad - (B_{(T,ij)}^{[uw]} + B_{(T,ij)}^{[wu]}) (A_{\pi}^{[20]}(l,u) A_{\pi}^{[10]}(l-w,u) + A_{\pi}^{[00]}(l,u) A_{\pi}^{[12]}(l-w,u)) \\
&\quad + B_{(T,ij)}^{[uu]} (A_{\pi}^{[22]}(l,u) A_{\pi}^{[00]}(l-w,u) + 2 A_{\pi}^{[20]}(l,u) A_{\pi}^{[20]}(l-w,u) \\
&\quad + A_{\pi}^{[00]}(l,u) A_{\pi}^{[22]}(l-w,u)), \tag{E.1}
\end{aligned}$$

$$\begin{aligned}
\Im\Pi_{(\rho,2)}^{(T,ij)}(w,u) &= g_{\omega\rho\pi}^2 \int \frac{d^4l}{2(2\pi)^4} (n_B(l\cdot u) + n_B((l-w)\cdot u)) \\
&\quad \left[(D_{(T,ij;22)}^{[ll]} A_{22}^{(\omega)}(l,u) + D_{(T,ij;T)}^{[ll]} A_T^{(\omega)}(l,u)) A_{\pi}^{[11]}(l-w,u) \right. \\
&\quad + (D_{(T,ij;22)}^{[lu]} A_{22}^{(\omega)}(l,u) + D_{(T,ij;T)}^{[lu]} A_T^{(\omega)}(l,u)) A_{\pi}^{[12]}(l-w,u) \\
&\quad + (D_{(T,ij;22)}^{[ul]} A_{22}^{(\omega)}(l,u) + D_{(T,ij;T)}^{[ul]} A_T^{(\omega)}(l,u)) A_{\pi}^{[21]}(l-w,u) \\
&\quad \left. + (D_{(T,ij;22)}^{[uu]} A_{22}^{(\omega)}(l,u) + D_{(T,ij;T)}^{[uu]} A_T^{(\omega)}(l,u)) A_{\pi}^{[22]}(l-w,u) \right]. \tag{E.2}
\end{aligned}$$

$$\begin{aligned}
 \Im\Pi_{(\rho,3)}^{(T)}(w, u) &= g_{\rho\pi\pi}^2 \int \frac{d^4l}{2(2\pi)^4} (H^{[T,T]} \Im\Pi_{(T)}^{(\rho\pi)}(l, u) + \sum_{ij=1}^2 H^{[T,ij]} \Im\Pi_{(ij)}^{(\rho\pi)}(l, u)) \\
 &\quad A_\pi(l+w, u)(n_B((l+w) \cdot u) + n_B(l \cdot u)) \\
 \Im\Pi_{(\rho,3)}^{(nm)}(w, u) &= g_{\rho\pi\pi}^2 \int \frac{d^4l}{2(2\pi)^4} (H^{[nm,T]} \Im\Pi_{(T)}^{(\rho\pi)}(l, u) + \sum_{ij=1}^2 H^{[nm,ij]} \Im\Pi_{(ij)}^{(\rho\pi)}(l, u)) \\
 &\quad A_\pi(l+w, u)(n_B((l+w) \cdot u) + n_B(l \cdot u)). \tag{E.3}
 \end{aligned}$$

Here we used the coefficient functions B and D specified in (E.9) and (E.8). The H functions are determined in Appendix B (B.1) We further decomposed the spectral function of the ω -meson

$$A_{\mu\nu}^{(\omega)}(l, u) = L_{\mu\nu}^{(22)}(l, u) A_{(22)}^{(\omega)}(l, u) + T_{\mu\nu}(l, u) A_{(T)}^{(\omega)}(l, u) \tag{E.4}$$

in the same way as the propagator (3.34). The functions $\Pi_i^{(\rho\pi)}$ are defined in (3.19) and we take the pion spectral functions $A_\pi^{[ij]}$ from (3.51). In the case without vertex corrections these expressions reduce to

$$\begin{aligned}
 \Im\Pi_{(\rho,1)}^{(T)}(w, u) &= g_{\rho\pi\pi}^2 \int \frac{d^4l}{2(2\pi)^4} (4 B_{(T)}^{[ll]} - 2 B_{(T)}^{[lq]} - 2 B_{(T)}^{[ql]} + B_{(T)}^{[qq]}) \\
 &\quad A_\pi(l, u) A_\pi(l+w, u) (n_B((l+w) \cdot u) + n_B(l \cdot u)) \\
 \Im\Pi_{(\rho,1)}^{(ij)}(w, u) &= g_{\rho\pi\pi}^2 \int \frac{d^4l}{2(2\pi)^4} (4 B_{(ij)}^{[ll]} - 2 B_{(ij)}^{[lq]} - 2 B_{(ij)}^{[ql]} + B_{(ij)}^{[qq]}) \\
 &\quad A_\pi(l, u) A_\pi(l+w, u) (n_B((l+w) \cdot u) + n_B(l \cdot u)) \tag{E.5}
 \end{aligned}$$

$$\begin{aligned}
 \Im\Pi_{(\rho,2)}^{(T)}(w, u) &= g_{\omega\rho\pi}^2 \int \frac{d^4l}{2(2\pi)^4} (D_{(T;22)}^{[ll]} A_{(22)}^{(\omega)}(l, u) + D_{(T;T)}^{[ll]} A_{(T)}^{(\omega)}(l, u)) \\
 &\quad A_\pi(l-w, u) (n_B(l \cdot u) + n_B((l-w) \cdot u)) \\
 \Im\Pi_{(\rho,2)}^{(ij)}(w, u) &= g_{\omega\rho\pi}^2 \int \frac{d^4l}{2(2\pi)^4} (D_{(ij;22)}^{[ll]} A_{(22)}^{(\omega)}(l, u) + D_{(ij;T)}^{[ll]} A_{(T)}^{(\omega)}(l, u)) \\
 &\quad A_\pi(l-w, u) (n_B(l \cdot u) + n_B((l-w) \cdot u)) \tag{E.6}
 \end{aligned}$$

$$\Im\Pi_{(\rho,3)}^{(T)}(w, u) = 0 \tag{E.7}$$

7. Appendix

It remains now to calculate the several contractions of the projectors. We specify only non-zero components.

$$\begin{aligned}
B_{(mn)}^{[ll]} &= L_{(mn)}^{\mu\nu}(w, u) l_\mu l_\nu & B_{(mn)}^{[uu]} &= L_{(mn)}^{\mu\nu}(w, u) u_\mu u_\nu \\
B_{(mn)}^{[lu]} &= L_{(mn)}^{\mu\nu}(w, u) l_\mu u_\nu & B_{(mn)}^{[ul]} &= L_{(mn)}^{\mu\nu}(w, u) u_\mu l_\nu \\
B_{(T)}^{[ll]} &= \frac{1}{2} T^{\mu\nu}(w, u) l_\mu l_\nu & B_{(T)}^{[uu]} &= \frac{1}{2} T^{\mu\nu}(w, u) u_\mu u_\nu \\
B_{(T)}^{[lu]} &= \frac{1}{2} T^{\mu\nu}(w, u) l_\mu u_\nu & B_{(T)}^{[ul]} &= \frac{1}{2} T^{\mu\nu}(w, u) u_\mu l_\nu \\
B_{(T)}^{[uu]} &= \frac{1}{2} T^{\mu\nu}(w, u) u_\mu u_\nu \\
\\
B_{(T)}^{[ll]} &= \frac{1}{2} \left(-\frac{(l \cdot w)^2 - 2(u \cdot l)(u \cdot w)(l \cdot w) + (u \cdot l)^2 w^2}{w^2 - (u \cdot w)^2} + l^2 \right) \\
B_{(11)}^{[ll]} &= \frac{(l \cdot w)^2}{w^2} & B_{(22)}^{[ll]} &= \frac{((u \cdot l) w^2 - (u \cdot w)(l \cdot w))^2}{w^2 (w^2 - (u \cdot w)^2)} \\
B_{(12)}^{[ll]} &= B_{(21)}^{[ll]} = \frac{(l \cdot w)((u \cdot w)(l \cdot w) - (u \cdot l) w^2)}{w^2 \sqrt{w^2 - (u \cdot w)^2}} \\
B_{(22)}^{[lu]} &= B_{(22)}^{[ul]} = (u \cdot l) - \frac{(u \cdot w)(l \cdot w)}{w^2} & B_{(22)}^{[uu]} &= 1 - \frac{(u \cdot w)^2}{w^2} \\
B_{(12)}^{[lu]} &= B_{(21)}^{[ul]} = -\frac{(l \cdot w) \sqrt{w^2 - (u \cdot w)^2}}{w^2} & B_{(11)}^{[qq]} &= w^2 \\
B_{(21)}^{[lu]} &= B_{(12)}^{[ul]} = \frac{(u \cdot w)((u \cdot w)(l \cdot w) - (u \cdot l) w^2)}{w^2 \sqrt{w^2 - (u \cdot w)^2}} \\
B_{(11)}^{[lu]} &= B_{(11)}^{[ul]} = \frac{(u \cdot w)(l \cdot w)}{w^2} & B_{(11)}^{[qu]} &= B_{(11)}^{[uq]} = (u \cdot w) \\
B_{(12)}^{[uu]} &= B_{(21)}^{[uu]} = -\frac{(u \cdot w) \sqrt{w^2 - (u \cdot w)^2}}{w^2} & B_{(11)}^{[lq]} &= B_{(11)}^{[ql]} = (l \cdot w) \\
B_{(11)}^{[uu]} &= \frac{(u \cdot w)^2}{w^2} & B_{(21)}^{[lq]} &= B_{(12)}^{[ql]} = \frac{(u \cdot w)(l \cdot w) - (u \cdot l) w^2}{\sqrt{w^2 - (u \cdot w)^2}} \\
B_{(12)}^{[qu]} &= B_{(21)}^{[uq]} = -\sqrt{w^2 - (u \cdot w)^2}
\end{aligned} \tag{E.8}$$

E. Coefficients of the vector-meson self-energies

$$\begin{aligned}
D_{(T;ij)}^{[ll]} &= \frac{1}{2} T_{\mu\nu}(w, u) \epsilon^{\mu\alpha\beta\gamma} \epsilon^{\nu\alpha'\beta'\gamma'} w_\alpha l_\beta w_{\alpha'} l_{\beta'} L_{\gamma\gamma'}^{(ij)}(l, u) \\
D_{(T;ij)}^{[lu]} &= \frac{1}{2} T_{\mu\nu}(w, u) \epsilon^{\mu\alpha\beta\gamma} \epsilon^{\nu\alpha'\beta'\gamma'} w_\alpha l_\beta w_{\alpha'} u_{\beta'} L_{\gamma\gamma'}^{(ij)}(l, u) \\
D_{(T;ij)}^{[ul]} &= \frac{1}{2} T_{\mu\nu}(w, u) \epsilon^{\mu\alpha\beta\gamma} \epsilon^{\nu\alpha'\beta'\gamma'} w_\alpha u_\beta w_{\alpha'} l_{\beta'} L_{\gamma\gamma'}^{(ij)}(l, u) \\
D_{(T;ij)}^{[uu]} &= \frac{1}{2} T_{\mu\nu}(w, u) \epsilon^{\mu\alpha\beta\gamma} \epsilon^{\nu\alpha'\beta'\gamma'} w_\alpha u_\beta w_{\alpha'} u_{\beta'} L_{\gamma\gamma'}^{(ij)}(l, u) \\
D_{(nm;ij)}^{[ll]} &= L_{\mu\nu}^{(nm)}(w, u) \epsilon^{\mu\alpha\beta\gamma} \epsilon^{\nu\alpha'\beta'\gamma'} w_\alpha l_\beta w_{\alpha'} l_{\beta'} L_{\gamma\gamma'}^{(ij)}(l, u) \\
D_{(nm;ij)}^{[lu]} &= L_{\mu\nu}^{(nm)}(w, u) \epsilon^{\mu\alpha\beta\gamma} \epsilon^{\nu\alpha'\beta'\gamma'} w_\alpha l_\beta w_{\alpha'} u_{\beta'} L_{\gamma\gamma'}^{(ij)}(l, u) \\
D_{(nm;ij)}^{[ul]} &= L_{\mu\nu}^{(nm)}(w, u) \epsilon^{\mu\alpha\beta\gamma} \epsilon^{\nu\alpha'\beta'\gamma'} w_\alpha u_\beta w_{\alpha'} l_{\beta'} L_{\gamma\gamma'}^{(ij)}(l, u) \\
D_{(nm;ij)}^{[uu]} &= L_{\mu\nu}^{(nm)}(w, u) \epsilon^{\mu\alpha\beta\gamma} \epsilon^{\nu\alpha'\beta'\gamma'} w_\alpha u_\beta w_{\alpha'} u_{\beta'} L_{\gamma\gamma'}^{(ij)}(l, u) \\
\\
D &= \frac{(l \cdot w)^2 - 2(u \cdot l)(u \cdot w)(l \cdot w) + (u \cdot l)^2 w^2 + l^2((u \cdot w)^2 - w^2)}{2(l^2 - (u \cdot l)^2)} \\
\\
D_{(T;22)}^{[ll]} &= l^2 D \quad D_{(T;22)}^{[lu]} = (u \cdot l) D \quad D_{(T;22)}^{[uu]} = \frac{(u \cdot l)^2}{l^2} D \\
\\
D_{(T;T)}^{[ll]} &= \frac{2(u \cdot l)^2(l \cdot w)^2 + l^4(u \cdot w)^2 - l^2(l \cdot w)((l \cdot w) + 2(u \cdot l)(u \cdot w))}{2((u \cdot l)^2 - l^2)} \\
&\quad - \frac{w^2((l \cdot w)^2 - 2(u \cdot l)(u \cdot w)(l \cdot w) + (u \cdot l)^2 w^2)}{2(w^2 - (u \cdot w)^2)} \\
\\
D_{(T;T)}^{[lu]} &= \frac{1}{2(l^2 - (u \cdot l)^2)} \left(-(u \cdot l)(l \cdot w)^2 + 2l^2(u \cdot w)(l \cdot w) \right. \\
&\quad \left. + (u \cdot l)((u \cdot l)^2 w^2 - l^2((u \cdot w)^2 + w^2)) \right) \\
\\
D_{(T;T)}^{[uu]} &= \frac{1}{2(l^2 - (u \cdot l)^2)} \left(-(l \cdot w)^2 + 2(u \cdot l)(u \cdot w)(l \cdot w) \right. \\
&\quad \left. + (u \cdot l)^2(w^2 - 2(u \cdot w)^2) + l^2((u \cdot w)^2 - w^2) \right) \\
\\
D_{(T;T)}^{[ul]} &= D_{(T;T)}^{[lu]} \quad D_{(T;22)}^{[ul]} = D_{(T;22)}^{[lu]} \tag{E.9}
\end{aligned}$$

All others being zero.

F. Analytic estimates for the ρ -meson self-energy

In this Appendix we analyse the imaginary part of ρ -meson self-energy resulting from the two pion loop

$$\begin{aligned} \Im\Pi_{T,22}^{(\rho)}(w_0, m_1, m_2) &= -\frac{g_{\rho\pi\pi}^2}{6\pi w_0} \left[|\vec{p}_d|^3 \left(n_B \left(\sqrt{|\vec{p}_d|^2 + m_1^2} \right) - n_B \left(-\sqrt{|\vec{p}_d|^2 + m_2^2} \right) \right) \right. \\ &\quad \left. - |\vec{p}_s|^3 \left(n_B \left(\sqrt{|\vec{p}_s|^2 + m_1^2} \right) - n_B \left(\sqrt{|\vec{p}_s|^2 + m_2^2} \right) \right) \right], \\ |\vec{p}_d| &= \frac{1}{2w_0} \left(((w_0)^2 - (m_1 + m_2)^2)((w_0)^2 - (m_1 - m_2)^2) \right)^{1/2} \Theta(w_0 - (m_1 - m_2)) \\ |\vec{p}_s| &= \frac{1}{2w_0} \left(((w_0)^2 - (m_1 + m_2)^2)((w_0)^2 - (m_1 - m_2)^2) \right)^{1/2} \Theta((m_1 - m_2) - w_0) \end{aligned}$$

at zero momentum on a perturbative level depending on the pion mass in order get some estimates on the possible in-medium effects.

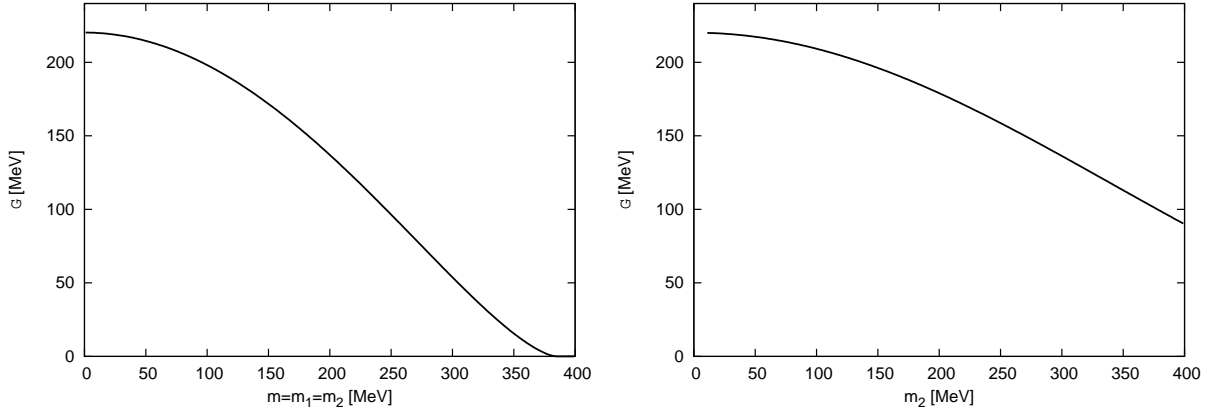


Figure F.1.: Dependence of the ρ -meson width $\Gamma = -\Im\Pi_T^\rho(m_\rho, m_1, m_2)/m_\rho$ on the pion mass at a temperature of 160 MeV. For equal masses of the pions (left plot) and for keeping one mass at 10 MeV (right plot).

The results for the influence of variations of the pion mass are shown in Fig. F.1. The increases of the width by about 20% when turning on temperature results from the Bose enhancement in the decay mode while the scattering contribution can completely be neglected at the ρ -meson pole. We studied the influence of changing both pion masses in the loop while keeping them equal or we kept on mass at 10 MeV while increasing the other one. The influence on the ρ -meson width is mainly given by phase space and results in a roughly linear slope. In the real calculations the pion will not be a sharp particle any more but will become board due to the interactions with the medium. This effect can be modeled in the present treatment by folding the ρ -meson self-energy with

one

$$\Im\Pi_T^\rho(w_0, m_2) = \int \Im\Pi_T(w_0, m_1, m_2) m_1 A_\pi(m_1, \vec{p}) dm_1$$

$$A_\pi(m, \Gamma_\pi) = \frac{2}{\pi} \frac{m\Gamma_\pi}{(m^2 - m_\pi^2)^2 + (m\Gamma_\pi)^2} \quad m_\pi = 140 \text{ MeV} \quad \Gamma_\pi = 30 \text{ MeV}$$

or two parameterised pion spectral functions. The result for such a calculation is shown in Fig. F.2 compared to case of a sharp pion. We see that the inclusion of a spectral distribution for the pion effectively reduces the width of the ρ -meson. The effect can be understood

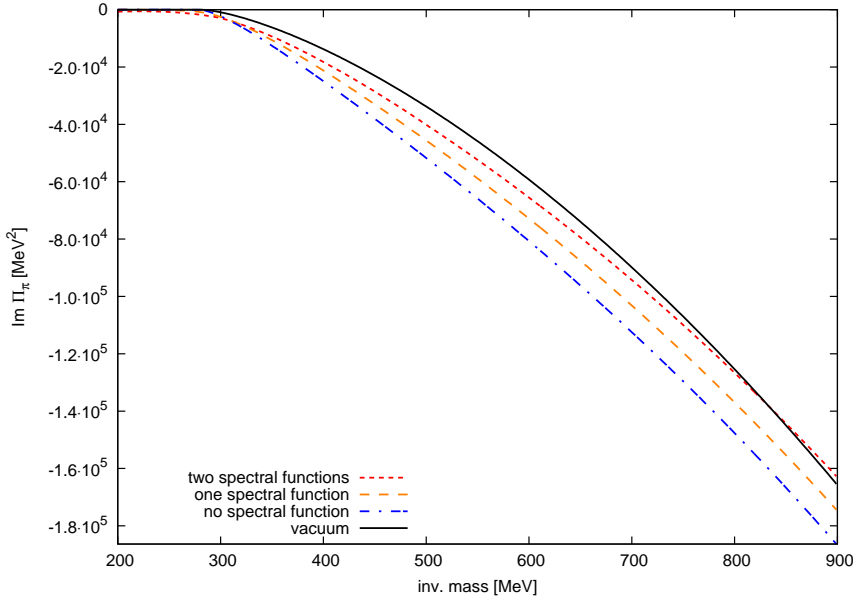


Figure F.2.: Dependence of the ρ -meson self-energy at a temperature of 160 MeV on the pion spectral function.

because in our spectral function we have several modes which become so heavy that they can't be balanced by an according low energy contribution. Therefore spacelike parts in the pion spectral function which are absent in our present treatment would be necessary. This effect can also be observed in the calculations done in the full system. Thus from this approximative treatment we can conclude that no large effects on the ρ -meson width are expected as long as no strong spacelike modes, which could emerge due to interactions with Baryons where particle hole excitations could serve as a source for such spacelike modes, are present.

G. Nucleon- and isobar-hole loop functions

Before we consider the calculation of the loops functions (4.15) in the general case we start with the perturbative limit. For the particle- and Δ -hole loops these calculations have already been done in [29] where the following zero temperature expressions have been found:

$$\begin{aligned} \chi_{ij}^{(Nh)}(\omega, \vec{q}) &= \frac{f_N^2}{m_\pi^2} \mathcal{P} \int_0^{k_F} \frac{d^3 p}{2(p_0 - \Sigma_V)(2\pi)^3} \frac{8 K_{ij}^{(Nh)}}{2 p \cdot q + q^2 + i \epsilon} \\ &+ \frac{i f_N^2}{m_\pi^2} \Im \int_0^{k_F} \frac{d^3 p}{2(p_0 - \Sigma_V)(2\pi)^3} \frac{8 K_{ij}^{(Nh)} \Theta(|\vec{p} + \vec{q}| - k_F)}{2 p \cdot q + q^2 + i \epsilon} \Theta(p_0 + \omega) \\ &+ (-1)^{i+j} (q_\mu \rightarrow -q_\mu), \end{aligned} \quad (\text{G.1})$$

where $q_\mu = (\omega, \vec{q})$, $p_0 = \sqrt{m_N^2 + \vec{p}^2} + \Sigma_V$ and

$$\begin{aligned} K_{11}^{(Nh)} &= 2 m_N^2, & K_{12}^{(Nh)} &= K_{21}^{(Nh)} = 0, \\ K_{22}^{(Nh)} &= \frac{\omega^2 - \vec{q}^2}{\vec{q}^2} \left(2 \vec{p}^2 + \omega (p_0 - \Sigma_V) + \vec{p} \cdot \vec{q} \right) + 2 m_N^2 \frac{\omega^2}{\vec{q}^2}, \\ K_T^{(Nh)} &= 3 m_N^2 + \omega (p_0 - \Sigma_V) - \vec{p} \cdot \vec{q} - \frac{1}{2} \left(K_{11}^{(Nh)} + K_{22}^{(Nh)} \right). \end{aligned} \quad (\text{G.2})$$

For a bare isobar propagator, $S_0^{\mu\nu}(w)$ as given in (4.4), the longitudinal isobar-hole loop functions were computed already in [29]. We present here longitudinal as well as the transverse loop functions:

$$\begin{aligned} \chi_{ij}^{(\Delta h)}(\omega, \vec{q}) &= \frac{4 f_\Delta^2}{9 m_\pi^2} \int_0^{k_F} \frac{d^3 p}{2(p_0 - \Sigma_V)(2\pi)^3} \frac{8 K_{ij}^{(\Delta h)} (m_N m_\Delta + m_N^2 + (p \cdot q))}{2 p \cdot q + q^2 - m_\Delta^2 + m_N^2 + i \epsilon} \\ &+ (-1)^{i+j} (q_\mu \rightarrow -q_\mu), \\ K_{11}^{(\Delta h)} &= 1 - \frac{(q^2 + p \cdot q)^2}{q^2 m_\Delta^2}, & K_{22}^{(\Delta h)} &= 1 + \frac{(\omega |\vec{p}| \cos(\vec{q}, \vec{p}) - |\vec{q}| p_0)^2}{m_\Delta^2 q^2}, \\ K_{12}^{(\Delta h)} &= K_{21}^{(\Delta h)} = i \frac{q^2 + p \cdot q}{q^2 m_\Delta^2} (|\vec{q}| p_0 - \omega |\vec{p}| \cos(\vec{q}, \vec{p})) \\ K_T^{(\Delta h)} &= 2 - \frac{(p + q)^2}{2 m_\Delta^2} - \frac{1}{2} \left(K_{11}^{(\Delta h)} + K_{22}^{(\Delta h)} \right), \end{aligned} \quad (\text{G.3})$$

where $q_\mu = (\omega, \vec{q})$, $p_0 = \sqrt{m_N^2 + \vec{p}^2} + \Sigma_V$. The kernels can be rewritten as:

$$\begin{aligned} K_{11}^{(\Delta h)} &= \frac{1}{q^2} K_1^{(\Delta h)} & K_T^{(\Delta h)} &= \frac{1}{2} \left(K_4^{(\Delta h)} - K_{11}^{(\Delta h)} - K_{22}^{(\Delta h)} \right) \\ K_{22}^{(\Delta h)} &= \frac{(q \cdot u)}{q^2 - (q \cdot u)^2} \left(\frac{(q \cdot u)}{q^2} K_1^{(\Delta h)} - 2 K_2^{(\Delta h)} + \frac{q^2}{(q \cdot u)} K_3^{(\Delta h)} \right) \\ K_{12}^{(\Delta h)} &= K_{21}^{(\Delta h)} = \frac{1}{\sqrt{q^2 - (q \cdot u)}} \left(\frac{(q \cdot u)}{q^2} K_1^{(\Delta h)} - K_2^{(\Delta h)} \right) \end{aligned} \quad (\text{G.4})$$

with

$$\begin{aligned}
 K_1^{(\Delta h)} &= q^2 - \frac{(q^2 + (p \cdot q))^2}{m_\Delta^2} & K_3^{(\Delta h)} &= 1 - \frac{((p \cdot u) + (q \cdot u))^2}{m_\Delta^2} \\
 K_2^{(\Delta h)} &= (q \cdot u) - \frac{(p \cdot u) + (q \cdot u)}{m_\Delta^2} ((p \cdot q) + q^2) \\
 K_4^{(\Delta h)} &= 4 - \frac{(p + q)^2}{m_\Delta^2}
 \end{aligned} \tag{G.5}$$

as to show the projector structure explicitly. This structure is also helpful when deriving the general results for the isobar-hole loop functions. We write

$$\begin{aligned}
 \chi_{11}^{(\Delta h)}(\omega, \vec{q}) &= \frac{1}{q^2} \chi_1^{(\Delta h)}(\omega, \vec{q}), \\
 \chi_{12}^{(\Delta h)}(\omega, \vec{q}) &= \frac{1}{\sqrt{q^2 - (q \cdot u)^2}} \left(\frac{q \cdot u}{q^2} \chi_1^{(\Delta h)}(\omega, \vec{q}) - \chi_2^{(\Delta h)}(\omega, \vec{q}) \right), \\
 \chi_{22}^{(\Delta h)}(\omega, \vec{q}) &= \frac{q \cdot u}{q^2 - (q \cdot u)^2} \left(\frac{q \cdot u}{q^2} \chi_1^{(\Delta h)}(\omega, \vec{q}) - 2 \chi_2^{(\Delta h)}(\omega, \vec{q}) \right. \\
 &\quad \left. + \frac{q^2}{q \cdot u} \chi_3^{(\Delta h)}(\omega, \vec{q}) \right), \\
 \chi_T^{(\Delta h)}(\omega, \vec{q}) &= \frac{1}{2} \left(\chi_4^{(\Delta h)}(\omega, \vec{q}) - \chi_{11}^{(\Delta h)}(\omega, \vec{q}) - \chi_{22}^{(\Delta h)}(\omega, \vec{q}) \right).
 \end{aligned} \tag{G.6}$$

This representation (G.6) simplifies the realization of the constraint equations (3.22). The first condition is satisfied for any functions $\chi_i(\omega, \vec{q})$ that are regular at $q^2 = 0$. The second equation in (3.22) implies the following constraint,

$$\begin{aligned}
 \chi_3(\omega, 0) &= \frac{1}{\omega^2} \chi_1(\omega, 0), & \chi_2(\omega, 0) &= \frac{1}{\omega} \chi_1(\omega, 0), \\
 \chi_4(\omega, 0) &= 3 \chi_{22}(\omega, 0) + \chi_{11}(\omega, 0),
 \end{aligned} \tag{G.7}$$

where we boosted into the rest frame of nuclear matter for convenience. Based on the representation (4.30) we define

$$\begin{aligned}
 \chi_i^{(\Delta h)}(\omega, \vec{q}) &= \left[\delta_{i4} \Pi_3^{(\Delta h)}(0, \vec{q}) \right. \\
 &\quad \left. - \frac{8}{3} \frac{f_\Delta^2}{m_\pi^2} \int_0^{k_F} \frac{d^3 p}{2(p_0 - \Sigma_V)(2\pi)^3} \int_{-\infty}^{+\infty} \frac{d\bar{\omega}}{\pi} \left(\frac{\omega}{\bar{\omega}} \right)^{n_i} \frac{\text{sign}(\bar{\omega}) \Im S_i^{(\Delta h)}(\bar{\omega}, \vec{q}, \vec{p})}{\bar{\omega} - \omega - i\bar{\omega}\epsilon} \right] \\
 &\quad + (-1)^{\epsilon_i} (q_\mu \rightarrow -q_\mu),
 \end{aligned} \tag{G.8}$$

where $p_0 = \sqrt{m_N^2 + \vec{p}^2} + \Sigma_V$ and $\epsilon_{1,3,4} = 0$ and $\epsilon_2 = 1$. Furthermore $n_{1,4} = 2$ but $n_2 = 1$ and $n_3 = 0$. We assure that the definition (G.8) leads to a polarisation tensor

7. Appendix

compatible with all constraints (3.22, C.2). This is a consequence of specific identities of the integral kernels (see G.11).

The integral kernels, $S_i^{(\Delta h)}(q, p, u)$, required in (G.8) are covariant functions of the 4-momenta q_μ, p_μ and u_μ . Their evaluation requires the contraction of the isobar propagator, $S_{\mu\nu}(p+q, u)$, with the q_μ and u_μ (see (4.8)). We express the 4-vector u_μ , in terms of v_μ and $X_\mu(v, u)$,

$$u_\mu = -\sqrt{(\hat{v} \cdot u)^2 - 1} X_\mu(v, u) + (\hat{v} \cdot u) \hat{v}_\mu, \quad (\text{G.9})$$

since the contraction of the isobar propagator with v_μ and $X_\mu(v, u)$ leads to more transparent expressions. In particular we can take over the results (O.3, O.4), where contractions of the isobar propagator with the latter 4-vectors were computed already. The results were decomposed into the extended algebra of projectors (4.26, 4.27) introducing the invariant expansion coefficients $S_{[ij]}^{(a)}(v, u)$ and $S_{[ij]}^{(ab)}(v, u)$ with $a, b = v, x$.

We present the integral kernels of (G.8), which have transparent representations in terms of the invariant functions introduced in (4.30, O.1, O.4, O.3) and $c_{[ij]}^{(p,q)}(q; v, u)$ of Appendix L. We establish:

$$\begin{aligned} S_1^{(\Delta h)} &= \sum_{i,j=3}^8 c_{[ij]}^{(p)} S_{[ij]}^{(p)} + \sum_{i,j=1}^2 c_{[ij]}^{(q)} S_{[ij]}^{(q)}, \\ S_2^{(\Delta h)} &= \sum_{i=1}^2 \sum_{j=3}^8 c_{[ij]}^{(p)} \left[(\hat{v} \cdot u) S_{[ij]}^{(v)} - \sqrt{(\hat{v} \cdot u)^2 - 1} S_{[ij]}^{(x)} \right], \\ S_3^{(\Delta h)} &= \sum_{i,j=1}^2 c_{[ij]}^{(p)} \left[(\hat{v} \cdot u)^2 S_{[ij]}^{(vv)} + \left((\hat{v} \cdot u)^2 - 1 \right) S_{[ij]}^{(xx)} \right. \\ &\quad \left. - (\hat{v} \cdot u) \sqrt{(\hat{v} \cdot u)^2 - 1} \left(S_{[ij]}^{(xv)} + S_{[ij]}^{(vx)} \right) \right], \\ S_4^{(\Delta h)} &= \sum_{i,j=1}^2 c_{[ij]}^{(p)} S_{[ij]}^{(g)}. \end{aligned} \quad (\text{G.10})$$

A straight forward computation reveals that the kernels $S_i^{(\Delta h)}$ are correlated at vanishing 3-momentum $\vec{q} = 0$. In this case it holds

$$\begin{aligned} S_3^{(\Delta h)} &= \frac{1}{\omega^2} S_1^{(\Delta h)}, & S_2^{(\Delta h)} &= \frac{1}{\omega} S_1^{(\Delta h)}, \\ S_4^{(\Delta h)} &= 3 S_3^{(\Delta h)} - \frac{2}{\omega^2} S_1^{(\Delta h)} - 3 \frac{d}{d\vec{q}^2} \Bigg|_{\vec{q}=0} \left(S_1^{(\Delta h)} - 2\omega S_2^{(\Delta h)} + \omega^2 S_3^{(\Delta h)} \right), \end{aligned} \quad (\text{G.11})$$

where we assumed an angle average, i.e. the presence of $d\Omega_{\vec{q}}$.

H. Coefficient functions $V_{[ij]}^{(p,q)}$

We derive

$$\begin{aligned}
 V_{[33]}^{(p)} &= \frac{f_\Delta^2}{m_\pi^2} \left[\frac{2 \delta_V \delta (m_\Delta + (\tilde{w} \cdot \hat{v}))}{9 m_\Delta^2 (m_\Delta^2 - \tilde{w}^2)} - \frac{Z (Z (\tilde{w} \cdot \hat{v}) - 2 m_\Delta (Z - 1))}{2 m_\Delta^2} \right], \\
 V_{[34]}^{(p)} &= \frac{i \delta f_\Delta^2}{m_\pi^2 m_\Delta^2 \sqrt{(u \cdot \hat{v})^2 - 1}} \left[\frac{-2 \delta_V \delta}{9 (m_\Delta^2 - \tilde{w}^2)} + \frac{Z}{6} (4 - 3 Z) \right], \\
 V_{[35]}^{(p)} &= \frac{f_\Delta^2}{\sqrt{3} m_\pi^2 m_\Delta^2} \left[\frac{3 m_\Delta (m_\Delta^2 - (\tilde{w} \cdot \hat{v})^2) - \delta_V \delta (2 (\tilde{w} \cdot \hat{v}) - m_\Delta)}{3 (m_\Delta^2 - \tilde{w}^2)} \right. \\
 &\quad \left. + \frac{Z}{2} (2 m_\Delta (Z - 1) - (\tilde{w} \cdot \hat{v}) (Z - 2)) \right], \\
 V_{[36]}^{(p)} &= -V_{[45]}^{(p)} = \frac{i \delta f_\Delta^2}{m_\pi^2 m_\Delta^2 \sqrt{3 (u \cdot \hat{v})^2 - 3}} \left[\frac{2 (m_\Delta^2 - (\tilde{w} \cdot \hat{v})^2)}{3 (m_\Delta^2 - \tilde{w}^2)} + \frac{Z}{6} (3 Z - 2) \right], \\
 V_{[37]}^{(p)} &= \frac{\sqrt{2} i \delta f_\Delta^2}{3 m_\pi^2 m_\Delta^2 \sqrt{(u \cdot \hat{v})^2 - 1}} \left[\frac{3 m_\Delta (m_\Delta + (\tilde{w} \cdot \hat{v})) + 2 \delta_V \delta}{3 (m_\Delta^2 - \tilde{w}^2)} - Z \right], \\
 V_{[38]}^{(p)} &= \frac{-f_\Delta^2 \delta (\delta_V (1 - (u \cdot \hat{v})^2) + 3 \delta) (m_\Delta - 2 (\tilde{w} \cdot \hat{v}))}{9 \sqrt{2} m_\pi^2 m_\Delta^2 (m_\Delta^2 - \tilde{w}^2) (1 - (u \cdot \hat{v})^2)}, \\
 V_{[44]}^{(p)} &= \frac{f_\Delta^2}{m_\pi^2 m_\Delta^2} \left[\frac{2 \delta_V \delta ((\tilde{w} \cdot \hat{v}) - m_\Delta)}{9 (m_\Delta^2 - \tilde{w}^2)} + \frac{Z}{2} (2 m_\Delta (Z - 1) + (\tilde{w} \cdot \hat{v}) Z) \right], \\
 V_{[46]}^{(p)} &= \frac{f_\Delta^2}{\sqrt{3} m_\pi^2 m_\Delta^2} \left[\frac{-3 m_\Delta (m_\Delta^2 - (\tilde{w} \cdot \hat{v})^2) - \delta_V \delta (2 (\tilde{w} \cdot \hat{v}) + m_\Delta)}{3 (m_\Delta^2 - \tilde{w}^2)} \right. \\
 &\quad \left. - \frac{Z}{2} (2 m_\Delta (Z - 1) + (\tilde{w} \cdot \hat{v}) (Z - 2)) \right], \\
 V_{[47]}^{(p)} &= \frac{-f_\Delta^2 \delta (\delta_V (1 - (u \cdot \hat{v})^2) + 3 \delta) (m_\Delta + 2 (\tilde{w} \cdot \hat{v}))}{9 \sqrt{2} m_\pi^2 m_\Delta^2 (m_\Delta^2 - \tilde{w}^2) (1 - (u \cdot \hat{v})^2)}, \\
 V_{[48]}^{(p)} &= \frac{\sqrt{2} i \delta f_\Delta^2}{3 m_\pi^2 m_\Delta^2 \sqrt{(u \cdot \hat{v})^2 - 1}} \left[\frac{3 m_\Delta (m_\Delta - (\tilde{w} \cdot \hat{v})) + 2 \delta_V \delta}{3 (m_\Delta^2 - \tilde{w}^2)} - Z \right], \\
 V_{[55]}^{(p)} &= \frac{f_\Delta^2}{3 m_\pi^2 m_\Delta^2} \left[\frac{-2 (m_\Delta - (\tilde{w} \cdot \hat{v})) (m_\Delta + (\tilde{w} \cdot \hat{v}))^2}{m_\Delta^2 - \tilde{w}^2} \right. \\
 &\quad \left. + \frac{Z}{2} (2 m_\Delta (Z - 1) - (\tilde{w} \cdot \hat{v}) (Z - 4)) \right],
 \end{aligned}$$

7. Appendix

$$\begin{aligned}
V_{[56]}^{(p)} &= \frac{i \delta f_{\Delta}^2}{m_{\pi}^2 m_{\Delta}^2 \sqrt{(u \cdot \hat{v})^2 - 1}} \left[\frac{-2(m_{\Delta}^2 - (\tilde{w} \cdot \hat{v})^2)}{3(m_{\Delta}^2 - \tilde{w}^2)} + \frac{Z^2}{6} \right], \\
V_{[57]}^{(p)} &= -\frac{\sqrt{2} i \delta f_{\Delta}^2}{3\sqrt{3} m_{\pi}^2 m_{\Delta}^2 \sqrt{(u \cdot \hat{v})^2 - 1}} \left[\frac{m_{\Delta}^2 + 3 m_{\Delta} (\tilde{w} \cdot \hat{v}) + 2 (\tilde{w} \cdot \hat{v})^2}{(m_{\Delta}^2 - \tilde{w}^2)} + Z \right], \\
V_{[58]}^{(p)} &= \frac{f_{\Delta}^2 \delta (\delta_V (1 - (u \cdot \hat{v})^2) + 3 \delta) (m_{\Delta} - 2 (\tilde{w} \cdot \hat{v}))}{3\sqrt{6} m_{\pi}^2 m_{\Delta}^2 (m_{\Delta}^2 - \tilde{w}^2) (1 - (u \cdot \hat{v})^2)}, \\
V_{[66]}^{(p)} &= \frac{f_{\Delta}^2}{3 m_{\pi}^2 m_{\Delta}^2} \left[\frac{-2(m_{\Delta} - (\tilde{w} \cdot \hat{v}))^2 (m_{\Delta} + (\tilde{w} \cdot \hat{v}))}{m_{\Delta}^2 - \tilde{w}^2} \right. \\
&\quad \left. + \frac{Z}{2} (2 m_{\Delta} (Z - 1) + (\tilde{w} \cdot \hat{v}) (Z - 4)) \right], \\
V_{[67]}^{(p)} &= -\frac{f_{\Delta}^2 \delta (\delta_V (1 - (u \cdot \hat{v})^2) + 3 \delta) (m_{\Delta} + 2 (\tilde{w} \cdot \hat{v}))}{3\sqrt{6} m_{\pi}^2 m_{\Delta}^2 (m_{\Delta}^2 - \tilde{w}^2) (1 - (u \cdot \hat{v})^2)}, \\
V_{[68]}^{(p)} &= \frac{\sqrt{2} i \delta f_{\Delta}^2}{3\sqrt{3} m_{\pi}^2 m_{\Delta}^2 \sqrt{(u \cdot \hat{v})^2 - 1}} \left[\frac{m_{\Delta}^2 - 3 m_{\Delta} (\tilde{w} \cdot \hat{v}) + 2 (\tilde{w} \cdot \hat{v})^2}{(m_{\Delta}^2 - \tilde{w}^2)} + Z \right], \\
V_{[77]}^{(p)} &= -\frac{f_{\Delta}^2 (m_{\Delta} + (\tilde{w} \cdot \hat{v}))}{m_{\pi}^2 (m_{\Delta}^2 - \tilde{w}^2)} \\
&\quad + \frac{f_{\Delta}^2 \delta (3 \delta (2 m_{\Delta} + (\tilde{w} \cdot \hat{v})) + \delta_V ((u \cdot \hat{v})^2 - 1) (2 m_{\Delta} + (\tilde{w} \cdot \hat{v})))}{9 m_{\pi}^2 m_{\Delta}^2 (m_{\Delta}^2 - \tilde{w}^2) (1 - (u \cdot \hat{v})^2)}, \\
V_{[78]}^{(p)} &= \frac{-i \delta f_{\Delta}^2 (9 \delta^2 + ((u \cdot \hat{v})^2 - 1) (-5 \delta_V \delta + 3 m_{\Delta}^2))}{9 m_{\pi}^2 m_{\Delta}^2 (m_{\Delta}^2 - \tilde{w}^2) \sqrt{(u \cdot \hat{v})^2 - 1}^3}, \\
V_{[88]}^{(p)} &= -\frac{f_{\Delta}^2 (m_{\Delta} - (\tilde{w} \cdot \hat{v}))}{m_{\pi}^2 (m_{\Delta}^2 - \tilde{w}^2)} \\
&\quad + \frac{f_{\Delta}^2 \delta (3 \delta (2 m_{\Delta} - (\tilde{w} \cdot \hat{v})) + \delta_V ((u \cdot \hat{v})^2 - 1) (2 m_{\Delta} - (\tilde{w} \cdot \hat{v})))}{9 m_{\pi}^2 m_{\Delta}^2 (m_{\Delta}^2 - \tilde{w}^2) (1 - (u \cdot \hat{v})^2)}, \\
V_{[11]}^{(q)} &= \frac{f_{\Delta}^2 (m_{\Delta} + (\tilde{w} \cdot \hat{v}))}{m_{\pi}^2 (\tilde{w}^2 - m_{\Delta}^2)}, \quad V_{[22]}^{(q)} = \frac{f_{\Delta}^2 (m_{\Delta} - (\tilde{w} \cdot \hat{v}))}{m_{\pi}^2 (\tilde{w}^2 - m_{\Delta}^2)}, \\
V_{[12]}^{(q)} &= \frac{i \delta f_{\Delta}^2}{m_{\pi}^2 (\tilde{w}^2 - m_{\Delta}^2) \sqrt{(u \cdot \hat{v})^2 - 1}}, \tag{H.1}
\end{aligned}$$

to be used in Eq. (4.39). Here

$$\tilde{w}_{\mu} = w_{\mu} - \mu_V u_{\mu}, \quad \delta = (u \cdot \hat{v})(\tilde{w} \cdot \hat{v}) - (u \cdot \tilde{w}), \quad \delta_V = \Sigma_V - \mu_V. \tag{H.2}$$

I. Coefficient functions $J_{[ij]}^{(p,q)}$ and master functions J_i

The matrix of loop functions $J_{[ij]}^{(p,q)}(v, u)$ to be used in contrast of Eq. (4.42) ff. are expressed in terms of 13 master functions $J_n(v, u)$. It holds

$$\begin{aligned}
J_{[33]}^{(p)} &= \frac{1}{3} \left(m_N (2 J_3 - J_5) + J_{12} - 2 J_7 \right), \\
J_{[44]}^{(p)} &= \frac{1}{3} \left(m_N (2 J_3 - J_5) - J_{12} + 2 J_7 \right), \\
J_{[55]}^{(p)} &= (m_N - 2 \sqrt{v^2}) J_4 + J_9 + m_N v^2 J_0 + (v^2 - 2 m_N \sqrt{v^2}) J_1, \\
J_{[66]}^{(p)} &= (m_N + 2 \sqrt{v^2}) J_4 - J_9 + m_N v^2 J_0 - (v^2 + 2 m_N \sqrt{v^2}) J_1, \\
J_{[77]}^{(p)} &= \frac{1}{3} \left(m_N (J_3 - 2 J_5) + J_7 - 2 J_{12} \right), \\
J_{[88]}^{(p)} &= \frac{1}{3} \left(m_N (J_3 - 2 J_5) - J_7 + 2 J_{12} \right), \\
J_{[35]}^{(p)} &= J_{[46]}^{(p)} = \frac{1}{\sqrt{3}} \left(2 J_7 - J_{12} - \sqrt{v^2} (2 J_3 - J_5) \right), \\
J_{[37]}^{(p)} &= J_{[48]}^{(p)} = i \frac{\sqrt{2}}{3} \left(2 J_8 - J_{11} \right), \\
J_{[57]}^{(p)} &= i \sqrt{\frac{2}{3}} \left((m_N - \sqrt{v^2}) J_6 + J_{10} - m_N \sqrt{v^2} J_2 \right), \\
J_{[68]}^{(p)} &= i \sqrt{\frac{2}{3}} \left((m_N + \sqrt{v^2}) J_6 - J_{10} - m_N \sqrt{v^2} J_2 \right), \\
J_{[34]}^{(p)} &= -\frac{i}{3} \left(2 J_8 - J_{11} \right), \quad J_{[78]}^{(p)} = \frac{i}{3} \left(5 J_8 + 2 J_{11} \right), \\
J_{[36]}^{(p)} &= -\frac{i}{\sqrt{3}} \left((m_N + \sqrt{v^2}) J_6 - J_{10} - m_N \sqrt{v^2} J_2 \right), \\
J_{[45]}^{(p)} &= -\frac{i}{\sqrt{3}} \left((m_N - \sqrt{v^2}) J_6 + J_{10} - m_N \sqrt{v^2} J_2 \right), \\
J_{[38]}^{(p)} &= \frac{\sqrt{2}}{3} \left(m_N (J_3 + J_5) - J_7 - J_{12} \right), \\
J_{[47]}^{(p)} &= \frac{\sqrt{2}}{3} \left(m_N (J_3 + J_5) + J_7 + J_{12} \right), \\
J_{[58]}^{(p)} &= J_{[67]}^{(p)} = \sqrt{\frac{2}{3}} \left(J_7 + J_{12} - \sqrt{v^2} (J_3 + J_5) \right), \\
J_{[56]}^{(p)} &= -i \left(J_{10} - 2 \sqrt{v^2} J_6 + v^2 J_2 \right), \tag{I.1}
\end{aligned}$$

7. Appendix

$$\begin{aligned}
J_{[11]}^{(q)} &= m_N J_3 + J_7, & J_{[22]}^{(q)} &= m_N J_3 - J_7, & J_{[12]}^{(q)} &= -i J_8, \\
J_{[11]}^{(p)} &= m_N J_0 + J_1, & J_{[22]}^{(p)} &= m_N J_0 - J_1, & J_{[12]}^{(p)} &= -i J_2, \\
J_{[13]}^{(p)} &= J_{[24]}^{(p)} = \frac{-1}{\sqrt{3}} (2 J_3 - J_5), & J_{[16]}^{(p)} &= J_{[25]}^{(p)} = +i (J_6 - \sqrt{v^2} J_2), \\
J_{[15]}^{(p)} &= +(\sqrt{v^2} - m_N) J_1 - J_4 + m_N \sqrt{v^2} J_0, \\
J_{[26]}^{(p)} &= -(\sqrt{v^2} + m_N) J_1 + J_4 + m_N \sqrt{v^2} J_0, \\
J_{[17]}^{(p)} &= -i \sqrt{\frac{2}{3}} (m_N J_2 + J_6), & J_{[28]}^{(p)} &= -i \sqrt{\frac{2}{3}} (m_N J_2 - J_6), \\
J_{[14]}^{(p)} &= +\frac{i}{\sqrt{3}} (m_N J_2 + J_6), & J_{[23]}^{(p)} &= +\frac{i}{\sqrt{3}} (m_N J_2 - J_6), \\
J_{[18]}^{(p)} &= J_{[27]}^{(p)} = -\sqrt{\frac{2}{3}} (J_3 + J_5),
\end{aligned}$$

where the remaining elements follow from the symmetry property $J_{[ij]}^{(p,q)} = J_{[ji]}^{(p,q)}$. It remains to specify the integral kernels, $K_n(l; v, \bar{v}, u)$, defining the loop functions introduced in (4.48) and (4.53). It is derived

$$\begin{aligned}
K_0 &= \frac{v^2}{\bar{v}^2}, \\
K_1 &= \left(\frac{\sqrt{v^2}}{2} + \frac{(\bar{l} \cdot \bar{v})}{\sqrt{v^2}} \right) \frac{v^2}{\bar{v}^2}, \\
K_2 &= -\frac{(v \cdot u)}{\sqrt{(v \cdot u)^2 - v^2}} \frac{(\bar{l} \cdot \bar{v})}{\sqrt{v^2}} \frac{v^2}{\bar{v}^2} + \frac{\sqrt{v^2} (\bar{l} \cdot u)}{\sqrt{(v \cdot u)^2 - v^2}}, \\
K_3 &= \frac{1}{2} K_5^P - \frac{1}{2} \frac{v^2}{\bar{v}^2} \left(\frac{(\bar{l} \cdot \bar{v})^2}{v^2} - \bar{l}^2 - \frac{\bar{v}^2 - v^2}{4} \right), \\
K_4 &= \left(\frac{\sqrt{v^2}}{2} + \frac{(\bar{l} \cdot \bar{v})}{\sqrt{v^2}} \right)^2 \frac{v^2}{\bar{v}^2}, \\
K_5 &= \frac{1}{(v \cdot u)^2 - v^2} \left\{ v^2 (\bar{l} \cdot u)^2 - 2 (v \cdot u) (\bar{l} \cdot \bar{v}) (\bar{l} \cdot u) \right. \\
&\quad \left. + (v \cdot u)^2 \frac{(\bar{l} \cdot \bar{v})^2}{\bar{v}^2} \right\} - \frac{\bar{v}^2 - v^2}{12 \bar{v}^2} v^2, \\
K_6 &= \frac{\sqrt{v^2}}{2} K_2^P + \frac{(\bar{l} \cdot \bar{v}) (\bar{l} \cdot u)}{\sqrt{(v \cdot u)^2 - v^2}} - \frac{(v \cdot u)}{\sqrt{(v \cdot u)^2 - v^2}} \frac{(\bar{l} \cdot \bar{v})^2}{\bar{v}^2}, \\
K_7 &= \frac{1}{2} K_{12}^P + \frac{1}{2} \frac{v^2}{\bar{v}^2} \left(\bar{l}^2 + \frac{\bar{v}^2 - v^2}{4} - \frac{(\bar{l} \cdot \bar{v})^2}{v^2} \right) \left(\frac{\sqrt{v^2}}{2} + \frac{(\bar{l} \cdot \bar{v})}{\sqrt{v^2}} \right),
\end{aligned}$$

$$\begin{aligned}
 K_8 &= \frac{1}{2} K_{11}^P + \frac{1}{2} \left(\bar{l}^2 + \frac{\bar{v}^2 - v^2}{4} - \frac{(\bar{l} \cdot \bar{v})^2}{v^2} \right) \left(-\frac{(v \cdot u)}{\sqrt{(v \cdot u)^2 - v^2}} \frac{(\bar{l} \cdot \bar{v}) v^2}{\sqrt{v^2} \bar{v}^2} \right. \\
 &\quad \left. + \frac{\sqrt{v^2} (\bar{l} \cdot u)}{\sqrt{(v \cdot u)^2 - v^2}} \right), \\
 K_9 &= \left(\frac{\sqrt{v^2}}{2} + \frac{(\bar{l} \cdot \bar{v})}{\sqrt{v^2}} \right)^3 \frac{v^2}{\bar{v}^2}, \\
 K_{10} &= -\frac{v^2}{4} \frac{v^2}{\bar{v}^2} \left(1 + 2 \frac{(\bar{l} \cdot \bar{v})}{v^2} + 4 \frac{(\bar{l} \cdot \bar{v})^2}{v^2 v^2} \right) \frac{(v \cdot u)}{\sqrt{(v \cdot u)^2 - v^2}} \frac{(\bar{l} \cdot \bar{v})}{\sqrt{v^2}} \\
 &\quad + \frac{v^2}{4} \left(1 + 2 \frac{(\bar{l} \cdot \bar{v})}{v^2} + 4 \frac{(\bar{l} \cdot \bar{v})^2}{v^2 v^2} \right) \frac{\sqrt{v^2} (\bar{l} \cdot u)}{\sqrt{(v \cdot u)^2 - v^2}} \\
 &\quad + \frac{1}{2} \frac{\sqrt{v^2} (v \cdot u)}{\sqrt{(v \cdot u)^2 - v^2}} \left(\frac{(\bar{l} \cdot u)}{(v \cdot u)} - \frac{(\bar{l} \cdot \bar{v})}{\bar{v}^2} \right) (\bar{l} \cdot \bar{v}), \\
 K_{11} &= \frac{\sqrt{v^2}}{[(v \cdot u)^2 - v^2]^{3/2}} \left\{ v^2 (\bar{l} \cdot u)^3 - 3 (v \cdot u) (\bar{l} \cdot u)^2 (\bar{l} \cdot \bar{v}) \frac{v^2}{\bar{v}^2} \right. \\
 &\quad \left. + 3 (v \cdot u)^2 (\bar{l} \cdot u) \frac{(\bar{l} \cdot \bar{v})^2}{v^2} - \frac{(v \cdot u)^3 (\bar{l} \cdot \bar{v})^3}{v^2 \bar{v}^2} \right\}, \\
 K_{12} &= \frac{1}{(v \cdot u)^2 - v^2} \left\{ \left(\frac{\sqrt{v^2}}{2} + \frac{(\bar{l} \cdot \bar{v})}{\sqrt{v^2}} \right) \frac{v^2}{\bar{v}^2} v^2 (\bar{l} \cdot u)^2 \right. \\
 &\quad - 2 \left(\frac{\sqrt{v^2}}{2} + \sqrt{v^2} \frac{(\bar{l} \cdot \bar{v})}{v^2} \right) (v \cdot u) (\bar{l} \cdot u) (\bar{l} \cdot \bar{v}) \\
 &\quad \left. + \left(\frac{\sqrt{v^2}}{2} + \frac{(\bar{l} \cdot \bar{v})}{\sqrt{v^2}} \right) (v \cdot u)^2 \frac{(\bar{l} \cdot \bar{v})^2}{\bar{v}^2} \right\} \\
 \bar{l}_\mu &= l_\mu - \bar{v}_\mu/2, \quad \bar{v}^2 = (\bar{v} \cdot u)^2 - (v \cdot u)^2 + v^2, \tag{I.2}
 \end{aligned}$$

The free space limit (4.45) can be recovered using the following identities valid in vacuum:

$$\begin{aligned}
 (\bar{l} \cdot \bar{v}) &= \frac{m_N^2 - m_\pi^2}{2}, \quad (\bar{l} \cdot u) = \frac{(\bar{v} \cdot u)}{\bar{v}^2} (\bar{l} \cdot \bar{v}) \\
 (\bar{l} \cdot u)^2 &= (\bar{l} \cdot \bar{v})^2 \frac{(\bar{v} \cdot u)^2}{(\bar{v}^2)^2} + \frac{1}{3} \left(\bar{l}^2 - \frac{(\bar{l} \cdot \bar{v})}{\bar{v}^2} \right) \left(1 - \frac{(\bar{v} \cdot u)^2}{\bar{v}^2} \right) \\
 (\bar{l} \cdot u)^3 &= (\bar{l} \cdot \bar{v})^3 \frac{(\bar{v} \cdot u)^3}{(\bar{v}^2)^3} + (\bar{l} \cdot \bar{v}) \frac{(\bar{v} \cdot u)}{\bar{v}^2} \left(\bar{l}^2 - \frac{(\bar{l} \cdot \bar{v})}{\bar{v}^2} \right) \left(1 - \frac{(\bar{v} \cdot u)^2}{\bar{v}^2} \right) \\
 \bar{l}^2 &= \frac{m_N^2 + m_\pi^2}{2} - \frac{\bar{v}^2}{4} \tag{I.3}
 \end{aligned}$$

Note that in K_3^P , K_5^P , K_7^P and K_8^P we need terms proportional to $\bar{v}^2 - v^2$ in order to regularise the \bar{l}^2 and $(u \cdot \bar{l})^2$ terms which would otherwise be UV-divergent. The

7. Appendix

subtraction terms are constructed according to

$$\begin{aligned}
J_0^C &= (v \cdot u) C_{0,1}^{000}, & J_1^C &= \frac{1}{2} \frac{v \cdot u}{\sqrt{v^2}} (v^2 C_{0,1}^{000} + 2 C_{0,1}^{100}), \\
J_2^C &= -\frac{v \cdot u}{\sqrt{(v \cdot u)^2 - v^2}} \frac{v \cdot u}{\sqrt{v^2}} C_{0,1}^{100}, \\
J_3^C &= \frac{1}{2} J_5^C + 2 (v \cdot u) C_{0,2}^{200} + 2 C_{+1,2}^{200}, \\
J_4^C &= \frac{1}{4} (v \cdot u) (v^2 C_{0,1}^{000} + 4 C_{0,1}^{100}), & J_5^C &= \frac{2 (v \cdot u)}{(v \cdot u)^2 - v^2} C_{-1,0}^{110}, \\
J_6^C &= \frac{1}{2} \sqrt{v^2} J_2^C - \frac{1}{\sqrt{(v \cdot u)^2 - v^2}} C_{-1,0}^{110}, \\
J_7^C &= \frac{1}{2} J_{12}^C + \frac{1}{2 \sqrt{v^2}} C_{+1,2}^{300} - \frac{1}{16} \sqrt{v^2} v^2 (C_{+1,1}^{000} + 4 C_{+1,2}^{001} - 16 C_{+1,3}^{200}) \\
&\quad - \frac{1}{16} \sqrt{v^2} (v \cdot u) (v^2 C_{0,1}^{000} + 2 C_{0,1}^{100} - 4 C_{0,2}^{200} + 16 C_{0,3}^{300}) \\
&\quad - \frac{1}{8} \sqrt{v^2} (C_{+1,1}^{100} + 4 C_{+1,2}^{101} - 8 C_{+1,2}^{200} - 8 C_{+1,3}^{300}), \\
J_8^C &= \frac{1}{2} J_{11}^C - \frac{1}{24 \sqrt{v^2} \sqrt{(v \cdot u)^2 - v^2}} [v^2 (3 C_{+1,0}^{010} + 12 C_{+1,1}^{011} + 8 C_{+1,2}^{210}) \\
&\quad - 12 C_{+1,1}^{210} - (v \cdot u)^2 (3 v^2 C_{0,1}^{100} + 8 C_{0,2}^{300}) + 12 (v \cdot u) (C_{+1,2}^{300} - C_{0,1}^{210}) \\
&\quad + v^2 (v \cdot u) (3 C_{0,0}^{010} + 12 C_{0,1}^{011} - 3 C_{+1,1}^{100} - 12 C_{+1,2}^{101} + 8 C_{0,2}^{210} - 8 C_{+1,3}^{300})], \\
J_9^C &= -\frac{1}{8 \sqrt{v^2}} [-(v \cdot u) v^2 (v^2 C_{0,1}^{000} + 6 C_{0,1}^{100}) + 16 (v \cdot u) C_{0,2}^{300} + 8 C_{+1,2}^{300}], \\
J_{10}^C &= -\frac{1}{12 \sqrt{v^2} \sqrt{(v \cdot u)^2 - v^2}} [v^2 (6 C_{-1,0}^{110} + 6 C_{+1,1}^{110} + 16 C_{+1,2}^{210}) \\
&\quad + 12 C_{+1,1}^{210} + (v \cdot u)^2 (3 v^2 C_{0,1}^{100} - 16 C_{0,2}^{300}) + 12 (v \cdot u) (C_{0,1}^{210} - C_{+1,2}^{300}) \\
&\quad + 2 (v \cdot u) v^2 (3 C_{0,1}^{110} - 3 C_{+1,2}^{200} + 8 C_{0,2}^{210} - 8 C_{+1,3}^{300})], \\
J_{11}^C &= -\frac{1}{\sqrt{v^2} ((v \cdot u)^2 - v^2)^{3/2}} [-2 (v \cdot u) (v^2)^2 C_{0,2}^{210} + 2 (v^2)^2 C_{+1,2}^{210} \\
&\quad + (v \cdot u)^2 (3 v^2 C_{0,1}^{120} + 3 C_{+1,1}^{210} - 2 v^2 C_{+1,2}^{210}) \\
&\quad + (v \cdot u)^3 (3 C_{0,1}^{210} + 2 v^2 C_{0,2}^{210} - C_{+1,2}^{300})], \\
J_{12}^C &= \frac{1}{6 \sqrt{v^2} ((v \cdot u)^2 - v^2)} [(v \cdot u) (12 C_{+1,1}^{210} + v^2 (3 v^2 (C_{0,1}^{020} - C_{-1,1}^{110}) \\
&\quad + 6 (C_{-1,0}^{110} + C_{0,1}^{120}) + 4 C_{+1,2}^{210})) + (v \cdot u)^3 (3 v^2 C_{-1,1}^{110} - 4 C_{0,2}^{300}) \\
&\quad + 6 (v \cdot u)^2 (2 C_{0,1}^{210} - C_{+1,2}^{300}) \\
&\quad + (v \cdot u)^2 v^2 (3 C_{0,1}^{110} - 3 C_{+1,2}^{200} + 12 C_{0,2}^{210} - 8 C_{+1,3}^{300}) \\
&\quad + (v^2)^2 (-3 C_{0,1}^{110} + 6 C_{+1,2}^{200} - 8 C_{0,2}^{210} + 4 C_{+1,3}^{300})]. \tag{I.4}
\end{aligned}$$

Please note that the K_i and J_i^C fulfill the constraints on the lightcone by themselves. No cancellation between these terms is needed to fulfill the constraints. In addition the J_i^C fulfill the lightcone-constraints independent of the values of the $\bar{C}_{m,n}^{ijk}$. The case is different at zero momentum where we need cancellations in order to get finite results. Therefore the zero momentum limit deserves closer investigation. First we observe that for zero momentum some of the functions get correlated

$$\bar{C}_{1,n}^{ijk} = \bar{C}_{0,(n-1)}^{(i-1)(j+1)k} + \mathcal{O}(\epsilon). \quad (\text{I.5})$$

In addition we already stated that we need the J_i^C only to cancel the kinematical singularities at zero momentum and to guarantee the right vacuum limit. Since in the vacuum limit all $\bar{C}_{m,n}^{ijk}$ become constants anyway we can ask what minimal polynomial ansatz would comply with the kinematical requirements. Expanding J_i and J_i^C around zero momentum we learn that to cancel the singularities it is enough to keep the terms given in tabular I.1. It remains to define the terms proportional to $1/[\bar{v}^2]^n$ for $n > 1$ because these terms are not defined using a normal principal value integral as soon as the imaginary part has support at the subtraction point. If this is not the case then we can also reformulate the basis loops as described in Appendix J. However in the general case an extended definition is required. Normally we are left with the following dispersion integral for the remainder terms:

$$\int_{-\infty}^{\infty} \frac{f(\bar{v}_0, |\vec{w}|)}{(\bar{v}^2)^n} d\bar{v}_0 \quad (\text{I.6})$$

with f some function depending on momentum and internal energy only. For $n = 1$ there is no problem and we can simply calculate this dispersion integral as a principal value integral. For higher values of n we first split f into a symmetric and an anti-symmetric part:

$$\begin{aligned} f_S(\bar{v}_0, |\vec{w}|) &= \frac{1}{2} (f(\bar{v}_0, |\vec{w}|) + f(-\bar{v}_0, |\vec{w}|)) \\ f_A(\bar{v}_0, |\vec{w}|) &= \frac{1}{2} (f(\bar{v}_0, |\vec{w}|) - f(-\bar{v}_0, |\vec{w}|)) \end{aligned} \quad (\text{I.7})$$

Then we define for $n = 2$:

$$\begin{aligned} \bar{f}^S(\bar{v}_0, |\vec{w}|) &= f_S(\bar{v}_0, |\vec{w}|) - f_S(|\vec{w}|, |\vec{w}|) \\ \bar{f}^A(\bar{v}_0, |\vec{w}|) &= f_A(\bar{v}_0, |\vec{w}|) - \frac{\bar{v}_0}{|\vec{w}|} f_A(|\vec{w}|, |\vec{w}|) \end{aligned} \quad (\text{I.8})$$

and for $n = 3$:

$$\begin{aligned} \bar{f}^S(\bar{v}_0, |\vec{w}|) &= f_S(\bar{v}_0, |\vec{w}|) - f_S(|\vec{w}|, |\vec{w}|) - \frac{\bar{v}_0^2}{2|\vec{w}|} f'_S(|\vec{w}|, |\vec{w}|) \\ \bar{f}^A(\bar{v}_0, |\vec{w}|) &= f_A(\bar{v}_0, |\vec{w}|) - \frac{\bar{v}_0}{2|\vec{w}|^3} [(3|\vec{w}|^2 - \bar{v}_0^2) f_A(|\vec{w}|, |\vec{w}|) \\ &\quad + |\vec{w}|(\bar{v}_0^2 - |\vec{w}|^2) f'_A(|\vec{w}|, |\vec{w}|)] \end{aligned} \quad (\text{I.9})$$

7. Appendix

	vacuum limit	singularity cancellation	
		const. term	quadratic term
$\bar{C}_{1,1}^{000}$	x	x	
$\bar{C}_{1,1}^{100}$	x	x	
$\bar{C}_{1,1}^{010}$		x	
$\bar{C}_{1,1}^{011}$		x	
$\bar{C}_{1,1}^{210}$		x	x
$\bar{C}_{1,1}^{110}$		x	
$\bar{C}_{1,2}^{300}$	x	o	x
$\bar{C}_{1,2}^{001}$	x	x	
$\bar{C}_{1,2}^{101}$	x	o	
$\bar{C}_{1,2}^{210}$		o	x
$\bar{C}_{1,2}^{200}$	x	o	x
$\bar{C}_{1,3}^{200}$	x	x	
$\bar{C}_{1,3}^{300}$	x	o	x
$\bar{C}_{0,1}^{000}$		x	
$\bar{C}_{0,1}^{100}$		x	
$\bar{C}_{-1,0}^{110}$	x	x	x
$\bar{C}_{0,1}^{210}$	x	x	x
$\bar{C}_{0,1}^{010}$	x		
$\bar{C}_{0,1}^{011}$	x	x	
$\bar{C}_{0,1}^{110}$	x	x	
$\bar{C}_{0,1}^{120}$		x	x
$\bar{C}_{0,1}^{020}$		x	x
$\bar{C}_{0,2}^{200}$		x	
$\bar{C}_{0,2}^{300}$		x	x
$\bar{C}_{0,2}^{210}$	x	x	x
$\bar{C}_{0,3}^{300}$		x	
$\bar{C}_{-1,1}^{110}$		x	

Table I.1.: Relevant orders of the $\bar{C}_{a,n}^{ijk}$ close to zero momentum. A cross denotes that this order is needed and an o is introduced for the terms which additionally have to fulfill (I.5). Note that the linear term vanishes.

I. Coefficient functions $J_{[ij]}^{(p,q)}$ and master functions J_i

The integral is then defined as:

$$\int_{-\infty}^{\infty} \frac{\bar{f}(\bar{v}_0, |\bar{w}|)}{(\bar{v}^2)^n} d\bar{v}_0 \quad (\text{I.10})$$

We immediately observe that the anti-symmetric part always leads to a vanishing result after performing the dispersion integral. So we can drop this part from the very beginning. The motivation for this procedure is that we would like to close the integration contour in the upper half plain without including the poles from the higher subtractions which by using (I.8,I.9) are moved to the lower half plain.

This procedure also complies with the correlations (I.5) at zero momentum. At zero momentum our functions f for the two cases look like:

$$f_1(\bar{v}_0, \epsilon) = (\bar{l}^2)^k (\bar{l}_0)^{i+j} (\bar{v}_0)^{i+1} + \mathcal{O}(\epsilon) \quad (\text{I.11})$$

for the case of $\bar{C}_{-1,n}^{ijk}$ and

$$f_2(\bar{v}_0, \epsilon) = (\bar{l}^2)^k (\bar{l}_0)^{i+j} (\bar{v}_0)^{i-1} + \mathcal{O}(\epsilon) \quad (\text{I.12})$$

for $\bar{C}_{0,(n-1)}^{(i-1)(j+1)k}$ leading to the relation:

$$f_1(\bar{v}_0, \epsilon) = (\bar{v}_0)^2 f_2(\bar{v}_0, \epsilon) + \mathcal{O}(\epsilon). \quad (\text{I.13})$$

Now we have to convert both functions according to the different prescriptions we have. We obtain:

$$\begin{aligned} \bar{f}_1(\bar{v}_0, \epsilon) &= f_1(\bar{v}_0, \epsilon) - \frac{(\bar{v}_0)^2}{2\epsilon} (2\epsilon f_2(0, 0)) \\ &= (\bar{v}_0)^2 f_2(\bar{v}_0, \epsilon) - (\bar{v}_0)^2 f_2(0, 0) \end{aligned} \quad (\text{I.14})$$

and of course

$$\bar{f}_1(\bar{v}_0, \epsilon) = f_2(\bar{v}_0, \epsilon) - f_2(0, 0). \quad (\text{I.15})$$

The additional factor $(\bar{v}_0)^2$ now compensates the higher subtraction done in the first case such that we arrive at the same result for both terms.

J. Reformulation of the master loop functions J_i

In (4.47) we splitted the J_i loops into parts containing one subtraction and a part J_i^C where higher subtractions on the lightcone are included. When we have no support from the imaginary part of the loop at the lightcone, like in the vacuum case or at reasonably small momenta for zero temperature, we can alternatively⁵ define the master loops as

$$J_n(v_0, \vec{w}) = \int_{-\infty}^{+\infty} \frac{d\bar{v}_0}{\pi} \frac{\Delta J_n(\bar{v}_0; v_0, \vec{w})}{\bar{v}_0 - v_0 - i\epsilon(\bar{v}_0 - \mu)}, \quad (\text{J.1})$$

with

$$\begin{aligned} \Delta J_n(\bar{v}_0; v_0, \vec{w}) &= \int \frac{d^3l}{2(2\pi)^3} \left(m_N^2 + \vec{l}^2\right)^{-\frac{1}{2}} \\ &\times \left\{ K_n^R(l_+, \bar{v}_0; v_0, \vec{w}) A_\pi(|\bar{v}_+|, \vec{w} - \vec{l}) \left[\Theta(+\bar{v}_+) - \Theta(k_F - |\vec{l}|) \right] \right. \\ &\quad \left. + K_n^R(l_-, \bar{v}_0; v_0, \vec{w}) A_\pi(|\bar{v}_-|, \vec{w} - \vec{l}) \Theta(-\bar{v}_-) \right\}, \\ l_\pm^\mu &= (\pm \sqrt{m_N^2 + \vec{l}^2}, \vec{l}), \quad \bar{v}_\pm = \bar{v}_0 \mp \sqrt{m_N^2 + \vec{l}^2}. \end{aligned} \quad (\text{J.2})$$

In this case the kernels K_n^R being a combination of the K_n and the kernels used in the definition of J_i^C (4.50) together with the algebra (I.4) are give by

$$\begin{aligned} K_0^R &= 1 - \frac{(\bar{v} \cdot u)}{\bar{v}^2} \left[(\bar{v} \cdot u) - (v \cdot u) \right], \\ K_1^R &= \left(\frac{\sqrt{v^2}}{2} + \frac{(\bar{l} \cdot \bar{v})}{\sqrt{v^2}} \right) \left(1 - \frac{(\bar{v} \cdot u)}{\bar{v}^2} \left[(\bar{v} \cdot u) - (v \cdot u) \right] \right), \\ K_2^R &= -\frac{(v \cdot u)}{\sqrt{(v \cdot u)^2 - v^2}} \frac{(\bar{l} \cdot \bar{v})}{\sqrt{v^2}} \left(1 - \frac{(\bar{v} \cdot u)}{\bar{v}^2} \left[(\bar{v} \cdot u) - (v \cdot u) \right] \right) \\ &\quad + \frac{\sqrt{v^2} (\bar{l} \cdot u)}{\sqrt{(v \cdot u)^2 - v^2}}, \\ K_3^R &= \frac{1}{2} K_5^R - \frac{1}{2} \frac{v^2}{\bar{v}^2} \left(\frac{(\bar{l} \cdot \bar{v})^2}{v^2} - \bar{l}^2 - \frac{\bar{v}^2 - v^2}{4} \right) + 2 \frac{\bar{v}^2 - v^2}{\bar{v}^2} \frac{(\bar{l} \cdot \bar{v})^2}{\bar{v}^2}, \\ K_4^R &= \left(\frac{\sqrt{v^2}}{2} + \frac{(\bar{l} \cdot \bar{v})}{\sqrt{v^2}} \right) K_1^R - \frac{(\bar{l} \cdot \bar{v})^2}{\bar{v}^2} \frac{(v \cdot u)}{v^2} \left[(\bar{v} \cdot u) - (v \cdot u) \right], \end{aligned}$$

⁵If there is no support for the imaginary part on the lightcone this is identical to the definition (4.47) and (4.50) without the Taylor expansion (4.51).

$$\begin{aligned}
 K_5^R &= \frac{1}{(v \cdot u)^2 - v^2} \left\{ v^2 (\bar{l} \cdot u)^2 - 2 \frac{(v \cdot u)^2}{(\bar{v} \cdot u)} (\bar{l} \cdot \bar{v}) (\bar{l} \cdot u) \right. \\
 &\quad \left. + (v \cdot u)^2 \frac{(\bar{l} \cdot \bar{v})^2}{\bar{v}^2} \right\} - \frac{\bar{v}^2 - v^2}{12 \bar{v}^2} v^2, \\
 K_6^R &= \frac{\sqrt{v^2}}{2} K_2^R + \frac{(\bar{l} \cdot \bar{v}) (\bar{l} \cdot u)}{\sqrt{(v \cdot u)^2 - v^2}} \frac{(v \cdot u)}{(\bar{v} \cdot u)} - \frac{(v \cdot u)}{\sqrt{(v \cdot u)^2 - v^2}} \frac{(\bar{l} \cdot \bar{v})^2}{\bar{v}^2}, \\
 K_7^R &= \frac{1}{2} K_{12}^R + \frac{1}{2} \frac{v^2}{\bar{v}^2} \left(\bar{l}^2 - \frac{(\bar{l} \cdot \bar{v})^2}{\bar{v}^2} \right) K_1^R + \frac{3}{4} \sqrt{v^2} [1 - K_0^R] \frac{\bar{v}^2 + v^2}{\bar{v}^2} \frac{(\bar{l} \cdot \bar{v})^2}{\bar{v}^2} \\
 &\quad + \frac{1}{2} \sqrt{v^2} \frac{\bar{v}^2 - v^2}{\bar{v}^2} \frac{(\bar{l} \cdot \bar{v})^3}{\bar{v}^2 \bar{v}^2} - \frac{1}{2} \frac{(v \cdot u)}{\sqrt{v^2}} \frac{(\bar{v} \cdot u) - (v \cdot u)}{\bar{v}^2} \left(1 + 3 \frac{v^2}{\bar{v}^2} \right) \frac{(\bar{l} \cdot \bar{v})^3}{\bar{v}^2}, \\
 K_8^R &= \frac{1}{2} K_{11}^R + \frac{1}{2} \frac{v^2}{\bar{v}^2} \left(\bar{l}^2 - \frac{(\bar{l} \cdot \bar{v})^2}{\bar{v}^2} \right) K_2^R - \frac{1}{3} \frac{\bar{v}^2 - v^2}{\bar{v}^2} \frac{(\bar{l} \cdot \bar{v})^2}{\bar{v}^2} K_2^R, \\
 K_9^R &= \left(\frac{\sqrt{v^2}}{2} + \frac{(\bar{l} \cdot \bar{v})}{\sqrt{v^2}} \right)^2 K_1^R - \frac{3}{2} \frac{(v \cdot u)}{\sqrt{v^2}} [(\bar{v} \cdot u) - (v \cdot u)] \frac{(\bar{l} \cdot \bar{v})^2}{\bar{v}^2} \\
 &\quad + \frac{1}{\sqrt{v^2}} \left(\frac{v^2 - \bar{v}^2}{v^2} K_0^R - 2 (v \cdot u) \frac{(\bar{v} \cdot u) - (v \cdot u)}{\bar{v}^2} \right) \frac{(\bar{l} \cdot \bar{v})^3}{\bar{v}^2}, \\
 K_{10}^R &= \frac{v^2}{4} \left(1 + 2 \frac{(\bar{l} \cdot \bar{v})}{\bar{v}^2} + 4 \frac{(\bar{l} \cdot \bar{v})^2}{\bar{v}^2 \bar{v}^2} \right) K_2^R + \frac{1}{3} \frac{v^2 - \bar{v}^2}{\bar{v}^2} \frac{(\bar{l} \cdot \bar{v})^2}{\bar{v}^2} K_2^R \\
 &\quad + \frac{1}{2} \frac{\sqrt{v^2} (v \cdot u)}{\sqrt{(v \cdot u)^2 - v^2}} \left(\frac{(\bar{l} \cdot u)}{(\bar{v} \cdot u)} - \frac{(\bar{l} \cdot \bar{v})}{\bar{v}^2} \right) (\bar{l} \cdot \bar{v}), \\
 K_{11}^R &= \frac{\sqrt{v^2}}{[(v \cdot u)^2 - v^2]^{3/2}} \left\{ v^2 (\bar{l} \cdot u)^3 - 3 (v \cdot u) (\bar{l} \cdot u)^2 (\bar{l} \cdot \bar{v}) K_0^R \right. \\
 &\quad \left. + 3 (v \cdot u)^2 (\bar{l} \cdot u) \frac{(\bar{l} \cdot \bar{v})^2}{\bar{v}^2} - \frac{(v \cdot u)^3}{v^2} \frac{(\bar{l} \cdot \bar{v})^3}{\bar{v}^2} K_0^R \right\} \\
 &\quad + 2 \frac{\sqrt{v^2}}{[(v \cdot u)^2 - v^2]^{1/2}} \frac{[(\bar{v} \cdot u) - (v \cdot u)]^2}{\bar{v}^2} (\bar{l} \cdot u) \frac{(\bar{l} \cdot \bar{v})^2}{\bar{v}^2}, \\
 K_{12}^R &= \frac{1}{(v \cdot u)^2 - v^2} \left\{ \left(\frac{\sqrt{v^2}}{2} + \frac{(\bar{l} \cdot \bar{v})}{\sqrt{v^2}} \right) K_0^R v^2 (\bar{l} \cdot u)^2 \right. \\
 &\quad - 2 \left(\frac{\sqrt{v^2}}{2} \frac{(v \cdot u)}{(\bar{v} \cdot u)} + \sqrt{v^2} \left[1 - \frac{1}{3} \frac{\bar{v}^2 - v^2}{\bar{v}^2} \right] \frac{(\bar{l} \cdot \bar{v})}{\bar{v}^2} \right) (v \cdot u) (\bar{l} \cdot u) (\bar{l} \cdot \bar{v}) \\
 &\quad + \left(\frac{\sqrt{v^2}}{2} [2 - K_0^R] + \frac{(\bar{l} \cdot \bar{v})}{\sqrt{v^2}} \left[1 - \frac{2}{3} \frac{\bar{v}^2 - v^2}{\bar{v}^2} \right] K_0^R \right) (v \cdot u)^2 \frac{(\bar{l} \cdot \bar{v})^2}{\bar{v}^2} \left. \right\} \\
 &\quad - \sqrt{v^2} [1 - K_0^R] \left(1 + \frac{2}{3} \frac{(\bar{l} \cdot \bar{v})}{\bar{v}^2} - \frac{4}{3} \frac{1}{(\bar{v} \cdot u)} (\bar{l} \cdot u) \right) \frac{(\bar{l} \cdot \bar{v})^2}{\bar{v}^2} \\
 &\quad + \frac{\sqrt{v^2}}{2} \frac{\bar{v}^2 - v^2}{(\bar{v} \cdot u)} (\bar{l} \cdot u) \frac{(\bar{l} \cdot \bar{v})}{\bar{v}^2}, \tag{J.3}
 \end{aligned}$$

7. Appendix

with

$$\bar{l}_\mu = l_\mu - \bar{v}_\mu/2, \quad \bar{v}^2 = (\bar{v} \cdot u)^2 - (v \cdot u)^2 + v^2. \quad (\text{J.4})$$

This formulation of the master loops makes it also easier to prove the constraints (4.43, 4.44) we need to fulfill. The transition to the splitted version used in (4.47) and presented in Appendix I can be achieved in the following way. From the K_i^R we first take all which terms which lead to a converging dispersion integral and have at most one subtraction. These terms will then build up the K_i given in Appendix I. Note hereby that according to the vacuum limits (I.3) we minimally need to combine

$$\begin{array}{ll} (\bar{l} \cdot \bar{v})^n & \text{with } \frac{v^2}{\bar{v}^2} \\ (u \cdot \bar{l}) & \text{with } 1 \end{array} \quad (\text{J.5})$$

in order to get convergence of the dispersion integrals. The situation for $(u \cdot \bar{l})^2$, $(u \cdot \bar{l})^3$ and \bar{l}^2 is more involved because here we need to compensate the \bar{v}^2 of the \bar{l}^2 terms. This can be done by adding

$$\bar{l}^2 \longrightarrow \bar{l}^2 + \frac{\bar{v}^2 - v^2}{4} \quad (\text{J.6})$$

and extra term which changes the \bar{v}^2 into a v^2 behaviour. After having moved these minimally subtracted terms into the K_i we will be left with terms including higher subtractions and the terms compensating the additional term in (J.6). These terms will then be brought into a form

$$((\bar{v} \cdot u) - (v \cdot u)) \times \text{remainder} \quad (\text{J.7})$$

using the identities of Appendix K. Thereby the factor $((\bar{v} \cdot u) - (v \cdot u))$ cancels the denominator in the dispersion integral resulting in a trivial energy dependence of the $\bar{C}_{n,m}^{ijk}$ which is given by external energy variable only.

K. Reformulations in the dispersion integrals

In this appendix we derive some tricks used in the calculation of the master loop functions for the delta isobar. In order to calculate the real parts of these loops we use dispersion relations. Doing so we are always facing integrals like⁶:

$$\int_{-\infty}^{\infty} d\bar{v}^0 \frac{f(\bar{v}^0, |\vec{w}|)}{\bar{v}^0 - v^0} (v^0)^n (\bar{v}^0)^m \quad (\text{K.1})$$

where $f(\bar{v}^0, |\vec{w}|)$ is our integration kernel. In vacuum these kernels always fulfill the condition $f(\bar{v}^0, |\vec{w}|) = -f(-\bar{v}^0, |\vec{w}|)$ due to the symmetry of the imaginary parts of the loops. This leads us to

$$\begin{aligned} & \int_{-\infty}^{\infty} d\bar{v}^0 \frac{f(\bar{v}^0, |\vec{w}|)}{\bar{v}^0 - v^0} (v^0)^n (\bar{v}^0)^m \\ &= \int_0^{\infty} d\bar{v}^0 f(\bar{v}^0, |\vec{w}|) (v^0)^n (\bar{v}^0)^m \left[\frac{(\bar{v}^0 + v^0) + (-1)^m (\bar{v}^0 - v^0)}{(\bar{v}^0)^2 - (v^0)^2} \right]. \end{aligned} \quad (\text{K.2})$$

If m is even we thus find:

$$= 2 \int_0^{\infty} d\bar{v}^0 (v^0)^n (\bar{v}^0)^{(m+1)} \left[\frac{f(\bar{v}^0, |\vec{w}|)}{(\bar{v}^0)^2 - (v^0)^2} \right],$$

and in the odd case:

$$= 2 \int_0^{\infty} d\bar{v}^0 (v^0)^{(n+1)} (\bar{v}^0)^m \left[\frac{f(\bar{v}^0, |\vec{w}|)}{(\bar{v}^0)^2 - (v^0)^2} \right].$$

We see that in the odd case we are free to move one power of \bar{v}^0 into a power of v^0 without changing the result. For example we would have:

$$= \int_{-\infty}^{\infty} d\bar{v}^0 (v^0 - \bar{v}^0) \left[\frac{f(\bar{v}^0, |\vec{w}|)}{(\bar{v}^0) - (v^0)} \right] = 0.$$

and we could make the replacements:

$$\begin{aligned} \bar{v}^0 &\longleftrightarrow v^0 \\ (\bar{v}^0)^2 &\longleftrightarrow (\bar{v}^0)^2 \\ (\bar{v}^0)^3 &\longleftrightarrow (v^0)(\bar{v}^0)^2 \end{aligned} \quad (\text{K.3})$$

and so on without changing the value of the dispersion integral. This allows us to rewrite some subtraction terms:

$$\frac{v^2}{\bar{v}^2} = \frac{v^2 - \bar{v}^2}{\bar{v}^2} + 1 = \frac{(v^0)^2 - (\bar{v}^0)^2}{\bar{v}^2} + 1 = \frac{\bar{v}^0(v^0 - \bar{v}^0)}{\bar{v}^2} + 1 \quad (\text{K.4})$$

⁶Note that all calculations of the dispersion integrals are done in the nuclear matter rest frame $u_\mu = (1, \vec{0})$

7. Appendix

where the last equality is valid only in vacuum. This is a nice trick to rewrite the subtraction term v^2/\bar{v}^2 for the following reason. In vacuum the subtraction with v^2/\bar{v}^2 is perfectly doable because we know that the realpart will be a function of v^2 only and our subtraction doesn't spoil this. In contrast to this in medium we have an additional dependence on $(u \cdot v)$ which will not be covered when v^2/\bar{v}^2 is used. The mentioned rewriting of this term will then serve for this additional dependence. In addition we can write equivalent substitutions for higher subtractions:

$$\begin{aligned} \left[\frac{v^2}{\bar{v}^2} \right]^2 &= \left[\frac{v^2}{\bar{v}^2} \right] \left(\frac{v^2 - \bar{v}^2}{\bar{v}^2} + 1 \right) \\ &\longrightarrow 1 - \frac{(u \cdot \bar{v})}{\bar{v}^2} [(u \cdot \bar{v}) - (u \cdot v)] - v^2 \frac{\bar{v}^2 - v^2}{\bar{v}^2 \bar{v}^2}. \end{aligned} \quad (\text{K.5})$$

L. Coefficient functions $c_{[ij]}^{(p,q)}$

We recall the form of the invariant functions $c_{[ij]}^{(p,q)}(q; v, u)$:

$$\begin{aligned}
 c_{[11]}^{(q)} &= \frac{1}{2} E_+ \left(E_+ E_- + (X \cdot q)^2 \right), & c_{[11]}^{(p)} &= E_+, \\
 c_{[12]}^{(q)} &= -\frac{i}{2} (X \cdot q) \left(E_+ E_- + (X \cdot q)^2 \right), & c_{[12]}^{(p)} &= -i (X \cdot q), \\
 c_{[22]}^{(q)} &= \frac{1}{2} E_- \left(E_+ E_- + (X \cdot q)^2 \right), & c_{[22]}^{(p)} &= E_-, \\
 c_{[13]}^{(p)} &= c_{[24]}^{(p)} = -\frac{1}{\sqrt{3}} E_+ E_-, & c_{[25]}^{(p)} &= c_{[16]}^{(p)} = -i (\hat{v} \cdot q) (X \cdot q), \\
 c_{[17]}^{(p)} &= -i \sqrt{\frac{2}{3}} E_+ (X \cdot q), & c_{[15]}^{(p)} &= (\hat{v} \cdot q) E_+, & c_{[14]}^{(p)} &= \frac{i}{\sqrt{3}} E_+ (X \cdot q), \\
 c_{[28]}^{(p)} &= -i \sqrt{\frac{2}{3}} E_- (X \cdot q), & c_{[26]}^{(p)} &= (\hat{v} \cdot q) E_-, & c_{[23]}^{(p)} &= \frac{i}{\sqrt{3}} E_- (X \cdot q), \\
 c_{[27]}^{(p)} &= c_{[18]}^{(p)} = -\sqrt{\frac{3}{2}} \left(\frac{1}{3} E_+ E_- + (X \cdot q)^2 \right), & & & &
 \end{aligned} \tag{L.1}$$

and

$$\begin{aligned}
 c_{[33]}^{(p)} &= \frac{1}{3} E_-^2 E_+, & c_{[44]}^{(p)} &= \frac{1}{3} E_+^2 E_-, \\
 c_{[55]}^{(p)} &= E_+ (\hat{v} \cdot q)^2, & c_{[77]}^{(p)} &= \frac{1}{2} E_+ \left(\frac{1}{3} E_+ E_- - (X \cdot q)^2 \right), \\
 c_{[66]}^{(p)} &= E_- (\hat{v} \cdot q)^2, & c_{[88]}^{(p)} &= \frac{1}{2} E_- \left(\frac{1}{3} E_+ E_- - (X \cdot q)^2 \right), \\
 c_{[35]}^{(p)} &= c_{[46]}^{(p)} = -\frac{1}{\sqrt{3}} (\hat{v} \cdot q) E_+ E_-, & c_{[57]}^{(p)} &= -i \sqrt{\frac{2}{3}} (X \cdot q) (\hat{v} \cdot q) E_+, \\
 c_{[37]}^{(p)} &= c_{[48]}^{(p)} = i \frac{\sqrt{2}}{3} (X \cdot q) E_+ E_-, & c_{[68]}^{(p)} &= -i \sqrt{\frac{2}{3}} (X \cdot q) (\hat{v} \cdot q) E_-, \\
 c_{[34]}^{(p)} &= -\frac{i}{3} (X \cdot q) E_+ E_-, & c_{[56]}^{(p)} &= -i (\hat{v} \cdot q)^2 (X \cdot q), \\
 c_{[78]}^{(p)} &= i (X \cdot q) \left(\frac{3}{2} (X \cdot q)^2 + \frac{5}{6} E_+ E_- \right), \\
 c_{[36]}^{(p)} &= \frac{i}{\sqrt{3}} (\hat{v} \cdot q) E_- (X \cdot q), & c_{[38]}^{(p)} &= \frac{1}{\sqrt{2}} E_- \left(\frac{1}{3} E_+ E_- + (X \cdot q)^2 \right), \\
 c_{[45]}^{(p)} &= \frac{i}{\sqrt{3}} (\hat{v} \cdot q) E_+ (X \cdot q), & c_{[47]}^{(p)} &= \frac{1}{\sqrt{2}} E_+ \left(\frac{1}{3} E_+ E_- + (X \cdot q)^2 \right), \\
 c_{[58]}^{(p)} &= c_{[67]}^{(p)} = -\sqrt{\frac{3}{2}} (\hat{v} \cdot q) \left(\frac{1}{3} E_+ E_- + (X \cdot q)^2 \right), & & & &
 \end{aligned} \tag{L.2}$$

where $X_\mu = X_\mu(v, u)$ and

$$E_\pm \equiv m_N \pm \left(\sqrt{v_0^2 - \vec{v}^2} - q \cdot \hat{v} \right), \quad E_+ E_- = q^2 - (q \cdot \hat{v})^2. \tag{L.3}$$

M. u -channel contributions to the πN scattering amplitude

In this Appendix we construct the interaction kernels $K_{\pi N}^{(N,\pm)}$ and $K_{\pi N}^{(\Delta,\pm)}$ for the u -channel contributions to the πN scattering amplitude. We begin with the calculation of the coefficients for the u -channel nucleon pole diagram

$$K_{u,\pi N}^{(N)} = \begin{array}{c} \begin{array}{ccc} & q & \bar{q} \\ & \text{---} & \text{---} \\ & \diagdown & / \\ & \text{---} & \text{---} \\ & / & \diagdown \\ p & & \bar{p} \end{array} \end{array} \quad (\text{M.1})$$

where we define $w = p + q = \bar{p} + \bar{q}$ and $\tilde{w} = p - \bar{q} = \bar{p} - q$. This contribution

$$K_{u,\pi N}^{(N)}(\bar{p}, p; w) = \frac{g_{\pi NN}^2}{m_N^2} \left(\not{w} + m_N - (\not{\bar{p}} + m_N) \frac{1}{\not{w} + m_N} (\not{p} + m_N) \right) \quad (\text{M.2})$$

has already been calculated in [90] from where we also take the value $g_{\pi NN} = 12.61$. We now decompose this expression into the projectors P^+ and P^- (4.25)

$$K_{u,\pi N}^{(N)}(\bar{p}, p; w) = K_{\pi N}^{(N,+)} P^+ + K_{\pi N}^{(N,-)} P^- \quad (\text{M.3})$$

and determine the coefficient functions which are used in (4.67). Using the on-shell conditions we arrive at:

$$K_{\pi N}^{(N,\pm)} = g_{\pi NN}^2 \left(\frac{\sqrt{s}}{(m_N)^2} \pm \frac{1}{m_N} + 4 \frac{\sqrt{s} - m_N}{u - (m_N)^2} \right) \quad (\text{M.4})$$

The same decomposition has to be done for the case of the isobar u -channel diagram.

$$K_{u,\pi N}^{(\Delta)} = \begin{array}{c} \begin{array}{ccc} & q & \bar{q} \\ & \text{---} & \text{---} \\ & \diagdown & / \\ & \text{---} & \text{---} \\ & / & \diagdown \\ p & & \bar{p} \end{array} \end{array} \quad (\text{M.5})$$

Since we would like to have only a qualitative estimate about the possible effect due to u -channel corrections we use the free isobar propagator in this diagram. The computation is a little bit more complicated because of the more complicated structure of the

propagator:

$$\begin{aligned}
 K_{u,\pi N}^{(\Delta)}(\bar{p}, p; w) = & \\
 & \frac{\tilde{C}_{[10]}^{(\frac{3}{2},\Delta)}}{4f_\pi} \left[\frac{(\bar{q} \cdot q)}{\tilde{\psi} - m_\Delta} - \frac{(\bar{q} \cdot \tilde{w})(\tilde{w} \cdot q)}{(m_\Delta)^2(\tilde{\psi} - m_\Delta)} \right. \\
 & + \frac{1}{3} \left(\bar{p} + m_\Delta + \frac{(q \cdot \tilde{w})}{m_\Delta} \right) \frac{1}{\tilde{\psi} + m_\Delta} \left(p + m_\Delta + \frac{(\bar{q} \cdot \tilde{w})}{m_\Delta} \right) - \frac{\tilde{w} \cdot (q + \bar{q})}{3m_\Delta} \\
 & - \frac{1}{3}(\psi + m_\Delta) + \frac{Z}{3m_\Delta} (\bar{q}(\tilde{w} \cdot q) + (\bar{q} \cdot \tilde{w})\not{q} + m_\Delta(\bar{q}\not{q} - 2(\bar{q} \cdot q))) \\
 & \left. \frac{Z^2}{6m_\Delta} \left(\bar{p}\tilde{\psi}p - \tilde{w}^2\psi + 2m_\Delta(\bar{q}\not{q} - 2(q \cdot q)) \right) \right] \tag{M.6}
 \end{aligned}$$

The coupling $\tilde{C}_{[10]}^{(\frac{3}{2},\Delta)} = 6.845$ is taken from [90]. This leads to the following results for the K^\pm :

$$\begin{aligned}
 K_{\pi N}^{(\Delta,\pm)} = & \frac{\tilde{C}_{[10]}^{(\frac{3}{2},\Delta)}}{24f_\pi^2 m_\Delta^2} \left[\frac{1}{(m_\Delta)^2 - u} (\mp 10(m_\Delta)^5 + 6\sqrt{s}(m_\Delta)^4 \right. \\
 & + m_\Delta^3(\pm 12m_N^2 \pm 6m_\pi^2 \mp 9s \mp u) - \sqrt{s}(-m_N^2 + m_\pi^2 + u)^2 \\
 & + m_\Delta^2\sqrt{s}(-2m_N^2 - 4m_\pi^2 + 3s + u) \\
 & \left. \pm 2m_\Delta(m_N^2 - m_\pi^2 - u)(2m_N^2 - 2m_\pi^2 - u) \right] \\
 & Z_{[10]}((\pm 2m_\pi^2 \mp s \pm u) - 2\sqrt{s}(-m_N^2 + m_\pi^2 + u)) \\
 & Z_{[10]}^2(\mp(m_\Delta)^3 + \sqrt{s}(m_\Delta)^2 + m_\Delta^2(\pm 2m_N^2 \pm m_\pi^2 \mp s \pm u) - u\sqrt{s}) \tag{M.7}
 \end{aligned}$$

Note that the nucleon u -channel contribution is proportional to $1/\sqrt{s}$ while the contribution of the delta is $\sim \sqrt{s}$ respectively. Compared to the treatment of the isobar we had up to now here we have to mention a difference. The value of m_Δ is in this perturbative treatment not given by the effective mass we introduced to get a better description of the scattering data but is fixed to the value $m_\Delta = 1232$ MeV. One could speculate whether a more complete description using a dressed isobar might improve the quality of the description of the scattering amplitude. However since a complete description which than would also have to include unitarisation effects is beyond the scope of this work we restrict ourself to this perturbative treatment.

N. Photon transition function \mathbf{U}

We provide explicit expressions for the photon transition function $U(q, u)$, introduced in (4.79, 4.82). For nuclear matter at rest we write

$$q^2 U(\omega, \vec{q}) = -\frac{8}{3} \frac{f_\Delta^2}{m_\pi^2} \int_0^{k_F} \frac{d^3 p}{2(p_0 - \Sigma_V) (2\pi)^3} S_{\Delta h}^{(U)}(\omega, \vec{q}, \vec{p}) + (q_\mu \rightarrow -q_\mu). \quad (\text{N.1})$$

The evaluation of the integral kernel of (N.1) is analogous to the derivation of (G.10). The first term in (4.82) implies a contribution proportional to $S_T^{(\Delta h)}$. The second term in (4.82) is treated with ease upon inserting (G.9) into the decomposition

$$\begin{aligned} [(q \cdot u) q_\mu - q^2 u_\mu] T_{\nu\alpha}(q, u) v^\alpha &= -[(q \cdot u) (q \cdot v) - q^2 (v \cdot u)] L_{\mu\nu}^{(22)}(q, u) \\ &\quad - (q \cdot v) \sqrt{q^2 - (q \cdot u)^2} L_{\mu\nu}^{(21)}(q, u) + [(q \cdot u) q_\mu - q^2 u_\mu] v_\nu. \end{aligned} \quad (\text{N.2})$$

We obtain:

$$\begin{aligned} S_{\Delta h}^{(U)} &= \frac{1}{2} \Sigma_V^N \left[q^2 S_4^{(\Delta h)} - S_1^{(\Delta h)} - S_{22}^{(\Delta h)} \right] \\ &\quad + \frac{1}{2} \frac{(q \cdot u) (q \cdot v) - q^2 (v \cdot u)}{(q \cdot u)^2 - q^2} \left[q^2 S_4^{(\Delta h)} - S_1^{(\Delta h)} \right] \\ &\quad - \frac{1}{2} \frac{(q \cdot v)}{\sqrt{q^2 - (q \cdot u)^2}} S_{12}^{(\Delta h)} - \frac{1}{2} \frac{q^2 (q \cdot u) \sqrt{v^2}}{(q \cdot u)^2 - q^2} \sum_{j=1}^2 \sum_{i=3}^8 c_{[ij]}^{(p)} S_{[ij]}^{(v)} \\ &\quad - \frac{1}{2} \frac{q^2 (v \cdot u) q^2}{(q \cdot u)^2 - q^2} \sum_{i,j=1}^2 c_{[ij]}^{(p)} \left[\sqrt{1 - \frac{v^2}{(v \cdot u)^2}} S_{[ij]}^{(xv)} - S_{[ij]}^{(vv)} \right], \end{aligned} \quad (\text{N.3})$$

with

$$\begin{aligned} S_{12}^{(\Delta h)} &= \frac{(q \cdot u)}{\sqrt{q^2 - (q \cdot u)^2}} S_1^{(\Delta h)} - \frac{q^2}{\sqrt{q^2 - (q \cdot u)^2}} S_2^{(\Delta h)}, \\ S_{22}^{(\Delta h)} &= \frac{(q \cdot u)^2}{q^2 - (q \cdot u)^2} S_1^{(\Delta h)} - 2 \frac{(q \cdot u) q^2}{q^2 - (q \cdot u)^2} S_2^{(\Delta h)} + \frac{q^2 q^2}{q^2 - (q \cdot u)^2} S_3^{(\Delta h)}. \end{aligned} \quad (\text{N.4})$$

O. Contractions of the isobar propagator

We specify the invariant functions

$$\begin{aligned}
 g_{\mu\nu} S^{\mu\nu}(w, u) &= \sum_{i,j=1}^2 S_{[ij]}^{(g)}(v, u) P_{[ij]}(v, u), \\
 \zeta_\mu S^{\mu\nu}(w, u) \zeta_\nu &= \sum_{i,j=1}^2 S_{[ij]}^{(\zeta\zeta)}(v, u) P_{[ij]}(v, u), \\
 \zeta_\mu S^{\mu\nu}(w, u) &= \sum_{i=1}^2 \sum_{j=3}^8 S_{[ij]}^{(\zeta)}(v, u) \bar{P}_{[ij]}^\nu(v, u), \\
 S^{\mu\nu}(w, u) \zeta_\nu &= \sum_{i=3}^8 \sum_{j=1}^2 S_{[ij]}^{(\zeta)}(v, u) P_{[ij]}^\mu(v, u), \tag{O.1}
 \end{aligned}$$

in terms of the components, $S_{[ij]}^{(p)}(v, u)$ and $S_{[ij]}^{(q)}(v, u)$, of the isobar propagator as defined in (4.30):

$$\begin{aligned}
 S_{[ij]}^{(g)} &= S_{[ij]}^{(q)} + S_{[4+i,4+j]}^{(p)} + \frac{1}{3} (4\delta_{ij} - 1) S_{[5-i,5-j]}^{(p)} + \frac{1}{3} (1 + 2\delta_{ij}) S_{[6+i,6+j]}^{(p)} \\
 &\quad + \frac{\sqrt{8}}{3} (\delta_{ij} - 1) [S_{[5-i,6+j]}^{(p)} + S_{[6+i,5-j]}^{(p)}], \\
 S_{[ij]}^{(\zeta\zeta)} &= (\zeta \cdot \hat{v})^2 S_{[ij]}^{(vv)} + (\zeta \cdot X)^2 S_{[ij]}^{(xx)} - (\zeta \cdot X) (\zeta \cdot \hat{v}) \left(S_{[ij]}^{(vx)} + S_{[ij]}^{(xv)} \right), \\
 S_{[ij]}^{(\zeta)} &= (\zeta \cdot \hat{v}) S_{[ij]}^{(v)} - (\zeta \cdot X) S_{[ij]}^{(x)}, \tag{O.2}
 \end{aligned}$$

where $\hat{v}_\mu = v_\mu / \sqrt{v^2}$ and $X_\mu = X_\mu(v, u)$ and

$$\begin{aligned}
 \hat{v}_\mu S^{\mu\nu} &= \sum_{i=1}^2 \sum_{j=3}^8 S_{[ij]}^{(v)} \bar{P}_{[ij]}^\nu, & S^{\mu\nu} \hat{v}_\nu &= \sum_{i=3}^8 \sum_{j=1}^2 S_{[ij]}^{(v)} P_{[ij]}^\mu, \\
 \hat{v}_\mu S^{\mu\nu} \hat{v}_\nu &= \sum_{i,j=1}^2 S_{[ij]}^{(vv)} P_{[ij]}, & X_\mu S^{\mu\nu} X_\nu &= \sum_{i,j=1}^2 S_{[ij]}^{(xx)} P_{[ij]}, \\
 X_\mu S^{\mu\nu} \hat{v}_\nu &= \sum_{i,j=1}^2 S_{[ij]}^{(xv)} P_{[ij]}, & \hat{v}_\mu S^{\mu\nu} X_\nu &= \sum_{i,j=1}^2 S_{[ij]}^{(vx)} P_{[ij]}, \\
 X_\mu S^{\mu\nu} &= \sum_{i=1}^2 \sum_{j=3}^8 S_{[ij]}^{(x)} \bar{P}_{[ij]}^\nu, & S^{\mu\nu} X_\nu &= \sum_{i=3}^8 \sum_{j=1}^2 S_{[ij]}^{(x)} P_{[ij]}^\mu. \tag{O.3}
 \end{aligned}$$

7. Appendix

We obtain:

$$\begin{aligned}
S_{[ij]}^{(xx)} &= \frac{\sqrt{2}}{3} (S_{[5-i,6+j]}^{(p)} + S_{[6+i,5-j]}^{(p)}) - \frac{1}{3} (S_{[5-i,5-j]}^{(p)} + 2S_{[6+i,6+j]}^{(p)}), \\
S_{[ij]}^{(xv)} &= -\frac{i}{\sqrt{3}} S_{[5-i,4+j]}^{(p)} + i \sqrt{\frac{2}{3}} S_{[6+i,4+j]}^{(p)}, \\
S_{[ij]}^{(vx)} &= -\frac{i}{\sqrt{3}} S_{[4+i,5-j]}^{(p)} + i \sqrt{\frac{2}{3}} S_{[4+i,6+j]}^{(p)}, \quad \text{for } i, j = 1, 2 \\
S_{[ij]}^{(x)} &= -\frac{i}{\sqrt{3}} S_{[5-i,j]}^{(p)} + i \sqrt{\frac{2}{3}} S_{[6+i,j]}^{(p)}, \quad \text{for } i = 1, 2 \text{ \& } j > 2, \\
S_{[ij]}^{(x)} &= -\frac{i}{\sqrt{3}} S_{[i,5-j]}^{(p)} + i \sqrt{\frac{2}{3}} S_{[i,6+j]}^{(p)}, \quad \text{for } i > 2 \text{ \& } j = 1, 2. \\
S_{[1j]}^{(v)} &= S_{[5j]}^{(p)}, \quad S_{[2j]}^{(v)} = S_{[6j]}^{(p)}, \quad S_{[j1]}^{(v)} = S_{[j5]}^{(p)}, \quad S_{[j2]}^{(v)} = S_{[j6]}^{(p)}, \quad \text{for } j > 2, \\
S_{[ij]}^{(vv)} &= S_{[4+i,4+j]}^{(p)}, \quad \text{for } i, j = 1, 2.
\end{aligned} \tag{O.4}$$

P. Nucleon contributions to the Photoabsorption

In this Appendix we calculate the relevant background contributions to the photoabsorption.

The kernels (4.77) are defined

$$\begin{aligned} K_{ij,lm}^{channel} &= -g^{\mu\nu} \text{Tr} \left[\bar{T}_{\mu;i;l}^{channel} T_{\nu;j;m}^{channel} \right] \\ K_{g;lm}^{channel} &= -g^{\mu\nu} g^{\alpha\beta} \text{Tr} \left[\bar{T}_{\mu\alpha;g;l}^{channel} T_{\nu\beta;g;m}^{channel} \right] \end{aligned} \quad (\text{P.1})$$

in terms of the amplitudes T . We will specify only the amplitudes actually used in the calculation while setting all other to zero for simplicity.

$$\begin{aligned} T_{\delta;1;1}^{\gamma p \rightarrow p \pi^0} &= \frac{2f_\Delta}{3m_\pi^3} \bar{N}(p, u) k_\mu S^{\mu\nu}(w, u) [f_\gamma \epsilon_{\delta\nu\alpha\beta} q^\alpha w^\beta \\ &\quad + i f'_\gamma \gamma_5 ((q \cdot w) g_{\nu\delta} - q_\nu w_\delta)] N(l, u) \\ T_{\delta;1;2}^{\gamma p \rightarrow p \pi^0} &= ie \frac{f_N}{m_\pi} \bar{N}(p, u) \left[\gamma_5 \not{k} \frac{\not{p} + \not{q} + m_N}{2(p \cdot q)} \gamma_\delta - \gamma_\delta \frac{\not{l} - \not{q} + m_N}{2(l \cdot q)} \gamma_5 \not{k} \right] N(l, u) \\ T_{\delta;2;1}^{\gamma p \rightarrow p \pi^0} &= \frac{2f_\Delta}{3m_\pi^3} \bar{N}(p, u) u_\mu S^{\mu\nu}(w, u) [f_\gamma \epsilon_{\delta\nu\alpha\beta} q^\alpha w^\beta \\ &\quad + i f'_\gamma \gamma_5 ((q \cdot w) g_{\nu\delta} - q_\nu w_\delta)] N(l, u) \\ T_{\delta;2;2}^{\gamma p \rightarrow p \pi^0} &= ie \frac{f_N}{m_\pi} \bar{N}(p, u) \left[\gamma_5 \not{q} \frac{\not{p} + \not{q} + m_N}{2(p \cdot q)} \gamma_\delta - \gamma_\delta \frac{\not{l} - \not{q} + m_N}{2(l \cdot q)} \gamma_5 \not{q} \right] N(l, u) \\ T_{\delta\mu;g;1}^{\gamma p \rightarrow p \pi^0} &= \frac{2f_\Delta}{3m_\pi^3} \bar{N}(p, u) S_\mu^\nu(w, u) [f_\gamma \epsilon_{\delta\nu\alpha\beta} q^\alpha w^\beta \\ &\quad + i f'_\gamma \gamma_5 ((q \cdot w) g_{\nu\delta} - q_\nu w_\delta)] N(l, u) \\ T_{\delta\mu;g;2}^{\gamma p \rightarrow p \pi^0} &= ie \frac{f_N}{m_\pi} \bar{N}(p, u) \left[\gamma_5 \gamma_\mu \frac{\not{p} + \not{q} + m_N}{2(p \cdot q)} \gamma_\delta - \gamma_\delta \frac{\not{l} - \not{q} + m_N}{2(l \cdot q)} \gamma_5 \gamma_\mu \right] N(l, u) \end{aligned} \quad (\text{P.2})$$

7. Appendix

$$\begin{aligned}
T_{\delta;1;1}^{\gamma p \rightarrow n\pi^+} &= -\frac{1}{\sqrt{2}} T_{\delta;1;1}^{\gamma p \rightarrow p\pi^0} & T_{\delta;2;1}^{\gamma p \rightarrow n\pi^+} &= -\frac{1}{\sqrt{2}} T_{\delta;2;1}^{\gamma p \rightarrow p\pi^0} & T_{\delta\mu;g;1}^{\gamma p \rightarrow n\pi^+} &= -\frac{1}{\sqrt{2}} T_{\delta\mu;g;1}^{\gamma p \rightarrow p\pi^0} \\
T_{\delta;1;2}^{\gamma p \rightarrow n\pi^+} &= i\sqrt{2}e \frac{f_N}{m_\pi} \bar{N}(p, u) \left[\gamma_5 \not{k} \frac{\not{p} + \not{q} + m_N}{2(p \cdot q)} \gamma_\delta - \gamma_5 \gamma_\delta \right. \\
&\quad \left. - \gamma_5 (\not{q} - \not{k}) \frac{2k_\delta - q_\delta}{(k - q)^2 - m_\pi^2} \right] N(l, u) \\
T_{\delta;2;2}^{\gamma p \rightarrow n\pi^+} &= T_{\delta\mu;g;2}^{\gamma p \rightarrow n\pi^+} = 0
\end{aligned} \tag{P.3}$$

$$\begin{aligned}
T_{\delta;1;1}^{\gamma n \rightarrow n\pi^0} &= T_{\delta;1;1}^{\gamma p \rightarrow p\pi^0} & T_{\delta;2;1}^{\gamma n \rightarrow n\pi^0} &= T_{\delta;2;1}^{\gamma p \rightarrow p\pi^0} & T_{\delta\mu;g;1}^{\gamma n \rightarrow n\pi^0} &= T_{\delta\mu;g;1}^{\gamma p \rightarrow p\pi^0} \\
T_{\delta;1;2}^{\gamma n \rightarrow n\pi^0} &= T_{\delta;2;2}^{\gamma n \rightarrow n\pi^0} = T_{\delta\mu;g;2}^{\gamma n \rightarrow n\pi^0} = 0
\end{aligned} \tag{P.4}$$

$$\begin{aligned}
T_{\delta;1;1}^{\gamma n \rightarrow p\pi^-} &= \frac{1}{\sqrt{2}} T_{\delta;1;1}^{\gamma p \rightarrow p\pi^0} & T_{\delta;2;1}^{\gamma n \rightarrow p\pi^-} &= \frac{1}{\sqrt{2}} T_{\delta;2;1}^{\gamma p \rightarrow p\pi^0} & T_{\delta\mu;g;1}^{\gamma n \rightarrow p\pi^-} &= \frac{1}{\sqrt{2}} T_{\delta\mu;g;1}^{\gamma p \rightarrow p\pi^0} \\
T_{\delta;1;2}^{\gamma n \rightarrow p\pi^-} &= i\sqrt{2}e \frac{f_N}{m_\pi} \bar{N}(p, u) \left[-\gamma_\delta \frac{\not{l} - \not{q} + m_N}{2(l \cdot q)} \gamma_5 \not{k} + \gamma_5 \gamma_\delta \right. \\
&\quad \left. + \gamma_5 (\not{q} - \not{k}) \frac{2k_\delta - q_\delta}{(k - q)^2 - m_\pi^2} \right] N(l, u) \\
T_{\delta;2;2}^{\gamma n \rightarrow p\pi^-} &= T_{\delta\mu;g;2}^{\gamma n \rightarrow p\pi^-} = 0
\end{aligned} \tag{P.5}$$

where we have $p_\mu + q_\mu = w_\mu = l_\mu + k_\mu$. To build up the effective spectral functions (4.78) we define:

$$\begin{aligned}
\Gamma_{11}^{(11)}(q, u) &= -\frac{1}{q^2} \left(\chi_{33}^{(L)} + \frac{q \cdot u}{\sqrt{q^2 - (q \cdot u)^2}} (\chi_{34}^{(L)} + \chi_{43}^{(L)}) \right. \\
&\quad \left. + \frac{(q \cdot u)^2}{q^2 - (q \cdot u)^2} \chi_{44}^{(L)} - \frac{q^2}{q^2 - (q \cdot u)^2} \chi_{(22)}^{(T)} \right), \\
\Gamma_{12}^{(11)}(q, u) &= \Gamma_{21}^{(11)}(q, u) = \frac{1}{\sqrt{q^2 - (q \cdot u)^2}} \chi_{34}^{(L)} + \frac{q \cdot u}{q^2 - (q \cdot u)^2} (\chi_{44}^{(L)} - \chi_{22}^{(T)}), \\
\Gamma_{22}^{(11)}(q, u) &= -\frac{q^2}{q^2 - (q \cdot u)^2} (\chi_{44}^{(L)} - \chi_{22}^{(T)}), & \bar{\Gamma}_{00}^{(11)}(q, u) &= -\chi_{22}^{(T)}.
\end{aligned} \tag{P.6}$$

These functions are equal to the ones defined in (4.56). In addition we could now have the case where the external state is not a nucleon and a Δ -isobar but due to the background

terms we have also the situation with two nucleons. For these we need in addition:

$$\begin{aligned}
\Gamma_{11}^{(12)}(q, u) &= -\frac{1}{q^2} \left(\chi_{13}^{(L)} + \frac{q \cdot u}{\sqrt{q^2 - (q \cdot u)^2}} (\chi_{14}^{(L)} + \chi_{23}^{(L)}) \right. \\
&\quad \left. + \frac{(q \cdot u)^2}{q^2 - (q \cdot u)^2} \chi_{24}^{(L)} - \frac{q^2}{q^2 - (q \cdot u)^2} \chi_{(12)}^{(T)} \right), \\
\Gamma_{12}^{(12)}(q, u) &= \Gamma_{21}^{(12)}(q, u) = \frac{1}{\sqrt{q^2 - (q \cdot u)^2}} \chi_{14}^{(L)} + \frac{q \cdot u}{q^2 - (q \cdot u)^2} (\chi_{24}^{(L)} - \chi_{12}^{(T)}), \\
\Gamma_{22}^{(12)}(q, u) &= -\frac{q^2}{q^2 - (q \cdot u)^2} (\chi_{24}^{(L)} - \chi_{12}^{(T)}), \quad \bar{\Gamma}_{00}^{(12)}(q, u) = -\chi_{12}^{(T)}, \quad (P.7)
\end{aligned}$$

and

$$\begin{aligned}
\Gamma_{11}^{(22)}(q, u) &= -\frac{1}{q^2} \left(\chi_{11}^{(L)} + \frac{q \cdot u}{\sqrt{q^2 - (q \cdot u)^2}} (\chi_{12}^{(L)} + \chi_{21}^{(L)}) \right. \\
&\quad \left. + \frac{(q \cdot u)^2}{q^2 - (q \cdot u)^2} \chi_{22}^{(L)} - \frac{q^2}{q^2 - (q \cdot u)^2} \chi_{(11)}^{(T)} \right), \\
\Gamma_{12}^{(22)}(q, u) &= \Gamma_{21}^{(22)}(q, u) = \frac{1}{\sqrt{q^2 - (q \cdot u)^2}} \chi_{12}^{(L)} + \frac{q \cdot u}{q^2 - (q \cdot u)^2} (\chi_{22}^{(L)} - \chi_{11}^{(T)}), \\
\Gamma_{22}^{(22)}(q, u) &= -\frac{q^2}{q^2 - (q \cdot u)^2} (\chi_{22}^{(L)} - \chi_{11}^{(T)}), \quad \bar{\Gamma}_{00}^{(22)}(q, u) = -\chi_{11}^{(T)}. \quad (P.8)
\end{aligned}$$

Of course also the definition of the Γ_i (4.24) has to be extended:

$$\begin{aligned}
\Gamma_1^{(1)} &= 1 + \sum_{i \in \{3\} j \in \{1,3\}} \left[(\mathbb{1} - \chi^{(L)} g^{(L)})^{-1} \chi^{(L)} g^{(L)} \right]_{ij} \\
&\quad + \sum_{i \in \{4\} j \in \{1,3\}} \frac{(u \cdot q)}{\sqrt{q^2 - (u \cdot q)^2}} \left[(\mathbb{1} - \chi^{(L)} g^{(L)})^{-1} \chi^{(L)} g^{(L)} \right]_{ij} \quad (P.9)
\end{aligned}$$

$$\Gamma_2^{(1)} = \sum_{i \in \{4\} j \in \{1,3\}} \frac{-q^2}{\sqrt{q^2 - (u \cdot q)^2}} \left[(\mathbb{1} - \chi^{(L)} g^{(L)})^{-1} \chi^{(L)} g^{(L)} \right]_{ij}.$$

$$\begin{aligned}
\Gamma_1^{(2)} &= 1 + \sum_{i \in \{1\} j \in \{1,3\}} \left[(\mathbb{1} - \chi^{(L)} g^{(L)})^{-1} \chi^{(L)} g^{(L)} \right]_{ij} \\
&\quad + \sum_{i \in \{2\} j \in \{1,3\}} \frac{(u \cdot q)}{\sqrt{q^2 - (u \cdot q)^2}} \left[(\mathbb{1} - \chi^{(L)} g^{(L)})^{-1} \chi^{(L)} g^{(L)} \right]_{ij} \quad (P.10)
\end{aligned}$$

$$\Gamma_2^{(2)} = \sum_{i \in \{2\} j \in \{1,3\}} \frac{-q^2}{\sqrt{q^2 - (u \cdot q)^2}} \left[(\mathbb{1} - \chi^{(L)} g^{(L)})^{-1} \chi^{(L)} g^{(L)} \right]_{ij}.$$

7. Appendix

Bibliography

- [1] R. Rapp, Nucl. Phys. **A725**, 254 (2003).
- [2] M. Naruki *et al.*, Phys. Rev. Lett. **96**, 092301 (2006).
- [3] T. Eberl *et al.*, Nucl. Phys. **A752**, 433 (2005).
- [4] H. S. Matis *et al.*, Nucl. Phys. **A583**, 617C (1995).
- [5] J. P. Wessels *et al.*, Nucl. Phys. **A715**, 262 (2003).
- [6] A. L. S. Angelis *et al.*, Eur. Phys. J. **C13**, 433 (2000).
- [7] K. Ozawa *et al.*, Phys. Rev. Lett. **86**, 5019 (2001).
- [8] R. Arnaldi *et al.*, Phys. Rev. Lett. **96**, 162302 (2006).
- [9] F. Riek and J. Knoll, Nucl. Phys. **A740**, 287 (2004).
- [10] H. van Hees and J. Knoll, Nucl. Phys. **A683**, 369 (2000).
- [11] C. Gaarde, Ann. Rev. Nucl. Part. Sci. **41**, 187 (1991).
- [12] A. B. Migdal, Rev. Mod. Phys. **50**, 107 (1978).
- [13] A. B. Migdal, E. E. Saperstein, M. A. Troitsky, and D. N. Voskresensky, Phys. Rept. **192**, 179 (1990).
- [14] E. Oset, H. Toki, and W. Weise, Phys. Rept. **83**, 281 (1982).
- [15] E. Oset and L. L. Salcedo, Nucl. Phys. **A468**, 631 (1987).
- [16] L.-h. Xia, P. J. Siemens, and M. Soyeur, Nucl. Phys. **A578**, 493 (1994).
- [17] C. L. Korpa and R. Malfliet, Phys. Rev. **C52**, 2756 (1995).
- [18] P. Arve and J. Helgesson, Nucl. Phys. **A572**, 600 (1994).
- [19] H.-c. Kim, S. Schramm, and S. H. Lee, Phys. Rev. **C56**, 1582 (1997).
- [20] C. L. Korpa and M. F. M. Lutz, Nucl. Phys. **A742**, 305 (2004).

BIBLIOGRAPHY

- [21] M. Post, S. Leupold, and U. Mosel, Nucl. Phys. **A741**, 81 (2004).
- [22] C. L. Korpa and A. E. L. Dieperink, Phys. Rev. **C70**, 015207 (2004).
- [23] H. van Hees and R. Rapp, Phys. Lett. **B606**, 59 (2005).
- [24] T. Ericson and W. Weise, Clarendon Press, Oxford (1988).
- [25] J. Nieves, E. Oset, and C. Garcia-Recio, Nucl. Phys. **A554**, 554 (1993).
- [26] M. Hirata, J. H. Koch, E. J. Moniz, and F. Lenz, Annals Phys. **120**, 205 (1979).
- [27] M. Kohl *et al.*, Phys. Lett. **B530**, 67 (2002).
- [28] R. C. Carrasco and E. Oset, Nucl. Phys. **A536**, 445 (1992).
- [29] M. F. M. Lutz, Phys. Lett. **B552**, 159 (2003).
- [30] V. F. Dmitriev and T. Suzuki, Nucl. Phys. **A438**, 697 (1985).
- [31] T. Inoue and E. Oset, Nucl. Phys. **A710**, 354 (2002).
- [32] M. Nakano *et al.*, Int. J. Mod. Phys. **E10**, 459 (2001).
- [33] S. Afanasiev *et al.*, arXiv:0706.3034 [nucl-ex] (2007).
- [34] M. Asakawa, C. M. Ko, P. Levai, and X. J. Qiu, Phys. Rev. **C46**, 1159 (1992).
- [35] M. Herrmann, B. L. Friman, and W. Norenberg, Nucl. Phys. **A560**, 411 (1993).
- [36] B. Friman and H. J. Pirner, Nucl. Phys. **A617**, 496 (1997).
- [37] R. Rapp, G. Chanfray, and J. Wambach, Nucl. Phys. **A617**, 472 (1997).
- [38] W. Peters, M. Post, H. Lenske, S. Leupold, and U. Mosel, Nucl. Phys. **A632**, 109 (1998).
- [39] M. Urban, M. Buballa, and J. Wambach, Nucl. Phys. **A673**, 357 (2000).
- [40] M. Post, S. Leupold, and U. Mosel, Nucl. Phys. **A689**, 753 (2001).
- [41] D. Cabrera, E. Oset, and M. J. Vicente Vacas, Nucl. Phys. **A705**, 90 (2002).
- [42] H. van Hees and R. Rapp, Phys. Rev. Lett. **97**, 102301 (2006).
- [43] H. van Hees and R. Rapp, hep-ph/0604269 .
- [44] G. E. Brown and M. Rho, Phys. Rev. Lett. **66**, 2720 (1991).

- [45] R. Rapp and C. Gale, Phys. Rev. **C60**, 024903 (1999).
- [46] R. Rapp and J. Wambach, Eur. Phys. J. **A6**, 415 (1999).
- [47] J. Ruppert and T. Renk, Phys. Rev. **C71**, 064903 (2005).
- [48] F. Riek, H. van Hees, and J. Knoll, Phys. Rev. C **75**, 059801 (2007).
- [49] J. Ruppert and T. Renk, Phys. Rev. C **75**, 059901(E) (2007).
- [50] G. Penner and U. Mosel, Phys. Rev. **C66**, 055211 (2002).
- [51] G. Penner and U. Mosel, Phys. Rev. **C66**, 055212 (2002).
- [52] M. F. M. Lutz, G. Wolf, and B. Friman, Nucl. Phys. **A706**, 431 (2002).
- [53] F. Klingl, N. Kaiser, and W. Weise, Nucl. Phys. **A624**, 527 (1997).
- [54] F. Eichstaedt, S. Leupold, and U. Mosel, hep-ph/0703170 (2007).
- [55] B. Kampfer and S. Zschocke, Prog. Part. Nucl. Phys. **53**, 317 (2004).
- [56] T. Hatsuda, Y. Koike, and S.-H. Lee, Nucl. Phys. **B394**, 221 (1993).
- [57] S. Leupold, Phys. Rev. **C64**, 015202 (2001).
- [58] X.-m. Jin and D. B. Leinweber, Phys. Rev. **C52**, 3344 (1995).
- [59] G. Aarts and J. M. Martinez Resco, Nucl. Phys. **B726**, 93 (2005).
- [60] P. Muehlich, V. Shklyar, S. Leupold, U. Mosel, and M. Post, Nucl. Phys. **A780**, 187 (2006).
- [61] V. L. Eletsky, M. Belkacem, P. J. Ellis, and J. I. Kapusta, Phys. Rev. **C64**, 035202 (2001).
- [62] G. Wolf, B. Friman, and M. Soyeur, Nucl. Phys. **A640**, 129 (1998).
- [63] R. A. Schneider and W. Weise, Phys. Lett. **B515**, 89 (2001).
- [64] F. Klingl, T. Waas, and W. Weise, Nucl. Phys. **A650**, 299 (1999).
- [65] A. T. Martell and P. J. Ellis, Phys. Rev. **C69**, 065206 (2004).
- [66] D. Trnka *et al.*, Phys. Rev. Lett. **94**, 192303 (2005).
- [67] V. Metag, Talk at the QM2006 conference (2006).
- [68] M. Wachs, Phd Thesis / TU Darmstadt (2000).

BIBLIOGRAPHY

- [69] L. Kadanoff and G. Baym, Addison Wesley Publishing Comp. (1994).
- [70] M. Urban, M. Buballa, R. Rapp, and J. Wambach, Nucl. Phys. **A641**, 433 (1998).
- [71] J. S. Schwinger, Phys. Lett. **B24**, 473 (1967).
- [72] J. Wess and B. Zumino, Phys. Lett. **B37**, 95 (1971).
- [73] E. Witten, Nucl. Phys. **B223**, 422 (1983).
- [74] M. Lutz, private communications .
- [75] S. Leupold, hep-ph/0610356 (2006).
- [76] M. Herrmann, Phd Thesis / TU Darmstadt (1992).
- [77] H. van Hees and J. Knoll, Phys. Rev. **D65**, 025010 (2002).
- [78] H. van Hees, Phd Thesis / TU Darmstadt (2000).
- [79] C. D. Froggatt and J. L. Petersen, Nucl. Phys. **B129**, 89 (1977).
- [80] S. R. Amendolia *et al.*, Phys. Lett. **B138**, 454 (1984).
- [81] L. M. Barkov *et al.*, Nucl. Phys. **B256**, 365 (1985).
- [82] H. van Hees, Diploma Thesis / TU Darmstadt (1997).
- [83] W. M. Yao *et al.*, J. Phys. **G33**, 1 (2006).
- [84] C. L. Korpa, Heavy Ion Phys. **5**, 77 (1997).
- [85] V. Pascalutsa, Phys. Rev. **D58**, 096002 (1998).
- [86] V. Pascalutsa, Phys. Lett. **B503**, 85 (2001).
- [87] C. Korpa, M. Lutz, and F. Riek, in preparation .
- [88] M. F. M. Lutz, C. L. Korpa, and M. Moller, arXiv:0707.1283 [nucl-th] (2007).
- [89] M. F. M. Lutz and C. L. Korpa, Nucl. Phys. **A700**, 309 (2002).
- [90] M. F. M. Lutz and E. E. Kolomeitsev, Nucl. Phys. **A700**, 193 (2002).
- [91] G. Passarino and M. J. G. Veltman, Nucl. Phys. **B160**, 151 (1979).
- [92] B. D. Serot and J. D. Walecka, Adv. Nucl. Phys. **16**, 1 (1986).
- [93] R. Brockmann and R. Machleidt, Phys. Rev. **C42**, 1965 (1990).

- [94] E. G. Drukarev and E. M. Levin, Prog. Part. Nucl. Phys. **27**, 77 (1991).
- [95] P. Finelli, N. Kaiser, D. Vretenar, and W. Weise, Nucl. Phys. **A735**, 449 (2004).
- [96] O. Plohl and C. Fuchs, Phys. Rev. **C74**, 034325 (2006).
- [97] T. Herbert, K. Wehrberger, and F. Beck, Nucl. Phys. **A541**, 699 (1992).
- [98] SAID, on-line program, <http://gwdac.phys.gwu.edu/> .
- [99] E. Oset and W. Weise, Nucl. Phys. **A368**, 375 (1981).
- [100] H. Garcilazo and E. Moya de Guerra, Nucl. Phys. **A562**, 521 (1993).
- [101] C. Fernandez-Ramirez, E. Moya de Guerra, and J. M. Udias, Annals Phys. **321**, 1408 (2006).
- [102] V. Pascalutsa and D. R. Phillips, Phys. Rev. **C67**, 055202 (2003).
- [103] M. MacCormick *et al.*, Phys. Rev. **C53**, 41 (1996).
- [104] H. van Pee *et al.*, Eur. Phys. J. **A31**, 61 (2007).
- [105] T. Fujii *et al.*, Nucl. Phys. **B120**, 395 (1977).
- [106] J. Ahrens *et al.*, Phys. Lett. **B146**, 303 (1984).
- [107] N. Bianchi *et al.*, Phys. Rev. **C54**, 1688 (1996).
- [108] T. Wakasa *et al.*, Phys. Rev. C **55**, 2909 (1997).
- [109] G. Baym, Phys. Rev. **127**, 1391 (1962).
- [110] Y. B. Ivanov, J. Knoll, and D. N. Voskresensky, Nucl. Phys. **A657**, 413 (1999).
- [111] H. Van Hees and J. Knoll, Phys. Rev. **D65**, 105005 (2002).
- [112] H. van Hees and J. Knoll, Phys. Rev. **D66**, 025028 (2002).
- [113] R. Rapp and J. Wambach, Adv. Nucl. Phys. **25**, 1 (2000).
- [114] K. Symanzik, J. Math. Phys. **1**, 249 (1960).
- [115] S. Weinberg, Phys. Rev. **124**, 2049 (1961).
- [116] A. Herglotz, Math Naturw. Kl. **63**, (1911).
- [117] E. Wigner, Ann. Math. **53**, 36 (1951).
- [118] H. Nussenzweig, Academic press New York and London (1972).

BIBLIOGRAPHY

Acknowledgements

First of all I would like to thank my adviser Jörn Knoll, who initiated the project and with whom I developed the framework concerning the vector-mesons. Thanks also to Matthias Lutz who suggested and supervised the $\pi N\Delta$ -project of my thesis. Both of them provided me with an interesting topic and had a permanent willingness for discussions. Thanks also to Jochen Wambach and Wolfgang Nörenberg for the hospitality at the GSI theory group and the possibility to write this thesis. I have also to mention Csaba Korpa and my fellow student Matthias Möller who provided me not only with many important numerical checks for the $\pi N\Delta$ -project but also discussed many important points. I also would like to thank Bengt Friman, Ralf Rapp and especially Hendrik van Hees for many interesting discussions concerning the behaviour of vector mesons in matter. Special thanks have to go to the people from the GSI computing department especially T. Roth, W. Schön, C. Huhn and to our administrator T. Neff who always provided the necessary support for the calculations. I also would like to thank the organisers and participants of the ECT* doctoral training program 2005 for the nice time and interesting physics program I was able to attend during my stay in Trento. Last but not least special thanks to my fellow students here at GSI.

BIBLIOGRAPHY

Lebenslauf

Felix Christopher Riek
Geb. am 05.04.1979
Ledig, keine Kinder

.....
Schule	Grundschule Königstädten Immanuel-Kant-Schule . Gymnasium Rüsselsheim Abitur, Durchschnittsnote 1,5	09.1984 - 07.1989 09.1989 - 06.1998
.....
Bundeswehr	Wehrdienst Grundausbildung: 7./Feldjägerbataillon 801 Verwendung: Stabsdienstsoldat in der Öffentlichkeitsarbeit beim Kreiswehrrersatzamt Mainz Letzter Dienstgrad: Hauptgefreiter 1./Feldjägerbataillon 740	07.1998 - 04.1999
.....
Studium	Physik Technische Universität Darmstadt Dipl.-Phys., Gesamturteil: sehr gut Diplomarbeit: Resonanzen in hadronischer Materie bei endlichen Temperaturen und Baryonendichten Betreuer: Prof. Dr. Jörn Knoll	04.1999 - 08.2003
	Wissenschaftliche Hilfskraft bei der Gesellschaft für Schwerionenforschung mbH Darmstadt	09.2003 - 12.2007